

Contribution to the Technique of Compressed Air Energy Storage - The Concept of Finned Piston

THÈSE N° 6738 (2015)

PRÉSENTÉE LE 18 SEPTEMBRE 2015

À LA FACULTÉ DES SCIENCES ET TECHNIQUES DE L'INGÉNIEUR
LABORATOIRE D'ÉLECTRONIQUE INDUSTRIELLE
PROGRAMME DOCTORAL EN ENERGIE

ÉCOLE POLYTECHNIQUE FÉDÉRALE DE LAUSANNE

POUR L'OBTENTION DU GRADE DE DOCTEUR ÈS SCIENCES

PAR

Mahbod HEIDARI

acceptée sur proposition du jury:

Prof. F. Maréchal, président du jury
Prof. A. Rufer, Prof. F. Gallaire, directeurs de thèse
Prof. E. Groll, rapporteur
Prof. M. H. Saidi, rapporteur
Prof. S. Haussener, rapporteuse



ÉCOLE POLYTECHNIQUE
FÉDÉRALE DE LAUSANNE

Suisse
2015

Acknowledgements

First of all, I would like to express my deepest gratitude to my advisor Prof. Alfred Rufer for his kind attention and outstanding support throughout my PhD. I feel privileged to have been provided with an amazing scientific environment as well as excellent facilities and experimental setups, which were of great importance for the completion of this thesis. He has also shown great confidence in my work and personality and has been constantly encouraging me to draw my own research line as well as guiding me through his valuable experience whenever needed. For me, Prof. Rufer was way more than a simple supervisor, and I am extremely blessed to have completed my Ph.D. thesis under his supervision, which was a great experience.

I would like also to thank my co-director Prof. Gallaire, a true scientist, who has always helped me to conduct the thesis in the right direction and based on a concrete and solid scientific basis and with a from simple to complicated approach.

I am also grateful to the European Commission and Solution consortium for their financial support of this research work in the framework of FP7 project.

I cannot express how profoundly honored I feel by the fact that Prof. Eckhard Groll agreed to serve as a member of the scientific committee evaluating this thesis. A very special thanks to Prof. Saidi, who attended my thesis defense all the way from Sharif University in Iran, providing a very helpful review of the thesis and very useful comments. Prof. Thome, Prof. Maréchal, Prof. Favrat, Prof. Schiffmann and Prof. Haussener are equally gratefully acknowledged for dedicating their time and eagerly providing their comments and industrial insight on my work.

I am also thankful to Dr. Philippe Barrade for kindly guiding me on how to approach the difficult and important task of research specially at the beginning of my PhD. Certainly, I would not have enjoyed, or been successful, without the help of my fellow lab mates. Dr. Sebastien Wasterlain, who did an amazing job in preparing the test bench and measurements. Mr. Fred Uriel who was my officemate for the last year and has been always helpful in practical works.

Many thanks also go to Mrs. Fabienne Vionnet Monterde, the former and Mrs. Maria Anitua, the current secretary of the LEI. They both helped me on various administrative issues during my studies at the LEI. I should also thank all my friends in Lausanne, for creating a very nice and friendly environment, which helped me and motivated me a lot during the last few years.

I cannot end without thanking my dear family, on whose unconditional love, support, and encouragement, I have relied throughout my studies. My parents that have provided me with everything I needed and my lovely sister Mahta, who was always supportive and kind to me.

Lausanne, 3 June 2015

Abstract

Development of intermittent solar and wind energies and the demand peak increase has made energy storage very important in energy policy. Thus, energy storage will play a key role in enabling the world to develop a low-carbon electricity system. An interesting approach to do so can be storing energy in form of the compressed air.

Recently Compressed Air Energy Storage system (CAES) has attracted attentions as a promising technology for energy storage. In the general frame of CAES and after presenting liquid piston, the LEI Laboratory of EPFL has introduced the concept of finned piston. The main goal is to achieve energy storage by means of compressed air thanks to high isothermal efficiency compression/expansion processes.

As mentioned, compressed air with a liquid piston and with a performance of nearly 65% has been realized already as a promising solution for the cost-effective small/medium electricity storage applications. As a post-development, and to improve the problems related to the complexity of a liquid piston, a so called "dry finned piston" system was proposed. The effective work for this new system at LEI was to realize an analytical and a finite element model for such a system. The key development of this task is to solve the problem of non-isothermal behavior of the dry piston systems utilizing a directly integrated exchanger, inside of the compression / expansion chambers.

In this regard, theoretical modeling and simulation has been started with a classic reciprocating piston based on principles of mass and energy conservation. The model consists of different subsystems like driver mechanism, cylinder head, valves, heat transfer, etc. This will serve as a basis for developing the more complicated finned piston compressor.

Besides, the Finite Element Method (FEM) has been used to account for the detailed local thermal characterization in 3D geometry. Next, analytical modeling has been extended to finned piston. The heat and mass transfer has been accounted for using thermoelectric and pneumatic-electric analogy. Also FEM modeling has been carried out for the finned piston.

The analytical model was verified using experimentation. In order to propose an experimental validation, a test bench has been developed for both of the pistons. The experimental results confirms a higher exergetic efficiency for the finned piston due to its close to isothermal behavior thanks to increased heat transfer surface. The last chapter is dedicated to a parametric study to investigate the effect of change of the design parameters on system performance.

This thesis open doors toward more investigation to improve the design. The effective tool here is the comprehensive model developed in an innovative way.

Keywords: Reciprocating compressor, Finned piston, Energy storage, Heat transfer, EMR, Bond graph, Thermo-electric Analogy, Pneumatic-electric Analogy.

Résumé

Le développement des énergies intermittentes, notamment solaires et éoliennes, ainsi que l'augmentation de la demande de pointe ont rendu le stockage d'énergie très important dans la politique énergétique. Cet aspect jouera un rôle clé dans le développement d'un système électrique à faible émission de carbone. Une approche intéressante du concept consiste à utiliser l'air comprimé. Le système de stockage d'énergie par l'air comprimé (CAES) est apparu récemment comme une technologie prometteuse. Dans le cadre général de la CAES et après la présentation du piston liquide, le LEI de l'EPFL a introduit le concept de piston à ailettes. L'objectif principal est de parvenir à stocker de l'énergie par le moyen de l'air comprimé grâce à des procédés isothermes de compression et expansion à haut rendement.

Comme mentionné, l'air comprimé avec un piston liquide, d'un rendement de près de 65%, a déjà été présenté comme solution prometteuse et rentable pour les petites à moyennes installations de stockage d'électricité. Comme post-développement et dans le but de résoudre certains problèmes liés à la complexité d'un piston liquide, un système dénommé "piston sec à ailettes" a été proposé. Le travail effectif au LEI dans ce cadre a consisté à réaliser un modèle analytique ainsi qu'un modèle à éléments finis pour un tel système. Le cœur de cette tâche a été de résoudre le problème du comportement non-isotherme du système de piston sec utilisant un échangeur directement intégré à l'intérieur des chambres de compression - expansion.

À cet égard, la modélisation théorique et la simulation ont été tout d'abord réalisées avec un piston alternatif classique basé sur les principes de conservation de la masse et de l'énergie. Le modèle se compose de différents sous-systèmes comme mécanisme d'entraînement, tête de cylindre, soupapes, transferts de chaleur, etc. Ce travail servant comme base pour l'étude plus complexe du compresseur à piston à ailettes. La méthode des éléments finis (FEM) a été utilisée pour tenir compte de la géométrie locale et permettre la caractérisation thermique détaillée en 3D. Ensuite, la modélisation analytique a été étendue au piston à ailettes. Les transferts de chaleur et masse ont été comptabilisés par analogie thermoélectrique et pneumatique-électrique. De même, la modélisation FEM a été réalisée pour le piston à ailettes.

Le modèle analytique a été vérifié en pratique. Afin de réaliser une validation expérimentale, un banc d'essai a été développé pour les deux types de pistons. Les résultats expérimentaux confirment un rendement exégétique supérieur pour le piston à ailettes en raison de son rapprochement d'un comportement isotherme grâce à l'augmentation des surfaces de transfert de chaleur. Le dernier chapitre est consacré à l'étude des effets des changements des paramètres de conception sur les performances du système. Cette thèse laisse les portes ouvertes vers plus de recherche pour l'amélioration de la conception du système. L'outil de départ étant le modèle global innovant élaboré dans ce travail.

Mots-clés: compresseur à piston, piston à ailettes, le stockage d'énergie, transfert de chaleur, REM, Bond graph, l'analogie Thermo-électrique, l'analogie pneumatique-électrique.

Contents

Acknowledgements	v
Abstract	vi
Résumé	vii
List of Figures	xiii
List of Abbreviations	xix
Nomenclature	xx
Chapter 1 Introduction.....	23
1.1 Available Energy Storage Technology Assesment	23
1.2 CAES Fundamentals	24
1.3 Practical Challenges	26
1.4 Compression/Expansion Processes.....	27
1.5 Concept Of Directly Integrated Exchanger (DIE)	29
1.5.1 Multilayered annular piston-cylinder assembly.....	29
1.5.2 From the normal cylinder to the annular concept	29
1.6 Literature Survey	32
1.7 Theoretical Studies.....	33
1.7.1 Thermodynamic Models.....	33
1.7.2 Heat Transfer Models	33
1.7.3 In-cylinder fluid flow models	34
1.7.4 Valve dynamic models.....	35
1.7.5 Friction and leakage models.....	35
1.8 Attempts to approach isothermal compression/expansion.....	35
1.9 Methods used in the present research	36
1.10 Objectives of the present research.....	37
Chapter 2 Overview Of Compressed Air Energy Storage (CAES).....	39
2.1 Introduction.....	39
2.2 Principle of CAES Plant.....	39
2.3 First Law of Thermodynamics Analysis applied to CAES	40
2.3.1 Steady flow Conditions	42
2.3.2 Firt Law of Thermodynamic Efficiency.....	44

2.4	Exergy Analysis and Efficiency Applied to CAES	45
2.4.1	Air Stream Exergy	45
2.4.2	Storage Exergy in Reservoir	48
2.4.3	Exergy Efficiency of differnt parts of CAES	49
2.5	Conclusion	50
Chapter 3	Classic Piston Compressor Analytical Model.....	51
3.1	Introduction.....	51
3.2	Graphical Modelling Representation Tools.....	52
3.3	Bondgraph description	53
3.3.1	Adaptation of Bond Graph to Thermofluid Systems	55
3.4	EMR description	56
3.4.1	Adaptation of EMR to a Thermofluid Systems.....	56
3.5	Description of linear air compressor behavior	57
3.5.1	Linear driver mechanism.....	58
3.5.2	Cylinder head	59
3.5.3	Suction and discharge valves	61
3.5.4	Heat Transfer Model	63
3.5.5	Friction and Inertia Model.....	65
3.5.6	Leakage Model	68
3.5.7	Heat Exchanger Model	68
3.5.8	Reservoir Model.....	69
3.5.9	Complete Model of a Classic Compressor	69
3.6	Simulation results	71
3.6.1	Model Inputs.....	71
3.7	Multistage System	73
3.7.1	Multistage Air Compression	73
3.7.2	Optimum interstage pressure	74
3.7.3	Energy exchange in Multistage Compression	76
3.8	Conclusion	77
Chapter 4	Finned Piston Compressor Analytical Model	79
4.1	Introduction.....	79
4.2	Finned Compressor Description.....	79
4.3	Principle Of Thermoelectric Analogy	81
4.4	Adaptation Of Thermo-Electric Analogy To Cylinder-Piston Assembly	82
4.5	Development of Thermo-Electric Analogy For The Finned Piston Model.....	86
4.5.1	State space equations	90
4.6	Pneumatic- Electric Analogy	91
4.7	Developement of Pneumatic- Electric Analogy for the Finned piston Model	93

4.7.1	State space equations	94
4.8	Complete finned-piston model	94
4.9	Simulation results	97
4.9.1	Model Inputs.....	97
4.10	Inter-Fin Heat Transfer	100
4.10.1	Pneumatic losses	101
4.10.1	Conditions with thermal energy dissipation	102
4.11	Long term operation.....	104
4.12	Conclusion.....	105
Chapter 5	Finite Element Method	107
5.1	Introduction.....	107
5.2	Generalities of Finite Element Model	107
5.3	Use of COMSOL Multiphysics®	108
5.3.1	Global definitions.....	108
5.3.2	Definitions	108
5.4	Classic piston.....	109
5.4.1	Geometry.....	109
5.4.2	Moving mesh and meshes	109
5.4.3	Heat Transfer	110
5.4.4	Study	112
5.5	Finned piston	112
5.5.1	Geometry.....	112
5.5.2	Heat Transfer	114
5.6	Results.....	115
5.6.1	2D plots.....	116
5.7	Temperature distribution along the fins.....	118
5.8	Conclusions	119
Chapter 6	Experimental Method	121
6.1	Introduction.....	121
6.2	Loss characterization.....	121
6.2.1	Sliding force	121
6.2.2	Valve losses analysis	122
6.3	Driver setup description	123
6.4	Experimentation for a classic piston.....	123
6.4.1	Setup Description	123
6.5	Experimentation for Finned compressor	128
6.5.1	Setup Description	128
6.6	Comparision	133

Chapter 7	Parametric study.....	137
7.1	Introduction.....	137
7.2	Performance Parametres.....	137
7.2.1	Mass Flow of Compressed Gas Delivered.....	137
7.2.2	Work Consumed by the Compressor	137
7.2.3	Exergetic Efficiency	138
7.3	Finned compressor parametric study	138
7.3.1	Effect of clearance volume.....	138
7.3.2	Effect of velocity.....	140
7.3.3	Effect of Cylinder Wall(Fins) Temperature.....	143
7.3.4	Effect of Stroke Length to Bore Diameter (LD)	144
7.3.5	Effect of Number of Fins	146
7.3.6	Effect of gap between fins.....	146
7.4	Conclusion	148
Chapter 8	Conclusion and Future Research	151
8.1	Achieved results.....	151
8.2	Future Research.....	153
8.2.1	Liquid piston.....	153
8.2.2	Methodology	154
8.2.3	Analytic model	154
8.2.4	FEM model.....	155
	Bibliography	156
	Appendix.....	161
	I. Flow Characteristics in Concentric Annulus.....	162
I.1	Fluid Flow	162
I.2	Heat transfer.....	165
	A II. Other Efficiency Definitions.....	167
II.1	Introduction.....	167
II.2	Isothermal Efficiency	167
II.3	Volumetric Efficiency.....	168
II.3	Efficiency of delivery	170
	A III. Dynamic Valve Model	171
III.1	Pressure Dominant Mode.....	172
III.2	Mass-flux Dominant Mode.....	172
	A IV. Data sheets	176
IV.1	Swagelok Valve Data sheet	176
IV.2	SMC Valve Data sheet.....	177
IV.3	Seals datasheet.....	178

A V. Technical drawings	179
V.1 Classic Piston.....	179
V.1.1 Calculating the effective surface	179
V.2 Finned Piston.....	180
A VI. Simulink Model Representation	182
Curriculum Vitae	184

List of Figures

Figure 1.1 : Comparison of Power and Discharge Time for various energy storage devices(Courtesy of Electricity Storage Association).	24
Figure 1.2 : Comparison of efficiency and lifetime for various energy storage devices (Courtesy of Electricity Storage Association).	24
Figure 1.3 : Schematic of compressed air storage system (Courtesy of SustainX).	25
Figure 1.4 : p-V diagram of compression and expansion of different processes.....	27
Figure 1.5 : p-V diagrams of multi stage compression and expansion.	28
Figure 1.6 : p-V diagram of superposed multistage compression expansion round-trip cycle..	29
Figure 1.7 : Front surface of «Normal», « Interior-Differential » and «Exterior-Differential» pistons.	30
Figure 1.8 : Schematic representation of the Integrated Heat Exchanger Concept	31
Figure 1.9 : Three-stage finned piston compressor system circuit.....	32
Figure 2.1 : CAES general Scheme.....	40
Figure 2.2 : Compressor gas as an open thermodynamic system with work heat and mass flow interaction.	41
Figure 2.3 : Heat transfer rate in a classic and finned compressor.	41
Figure 2.4 : Delta Enthalpy, heat transfer rate and work change with Polytropic factor.....	42
Figure 2.5 : p-V diagram of a compression process while going from adiabatic to isothermal..	43
Figure 2.6 : P-V-T diagram of a compression process while changing from adiabatic (red) to polytropic (green) and finally to isothermal (blue).....	43
Figure 2.7 : T-S diagram of a compression process while going from adiabatic to isothermal..	44
Figure 2.8 : Pressure evolution in reservoir for different compression processes.....	46
Figure 2.9 : Temperature evolution in reservoir for different compression processes.....	47
Figure 2.10 : Exergetic content of reservoir during charging a tank with a specific pressure level.	47
Figure 2.11 : Exergy vs. polytropic factor.	48
Figure 2.12 : Exergetic efficiency vs. polytropic factor.	50
Figure 3.1 : Selection of bond graph couples in Thermodynamics based on Static or dynamic system.	55
Figure 3.2 : Bond graph representation of an accumulator as a multiport.	55
Figure 3.3 : Representation of a thermo-pneumatic multiport in EMR.	57
Figure 3.4 : Linear compressor schematic.	58
Figure 3.5 : Linear actuator mechanism.	58
Figure 3.6 Position and speed of piston during one cycle.....	58
Figure 3.7 : EMR of driver mechanism.	59
Figure 3.8 : Bond graph of driver mechanism.....	59
Figure 3.9 : EMR of cylinder head with inlet, outlet and heat transfer.....	61
Figure 3.10 : Bond graph of cylinder head with inlet, outlet and heat transfer.	61

Figure 3.11 : Isentropic nozzle.....	62
Figure 3.12 : Bond graph for the valve as isentropic nozzle.....	63
Figure 3.13 : EMR of Valves.....	63
Figure 3.14 : Gas temperature and heat transfer rate from gas to cylinder wall.....	64
Figure 3.15 : Thermoelectric analogy of the piston.....	65
Figure 3.16 : EMR of heat transfer process.	65
Figure 3.17 : Bond graph of heat transfer process.....	65
Figure 3.18 : Piston with piston ring. Note that the gas in the chamber applies pressure to the bottom and inside of the piston ring.....	66
Figure 3.19 : No load force and speed in classic compressor.....	67
Figure 3.20 : No load power in classic compressor.	67
Figure 3.21 : Schematic of an interstage heat exchanger.....	68
Figure 3.22 : EMR of heat exchanger.....	69
Figure 3.23 : EMR representation of Reservoir.....	69
Figure 3.24 : Bond graph representation of Reservoir.....	69
Figure 3.25 : complete system EMR.....	70
Figure 3.26 : complete system Bond Graph.....	70
Figure 3.27 : Pressure and temperature of the gas inside the cylinder.....	72
Figure 3.28 : Mass and volume of the gas inside the cylinder.....	72
Figure 3.29 : Effective work and power of the compressor.....	72
Figure 3.30 : Effect of pressure ratio and clearance on volumetric efficiency.....	73
Figure 3.31 : ideal indicator diagram for a three-stage air compressor.....	74
Figure 3.32 : Indicator diagram for three-stage compression.....	75
Figure 4.1 : Schematic representation of the Integrated Heat Exchanger Concept.....	80
Figure 4.2 : Fluid flow in a) Main Compression Chamber (MCC) and b) Inter Fins Space (IFS)....	81
Figure 4.3 : Thermal resistance network for combined series-parallel arrangement.....	82
Figure 4.4 : Thermo-electric analogy for a cylinder-piston assembly.....	85
Figure 4.5 : Bond graph representation of the developed thermo-electric analogy.....	85
Figure 4.6 : Thermal resistance variation during one cycle.....	86
Figure 4.7 : Analogy between low convection heat transfer between compressed gas and cylinder body and shortage of bus in the island (concept taken from [41]).....	86
Figure 4.8 : Classic and finned piston positions at BDC and TDC.....	87
Figure 4.9 : Gas temperature and heat transfer area from gas to cylinder wall in classic compressor.....	87
Figure 4.10 : Heat transfer area comparison during one cycle.....	88
Figure 4.11 : Equivalent electrical circuit for thermo-electric analogy.....	89
Figure 4.12 : Equivalent electrical circuit for thermoelectric analogy (entire piston).....	89
Figure 4.13 : Bond graph representation of the heat transfer in a finned compressor.....	90
Figure 4.14 : Pneumatic-electric analogy for a cylinder-piston assembly.....	92

Figure 4.15 : Equivalent electrical circuit for pneumatic-electric analogy.....	93
Figure 4.16 : Bond graph model of pneumatic part.....	93
Figure 4.17 : Bond graph model of Classic piston.....	95
Figure 4.18 : Bond graph model of finned piston.	96
Figure 4.19 : Bond graph representation of finned piston model.	96
Figure 4.20 : EMR representation of finned piston model.....	97
Figure 4.21 : Temperature evolution comparison.	99
Figure 4.22 : Pressure evolution comparison.	99
Figure 4.23 : Heat transfer rate comparison.....	99
Figure 4.24 : Effective work comparison.....	99
Figure 4.25 : Mass in the compression chamber.....	100
Figure 4.26 : Effective power comparison.	100
Figure 4.27 : Fluid flow direction in dry (finned) piston.....	101
Figure 4.28 : Pneumatic resistance with the losses of a compressible fluid.....	102
Figure 4.29 : Bond graph of energy dissipation in a resistance.....	102
Figure 4.30 : Mass flow in the inter-fin space.....	103
Figure 4.31 : Dissipated power in the inter-fin space.....	103
Figure 4.32 : Heat flow in the inter-fin space and total heat flow.	103
Figure 4.33 : Exergy efficiency degradation over time.....	104
Figure 4.34 : fins and sleeve temperature of finned and wall temperature of classic piston compressors over filling period.....	105
Figure 5.1 : Displacement and velocity of the piston in one cycle.....	108
Figure 5.2 : Geometry of a classic cylinder-piston assembly with axial symmetry (left) and zoom on inlet/outlet area (right).....	109
Figure 5.3 : Mesh of the classic piston for full expansion mid-travel and full compression respectively.	110
Figure 5.4 : Translational motion for the piston.	111
Figure 5.5 : Boundary conditions with no slip condition (left) for fixed wall and moving wall (right) respectively.....	111
Figure 5.6 : The three stages of the compressor.	112
Figure 5.7 : Geometry of finned piston with outlets and inlets.....	113
Figure 5.8 : The air can flow Inter fin space.	113
Figure 5.9 : Mesh of the finned piston for full expansion mid-travel and full compression respectively.	114
Figure 5.10 : Translational motion for the finned piston.	114
Figure 5.11 : Boundary conditions with no slip condition for fixed wall and moving wall respectively.	115
Figure 5.12 : Volume change during in one cycle.....	116
Figure 5.13 : Pressure evolution in one cycle.	116
Figure 5.14 : Temperature evolution in one cycle.....	116

Figure 5.15 : Power evolution in one cycle.	116
Figure 5.16 : Work during in one cycle.	116
Figure 5.17 : Mass change in the cylinder head in one cycle.....	116
Figure 5.18 : Temperature gradient – mid of last expansion travel.	117
Figure 5.19 : Velocity of air movement in the chambers and inter fin space.	117
Figure 5.20 : fins and sleeve temperature of finned piston compressor over filling period.....	118
Figure 6.1 : Check valve components.....	122
Figure 6.2 : Manufacturer data for determining mass flow from inlet pressure and pressure drop.	122
Figure 6.3 : Position and speed of piston during one cycle.	123
Figure 6.4 : Experimental setup.....	124
Figure 6.5 : Setup circuit schematic in filling mode.	124
Figure 6.6 : Friction force and speed in classic compressor (No Load mode).....	125
Figure 6.7 : Friction power in classic compressor (No Load mode).....	125
Figure 6.8 : Pressure evolution in reservoir for filling load mode in classic compressor.....	125
Figure 6.9 : Experimental and analytical power in load mode for classic compressor.	126
Figure 6.10 : Experimental and analytical Force and velocity in load mode (50 st cycle) in classic compressor.....	126
Figure 6.11 Experimental and analytical power in load mode (50 st cycle) in classic compressor.	127
Figure 6.12 : Effective, friction and total work and reservoir exergy content after cool down for classic compressor.....	127
Figure 6.13 : Setup schematic circuit in filling mode.	128
Figure 6.14 : Fix and mobile part of the finned piston cylinder.	128
Figure 6.15 : Finned piston experimental setup	129
Figure 6.16 : Experimental and analytical (a) Force and velocity (b) power in no-load mode in finned piston compressor.	129
Figure 6.17 : Experimental and analytical pressure increase in finned piston compressor.....	130
Figure 6.18 : Experimental and analytical power raise in finned piston compressor.....	130
Figure 6.19 : Experimental and analytical force and velocity in load mode (50 th cycle).....	131
Figure 6.20 : Experimental and analytical power in load mode (50 th cycle).	131
Figure 6.21 : Experimental and analytical Force and velocity in load mode (100 th cycle).....	132
Figure 6.22 : Experimental and analytical power in load mode (100 th cycle).	132
Figure 6.23 : Effective, friction and total work and reservoir exergy content after cool down for finned compressor.....	133
Figure 6.24 : Measured and calculated temperature for finned compressor sleeve.	133
Figure 6.25 : Pressure evolution in during filling the reservoir up to 5.8 Bar and after cool-down.	134
Figure 6.26 Temperature evolution for classic piston compressor during filling the reservoir.	134
Figure 6.27 Temperature evolution for finned piston compressor during filling the reservoir.	135
Figure 7.1 : Input and output variables and performance parameters of the system.	138

Figure 7.2 : Variation in volumetric, isothermal and exergetic efficiency.	140
Figure 7.3 : Variation in consumed energy, discharged mass and consumed energy per mass unit.	140
Figure 7.4 : Linear velocity.	140
Figure 7.5 : Reynolds number.	140
Figure 7.6 : Heat transfer rate.	141
Figure 7.7 : Total heat transfer.	141
Figure 7.8 : Gas temperature.	141
Figure 7.9 : Total work.	141
Figure 7.10 : Variation in consumed energy, discharged mass and consumed energy per mass unit.	142
Figure 7.11 : Variation in Heat transfer and discharged gas temperature.	142
Figure 7.12 : Simulated compared against experimental input work for finned piston compressor for filling mode up to 5.8 Bars.	143
Figure 7.13 : Effective Work change with wall(fins) Temperature.	143
Figure 7.14 : Efficiency change with wall(fins) Temperature.	143
Figure 7.15 : Discharged mass change with wall(fins) Temperature.	144
Figure 7.16 : Work Consumed per delivered mass change with wall(fins) Temperature.	144
Figure 7.17 : Finned piston geometry for different length to diameter ratio(*=Base case).	144
Figure 7.18 : Linear velocity.	145
Figure 7.19 : Piston position.	145
Figure 7.20 : Heat transfer rate.	145
Figure 7.21 : Total heat transfer.	145
Figure 7.22 : Gas temperature.	145
Figure 7.23 : Discharged mass.	145
Figure 7.24 : Work change with L/D ratio.	146
Figure 7.25 : Total exergetic efficiency(including friction) change with L/D ratio.	146
Figure 7.26 : Efficiency change with number of fins.	146
Figure 7.27 : Influence of g_{IFS} on dead volume.	147
Figure 7.28 : Influence of g_{IFS} on discharged mass and η_{vol}	147
Figure 7.29 : Influence of g_{IFS} and Δp on compression work and pneumatic dissipation in IFS . (Initial $\Delta p=1$ kPa for current design).	148
Figure 7.30 : Influence of g_{IFS} and Δp on η_{ex} (Initial $\Delta p=1$ kPa for current design).	148
Figure 8.1 : Placement of Finned piston in the roadmap (Results for FLP mode with PR=5.8).	152
Figure 8.2 : Liquid piston geometry (Left) and Dry (Finned) piston geometry (Right).	153
Figure 8.3 : Heat transfer mechanisms and assumed temperature profile across the bore wall.	155
Figure 8.4 : Heat transfer mechanisms and assumed temperature profile across the bore wall.	155

List of Abbreviations

ACD After Cool Down

BDC Bottom Dead Center

CAES Compressed Air Energy Storage

CV Control Volume

EMR Energetic Macroscopic Representation

FLP Fixed Pressure Level

FM Filling Mode

FEM Finite Element Method

IFS Inter Fin Space

LM Load Mode

MCC Main Compression Chambers

NLM No Load Mode

PR Pressure Ratio

RT Round Trip

RCC Radial Collecting Channels

TDC Top Dead Center

Nomenclature

Main Symbols

A	Area	(m^2)
C	Capacitance	(F)
D	Diameter	(m)
E	Enthalpy	(J)
\dot{E}	Enthalpy flow	(J/s)
F	Force	(N)
H	Heat transfer coefficient	(W /m^2K)
I	Electric current	(A)
Nu	Nusselt number	$(-)$
Pr	Prandtl number	$(-)$
Q	Heat Transfer	(J)
\dot{Q}	Heat Transfer rate	(J/s)
R	Resistance	(Ω)
Ra	Rayleigh number	$(-)$
Re	Reynolds number	$(-)$
R_g	Gas constant	$(J/kg.K)$
T	Temperature	(K)
U	Internal Energy	(J)
V	Volume	(m^3)
\dot{V}	Volume change	(m^3/s)
V_o	Electric potential	(V)
W	Work	(J)
\dot{W}	Power	(J/s)
X	Exergy	(J)

c_p	Specific heat at constant pressure	$(J/kg.K)$
c_v	Specific heat at constant volume	$(J/kg.K)$
e	effort	$(-)$
f	flow	$(-)$
g	gap	(m)
h	Specific enthalpy	(J/kg)
k	Heat conductivity	$(W/m.K)$
l	Length	(m)
m	Mass	(kg)
\dot{m}	Mass flow	(kg/s)
n	Polytropic exponent	$(-)$
p	Pressure	(Pa)
ρ	Density	(kg/m^3)
s	Specific entropy	$(J/kg.K)$
t	Time	(s)
w	work per unit of mass	(J/kg)
x	Position	(m)
\dot{x}	Speed	(m/s)
α	Load fraction	$(-)$
μ	Viscosity	$(kg/m.s)$
η	Efficiency	$(-)$
ϕ	Non-flow exergy	(J)
ψ	Flow exergy	(J)
ω	Rotational speed	(Hz)

Subscript

Atm	Atmosphere
Amb	Ambient
Res	Reservoir
a	air

<i>amb</i>	ambient
<i>b</i>	body of metal
<i>c</i>	cylinder
<i>cond</i>	conduction
<i>conv</i>	convection
<i>d</i>	downstream
<i>disch</i>	discharged
<i>e</i>	exit
<i>eff</i>	effective
<i>frc</i>	friction
<i>h</i>	hydraulic
<i>i</i>	inlet
<i>iso</i>	isothermal
<i>p</i>	piston
<i>r</i>	ratio
<i>s</i>	suction
<i>t</i>	total
<i>u</i>	upstream
<i>v</i>	volumetric
<i>va</i>	valve
<i>w</i>	wall

Chapter 1 Introduction

This chapter introduces the global context of energy storage and the motivation of using the finned piston compressor technology as the preferred option in the context of Compressed Air Energy Storage (CAES).

The global energy demand is rising continuously in line with the fast development in countries like India and China. In parallel, limited production and predicted shortage in fossil fuel resources induce increased prices on the energy market. In addition, greenhouse gas emissions related to the increasing consumption of these hydrocarbon fuels is the main reason for the present global warming and environmental instabilities. All the experts agree that two important energetic objectives must be achieved to mitigate these threats:

- More efficient and environmentally harmless energy conversion, distribution and use: Beside other technological breakthroughs, appropriate energy storage solutions are needed to achieve this objective. Storage is necessary both on the provider and consumer sides for supply-demand balancing, peak shaving, load leveling, power quality improvement, power system stability and control, etc.
- Shift towards alternative energy sources, mainly renewable: The inherent problem with some renewable sources such as wind and sunshine is their intermittent nature that makes their availability uncertain. Energy storage solutions are again necessary to circumvent this intermittency by storing these clean energies when they are available for use on demand.

Currently, there is a limited storage in the energy systems (around 5% of total installed capacity) almost exclusively from pumped hydro-storage, mainly in mountainous area. In other geographic areas it is of great interest to develop a feasible, efficient and environmentally friendly technology for energy storage. In this context, system with low aging or long life cycle must be developed.

1.1 Available Energy Storage Technology Assessment

Any discussion of a strategic vision for energy storage must begin with an assessment of the diverse technologies that comprise the sector. To assess the potential for future deployment of energy storage, policy makers and the public need an understanding of the current state of these technologies and the likely technological advancements that may occur in the near term.

Figure 1.1 compares the power and discharge time of various energy storage devices [1]. One can identify from this figure that the two technologies having both high rated power and high discharge time are pumped hydro and CAES. **Figure 1.2** compares the same storage technologies based on their efficiency and lifetime [2]. Here also the batteries place mostly on the lower left corner and do not look promising from this aspect. From these two figures one can conclude that apart from pumped hydro,

(that is available in certain geographical areas), the most promising technology for energy storage is CAES.

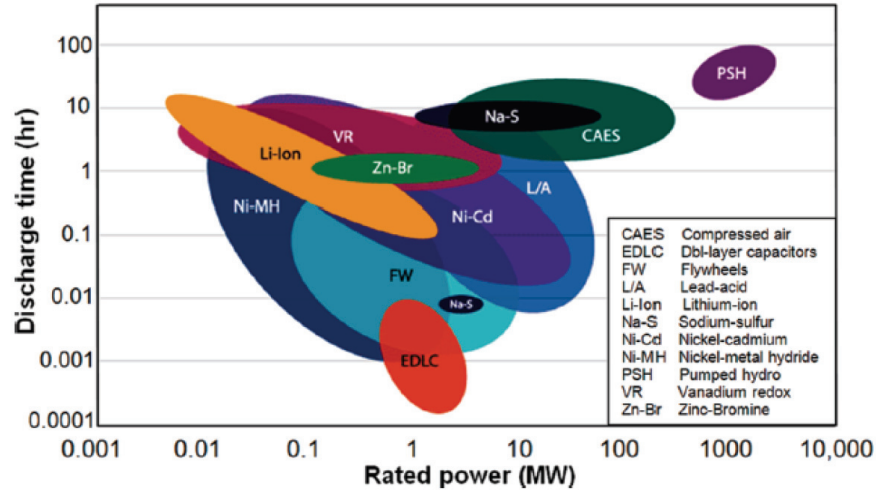


Figure 1.1 : Comparison of Power and Discharge Time for various energy storage devices (Courtesy of Electricity Storage Association).

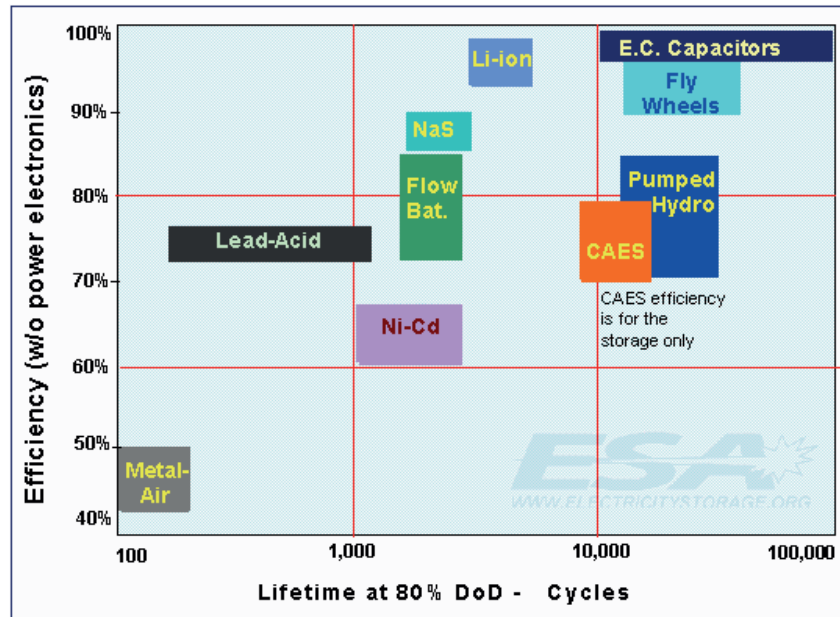


Figure 1.2 : Comparison of efficiency and lifetime for various energy storage devices (Courtesy of Electricity Storage Association).

1.2 CAES Fundamentals

CAES plants are mainly equivalent to pumped-hydro power plants in terms of their applications, output and storage capacity. But, instead of pumping water from a lower to an upper pond during periods of excess power, in a CAES plant, ambient air is compressed and stored under pressure in a reservoir or underground cavern [3]. When electricity is required, the pressurized air is heated and expanded in an expansion turbine driving a generator for power production. CAES is the closest

alternative to pumped-hydro power with high reliability, economic feasibility and low environmental impact [4].

Traditional CAES uses turbo machinery to compress air to around 70 bar before storage. In the absence of intercooling the air would heat up to around 900K, making it impossible (or prohibitively expensive) to process and store the gas [5]. In Advanced-Adiabatic CAES the heat of compression is stored separately and fed back into the compressed gas upon expansion, thereby removing the need to reheat with natural gas [6].

Isothermal CAES is an emerging technology, which attempts to overcome some of the limitations of traditional (diabatic or adiabatic) CAES. Rather than employing numerous stages to compress, cool, heat and expand the air, isothermal CAES technologies attempt to achieve true isothermal compression and expansion in situ, yielding improved round-trip efficiency and lower capital costs. In principle it also negates the need to store the heat of compression by some secondary means [7].

CAES is simply composed of a compression cycle, which delivers the gas to high-pressure storage, and an expansion cycle that expands the compressed air to extract its energy. The air compression system is driven by a hydraulic pump and cylinder, which is fed by an electric motor. On the other side the expander runs a hydraulic motor that is connected to an electric generator (Figure 1.3). Such typical systems are also described in [8] [9] and [10].

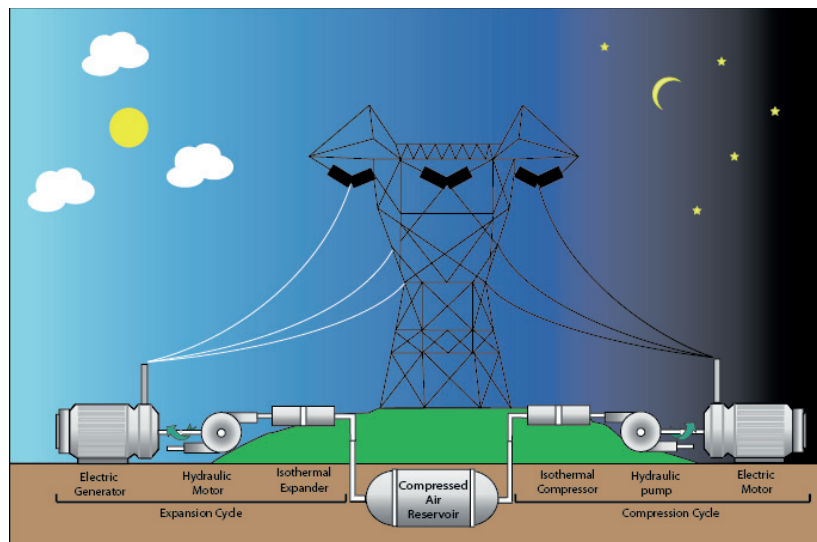


Figure 1.3 : Schematic of compressed air storage system (Courtesy of SustainX).

This system uses an efficient hydraulic drivetrain to convert electrical energy into potential energy stored as compressed air. The use of hydraulics, among other advantages, allows to precisely control gas expansion and compression, thus maximizing thermal efficiency, allowing for high-efficiency conversion of mechanical to electrical energy. The system works similarly in reverse mode to convert the potential energy stored in the compressed air back into electrical energy. The proposed concept belongs to a family of storage devices based on the compression and expansion of air, but where only electrical energy is used as changing resource and also only electric energy is produced. Such systems have their own advantages in the sense of sustainable development and emission free generation as alternatives to other CAES systems using combustion machines as described in [11] [12] and [13].

Compressed air energy storage is also intended to replace electrochemical batteries and to serve as low aging systems. The aspect of sustainability comprises also the general theme of Life Cycle Analysis (LCA), where wasted material, material resources and recycling are addressed.

1.3 Practical Challenges

Isothermal CAES is technologically challenging since it requires heat to be removed continuously from the air during the compression cycle and added continuously during expansion to maintain an isothermal process. Heat transfer occurs at a rate proportional to the temperature gradient multiplied by surface area of contact; therefore, to transfer heat at a high rate with a minimal temperature difference one requires a very large surface area of contact.

Although there are currently no commercial Isothermal CAES implementations, several possible solutions have been proposed based upon reciprocating machinery. One method is using foam as a heat exchange interface [14]. The other method is to spray fine droplets of water inside the piston during compression. The high surface area of the water droplets coupled with the high heat capacity of water relative to air means that the temperature stays approximately constant within the piston – the water is removed and either discarded or stored and the cycle repeats. A similar process occurs during expansion [15].

The technology compresses and expands gas near-isothermally over a wide pressure range, namely from atmospheric pressure (1 bar) to a maximum of about 200 bar. This large operating pressure range, along with the isothermal gas expansion (allowing for recovery of heat not achieved with adiabatic expansion), achieves a 7X reduction in storage cost as compared to classical CAES in vessels. The companies developing Isothermal CAES quote a potential round-trip efficiency of 70-80% [16].

In the framework of the European Union research project of SOLUTION, compressed air energy storage has been considered as the most promising solution for the cost effective small/medium electricity storage applications. As the first approach, a liquid piston compressor-expander with the performance of nearly 65% efficiency is selected based on the experiences with the pilot application at EPFL further innovative technological developments are foreseen within a dedicated work package.

Based on the first developments and investigations on compressed air energy storage at LEI, post-development has been defined and are currently the objective of investigation. Especially in the domain of increasing the energy capacity of small CAES (in vessels) the storage pressure should be increased.

Following the same arguments, research activities on compressed air energy storage have been initiated at EPFL's LEI with the PhD thesis realized by Sylvain Lemofouet [17]. In this work different solutions have been evaluated from air volumetric machines with very poor efficiency to the hydro-pneumatic concept where a so-called liquid piston is achieving the air compression and expansion function, driven by a hydrostatic volumetric actuator coupled to an electric machine.

This new contribution to the domain of compressed air energy storage is dedicated to the compression/expansion machine, and proposes the original concept of a "finned piston compression expansion system". With this concept the integrated heat transfer element is provided by an increased convection surface.

1.4 Compression/Expansion Processes

First let us investigate different possible processes from the point of view of work spent during compression and extracted during the expansion. **Figure 1.4** demonstrates such a comparison on a p-V diagram. The adiabatic process (red) is the compression/Expansion with no heat transfer to/ from surroundings, polytropic (green) involves some heat transfer and Isothermal involves the maximum heat transfer possible. As can be seen, adiabatic process consumes the highest and produces the lowest amount of work. In between lies the polytropic process and finally, isothermal compression consumes the lowest and produces the highest amount of work. This shows that the most promising process for CAES application is the isothermal one.

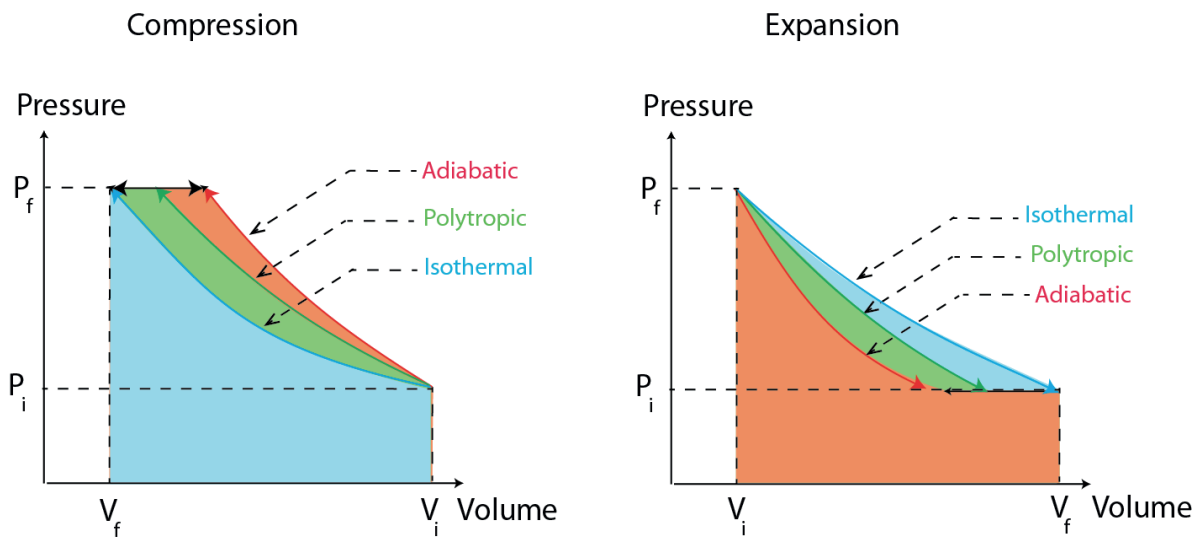


Figure 1.4 : p-V diagram of compression and expansion of different processes.

However, current compressor and expander provide poor heat transfer between mechanical boundaries and gas. The heat transfer is poor in these machines due to the high-speed operation and practical geometry requirements that dictate a poor surface area to volume ratio.

As mentioned, when the gas is compressed rapidly with minimal heat transfer, significant energy is converted into increasing the gas temperature. As the compressed gas cools in the storage reservoir the energy content of gas decreases. The same argument is true during the expansion: in rapid expansion gas cools down and in absence of efficient heat transfer to the gas, only a part of its energy can be extracted. These shortcomings reduce the round trip efficiency of the cycle.

As a result, current CAES systems suffer from two primary limitations:

1. Reduced round-trip efficiency associated with the cooling/reheating process, and
2. CO₂ emissions produced by the reheating process.

As mentioned, one of the most promising solutions to solve the above mentioned problem is Isothermal CAES.

Hence, the main goal of the new finned piston is to solve the problem of non-isothermal behavior of the compression system. In this regard two methods were introduced:

- Inter-stage heat exchangers
- Directly integrated exchanger

The first approach is rather classical and conventional, but it is not enough to reach the level of isothermal efficiency that is needed. Thus, a second approach is proposed, namely directly integrated exchanger, to reach higher isothermal efficiency. Controlling the pressure-volume (p-V) curve during compression and expansion is the key to efficient CAES. Roughly speaking, the closer the p-V curve resembles an isotherm, the less energy is wasted in the process.

In **Figure 1.5** (a) to (d), the compression process is represented and in **Figure 1.5** (e) to (h) the corresponding expansion is also illustrated. Four different cases are illustrated namely first the ideal isothermal process (curves (a) and (e)), and second the one stage polytropic process (curves (b) and (f)), where the shaded surfaces represent the spent recovered energy respectively. The compression and expansion surfaces correspond to be done or to be extracted work from the system for a state change from point 1 to 2 or in the inverse sequence. The third case (curves (c) and (g)), represents a 3 stage compression expansion machine with interstage heat exchangers. Finally, the fourth case represented in **Figure 1.5** ((d) and (h)) corresponds to a compression/expansion machine with increased thermodynamic performance due to the use of directly integrated exchangers (DIE).

To get a better illustration of the benefits provided by the directly integrated versus the benefits of the inter-stage exchangers the curves of **Figure 1.5** is superposed in **Figure 1.6**. By the classical approach of a multistage compression machine, the process gets close to isothermal line, as shown by large arrows. Furthermore, with the help of the second approach, using DIE, it is possible to go further close to isothermal line, which is demonstrated using small arrows. This explains the concept of the finned piston system design.

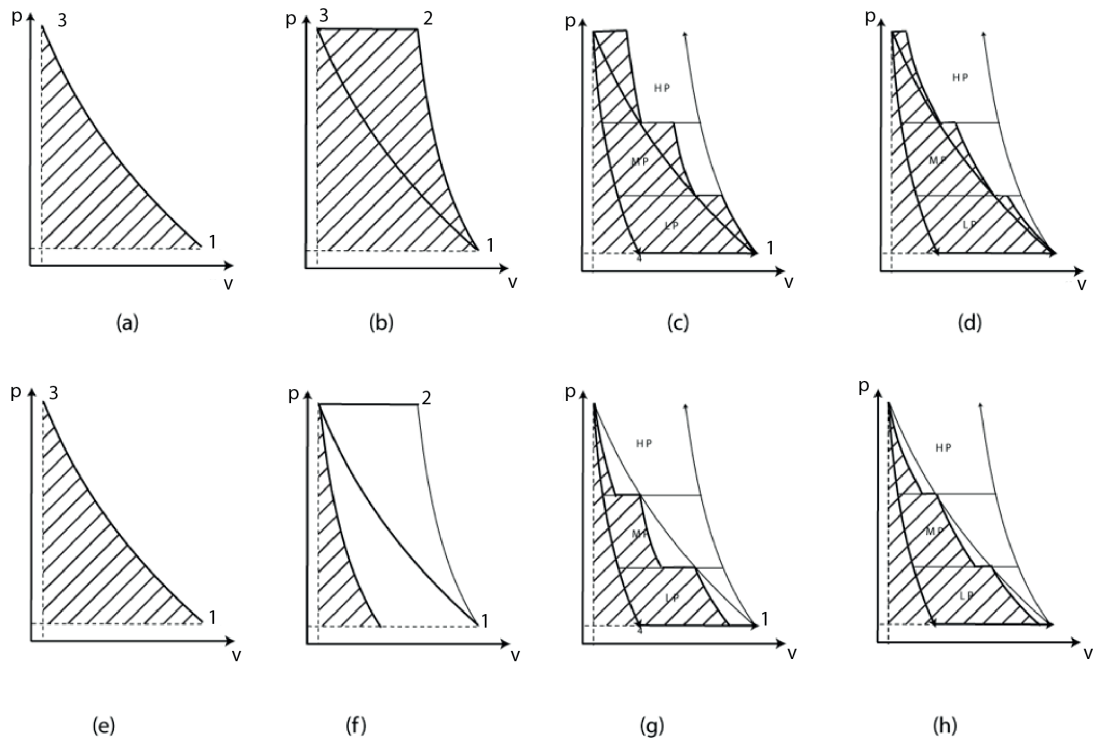


Figure 1.5 : p-V diagrams of multi stage compression and expansion.

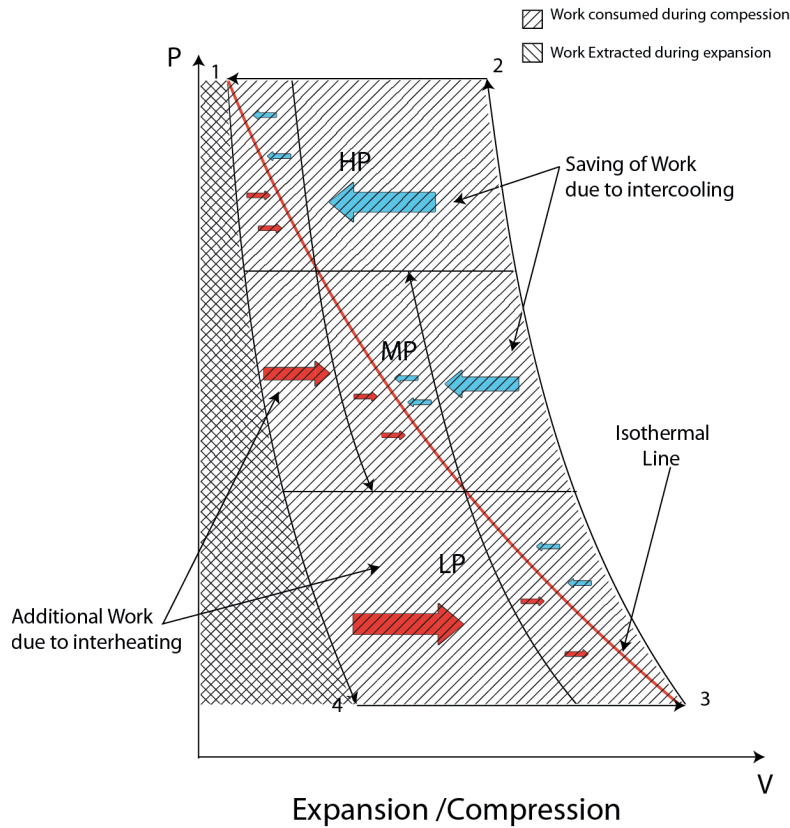


Figure 1.6 : p-V diagram of superposed multistage compression expansion round-trip cycle.

1.5 Concept Of Directly Integrated Exchanger (DIE)

1.5.1 Multilayered annular piston-cylinder assembly

As previously mentioned, in order to increase the energetic performances of a compression/expansion chamber, the heat exchange between the active volume of the gas inside of the chamber and the surrounding should be increased. In addition to the principle of the interstage coolers, the trial here is to reduce the mechanical work during the compression / expansion process. This better heat transfer should allow « moving » the PV curve of the polytropic compression/expansion in the direction of the curve of the isothermal behavior. For this purpose, the heat exchange surface of the cylinder is increased.

1.5.2 From the normal cylinder to the annular concept

The representation of **Figure 1.7** (a) to (l) show the active surface of one piston, realized in three different executions. **Figure 1.7** (a) to (d) show the active surface of a normal piston that corresponds to a simple circular surface. The piston surface is drawn for a situation where the pressure is increased, namely from 10 bar to successively 50 bar, 150 bar and finally 250 bar. This force-active surfaces, are calculated so as the forces developed by the pistons keep constant, independently from the pressure level. In this example, the exterior diameter for 10 bars is chosen equal to 5.5 cm. For the calculation of the active volume and for the maximum heat exchange surface, a stroke-length of 5.5 cm is also defined.

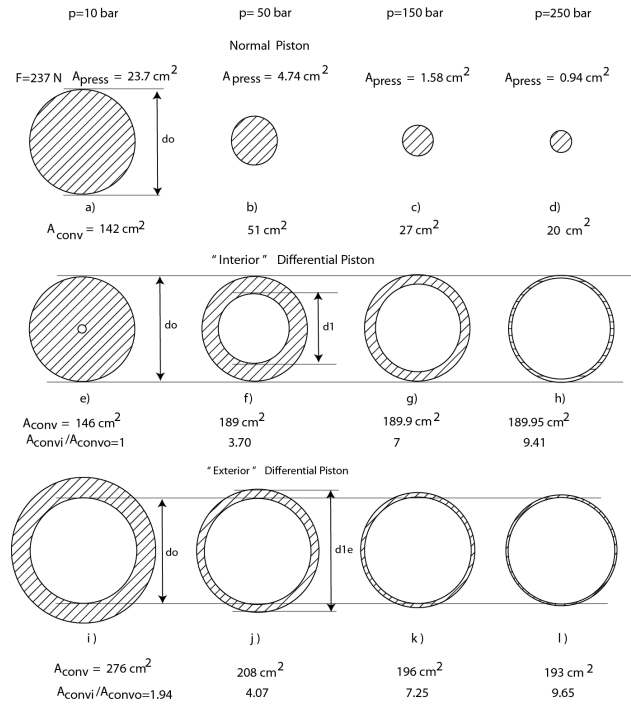


Figure 1.7 : Front surface of «Normal», « Interior-Differential » and «Exterior-Differential» pistons.

In the first column, the force-active surfaces are chosen in order to get the forces developed by all pistons are equal for all pressure levels. The force-active surface, which is indicated by A_{press} , varies from 23.7 cm^2 for 10 bar to 0.94 cm^2 for 250 bar pressure level.

For such cylinders, the heat exchange surfaces are then calculated. For the normal cylinder, the heat exchange surface is equal to the external surface of the cylinder. These values are noted A_{Conv0} . It is evident that for a piston suited for a higher pressure its diameter is reduced. Then the heat exchange surface is evaluated, under the assumption that the stroke of all pistons is identical. This leads to the fact that the mechanical works produced by different pistons of a multistage compression machine are also identical. In the figure, the heat exchange surface of the normal piston varies from 142 cm^2 for a 10 bar piston to 20 cm^2 for a 250 bar one.

Figure 1.7 (e) to (h) show a different concept, called here the « Interior Differential » Annular Concept. In this case, a differential piston is considered, that means that its active surface corresponds to an annular surface. The « Interior Differential Piston» (IDP) concept is based on the fact that the external diameter is identical to the diameter of a normal piston, and that an internal non-compressible cylindrical piece is used as a piston. The reduction of the force-active surface for an increased operating pressure is obtained by increasing the interior diameter of the non-compressible piece.

In the middle part of the **Figure 1.7 (e) to (h)**, the piston front-sides are represented for the interior differential pistons. In this case, the interior diameter varies from nearly zero for the lower pressure case (10 bar) to a diameter near to the exterior diameter for the high pressure storage (250 bar). The force-active surface is equal to the value of the corresponding normal piston for all indicated pressure levels. The interesting results in these cases are that the heat exchange surface A_{Conv1} is increased when the force active surface A_{press} is decreased. The values indicated in the figure goes from 146 cm^2 for a 10 bar piston to 189.95 cm^2 for the 250 bar piston.

It has to be noted that in the calculation of the interior diameter, the outer piston diameter is kept constant, and that the force-active surface is « inside » of the external (primitive) diameter. The possibility exists also to design a so called « Exterior Differential Piston » (EDP), by placing the force-active surface « outside » the primitive diameter. Four different cases of this design are represented in **Figure 1.7** (i) to (l). The first case considers a piston designed for the same case as in **Figure 1.7** (a). The same value of force is developed by the front-side of the piston. The same procedure is followed by the other pressure levels.

Figure 1.8 (a) shows the variation of the diameter for the normal piston, the variation of the interior piece for the IDP and the diameter of the outer cylinder for the EDP in dependency of gas pressure. The force is kept constant independently of the pressure. **Figure 1.8** (b) shows the heat exchange surfaces for the normal, interior differential and exterior differential pistons respectively. A comparison between these pistons shows that for the same force developed by increasing the pressure level, differential pistons can achieve around 9 times more heat exchange surface comparing to normal pistons.

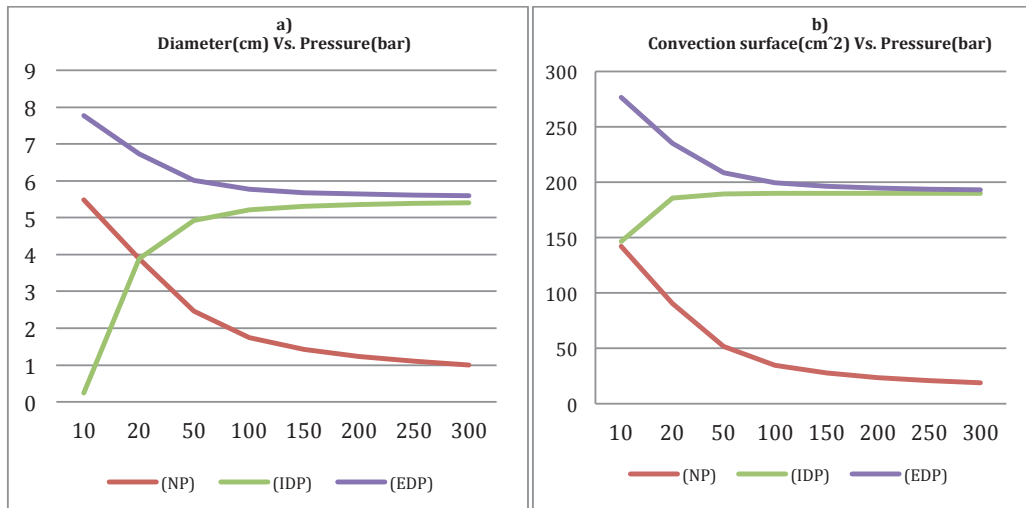


Figure 1.8 : Schematic representation of the Integrated Heat Exchanger Concept.

The details of the whole system including cooling system have been demonstrated in **Figure 1.9**. As it is shown air enters the LP, MP and HP stages respectively and stored in a compressed air reservoir. The hot air is cooled down using cooling water, which gets cooled down itself in turn, using an air cooling fan. Each stage of double-acting compressor is driven by a hydraulic cylinder fed by an electrically driven motor-pump system. low speed operation is essential in the compression process because the slower a compressor, the longer will be of course the time available for heat transfer per cycle and hence its impact on the compression cycle.

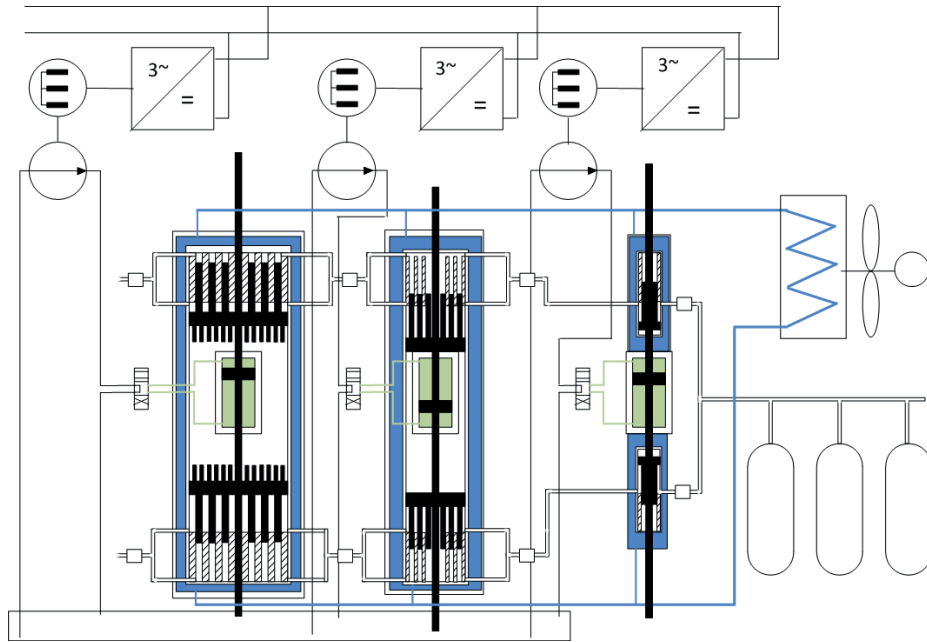


Figure 1.9 : Three-stage finned piston compressor system circuit.

1.6 Literature Survey

The effective work in this thesis will be the modeling and simulation of the introduced finned piston (which comprises several interconnecting annular compression chambers) and thermal characterization of such a compressor. As a step-by-step approach first the model for a classic compressor should be developed. This model will have a dual application in this thesis:

- It serves as the effective model of a classic piston compressor that is intended to be compared with the finned piston compressor performance
- It serves as a building block for developing the model of the more complicated finned piston.

Hence, a literature survey will be done on the models of the reciprocating compressors.

In general, research in the field of compressor technology has been led by Ray Harrick lab in Purdue University and is summarized in [18] and the conferences organized by this center comprise almost half of the articles published in this area.

The energetic performance of industrial product is described in [19], [20] and [21]. Compression process and performance analysis in high pressure machines has been documented more recently is reported as academic contributions by Wu [22]. Also recently, Instantaneous unsteady heat transfer has been evaluated in rapid compression expansion machines by Chen [23]. Isothermal compression and expansion dedicated to compressed air energy storage is studied by Lemofouet [18] and concerns the principal of liquid piston. More recently volumetric machines combined with hydraulic cylinders are proposed in the patent application by Bollinger [24].

In the current thesis two methods have been used for modeling the compressor: namely global and Finite Element (multidimensional) Models.

1.7 Theoretical Studies

Many mathematical models have been developed to describe the heat transfer, fluid flow and valve dynamics of reciprocating machinery. The works done in the area of modeling and simulation of compressors and expanders can be categorized in five main areas:

- 1) Thermodynamic models
- 2) Heat transfer models
- 3) In-cylinder fluid flow models
- 4) Valve dynamics models
- 5) Friction and leakage models

These areas will be discussed briefly.

1.7.1 Thermodynamic Models

Modeling the thermodynamic behavior of a compressor in an appropriate manner could solve most of the problems associated with compressor modeling. Various modeling methods have been developed for reciprocating compressors thermodynamic analysis. These methods can be roughly classified in global models and differential models where the variables depend on time (or crank angle).

Generally, the global models are simple and empirical while the second group sophisticated and time dependent. A representative of the first group is Cavallini [25], who developed a global model for analyzing thermal behavior of hermetic reciprocating compressors. Similar type of work carried out by Stouffs [26], who presented a more comprehensive global model for the thermodynamic analysis of reciprocating compressors. As an example of the second group, Si Yung Sun [27] developed a new method of computing thermodynamic behavior and simulated all the working processes for instantaneous values of thermodynamic parameters such as pressure, temperature, mass and enthalpy.

1.7.2 Heat Transfer Models

In the reciprocating piston compressors literature there exist many works that have investigated the heat transfer. Adair [28] is one of the pioneers of such investigations, which has introduced one of the most well known relations in this regard. Generally, as Rao [29] indicates heat transfer in a compressor or expander is quite complex because of the varying flow regimes within the cylinder and varying convection coefficient.

Also, Annand [30] and Kornhauser [31] point out that the other complexity is that heat transfer can be out of phase with the temperature difference between the bulk gas and the wall in a compressor and expander. The main reason that the bulk gas temperature does not closely follow the wall temperature is that the surface area to volume ratio in reciprocating piston systems is generally quite low.

Early correlations on cylinder heat transfer have been developed for internal combustion engines and formulate the heat transfer coefficient as a function of gas properties like pressure, temperature and volume or Reynolds number. Representative of this type of works are Nusselt [32], Eichelberg [33] and Woschni [34].

These correlations include constants that have to be determined experimentally and are, therefore, empirical or semi empirical.

More recently, dimensionless heat transfer models were adopted to develop the functional relationship governing the gas-side heat transfer coefficient. The basis of these models is that the following relationship between the Nusselt, Reynolds and Prandtl numbers, may be used:

$$Nu = a(Re)^b(Pr)^c \quad (1:1)$$

The representative of this type of modeling is work done by Wu [22] and Chen [23].

The Heat transfer models described so far are similar to the form of turbulent heat transfer for internal flows, however they can be employed for laminar flows as well [34]. Also for laminar flow regime as Kim and Groll [35] suggested, the heat transfer coefficient of Annand [30] is multiplied by a factor of three for a better prediction of the heat transfer rate as Todescat [36] recommended.

Regarding the special geometry at hand in this study, which is a series of circular annuli a research has been performed by Chung et al. in two parts, namely, fluid flow [37] and Heat transfer [38]. Also similar research for the same geometry but a laminar regime can be found in the works of Shah and London [39], which is the main reference, used in this thesis.

In heat transfer, it is widely known that many textbooks [40] and [41] incorporate the electric circuit analogy. Historically, this analogy comes from the experimental works of Paschakis [42,43]. Regarding the cylindrical geometry [43] have concluded that the “Finite Difference” or “equal geometrical size of lumps” is the most accurate method.

Educational publications [44] have used a similar approach but with emphasize on non-linear models for thermal conductivity and specific heat based on their dependency on temperature. More recently, [45] have proposed an electrical software (SPICE) to model the multidimensional transient heat transfer.

In a similar approach with application to compressor technology, Chen et al. [46] have used a “lumped capacitance method” to model the heat transfer in scroll compressor, considering a network of resistance and capacitance between different components of the compressor.

As another important work in this area, Faulkner has calculated the instantaneous spatially averaged heat transfer using the T-s diagram [47]. He concludes that the shape of the gas temperature perpendicular to the wall can be inferred from T-s diagram and is non-monotonic and changing over a cycle.

1.7.3 In-cylinder fluid flow models

Prediction of fluid flow in a reciprocating compressor cylinder is of great importance to predict local velocities and effects like swirl and turbulences.

Fluid flow in reciprocating compressors is a challenging fluid dynamics problem to model because the flow is unsteady, cyclic and non-stationary both spatially and temporally. Most of the works in this area are related to combustion engines that were adapted to reciprocating compressors.

A representative of numerical works in this area is Chiu [48] who has developed a numerical solution to predict axisymmetric two-dimensional in-cylinder flows for compressors. Some mathematicians also developed analytical solutions for piston strokes flow in two dimensional [49] and infinite channels [50].

1.7.4 Valve dynamic models

The pioneer in modeling the compressor valve and its design has been Soedel [20] with focus on reed valves. Pollack [51] has continued his work extending the analysis to spring-backed valves. Recently CFD has helped a lot in modeling valve dynamics by Song [52] and Chabane [53].

As an academic contribution Habing [54] has obtained semi-empirical coefficient for valve model followed by a CFD study. As another example Aigner [55] presented a numerical model to calculate the valve dynamics.

Finally, Kim and Groll [35] introduced a realistic and easy to use model dividing the valve operation in pressure and mass-flux dominant mode.

1.7.5 Friction and leakage models

The major source of friction in a kinematic reciprocating piston is the sliding friction of the piston seals [56]. Also the major source of the leakage is the leakage past the piston [35]. Hence decreasing the leakage gap can reduce the leakage while may increase the friction.

Modeling leakage in positive displacement machines has been seen in the works of Bell [57] and Fan [58]. Friction in reciprocating compressors is studied for lubricated seals by Dennis [59] and non-lubricated (dry) friction by Ren [60]. Also, friction in reciprocating compressors with Teflon rings is studied by Lewis [61].

As a recent trend in compressor technology, the comprehensive compressor analysis has been followed by researchers integrating all the sub-domains in one comprehensive model. Representatives of this approach are Bradshaw [62] Mathison [63], Chen [64, 46] and Kim [35, 65]. These models are based on mass and energy conservation and solve the compression process by integrating these equations. The process starts by geometric modeling which defines the change of compression chamber as a function of time or crank angle based on the type of the compressor. Then the modeling is preceded with mass flow model that includes valve modeling as a sub-model of mass flow model. Next heat transfer is modeled and finally friction and mechanical losses are taken into account. A numerical method is used to solve all these sub-models instantaneously.

1.8 Attempts to approach isothermal compression/expansion

There have been efforts to approach isothermal conditions using different techniques. One approach is to use multi-stage processes with intercooling. However, the additional required equipments is relatively expensive and increase the size of the system considering the number of cylinders, valves and heat exchangers, which are required in multi-stage units. Furthermore, external heat exchangers introduce additional pressure drop and thermal difference.

These problems have motivated the researchers to develop compressors that perform the heat exchange in the working chamber using liquid in compression or expansion process. These machines try to benefit from water as an external agent to absorb the heat of compression.

As an example of these kinds of machines, Coney [66] developed a novel compressor using water injection. He claimed to reach quasi-isothermal compression benefiting from of increasing the heat transfer surface area of water droplets by spraying it through nozzles as well as the high density and heat capacity of liquid water.

Another example of the second category is liquid piston. As Van de Ven [67] describes, in this method liquid column is utilized to directly compress the gas and is used as a medium to carry heat into an out of compression chamber. One of the industrial realized examples of liquid piston is the work by Lemoufouet and Rufer [8]. In their system, the liquid piston is controlled with a valve by switching the inlet and outlet of the hydraulic valve between two chambers. In this arrangement, one liquid piston is emptying while the other is filling. However, liquid piston has its own drawbacks: Firstly, in high pressures air can be solved in liquid and possibly causing cavitation in low-pressure areas of the system. Second, the liquid can leave the gas chamber when discharging the gas through valves. Besides, another drawback is the complexity of the system and additional equipments needed for water spray and separation of water and air at downstream.

The limitation mentioned has encouraged us to develop a compressor/expander machine that produce isothermal conditions by performing the heat exchange in the working chamber using only a dry mechanism (which works only with pure air and water is not involved). Of course as mentioned the operation must be at low speed. The slower the compressor is, the longer will be the time available for heat transfer per cycle and hence the more isothermal the process will be. This led to the idea of finned (dry) piston compressor.

1.9 Methods used in the present research

In this research 3 methods are used to evaluate and characterize the performance of classic and finned piston:

- Global Thermodynamic model.
- Multidimensional model (Finite Element Method).
- Experimental method.

Global thermodynamic models assume that the gas cylinder of a compressor is a single zone (bulk) and all properties are uniform inside the cylinder. For example, temperature and pressure have the same values at both the head and the end of the cylinder. In contrast, dimensional dependence is considered in multidimensional numerical fluid-dynamic models. So, all properties have different values at different locations in the cylinder. Global models use the conservation of mass and energy to solve problems. Similarly, multidimensional models apply conservation concepts, but they obtain temporal and spatial solutions by solving the three-dimensional conservation equations such as the continuity, momentum, and energy equations. Since global models use the single-zone assumption to simplify engine heat transfer, they are easy to use in modeling and require less CPU time and memory for computer calculations. On the other hand, multidimensional models are very complicated for computer simulation. For instance, they must create grid patterns to match cylinder geometry, yield a set of finite difference equations for the grid patterns, and use effective numerical algorithms to obtain convergent and correct solutions. During numerical computation, they need plenty of CPU time and memory to run the computer code and store data.

It should be noted that global models couldn't describe the details of local heat transfer effects because they deal with overall effects of the cylinder gas as a whole. Generally, they predict the overall system performance such as volumetric efficiency, energy consumption, total heat loss, discharge temperature and pressure, etc.

Multidimensional models, unlike global models, are able to predict detailed information not only on heat transfer, but also on velocity, turbulence, gas composition, etc. Besides that detailed information, multidimensional models, of course, can predict the overall system performance. Obviously, multidimensional models are much more powerful than global models. However, developing a multidimensional computer code requires putting lots of effort into complicated modeling. The global thermodynamic models still have advantages due to simplicity and less cost.

A finite element method developed by COMSOL Multiphysics® is used as a multi-dimensional model in this thesis to study the local and details of the thermal properties and heat transfer.

Finally an experimental method is used to verify the aforementioned models.

1.10 Objectives of the present research

The overall objective of this research is to develop a comprehensive model for the finned air compressors and to achieve a better understanding of the in-cylinder heat-transfer and fluid-flow processes by theoretical modeling and experimental measurement. The specific objectives of this research are:

- To define appropriate efficiency terms to evaluate the CAES systems.
- To develop a comprehensive model to predict the thermal behavior of classic pistons.
- To extend the developed model for a finned piston.
- To develop a finite element (Multidimensional) model for both the classic and finned piston.
- To verify the simulation results with experimental measurement from test bench.
- To investigate the design parameters like velocity on system performance.

Chapter 2 Overview Of Compressed Air Energy Storage (CAES)

2.1 Introduction

The main intention of this chapter is to give an insight to round-trip nature of a CAES system from energetic and thermodynamic point of view and to define appropriate efficiency terms for evaluating such systems. The principles of energy and exergy efficiency will be applied to the CAES system.

In the first section different parts of a CAES system is characterized and defined. Next, a first law of thermodynamics analysis was carried out considering the compressor and expander as a steady flow device. Then combining first and second laws of thermodynamics, exergy efficiency for the compressor/expander is defined. Finally, gradual roadmap from adiabatic towards isothermal process is illustrated from thermodynamics and heat transfer point of view. It will be seen what is the effect of changing polytropic factor on the system performance.

It should be reminded that the plots and results presented in this chapter are based on the simulations carried out on models developed for a reciprocating compressor in filling mode, so the reader should not be surprised by the absence of all the equations needed to reach the results of this chapter. However in the next chapters these concepts will be applied again to evaluate the performance of classic and finned compressors.

Previously Kim and Favrat [68] have studied several different CAES plants from energetic and exergetic point of view.

Elmegraad and Brix [69] also developed terms for evaluating the efficiency of CAES plants, but with more emphasize on adiabatic CAES. So far, no serious work has been carried out on detailed Isothermal CAES modeling, characterization and exergetic analysis.

2.2 Principle of CAES Plant

The basic principle of a CAES plant is illustrated in **Figure 2.1**. The CAES system comprises of three main parts :

1. *Consumer Part* :mainly is a compressor, that is provided with the shaftwork from an electric motor. It takes in the ambient air (T_0, p_0), compresses it and delivers it at (a higher) pressure and temperature of (T_1, p_1).

2. *Storage Part* : is an underground cavern or above ground vessel. The compressed air is stored in a reservoir, cools down and after sufficient time reaches the temperature of ambient ($T_2 = T_0$) and pressure of (p_2).
3. *Producer Part* : is basically an expander or a turbine. The air stored in the reservoir is released and produces work while its pressure drops to ambient ($p_3 = p_0$), and its temperature to sub-ambient (T_3).

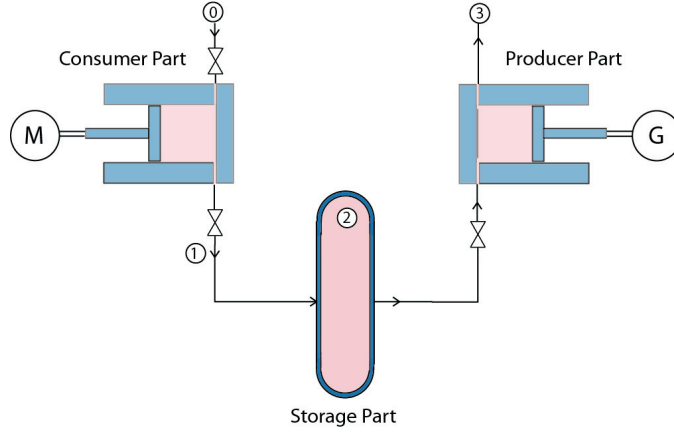


Figure 2.1 : CAES general Scheme

2.3 First Law of Thermodynamics Analysis applied to CAES

In some textbooks [19], the first law of thermodynamics is described generally as:

$$\sum_j \dot{W}^- + \sum_j \dot{Q}^- + \sum_j \dot{m}_j^- h_j + \frac{dU}{dt} = \sum_j \dot{W}^+ + \sum_j \dot{Q}^+ + \sum_j \dot{m}_j^+ h_j \quad (2:1)$$

Where + superscript represents (work, heat or mass) input to the system, while – superscript represents output from the system. Also work and heat interactions of the system with atmosphere are shown with subscript a and sources of other external systems are shown with subscript k .

1st law efficiency (effectiveness) has been described as all forms of energy given to the system divided by all outputs of energy:

$$\varepsilon = \frac{\sum_j \dot{W}_k^- + \sum_j \dot{Q}_k^- + \sum_j \dot{m}_j^- h_j}{\sum_j \dot{W}_k^+ + \sum_j \dot{Q}_k^+ + \sum_j \dot{m}_j^+ h_j} \quad (2:2)$$

Throughout this chapter, it is assumed that air behaves like an ideal gas and that the irreversible losses are negligible. Also, kinetic and potential energy changes associated with control volume is negligible.

The compressor can transport mass and energy through the “in” and “out” ports, but flow can go in only one direction at either port. Notice that we assume that one pressure; one temperature, one density, etc. characterize the entire internal volume of the control volume.

Assuming that the unsteady-flow process in a compressor or expander can be modeled as a *uniform-flow process*, which requires that the fluid flow at inlet or exit is uniform and steady, and thus the fluid

properties do not change with time or position over the cross section of inlet or exit. If they do, they are averaged and treated as constant for the entire process. The energy and mass balance relations in rate form for a uniform-flow compressor is expressed as

$$\dot{W}^+ + \dot{Q}^+ + \sum_j \dot{m}_j^+ h_j = \dot{Q}^- + \sum_j \dot{m}_j^- h_j + \frac{dU_{c.v}}{dt} \quad (2:3)$$

and

$$\sum_j \dot{m}_j^+ - \sum_j \dot{m}_j^- = \dot{m} \quad (2:4)$$

Considering the gas in the cylinder head as a control volume in **Figure 2.2**. \dot{Q}^+ and \dot{W}^+ are the heat and work *transferred to the gas* from the ambient, while \dot{Q}^- is the heat *transferred from gas* to ambient. Also, U is the internal energy of the control volume.

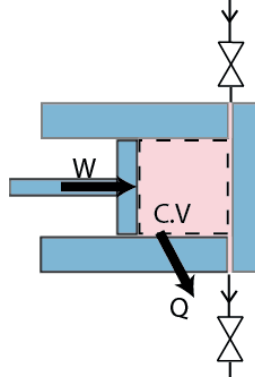


Figure 2.2 : Compressor gas as an open thermodynamic system with work, heat and mass flow interaction.

One should note that the direction of the heat transfer in a compressor can change within a cycle, specially if the heat transfer rate is high which is the case for a cooled or finned compressor. This fact is shown in **Figure 2.3**. It is observed that during the first half of the cycle (compression and discharge), the gas is hotter from the cylinder wall, so the heat transfer rate is negative, while during the second half (expansion and intake) the temperature of the gas drops below the wall temperature so the heat transfer is from cylinder wall to ambient, which is considered positive.

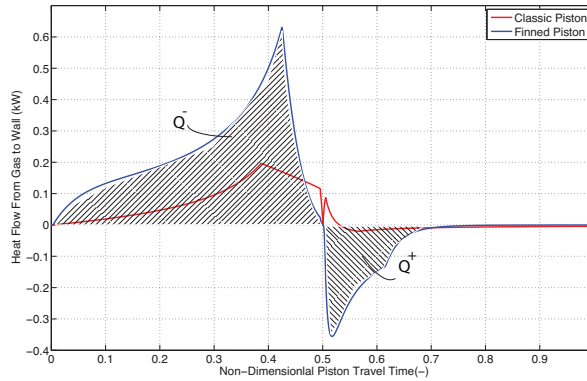


Figure 2.3: Heat transfer rate in a classic and finned compressor.

2.3.1 Steady flow Conditions

For simpler analysis let us assume that the flow in compressor is steady. Hence the total Energy and consequently internal energy of the control volume remains constant (Kinetic and potential energies were neglected already). Thus the change in internal energy of the control volume is zero ($\frac{dU_{cv}}{dt} = 0$). Therefore, the amount of energy entering the control volume in all form should be equal to the amount of energy leaving it. Then the rate form of First law of thermodynamics for open steady state systems (**Figure 2.2**) reduces to:

$$\dot{W}^+ = \dot{Q}^- + \dot{m}_e h_e - \dot{m}_i h_i \quad (2:5)$$

This means that the power input to a compressor may be written as the sum of heat transfer rate rejected to ambient plus the enthalpy change of the gas leaving and entering the chamber.

Integrating over one cycle of compressor performance, one can calculate work input, heat rejected and difference of input and output enthalpy in the piston. If one changes the polytropic factor from 1.4 (adiabatic process) to 1 (isothermal process) the parameters in Eq (2:5) will change according to **Figure 2.4** from right to left. It is observed that in the adiabatic case, however the heat transfer is zero, but the delta enthalpy is at its maximum. By decreasing the polytropic factor heat transfer increases but the decrease in enthalpy difference is more dominant, resulting in reduction in total work. The same argument is true in an expander, which means maximizing the heat transfer (isothermal expansion) can maximize the output work.

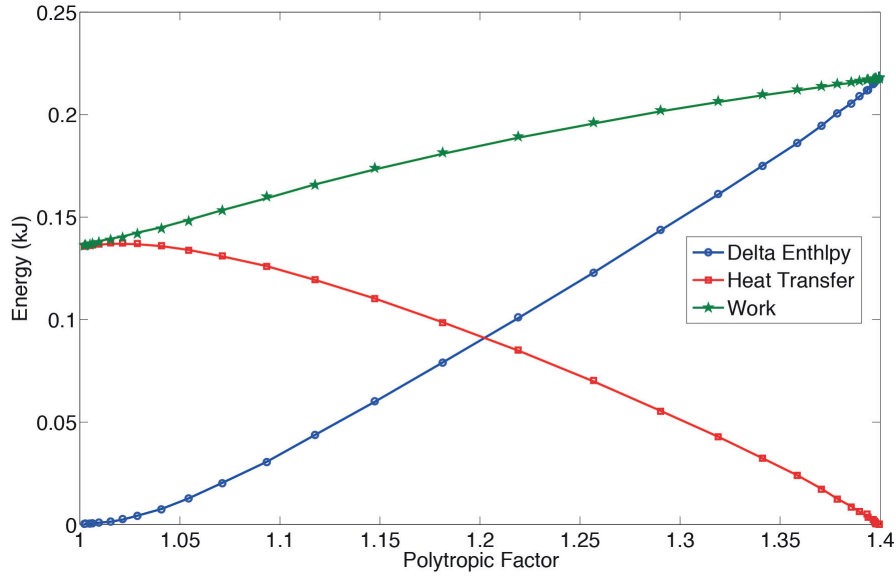


Figure 2.4 : Delta Enthalpy, heat transfer rate and work change with Polytropic factor.

On the other hand, neglecting any losses, work can be written as

$$W = \int p dV \quad (2:6)$$

Similarly, heat can be written as

$$Q = \int TdS \quad (2:7)$$

One can see in **Figure 2.5** that as the process changes gradually from adiabatic (red) to isothermal (blue), the surface enclosed by p-V diagram (which represents the required work input) decreases.

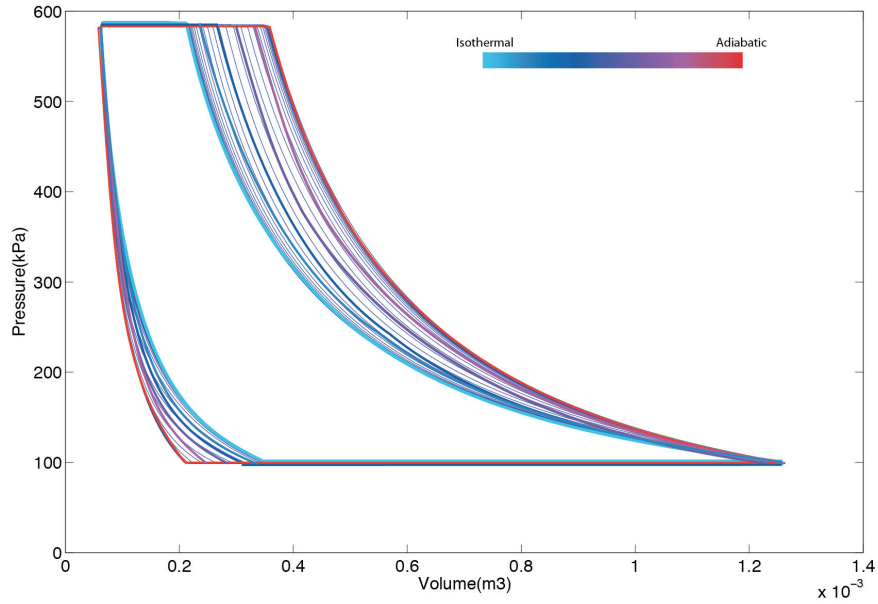


Figure 2.5 : p-V diagram of a compression process while going from adiabatic to isothermal.

Figure 2.6 Shows temperature on a third axis added to a p-V diagram in a 3D graph for 3 cases of adiabatic, polytropic and isothermal processes.

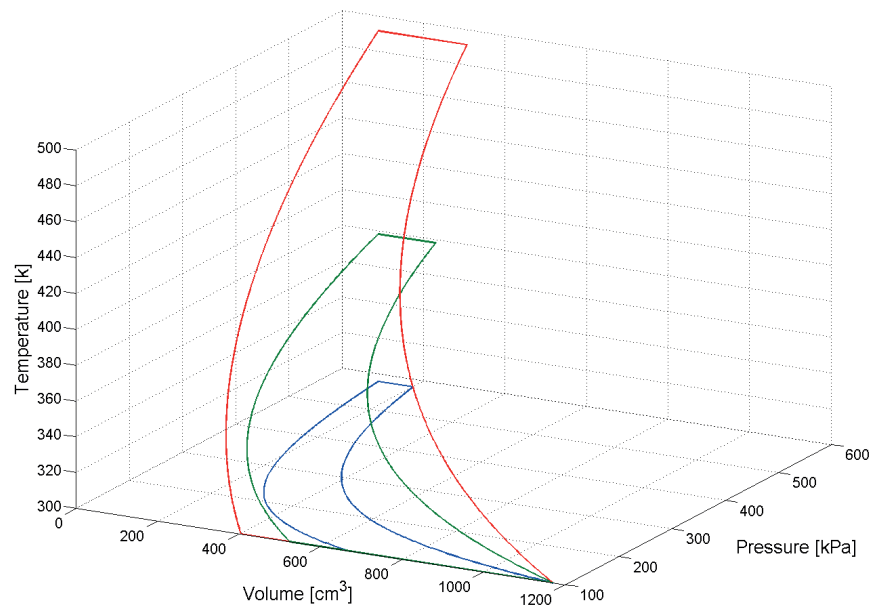


Figure 2.6 : P-V-T diagram of a compression process while changing from adiabatic (red) to polytropic (green) and finally to isothermal (blue).

At the same time in **Figure 2.7** the surface enclosed by T-S (Temperature-Entropy) diagram which is the energy wasted to heat generation decreases to almost zero for isothermal processes.

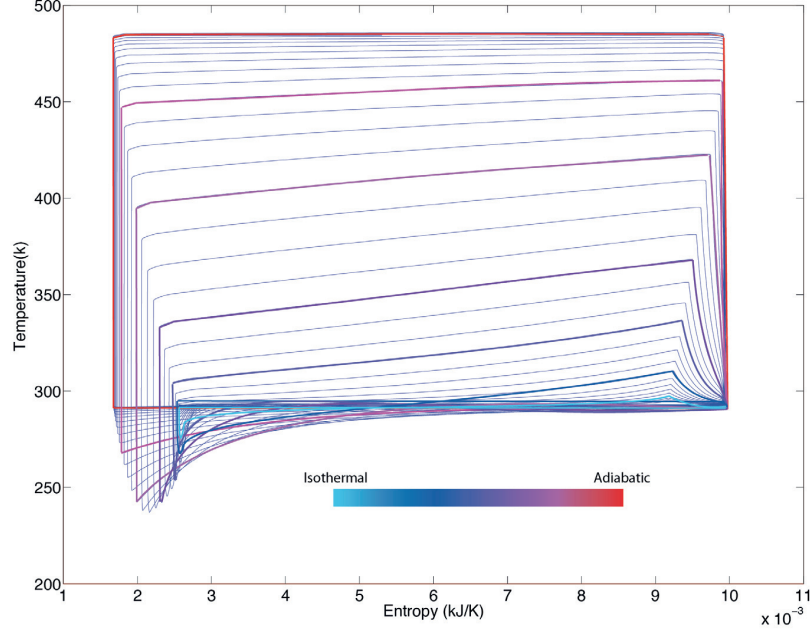


Figure 2.7 : T-S diagram of a compression process while going from adiabatic to isothermal.

2.3.2 First Law of Thermodynamics Efficiency

Back again to Eq. (2:3), separating the work and heat interactions of the system with atmosphere (with subscript a) and sources of other external systems (with subscript k), yields:

$$\dot{W}_k^+ + \dot{W}_a^+ + (\dot{Q}_k^+ + \dot{Q}_a^+) + \sum_j \dot{m}_j^+ h_j = \frac{dU}{dt} \quad (2:8)$$

For the case of the compressor, the only input is the work provided to the shaft, and the only useful output is the outgoing enthalpy. One may note that the definition of efficiency should be independent of the reference state. So the first law efficiency can be written as:

$$\varepsilon = \frac{\dot{m}_e h_e - \dot{m}_i h_i}{\dot{W}} \quad (2:9)$$

If we calculate the first law efficiency for the first two parts of the system (compressor and storage), since $(T_2 = T_0)$, and so $(h_2 = h_0)$, one may conclude that the compressed air produced by the storage process does not contain any part of the work invested in compressing it, however it is not the case. In fact the first law accounts for the energy balance during the conversion process but does not reflect the quality or grade of the different resultant forms of energy. Hence, energy (1st law) analysis alone is insufficient to evaluate the performance of CAES and an exergy evaluation is needed to figure out the real work potential of the system. This will be seen in the next section.

2.4 Exergy Analysis and Efficiency Applied to CAES

According to the same reference [19] exergy balance (combined first and second laws) for steady flow conditions can be written as:

$$\dot{W}_k^- + \left(1 - \frac{T_0}{T_k}\right) \dot{Q}_k^- + \sum_j \dot{m}_j^- \psi_j + \frac{d}{dt} (U + P_0 v - T_0 S) = \dot{W}_k^+ + \left(1 - \frac{T_0}{T_k}\right) \dot{Q}_k^+ + \sum_j \dot{m}_j^+ \psi_j - \dot{X}_{destroyed} \quad (2:10)$$

For the compressor, assuming steady state conditions, the storage term can be neglected and with a positive entering convention:

$$\dot{W}_k^+ + \left(1 - \frac{T_0}{T_k}\right) \dot{Q}_k^+ = \left(1 - \frac{T_0}{T_k}\right) \dot{Q}_k^- + \sum_j \dot{m}_j^- \psi_j - \sum_j \dot{m}_j^+ \psi_j + \dot{X}_{destroyed} \quad (2:11)$$

Exergy efficiency (combined 1st and 2nd law) has been described by [19] as all forms of energy given to the system divided by all outputs of energy:

$$\eta_x = \frac{\dot{W}_k^- + \left(1 - \frac{T_0}{T_k}\right) \dot{Q}_k^- + \sum_j \dot{m}_j^- \psi_j}{\dot{W}_k^+ + \left(1 - \frac{T_0}{T_k}\right) \dot{Q}_k^+ + \sum_j \dot{m}_j^+ \psi_j} \quad (2:12)$$

Where ψ is the stream exergy that will be defined in the next section.

2.4.1 Air Stream Exergy

In Eq. (2:11) ψ is the flow exergy and is defined by [70] (assuming that potential and kinematic energy effects are negligible):

$$\psi = (h - h_0) - T_0(s - s_0) \quad (2:13)$$

h and s are specific enthalpy and entropy, respectively, and the subscript 0 indicates that the properties are taken at reference temperature and pressure ($T_0 = 20^\circ\text{C}$, $p_0 = 1 \text{ Bar}$) as a dead state.

So the exergy of an air stream can be expressed as:

$$\dot{X} = \dot{m}[h - h_0 - T_0(s - s_0)] \quad (2:14)$$

In the case of ideal gas flow,

$$h - h_0 = c_p(T - T_0) \quad (2:15)$$

$$s - s_0 = c_p \ln \frac{T}{T_0} - R \ln \frac{p}{p_0} \quad (2:16)$$

The air stream exergy -as also practiced by [68]- can be split into two parts -the Pneumatical part and the Thermal part- as follows:

$$\dot{X} = \dot{X}_{(P)} + \dot{X}_{(T)} \quad (2:17)$$

$$\dot{X}_{(P)} = \dot{m} R T_0 \ln \frac{p}{p_0} \quad (2:18)$$

$$\dot{X}_{(T)} = \dot{m} c_p \left(T - T_0 - T_0 \ln \frac{T}{T_0} \right) \quad (2:19)$$

Although the compression work varies according to various processes, e.g., isothermal, adiabatic... , the compressed air is stored in the air storage, and the thermal exergy of compressed air is dissipated by cooling down the reservoir (unless it can be stored in a thermal energy storage and reused during expansion process). Hence, the only useful part of exergy is the pneumatical one.

However even the pneumatical part is not extractable entirely depending on the type of the compression process. This is due to the fact that the temperature of the stored gas in the reservoir decreases and since the volume of the reservoir and mass of the gas is constant, as a result the pressure decreases as well. So the final pressure of the reservoir will be:

$$p_2 = p \left(\frac{T_0}{T} \right) \quad (2:20)$$

Let us now investigate the filling of a reservoir with the compressor to a given pressure level (6 Bar here). After reaching this pressure, the compressor stops working and we let the air in the reservoir to cool down. It is interesting to investigate the different compression processes from isothermal ($n = 1$) to adiabatic ($n = 1.4$). One should note that the heat transfer from reservoir to ambient air is considered identically for all the cases as natural convection (will be described in chapter 3).

The evolution of pressure and temperature is shown respectively in **Figure 2.8** and **Figure 2.9** based on different compression processes. The first part of the diagrams show the charging phase, where pressure and temperature rises. One may note that the lower the polytropic factor is the longer it takes to fill the reservoir with a constant pressure level, and also the lower will be the temperature in the reservoir. In the second phase the charging of the tank is stopped and the pressure and temperature drops. It is evident that the temperature drop is much more in the case of an adiabatic compression. Also the exergy content of the reservoir is calculated based on Eq. (2:22) and plotted in **Figure 2.10**.

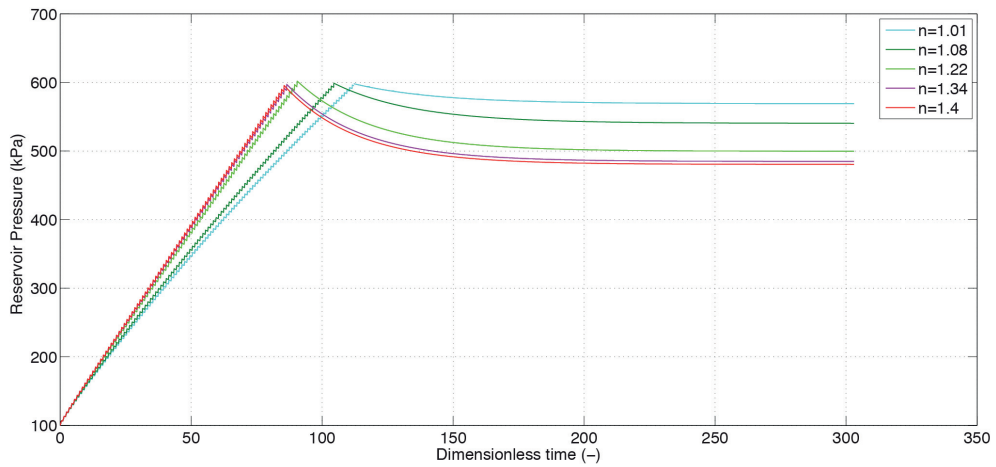


Figure 2.8 : Pressure evolution in reservoir for different compression processes.

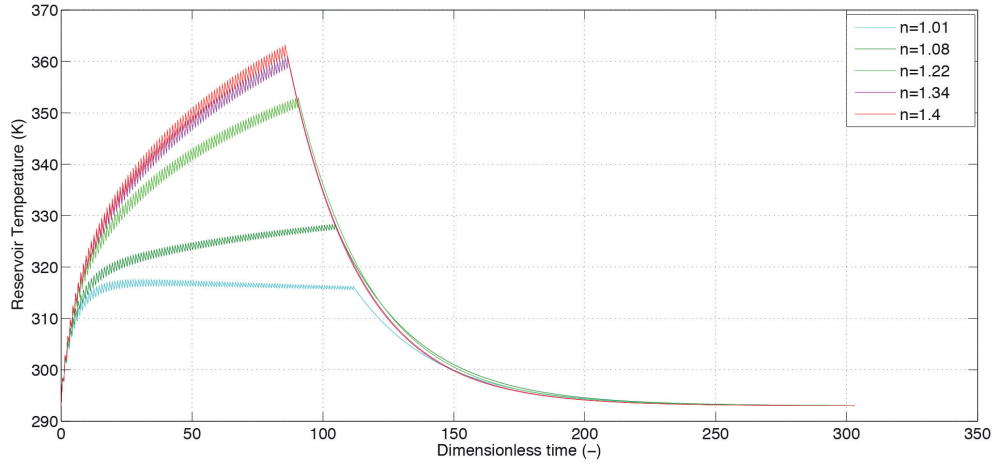


Figure 2.9 : Temperature evolution in reservoir for different compression processes.

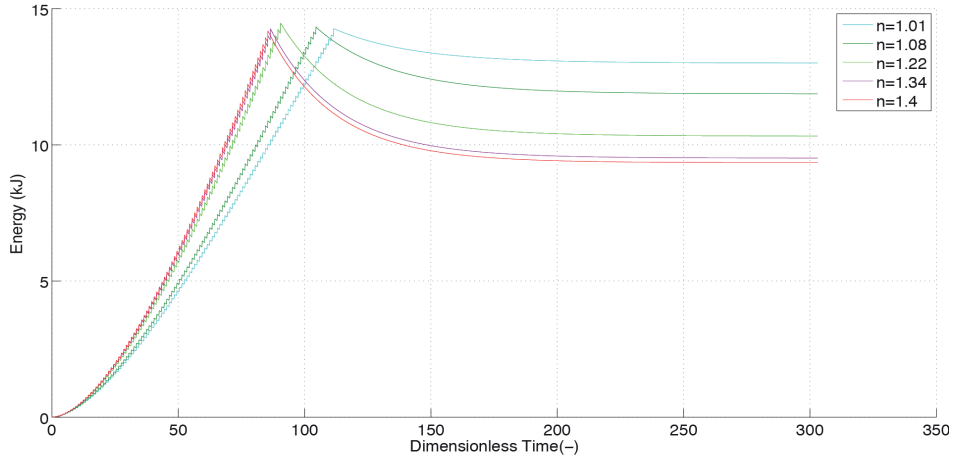


Figure 2.10 : Exergetic content of reservoir during charging a tank with a specific pressure level.

Replacing Eq.(2:20) in Eq. (2:18) yields

$$\dot{X}_{(P)2} = \dot{m}RT_0 \ln \frac{p}{p_0} \left(\frac{T_0}{T} \right) \quad (2:21)$$

Which is the recoverable exergy in an air stream after cool-down. It is evident from Eq. (2:21) that the higher the temperature of the air stream is the lower its recoverable exergy will be.

Figure 2.11 represent the variation of the mentioned terms with polytropic factor. The blue line represents the input work to the system. The green line represents the total stream exergy, which is the sum of pneumatic and thermal exergies. It is interesting to notice that fortunately the share of thermal exergy is much less than the pneumatic exergy, however this share increases with increment of polytropic factor. While one may think that the total stream exergy and also pneumatic exergy increases with polytropic factor but finally what is important is the exergy after cool-down (Eq. (2:21)) that is represented by dotted red line, which decreases.

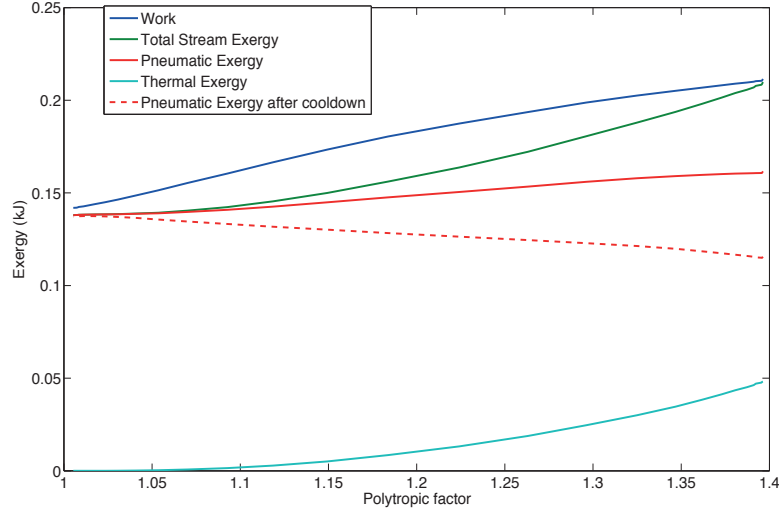


Figure 2.11 : Exergy vs. polytropic factor.

2.4.2 Storage Exergy in Reservoir

The amount of exergy available in a compressed air reservoir can be determined from:

$$X_1 = m\phi_1 \quad (2:22)$$

Where ϕ is the *non-flow* exergy and is defined by (again assuming that potential and kinematic energy effects are negligible):

$$\phi = (u - u_0) + p_0(v - v_0) - T_0(s - s_0) \quad (2:23)$$

Where,

$$u - u_0 = c_v(T - T_0) \quad (2:24)$$

And $(s - s_0)$ is already defined in Eq. (2:16), which after calculation will result in:

$$X_1 = m_1 R T_0 \left[\ln \left(\frac{p_1}{p_0} \right) + \frac{T_1}{T_0} \left(\frac{p_0}{p_1} + \frac{5}{2} \right) - \frac{7}{2} \left(1 + \ln \left(\frac{T_1}{T_0} \right) \right) \right] \quad (2:25)$$

Since the gas cools down due to heat transfer to ambient, the temperature and as a result the pressure will drop, leading to loss in exergy. The final pressure after cool down is determined from Eq. (2:20).

The exergy of the compressed air in the reservoir after reaching thermal equilibrium with ambient can be calculated by replacing $p = p_1$ and $T = T_0$ in Eq. (2:23), which results in

$$X_2 = m_1 R T_0 \left[\ln \left(\frac{p_2}{p_0} \right) + \frac{p_0}{p_2} - 1 \right] \quad (2:26)$$

One can derive Eq. (2:26) also by integrating by parts, Eq.(2:21) over the filling process:

$$\begin{aligned}
X_2 &= \int_{p=p_0}^{p=p_2} \dot{X}_{(P)2} dp = \int_{p=p_0}^{p=p_2} \dot{m} R T_0 \ln \frac{p}{p_0} \left(\frac{T_0}{T} \right) dp \\
&= p_2 V \left(\frac{1}{p_2} + \ln(p_2) - 1 \right) (kJ) \\
&= m_1 R T_0 \left[\ln \left(\frac{p_2}{p_0} \right) + \frac{p_0}{p_2} - 1 \right]
\end{aligned} \tag{2:27}$$

2.4.3 Exergy Efficiency of differnt parts of CAES

As proposed by [69], the round-trip efficiency of a CAES plant can be written as the product of the three parts introduced in section 2.2. Since there is no work output from the compressor, the exergy efficiency for the compression part from Eq. (2:12) reduces to:

$$\eta_x = \frac{\left(1 - \frac{T_0}{T_k}\right) \dot{Q}_k^- + \dot{m}_j^- \psi_j}{\dot{W}_k^+ + \left(1 - \frac{T_0}{T_k}\right) \dot{Q}_k^+ + \dot{m}_j^+ \psi_j} \tag{2:28}$$

Looking more accurately to the system, we can assume that the heat exergy is neither a product nor a service, and thus can be eliminated from both numerator and denominator. Integrating over the whole filling process, the exergetic efficiency of the compression process can be further reduced to the exergy in the reservoir before cool-down of the reservoir divided by the work input to the compressor:

$$\eta_{x,comp} = \frac{X_1}{W_c^+} \tag{2:29}$$

The exergy efficiency of the storage part can also be reduced from Eq. (2:12) to the ratio of the exergy of the fluid coming to the reservoir to the exergy of the air leaving the reservoir. The efficiency of the reservoir can be defined as the ratio of the exergy of the air coming to the reservoir to the exergy of the air leaving the reservoir. Integrating over the whole filling process,

$$\eta_{x,stor} = \frac{X_2}{X_1} \tag{2:30}$$

Also the compression-storage exergetic efficiency can be defined as the product of producer and storage parts:

$$\eta_{x,cs} = \eta_{x,comp} \cdot \eta_{x,stor} = \frac{X_1}{W_c^+} \frac{X_2}{X_1} = \frac{X_2}{W_c^+} \tag{2:31}$$

The exergetic efficiency of the expansion process can be defined similar to the compression process as the work produced by expansion divided by the exergy of incoming fluid:

$$\eta_{x,exp} = \frac{W_e^-}{X_2} \tag{2:32}$$

The round-trip exergy efficiency is the multiplication of the tree parts:

$$\eta_{RT,x} = \eta_{x,comp} \eta_{x,stor} \eta_{x,exp} \quad (2:33)$$

Which can be reduced to:

$$\eta_{RT,x} = \frac{X_1}{W_c^+} \frac{X_2}{X_1} \frac{W_e^-}{X_2} = \frac{W_e^-}{W_c^+} \quad (2:34)$$

So finally the round trip efficiency is the work provided by expansion divided by the work consumed by compression. The terms developed in Eqs. (2:29) to (2:34) are plotted in **Figure 2.12** against polytropic factor. It is interesting to notice that not only the compression, storage and expansion will decrease with polytropic factor, but also their product which is round-trip efficiency reduces much further. In other words the round-trip efficiency of a classic compressor (which can be considered almost adiabatic) is almost less than 50%, which means half of the energy input will be wasted into heat, and unless recovered will be wasted.

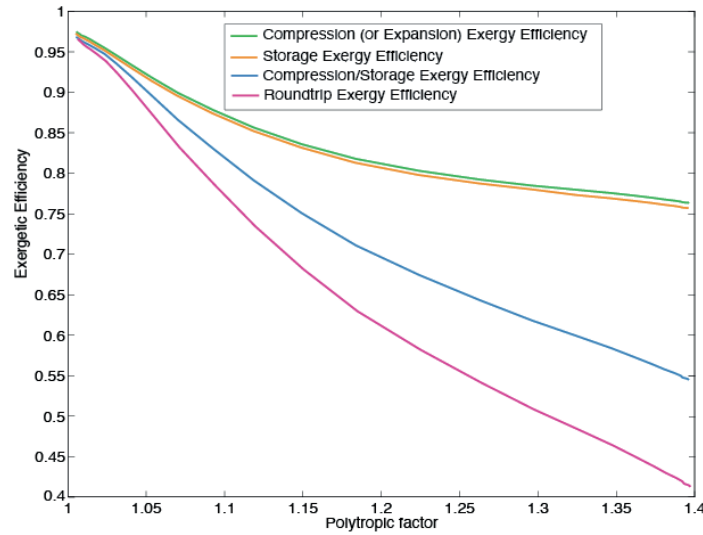


Figure 2.12 : Exergetic efficiency vs. polytropic factor.

It is evident that if the compression and expansion processes are close to isothermal, the exergy loss in the reservoir will be much less than if it is closer to isentropic compression. This makes the isothermal process benefit double and the preferable compression process in the absence of thermal storage facilities.

2.5 Conclusion

In this chapter, a CAES system was analyzed from energetic and exergetic point of view. The variation of different energetic terms like work and heat flow were investigated with regard to polytropic factor. It was shown that the 1st law of thermodynamics is not sufficient to evaluate the compressor performance for applications of CAES, and in addition an exergy analysis is necessary to account for real work potential of the system. Finally, isothermal compression and expansion was proved to be the most promising process for CAES applications without thermal storage facilities. The techniques and definitions developed in this chapter will be used to evaluate the system in the next chapters.

Chapter 3 Classic Piston Compressor

Analytical Model

3.1 Introduction

Reciprocating compressors is one the most important machines used throughout various industries. Due to its importance considerable effort has been devoted by many researchers toward the development of mathematical models for computer simulation of this type of machine.

In general, a cycle of operation of a high speed positive displacement compressor can be described as a number of complicated phenomena, interacting and taking place in a short period of time.

It is always a good idea to start modeling a complicated system by dividing it to simpler systems. The model can be extended by adding more details and combining the simple systems to build a comprehensive model. As well, In order to model a complicated finned piston, it is better to model a simple piston compressor first. This model will include inlet and outlet valves as well as the driving mechanism but will only include one chamber with uniform pressure and temperature distributions.

Global thermodynamic models (as utilized in this chapter) assume that the cylinder of a compressor is a single zone and all properties are uniform inside the cylinder. For example, temperature and pressure have the same values at both the head and the end of the cylinder. In contrast, dimensional dependence is considered in multidimensional numerical fluid-dynamic models. So, all properties have different values at different locations in the cylinder. CFD models (as will be seen in Chapter 5) can be categorized in this group.

Global models use the conservation of mass and energy to solve problems. Similarly, multidimensional models apply conservation concepts, but they obtain temporal and spatial solutions by solving the three-dimensional conservation equations such as the continuity, momentum, and energy equations. Since global models use the single-zone assumption to simplify engine heat transfer, they are easy to use in modeling and require less CPU time and memory for computer calculations. This is why these type of models were used in this chapter.

On the other hand, multidimensional models are very complicated for computer simulations. For instance, they must create grid patterns to match cylinder geometry, yield a set of finite difference equations for the grid patterns, and use effective numerical algorithms to obtain convergent and correct solutions. During numerical computation, they need plenty of CPU time and memory to run the computer code and store data. A representative of this type of models are described in Chapter 5.

It should be noted that global models couldn't describe the details of local heat transfer effects because they deal with overall effects of the cylinder gas as a whole. Generally, they predict the overall system performance such as volumetric efficiency, energy consumption, total heat loss, discharge temperature and pressure, etc.

Multidimensional models, unlike global models, are able to predict detailed information not only on heat transfer, but also on velocity, turbulence, gas composition, etc. Besides that detailed information, multidimensional models, of course, can predict the overall system performance. Obviously, multidimensional models are much more powerful than global models. However, developing a multidimensional computer code requires putting lots of effort into complicated modeling. The global thermodynamic models still have advantages due to simplicity and less cost.

In this chapter two graphic representation tool has been used to describe the model: EMR (Energetic Macroscopic Representation) and bond graph. Each of them has its own strength.

This chapter first introduces the two aforementioned graphic modeling tools. EMR and bond graph are the two approaches for representing the dynamic nonlinear model of a reciprocating air compressor. While bond graph is an established tool for representing mathematical model of physical systems, EMR has been introduced recently for research development in complex electromechanical systems. Both are based on action reaction principle, which organize the system as interconnected subsystems according to the integral causality. The graphical modeling based on EMR has advantages such as readability, modularity, structural and functional characteristics, while bond graph distinguishes resistance capacitance and inertia effect in physical systems more clearly. The air compressor system containing: slider-crank mechanism, cylinder head, valves, and reservoir is divided into multitude simple subsystems. Each subsystem describes an elementary step of the energy conversion, several of these blocks may occur in a single module. Calculations are carried out using two basic principles: mass and energy balances. Models are developed for different subsystems, which are assembled into a final overall system bond graph or EMR. The graphical modeling procedure presented here allows the modeling of multi-physics components and highlights the interactions of the electromechanical, thermodynamical, heat transfer and fluid flow phenomena that occur simultaneously in an air compressor.

3.2 Graphical Modelling Representation Tools

Comprehensive compressor models have been developed for different compressor types [62,63,64] and [65]. However, graphical representation of such models has been scarce so far.

Bond graphs are valuable and powerful tools in constructing mathematical model of variety of systems especially mechanical and hydraulic systems. Components or systems of which the behaviour must be described by thermodynamic relations are not considered to the same degree. This is especially true for open thermodynamic systems, which involve flow of mass and energy in and out of a device. A problematic bloc has been a correct bond graph description of convective transport. A breakthrough in practical thermofluid system modelling was made when Karnopp [71] presented his class of double bond pseudo bond graphs for compressible thermofluid systems.

In some literature, graphical models of air compressor can be found [72,73]. They are based on the same equations and theoretical backgrounds than the previous ones but the graphical methodology highlights the understanding of the device behaviour in a significant extent. To describe the modelling of thermodynamic systems, [74] uses bond graph approach. Using the same tool, [73] proposes an

overall picture of the considered system in a synthetic approach.

Even if bond graph tool is able to describe complex systems, Energetic Macroscopic Representation (EMR) has its own strengths. In fact, beyond its modularity and readability, EMR reveals functional characteristics to provide a good model description in agreement with physical (e.g. integral) causality [75]. Both bond graph and EMR are obviously able to describe multiphysical systems, but there are nevertheless different features between them. The former is based on energy and data flow and uses a uniform representation for all types of physical systems; while with the latter specific pictograms are used and associated to each power component increasing its readability. As a matter of fact, it shows the different physical domains crossed by the energy flows.

The graphical modelling based on EMR has advantages such as readability, modularity and functional characteristics. As regards the graphical modelling tools, their interest is double: firstly during the modelling phase itself and secondly as the easiest transfer of knowledge to the other users [76].

Therefore, a complex system of several energy sources and several energy conversion units can be accurately modelled and then described by the EMR tool with a clear readability.

Though EMR has been firstly developed to describe electromechanical system [77], made it possible to extend it to new energy domains. Expanded to electrochemical, thermodynamical, heat transfer and fluid mechanics domains, EMR has allowed describing many devices such as fuel cells systems, electromechanical systems, electrical or hybrid vehicle systems.

3.3 Bondgraph description

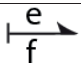
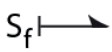
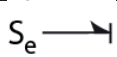



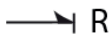

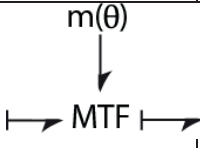
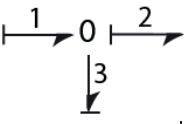
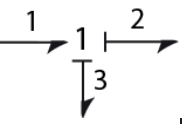
In the bond graph representation, a physical system can be represented by symbols and lines, identifying the power flow paths. The fundamental idea of a bond graph is that power is transmitted between connected components by a product of "effort" and "flow".

In other words, the bond graph is composed of the "bonds" which link together "single port", "double port" and "multi port" elements (see below for details). As mentioned, each bond represents the instantaneous flow of energy or power. The flow in each bond is denoted by a pair of variables called 'power variables' whose product is the instantaneous power of the bond. For example, the bond of an electrical system would represent the flow of electrical energy and the power variables would be voltage and current, whose product is power. Each domain of power variables are broken into two types: "effort" and "flow". Effort multiplied by flow produces power, thus every domain has a pair of power variables with a corresponding effort and flow variable. Examples of effort include force, torque, voltage, or pressure; while flow examples include velocity, current, and volumetric flow. **Table 3:1** contains the most common energy domains and the corresponding "effort" and "flow".

A bond has another features described briefly here. One is the "half-arrow" sign convention. This defines the assumed direction of positive energy flow. As with electrical circuit diagrams and free-body diagrams, the choice of positive direction is arbitrary, with the caveat that the analyst must be consistent throughout with the chosen definition. The other feature is the "causal stroke". This is a vertical bar placed on only one end of the bond. It is not arbitrary. As described below, there are rules for assigning the proper causality to a given port, and rules for the precedence among ports. Any port (single, double or multi) attached to the bond shall specify either "effort" or "flow" by its causal stroke, but not both. The port attached to the end of the bond with the "causal stroke" specifies the "flow" of the bond. And the bond imposes "effort" upon that port. Equivalently, the port on the end without the

"causal stroke" imposes "effort" to the bond, while the bond imposes "flow" to that port. Various symbols used in the bond graph are summarized in **Table 3:1**.

Table 3:1 Bond graph Standard Elements

	Symbols	Relation	Causality Constraints
Bonds			
			Effort or flow (here f)
Sources			
Flow		$f \text{ given}$	Fixed flow out
Effort		$e \text{ given}$	Fixed effort out
Energetic Elements			
Inertia		$f = \phi_I^{-1}(\int edt)$	Preferred Integral
Capacitor		$e = \phi_C^{-1}(\int fdt)$	Preferred Integral
Resistance		$e = \phi_R(f)$	Indifferent
		$f = \phi_R^{-1}(e)$	
2-port Elements			
Transformer			Only one casual stroke on TF
Modulated transfer function			Flow in flow out or Effort in effort out, But only one casual stroke on MTF
Junctions			
0-junction		$e_1 = e_2 = e_3$ $f_1 + f_2 + f_3 = 0$	Only one effort gives its value to others (here e_2) Only one casual stroke on 0 junction
1-junction		$f_1 = f_2 = f_3$ $e_1 + e_2 + e_3 = 0$	Only one flow gives its value to others (here f_2) Only one bond without casual stroke on 1 junction

3.3.1 Adaptation of Bond Graph to Thermofluid Systems

It is important to well distinguish a thermodynamic model with matter at rest, the Lagrangian Reference Frame, and a model with mass in movement, the Eulerian Frame. This difference is shown in **Figure 3.1**.

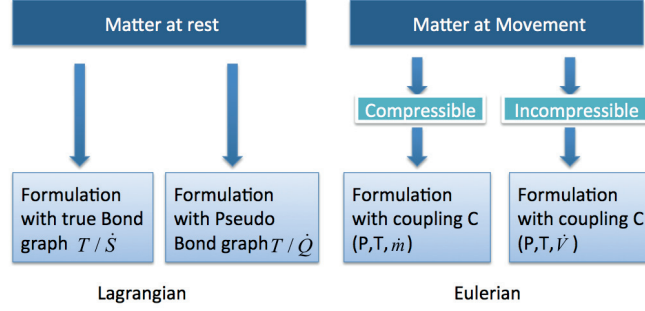


Figure 3.1 : Selection of bond graph couples in thermodynamics based on static or dynamic system.

Applying bond graph concept to open (with mass in movement or convective) thermo-fluid systems is a bit more complicated than other systems, because two independent intensive properties should be fixed for specifying completely the state of even a simple compressible system. A good choice for these two intensive variables in a system with matter at movement (like a compressor in our case) can be pressure and temperature. Since these two are effort variables they need also a flow variable to be coupled with. So, as it can be seen in **Figure 3.2**, we need two bonds to specify the state of a dynamic thermo fluid system.

It was also shown by some pioneer authors in bond graph development [72], [73] and [74], that using a pseudo-bond graph could facilitate the modeling of compressible gas dynamics system. In such a model the product of effort and flow variable is not necessarily power, however it possesses all other bond graph characteristics like causality. In such an approach a thermodynamic accumulator can be regarded as a control volume with mass and energy transport through "in" and "out" ports.

Karnopp [73] has shown that a cylinder head, which is a typical thermodynamic accumulator, can be represented by a multiport that has one true and three pseudo pairs (**Figure 3.2**). The true pair has pressure P as its effort variable \dot{V} as its flow variable. For the both pseudo-bonds (T, \dot{Q} and P, \dot{m}), the product of their effort and flow variables is not power. As it can be seen the shaft power is being converted to pneumatic and thermal energy.

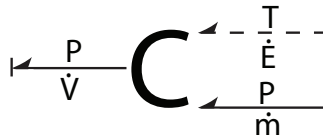


Figure 3.2 : Bond graph representation of an accumulator as a multiport.

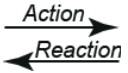
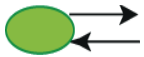



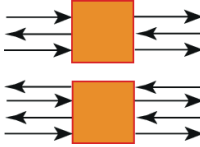
The T and \dot{E} (or \dot{Q}) dotted bond is necessary to properly account for the heat transfer in the control volume, while the P and \dot{m} is related to pneumatic energy.

3.4 EMR description

As mentioned before, EMR is used for the modeling of this multi-physics compressor. **Table 3:2** presents the generalized EMR pictograms used in the presented model. The detailed description of each element was not presented in this paper. For more details, please refer to [78] and [77]. All the elements are interconnected according to the action and reaction principle using exchange variable (arrows). The product of action and reaction variables between two elements leads to the instantaneous power exchanged.

In EMR only the integral causality is considered. This property leads to define accumulation element by a time-dependent relationship between its variables, in which its output is an integral function of its inputs. This is logical since derivative causality can lead to discontinuity in the output if the input of the system has a considerable dynamic behavior. Other elements are described using relationships without time dependence. Also, In order to respect the integral causality specific association rules are defined.

Table 3:2 Energetic Macroscopic Representation blocs

Pair of action a reaction	
Source of energy	
Energy conversion Same domain	
Energy conversion Different domains	
Energy accumulation	
Thermofluid causalities (three and four variables both for gas and liquid)	

3.4.1 Adaptation of EMR to a Thermofluid Systems

As mentioned in the introduction, EMR can be used for the modeling of this multi-physics compressor. The EMR methodology is based on the assumption that every energy exchange can be described using

one action and one reaction parameter. As in other graphic representation methodologies, the product of the causal parameter pair (here called action and reaction pair) gives the power exchanged between the blocks [79]. However, [77] argues that in the case of a multiport this does not have to be true all the time, and this relation has not necessarily to be a product. This approach might be called pseudo-EMR [77] in analogy to pseudo-bond graph [74]. It gives the possibility to handle the parameter pair in some areas more freely. It leads to defining EMR elements such as that one presented in Table 4:1 (Thermofluid causalities).

The basic ideas of EMR contain the fact that all systems can be subdivided into small parts, which follow either a simple conversion, a Kirchhoff law or a first order differential equation in integral form. For most systems this subdivision can be obtained. However, in some cases the link between energetic domains cannot be detached, they can only be described in matrix form. In this case the energetic domains inside the gas flows cannot be detached. The element has two parameter pairs upstream and downstream. According to [80]. Such an element can be called EMR-multiport in analogy to bond graph multiport. As it will be seen in section 3.5.2 an example used for this model is the connection between thermo-pneumatic systems. They have parameter pairs: pressure p and mass flow \dot{m} as well as temperature T and energy \dot{E} . Since they are connected via the ideal gas law, it is proposed that as the equation cannot be separated into the two energetic domains a multiport using both parameter pairs is used, see Figure 3.3.

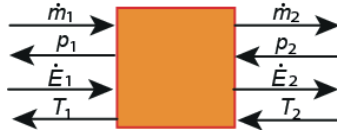


Figure 3.3 : Representation of a thermo-pneumatic multiport in EMR.

3.5 Description of linear air compressor behavior

A schematic of a linear compressor is shown in **Figure 3.4**. For modeling purposes the compressor is divided into five subsystems, namely:

1. Linear driver,
2. Cylinder head,
3. Valves,
4. Heat transfer
5. Reservoir,

Each subsystem is modeled independently and the sub-models are then combined into a complete model of the total system.

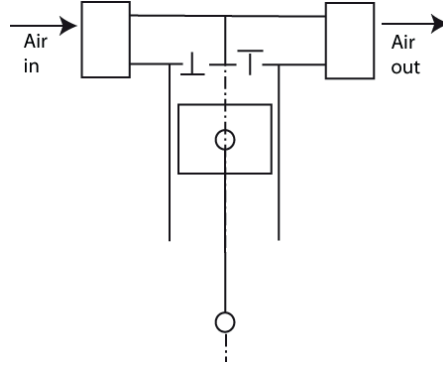


Figure 3.4 : Linear compressor schematic.

3.5.1 Linear driver mechanism

An electrical motor provides the compressor with a constant velocity during compression and expansion through a ball-screw driver (**Figure 3.5**). Eq. (3:1) shows the relationship between rotational speed of electrical motor ω , and the piston speed \dot{x}_p , as well as the relation between motor torque τ , and piston force F .

$$m(\theta) = \frac{\dot{x}_p}{\omega} = \frac{\tau}{F} \quad (3:1)$$

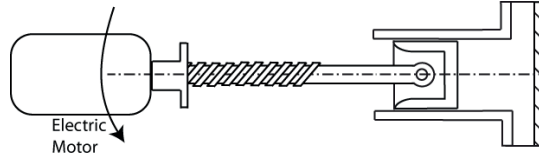


Figure 3.5 : Linear actuator mechanism.

The velocity has been set to be linear and constant during compression and expansion mode except at the very beginning and end of each movement. Of course as mentioned in chapter 1, operation must be at low speed (100 mm/s). Velocity and piston position is shown in **Figure 3.6**. It should be mentioned that here, velocity is cause and force is the effect, from the causality point of view.

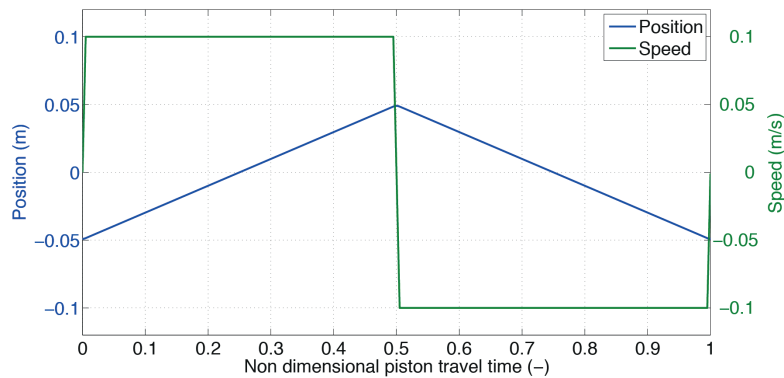


Figure 3.6 Position and speed of piston during one cycle.

Plus, the relation between the volume change and piston displacement can be deduced from Eq. (3:2), Where A_p is the piston surface:

$$\dot{V} = -A_p \dot{x}_p \quad (3:2)$$

One may represent the driver mechanism by the EMR of **Figure 3.7**. Also bond graph model is represented in **Figure 3.8**.

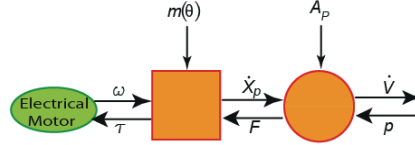


Figure 3.7 : EMR of driver mechanism.

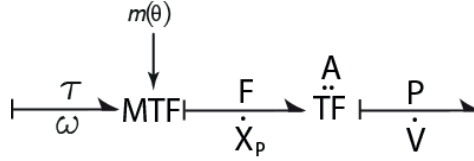


Figure 3.8 : Bond graph of driver mechanism.

Here as can be seen, the electric motor as a source of flow defines the rotational speed and in the next step, linear velocities causally, while symmetrically the other side (in this case cylinder head that will be described later) defines the force and then torque. Accordingly volume change is the cause and pressure is the effect.

3.5.2 Cylinder head

The core of the model is the cylinder head, which is shown by an energy conversion block. It can be considered as a control volume that transports mass and energy through the “in” and “out” ports. The mechanism of energy conversion is that the cylinder head receives the energy of shaft work and converts it to pneumatic (represented by the two upper bonds) and thermal (the two lower bonds) form.

The mass and energy balances for the mentioned control volume can be demonstrated using Eqs. (3:3) and (3:4)

$$\dot{m} = \dot{m}_i - \dot{m}_e \quad (3:3)$$

$$\dot{E} = \dot{E}_i - \dot{E}_e - p\dot{V} + \dot{Q} \quad (3:4)$$

Neglecting kinetic and potential energy:

$$E = U + KE + PE \quad (3:5)$$

Yields:

$$\dot{U} = \dot{E}_i - \dot{E}_e - p\dot{V} + \dot{Q} \quad (3:6)$$

Here U is the internal energy of the control volume, and \dot{E}_i and \dot{E}_e are inlet and exit transported energy flows (enthalpy) defined as:

$$\dot{E}_i = \dot{m}_i h_i \quad (3:7)$$

$$\dot{E}_e = \dot{m}_e h_e \quad (3:8)$$

It is assumed that the air obeys the gas law. Equations (3:3) and (3:4) look like first order state equations, and they motivate the construction of EMR of **Figure 3.9** and bond graph of **Figure 3.10**. The EMR and bond graph multiports in the aforementioned figures have one true and three pseudo pairs. The true pair has pressure p as its effort variable \dot{V} as its flow variable. For the both pseudo-bonds, the product of their effort and flow variables is not power. In fact \dot{E} is already power on the lower pseudo pair in EMR and upper bond in bond graph.

Even though the EMR or bond graph representation are not a true ones, nevertheless, they operates on associated action reaction pairs in a manner identical to a true EMR or bond graph. As the causality indicates, they possess all integral causality and therefore accept flow input on all three pairs (\dot{U} , \dot{m} and \dot{V}). It then integrates these flows to produce the state variables E , m and V . And finally the accumulator operates on these variables through appropriate constitutive laws to produce the outputs p and T . The constitutive relations are based on ideal gas equation and are given by Eqs. (3:9) and (3:10).

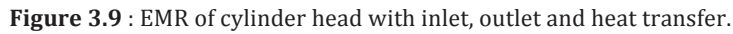
$$T = \frac{1}{c_v} \frac{U}{m} \quad (3:9)$$

$$P = \frac{mRT}{V} = \frac{mR}{V} \frac{1}{c_v} \frac{U}{m} = \frac{R}{c_v} \left(\frac{U}{V} \right) \quad (3:10)$$

Thus, if \dot{U} , \dot{m} and \dot{V} are prescribed (causally), then the thermodynamic accumulator will output T and p via the constitutive laws mentioned. The T, \dot{E} arrow (or stick in the case of bond graph) tells the accumulator the enthalpy flows \dot{E}_i and \dot{E}_e from whatever system is attached to accumulator and as the causality enforces the attached system learns of the temperature of the control volume. Similarly, the p, \dot{m} pseudo EMRs (or pseudo bond graphs), causally prescribe the mass flow from the attached system, while these arrows (or stick in the case of bond graph) also prescribe the control volume pressure to the attached system.

Considering the principals described in section 3.5, The EMR representation of the cylinder head is shown in **Figure 3.9**. As it can be seen the shaft power is being converted to enthalpy difference and heat flow. Like wise the bond graph representation of such a model is illustrated in **Figure 3.10**.

The T and \dot{Q} pair is also necessary to properly account for the heat transfer in the control volume, which will be described in details in section 0.



61

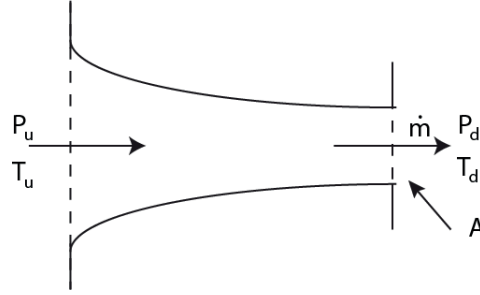


Figure 3.11 : Isentropic nozzle.

If we assume that isentropic flow exists, then it turns out that \dot{m} depends on the pressure ratio

$$p_r = p_u / p_d \quad (3:12)$$

rather than just the pressure drop $p_u - p_d$ across the nozzle.

The mass flow rate, \dot{m}_v through the valve as a function of valve area, upstream pressure P_u , temperature T_u , and downstream pressure, P_d can be calculated using Eq. (3:13).

$$\dot{m}_v = A_{va} p_u \sqrt{\frac{2k}{(k-1)RT_u}} \sqrt{(p_r)^{2/k} - (p_r)^{(k+1)/k}} \quad (3:13)$$

Where k is the ratio of specific heats and R is the ideal gas constant. This model assumes that the fluid is an ideal gas with compressibility taken into account, but there is no friction.

The area modulations A_i for the inlet and A_e for the discharge are needed to be specified by a logic expression. For example, for A_i can be defined by Eq.(3:14).

$$\text{If } v_p \leq 0 \text{ and } p \leq p_i, \quad A_i = A_{i \max} \quad (3:14)$$

$$\text{Otherwise,} \quad A_i = 0$$

This will keep the inlet open as long as pressure inside the cylinder is less than the atmospheric pressure. The similar logic can be defined for discharge valve.

And for the condition of Eq. (3:15),

$$p_r \leq p_{r \text{crit}} = \left(\frac{2}{k+1} \right)^{k/(k-1)} \quad (3:15)$$

The flow is choked, and the mass flow is independent of the downstream pressure.

The transported energy \dot{E}_h associated with the mass flow \dot{m} is given by Eq.(3:16).

$$\dot{E}_h = \dot{m} c_p T_u \quad (3:16)$$

The causality is indifferent for a conversion element like a valve, but since the cylinder head and ambient, prescribe pressure and temperature causally, then symmetrically, the valves will define mass and enthalpy flow.

Consider the 4-port R -element now called a pseudo-bond graph restrictor of **Figure 3.12**. As before the thermal bonds are shown dashed to distinguish them from the pneumatic bonds. Note that all bonds have effort in causality. This causality is the one most useful for the restrictor.

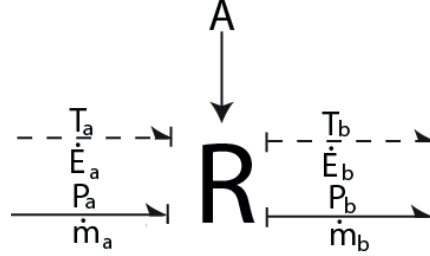


Figure 3.12 : Bond graph for the valve as isentropic nozzle.

Considering the principals described in section 4:2, the EMR representation of the valve is shown in Figure 3.13.

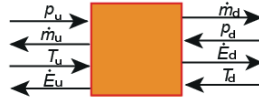


Figure 3.13 : EMR of Valves.

3.5.4 Heat Transfer Model

The rate of heat transfer between the gas and the cylinder head wall is modeled by a general approach given in Eq.(3:17).

$$\dot{Q}(t) = H_c(t)A_c(t)(T(t) - T_w(t)) \quad (3:17)$$

Where $H_c(t)$ is the instantaneous heat transfer coefficient, $A_c(t)$ the cylinder surface area exposed to convection, $T_w(t)$ the surface area temperature and $T(t)$ the instantaneous gas temperature.

One approach to model the heat transfer in reciprocating compressors may be that given by Eq. (12) developed by Adair [28]

$$H_c(t) = 0.053 \frac{k(t)}{D_p} (Re(t))^{0.6} (Pr)^{0.8} \quad (3:18)$$

Where Re and Pr numbers are based on flow prosperities, the flow speed and the cylinder diameter.

Since the flow regime is laminar ($500 < Re < 1500$) in the case under the study, and as Kim and Groll [35] suggested, the heat transfer coefficient of Annand [29] for reciprocating compressors is multiplied by a factor of three for heat transfer coefficient for a better prediction of the heat transfer rate as Todescat et al. [36] recommended. This method is applied in the simulation model. The resulting equation is setup as follows:

$$H_c(t) = 3 * 0.7 \frac{k(t)}{D_p} (Re(t))^{0.7} \quad (3:19)$$

Where Re is a function of the piston speed and diameter and thermal properties of air. Figure 3.14 Shows heat transfer rate between gas and wall and the average temperature in the cylinder during one cycle.

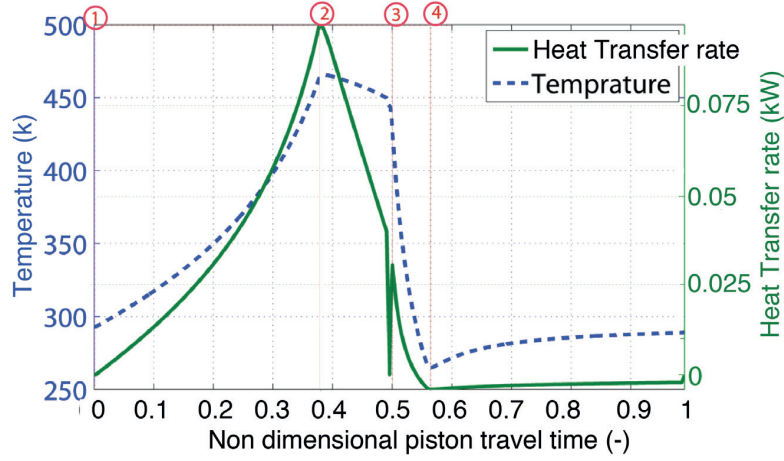


Figure 3.14 : Gas temperature and heat transfer rate from gas to cylinder wall.

One should note that the red numbers above the diagrams indicate the start of 1. Compression 2. Discharge 3. Expansion and 4. suction phase respectively.

Special attention has been paid to heat transfer considering the thermal resistor and capacitor effect of the walls, as well as effort generation due to prescribed temperature by cylinder head as a result of gas compression. The proposed thermoelectric analogy principal is showed in Figure 3.15.

One should note that resistor R_1 is the sum of the convection resistance between air and wall and half of conduction resistance in the wall, as shown by Eq.(3:20)

$$R_1 = R_a + \frac{R_b}{2} \quad (3:20)$$

As mentioned earlier, the cylinder head and ambient prescribes the temperature. Also as causality enforces, the piston wall as an accumulator can only define effort (temperature) variable to the resistances. On the other hand, the heat flows between gas and wall (\dot{Q}) and also between wall and ambient (\dot{Q}_2) will be prescribed by accumulator (note that the difference of these heat flows will be stored in the wall).

$$\dot{Q} = \dot{Q}_1 + \dot{Q}_2 \quad (3:21)$$

The heat stored in the wall of cylinder, is calculated by a capacitor C-element C_1 ,

$$T_w = \frac{1}{C_1} \int (\dot{Q} - \dot{Q}_2) dt \quad (3:22)$$

The details of the thermoelectric analogy will be described in Chapter 4, but it should be noted that throughout this text, the metal parts are shown in blue, while the gas is shown in pink.

Considering these facts the heat transfer EMR and bond graph will look like Figure 3.16 and **Figure 3.17** respectively.

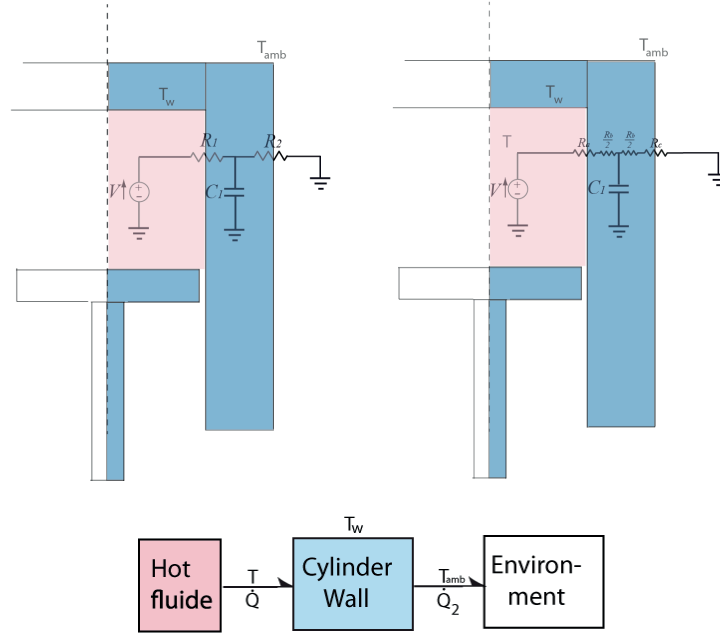


Figure 3.15 : Thermoelectric analogy of the piston.

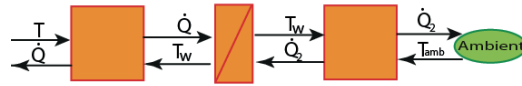


Figure 3.16 : EMR of heat transfer process.

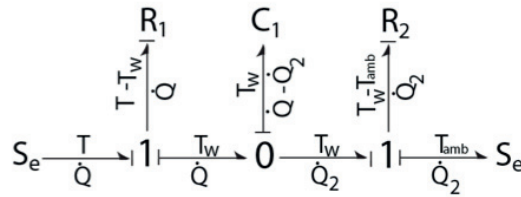


Figure 3.17 : Bond graph of heat transfer process.

3.5.5 Friction and Inertia Model

The major source of friction in a kinematic reciprocating piston is the sliding friction of the piston seals [56]. For most air compressor applications, the piston seals consist of split rings typically made of cast iron. The rings are preloaded against the cylinder walls by spring force in the rings. The design of the piston ring groove, seen **Figure 3.21**, allows the gas in the chamber to apply out-ward radial pressure to the piston ring, further increasing the pressure with the wall.

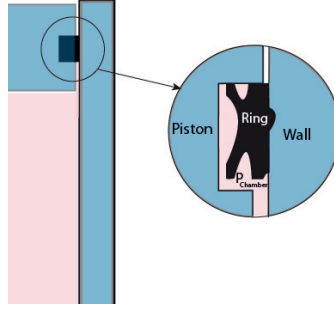


Figure 3.18 : Piston with piston ring. Note that the gas in the chamber applies pressure to the bottom and inside of the piston ring.

The force of the piston ring on the wall due to spring preload of the split piston ring is typically a fraction of the force created by the maximum gas pressure applied to the inner diameter of the piston ring [56]. The total pressure applied to the cylinder wall by the piston ring can be expressed as

$$p_{ring} = \alpha_{preload} p_{gas,max} + p_{gas} \quad (3:23)$$

Where p_{ring} is the ring pressure applied to the cylinder wall, $\alpha_{preload}$ is the fraction of the maximum gas pressure preload on the ring, $p_{gas,max}$ is the maximum gas pressure in the chamber, and p_{gas} is the gas pressure in the chamber. The sliding friction can be calculated from the normal force on the chamber wall and the coefficient of friction as follows:

$$F_f = p_{ring} A_p \varphi = (\alpha_{preload} p_{gas,max} + p_{gas})(\sigma \pi d) \varphi \quad (3:24)$$

Where F_f is the sliding friction, d is the inside diameter of the piston ring, σ is the vertical height of the piston ring, and μ is the sliding friction coefficient. Input variable to the numerical simulation of the frictional forces in classical compressor is given in **Table 3:3**.

The complete manufacturer data is available in Appendix IV.

Inertia of the moving mass should also be considered. The force of moving mass can be viewed as the product of cylinder mass and acceleration of the piston,

$$F_I = m_{cyl} \ddot{x}_p \quad (3:25)$$

This effect is shown in the very beginning and end of each compression and stroke as short pikes in **Figure 3.19**.

Table 3:3 input variables to the numerical simulation of the friction force in classical compressor.

Constant	Symbol	Value	Units
Piston ring sliding friction coefficient in compression	φ_1	0.18	-
Piston ring sliding friction coefficient in	φ_2	0.1	-

expansion			
Piston ring vertical height	σ	0.005	m
Piston ring preload fraction	$\alpha_{preload}$	0.25	-
Maximum gas pressure	$P_{gas,max}$	580	kPa

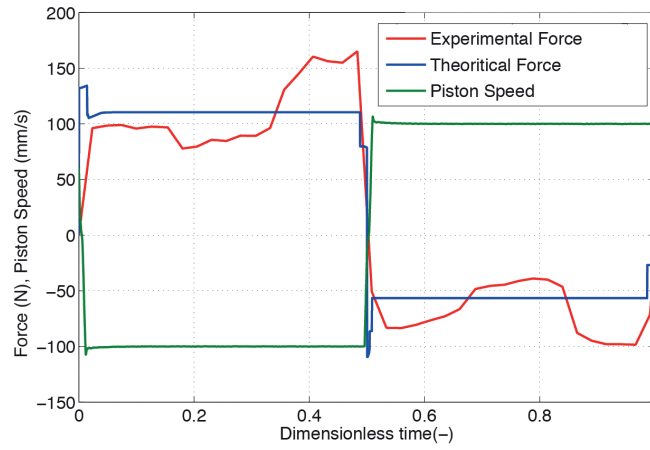


Figure 3.19 : No load force and speed in classic compressor.

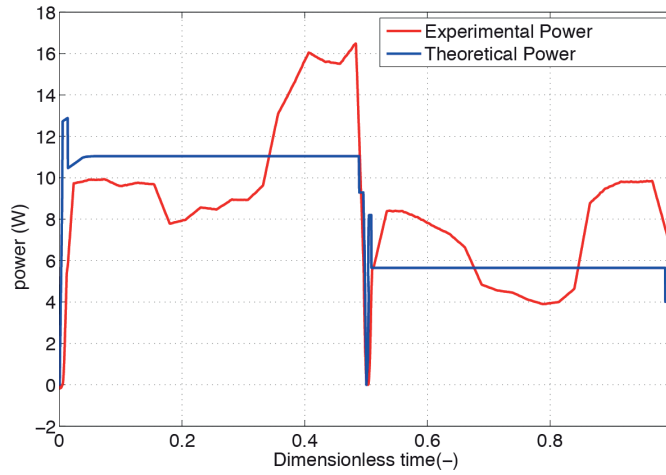


Figure 3.20 : No load power in classic compressor.

Experimental friction force in **Figure 3.19** indicates a stick-slip friction behavior. Simulation of such an effect is difficult because of strongly nonlinear behavior in the vicinity of zero velocity. Hence, for the sake of simplicity, we have considered a constant friction factor during compression and expansion. The theoretical and experimental friction power is also shown in **Figure 3.20**. The friction sub-model is integrated in the general model.

3.5.6 Leakage Model

Leakage can be simplest modeled as an isentropic compressible nozzle flow as described in Eq. (3:13), but the upstream and downstream pressures are chamber and ambient pressure respectively and throat area is the leakage area between cylinder and piston ring. This model assumes that the fluid is an ideal gas with compressibility taken into account, but there is no friction. If the imposed pressure ratio is large enough to obtain sonic conditions at the throat of the nozzle, the flow is choked.

3.5.7 Heat Exchanger Model

External heat exchangers like water intercoolers or water jacket around the cylinder can also be included. **Figure 3.21** shows a typical exchanger. The air enters the exchanger from inlet 1, and transfers its heat to cooling water and exits from outlet 2. Likewise the cooling water enters from 6 and absorbs the heat of hot air and exits from 7.

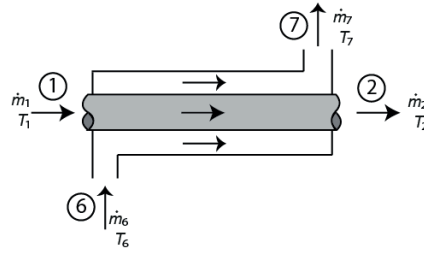


Figure 3.21 : Schematic of an interstage heat exchanger.

The conservation of mass and energy requires that:

$$\dot{m}_1 = \dot{m}_2, \dot{E}_2 = \dot{E}_1 - \dot{Q}_8, T_2 = \frac{\dot{E}_2}{\dot{m}_2 c_p} \neq T_1 \quad (3:26)$$

$$\dot{m}_6 = \dot{m}_7, \dot{E}_7 = \dot{E}_6 + \dot{Q}_5, T_7 = \frac{\dot{E}_7}{\dot{m}_2 c_p} \quad (3:27)$$

As described in section 0, one can consider a resistance for heat transfer between air and heat exchanger wall as R_1 and a resistance for heat transfer between heat exchanger wall and cooling water as R_2 .

$$R_8 = \frac{1}{h_8 A_8}, R_5 = \frac{1}{h_5 A_5} \quad (3:28)$$

The heat stored in the wall of heat exchange, is calculated by a capacitor C-element C_1 ,

$$T_4 = \frac{1}{C_1} \int (\dot{Q}_8 - \dot{Q}_5) dt \quad (3:29)$$

Figure 3.22 represents the model of the heat exchanger using EMR.

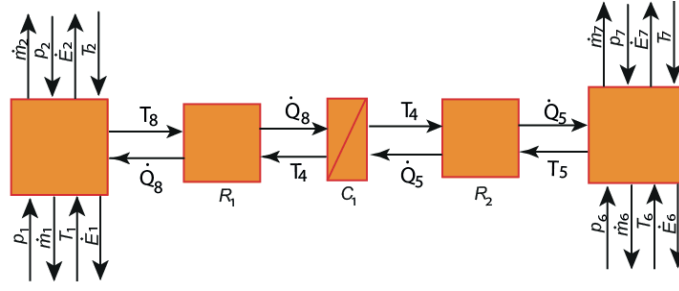


Figure 3.22 : EMR of heat exchanger.

3.5.8 Reservoir Model

If the compressor works between two fixed pressure levels, a source can be used for discharge and supply. But for the experimental verification, the compressed air provided by compressor will be stored in a reservoir. So, the discharge should be replaced by a reservoir. Due to the reservoir cumulative nature it can be demonstrated using EMR and bond graph representation as **Figure 3.23** and **Figure 3.24** respectively, which complies with causality principle. And the governing equations can be written as Eqs. (3:30) and (3:31)

$$m_{\text{Res}} = \int \dot{m} dt \quad (3:30)$$

$$U_{\text{Res}} = \int \dot{m}_e c_p T_e dt \quad (3:31)$$

The constitutive equations are similar to those developed for cylinder head.

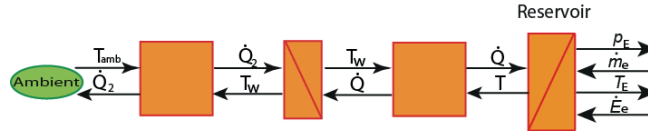


Figure 3.23 : EMR representation of Reservoir.

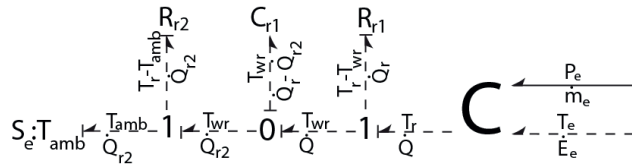


Figure 3.24 : Bond graph representation of Reservoir.

Heat transfer from reservoir can be considered, as done for the cylinder wall.

3.5.9 Complete Model of a Classic Compressor

The five previously developed sub models are assembled to form the complete EMR and bond graph model shown in **Figure 3.25** and **Figure 3.26** respectively. This EMR displays in one simple diagram the intricate mechanical-thermal interaction of the single stage compressor. The basic lumping process and the system structure are clearly indicated in these representations. They show all mass and

energy flow directions and causalities. The advantages of these techniques are clearly illustrated in that relatively complicated mechanical machines can be modeled by “assembling” a general set of building blocks.

The equations mentioned until now can be delivered to any explicit equation solver in any order desired. In this case we have used MATLAB Simulink for simulation. An integration algorithm will march the solution from one time step to next.

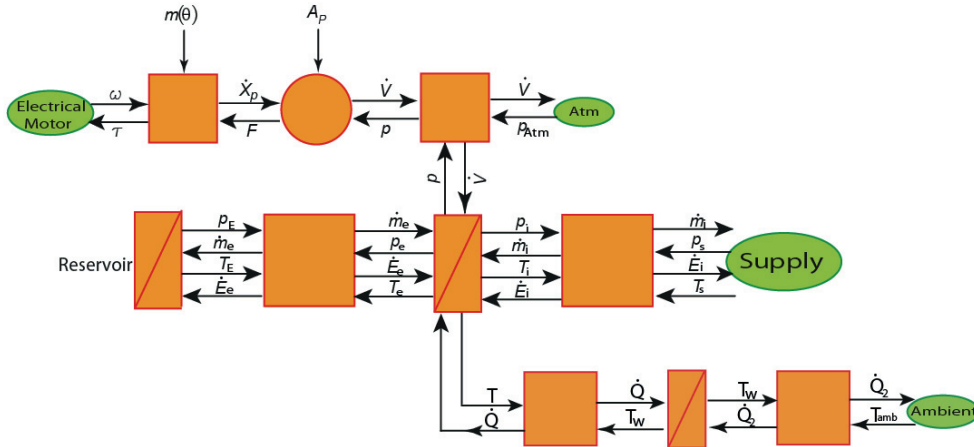


Figure 3.25 : complete system EMR.

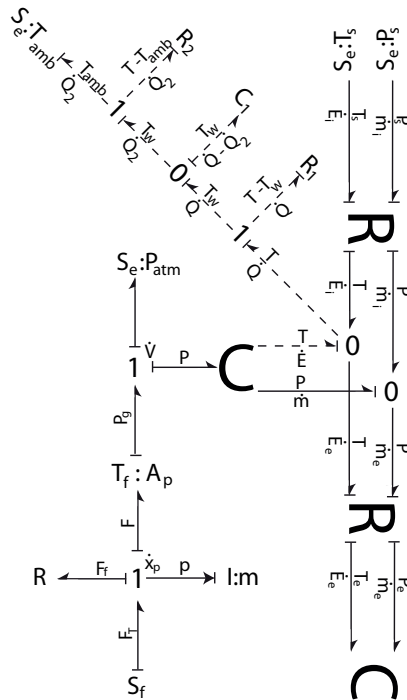


Figure 3.26 : complete system Bond Graph.

3.6 Simulation results

3.6.1 Model Inputs

The air compressor has a piston with diameter of 12.5 *cm* and a stroke of 98 *cm*. the dead volume was supposed to be 5% of the displacement volume. The period of a cycle is 1.98 seconds. The speed of the piston is constant during compression and expansion and is equal to 100 (*mm s*⁻¹). The reservoir is initially at ambient temperature and pressure and its volume is 25 liters, which is 20 times more than cylinder volume. Other inputs to the model are required to estimate the gas compression efficiency for the reciprocating piston and finned piston compressors using the above equations. These input variables are compiled in **Table 3:4**.

Table 3:4 Input variables to the numerical simulation of the classic piston model.

Constant	Symbol	Basic compressor	Units	Constant	Symbol	Basic compressor	Units
Maximum cylinder volume	V_{max}	0.0011	m^3	Reference dynamic viscosity	μ_0	$1.7 \cdot 10^{-5}$	$Pa \cdot s$
Dead Volume	V_0	0.00005	m^3	Initial temperature	T_0	293	kPa
Piston stroke	l	0.98	m	Initial pressure	p_0	100	kPa
Piston clearance	x_0	0.005	m	Maximum pressure	p_{max}	580	kPa
Piston Bore diameter	D_p	0.121	m	Inlet valve diameter	D_{vi}	0.006	m
Piston shaft diameter	D_0	0.03	m	Exit valve diameter	D_{ve}	0.006	m
Pressure compression ratio	p_r	5.8	—	Reservoir Volume	V_{Res}	0.025	m^3
Cycle period	T_{period}	1.98	s	Cylinder thickness	t_{cyl}	0.02	m
Piston linear speed	\dot{x}_p	0.1	m/s	Cylinder mass	m_{cyl}	3.2	kg

The model equations were programmed in a Matlab Simulink® environment for simulation. The results of the simulation have been shown in **Figure 3.27** and **Figure 3.28**. They show pressure, temperature, mass and volume for one cycle in a fixed pressure level mode. Above each figure the state of the piston is noted: point 1 is the start of the compression process and piston is its BDC, where the volume and mass in the cylinder has its maximum value. At the same time, pressure and temperature increases and when the pressure reaches the reservoir pressure (point 2) the discharge valve opens. Point 3 is the end of discharge process and immediately expansion begins, where in point 4 the inlet valve opens and the intake process starts. This cycle repeats over and over again but if the process is done in filling mode, of course the discharge (reservoir) pressure increases through the filling process.

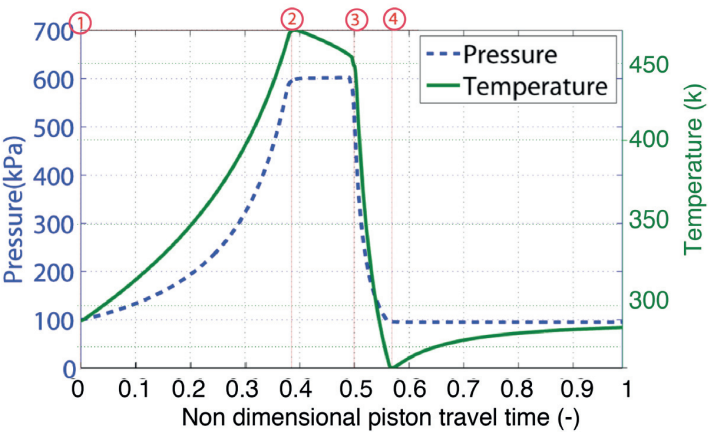


Figure 3.27 : Pressure and temperature of the gas inside the cylinder.

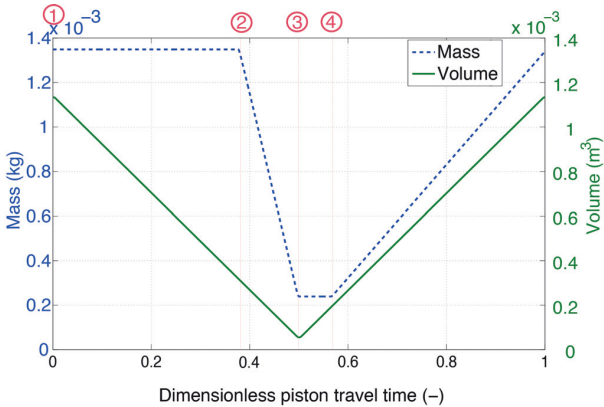


Figure 3.28 : Mass and volume of the gas inside the cylinder.

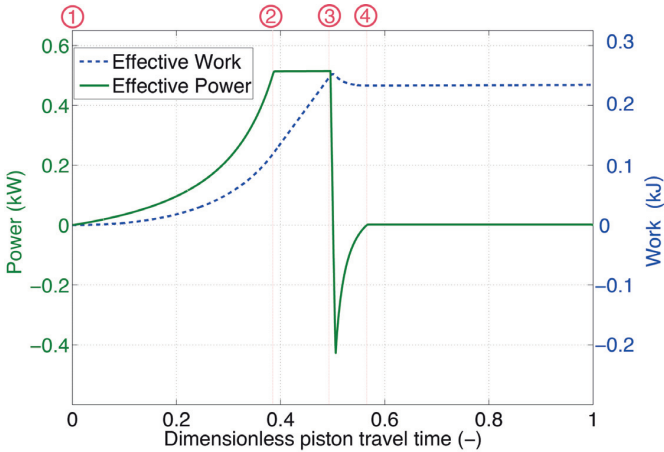


Figure 3.29 : Effective work and power of the compressor.

The results of the simulation are summarized in **Table 3:5**.

Table 3:5 Summary of the results of the numerical simulation of the classic piston model.

Constant	Symbol	Basic compressor	Units
Effective Work	W_{eff}	0.216	kJ/cyc
Friction Work	W_{frc}	0.038	kJ
Total Work	W_{tot}	0.255	kJ
Discharged Mass	m_{disch}	$1.098 \cdot 10^{-3}$	kg/cyc
Work per unit mass delivered	w_{eff}	195.3	kJ/kg
Volumetric efficiency	η_v	87.2	%
Exergy efficiency	$\eta_{x,cs}$	55.1	%
Isothermal efficiency	η_{iso}	76.2	%

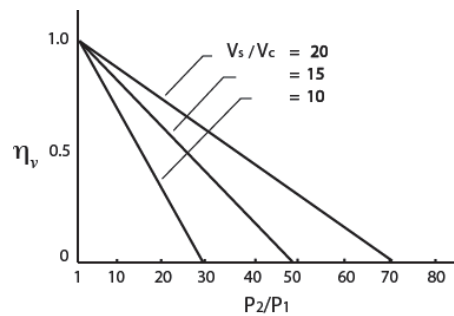
3.7 Multistage System

It is common practice for reaching high pressures to use several compression stages instead of one. In such configuration the discharge of each stage is the inlet of the next stage.

3.7.1 Multistage Air Compression

The use of single stage compression leads to low volumetric efficiencies if the pressure ratio p_2/p_1 is high, even if the valve pressure drops are small.

Based on Eq. AII:7, it can be seen from **Figure 3.30** that the volumetric efficiency diminishes rather rapidly as the clearance and the pressure ratio p_2/p_1 increases for a given magnitude of V_s . Indeed.

**Figure 3.30** : Effect of pressure ratio and clearance on volumetric efficiency.

Even with a machine where all processes are ideal there exists certain pressure ratio (p_2/p_1) at which no compressed air at all will be delivered. A single-stage compressor working at this pressure ratio would be a waste from practical standpoint. In a multistage compressor, air compression occurs in

several stages instead of one single stage. For total pressure ratio around 200 bar (for our case) usually 3-stage compression is enough [82].

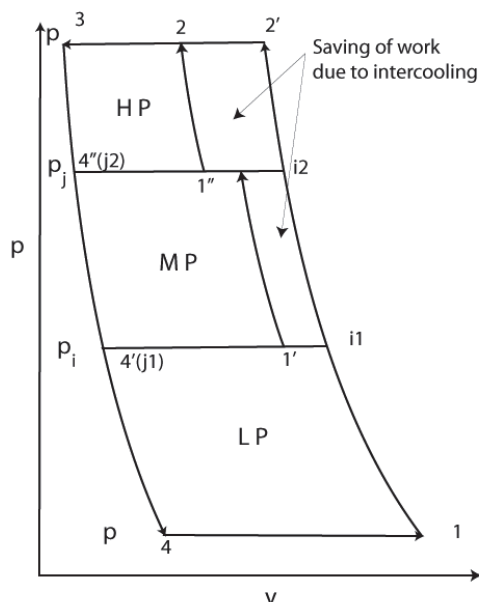


Figure 3.31 : ideal indicator diagram for a three-stage air compressor.

Each compressor stage is similar to a single-stage air compressor (**Figure 3.31**), except that the compressed air coming out of the first stage is the intake air for the second; the compressed air at a still higher pressure emerging from the second is the intake air for the third, and so on. The air from the last stage is delivered to a receiver where it will be stored for later use.

3.7.2 Optimum interstage pressure

Figure 3.31 shows the indicator diagram for an ideal three-stage compressor. For the low-pressure cylinder, 1-i1-j1-4 is the usual diagram. Let it be assumed that both compression and expansion processes are polytropic with exponent n , $1 < n < \gamma$. The temperature at i1, will naturally be higher than at the start of compression T_1 .

The air after leaving the low-pressure (LP) cylinder enters an intercooler where its temperature is brought down to $T_{1,}$, usually by using a cooling fluid at a temperature T_1 .

In practice the cooling process is accompanied by a pressure drop not considered here. Further the temperature of air after cooling 1' is never exactly equal to that at state 1, though for purposes of idealization we shall assume intercooling to be perfect with $T_1 = T_1$, if the valve pressure drop at entry and exit of the high pressure cylinder are neglected an indicator diagram for medium pressure cylinder will be 1'-2'-3'-4' as shown in **Figure 3.32**. It is seen from **Figure 3.32** that the polytropic compression between pressure p_1 and p_2 , while it is now the curve 1'-2'-4''-4'. There has been a saving in work input given by the area i1-1'-1''-2-2'-i2. If there are more than three stages, similar diagrams can be drawn to indicate saving in work in every intermediate pressure and high pressure cylinder.

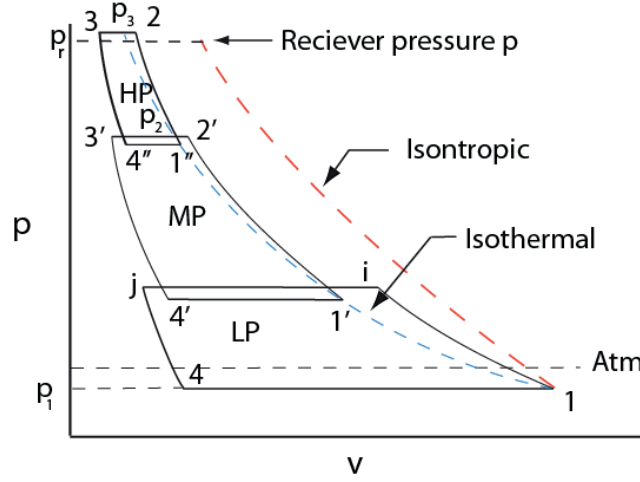


Figure 3.32 : Indicator diagram for three-stage compression.

The total work is the sum of the work in each stage as described by Eq. (3:32)

$$W = W_1 + W_2 + W_3 = \frac{mnRT_1}{n-1} \left\{ \left[1 - \left(\frac{P_{i1}}{P_1} \right)^{\frac{n-1}{n}} \right] + \left[1 - \left(\frac{P_{i2}}{P_{i1}} \right)^{\frac{n-1}{n}} \right] + \left[1 - \left(\frac{P_2}{P_{i2}} \right)^{\frac{n-1}{n}} \right] \right\} \quad (3:32)$$

In all three cylinders, the compression is assumed to be polytropic, with an exponent n such that $1 < n < \gamma$ as before. It is therefore seen that the total work $|W|$ is minimum for given magnitude of P_1 and P_2 if $\frac{dW}{dP_i} = 0$, One thus gets:

$$\frac{dW}{dP_i} = \frac{mnRT_1}{n-1} \left\{ -\frac{n-1}{n} \left(\frac{P_{i1}}{P_1} \right)^{-1/n} \left(\frac{1}{P_1} \right) + -\frac{n-1}{n} \left(\frac{P_{i2}}{P_{i1}} \right)^{-1/n} \left(\frac{1}{P_{i1}} \right) + -\frac{n-1}{n} \left(\frac{P_{i1}}{P_1} \right)^{-1/n} \left(\frac{1}{P_1} \right) + -\frac{n-1}{n} \left(\frac{P_2}{P_{i2}} \right)^{-1/n} \left(\frac{1}{P_{i2}} \right) \right\} \quad (3:33)$$

Which gives,

$$P_{i1} = (P_1^2 P_2)^{1/3} \quad (3:34)$$

And

$$P_{i2} = (P_1 P_2^2)^{1/3} \quad (3:35)$$

Eqs. (3:34) and (3:35) demonstrate that for minimum work input, the optimum interstage pressures should be the geometric means of its two intermediate neighboring pressures in our three-stage air compressor.

For our case since $P_1 = 1 \text{ Bar}$; $P_2 = 200 \text{ Bar}$ we have:

$$P_{i1} = 5.8 \text{ Bar} ; P_{i2} = 34 \text{ Bar} \quad (3:36)$$

With these intermediate pressures, the minimum work needed to drive a three-stage air compressor with perfect intercooling is seen to be:

$$W_{\min} = \frac{3mnRT_1}{n-1} \left[1 - \left(\frac{P_2}{P_1} \right)^{(n-1)/3n} \right] \quad (3:37)$$

Then equal amount of work are needed for each cylinders. In a similar way, for a multistage compressor with more than three stages, each intermediate pressure may be shown to be the geometric means of its two intermediate neighboring pressures. In the mathematical language this is equivalent to the equation:

$$\frac{P_{i1}}{P_1} = \frac{P_{i2}}{P_{i1}} = \dots = \frac{P_2}{P_{i(N-1)}} = \left(\frac{P_2}{P_1} \right)^{1/N} \quad (3:38)$$

Where $P_{i1}, P_{i2}, \dots, P_{i(N-1)}$ are the respective intermediate pressure in a compressor with N stages, P_1 and P_2 being respectively the intake and delivery pressures. Then, the work input to all the stages is the same. Eq. (3:38) applies to a multistage compressor with perfect intercooling, where the intercooler reduces the temperature at the end of each compression stage to the atmospheric value. If however, intercoolers are not perfect, the intercooler effectiveness will have to be taken into account. Since the intercooler is a simple heat exchanger its effectiveness (efficiency) may be defined by the expression:

$$\varepsilon = \frac{h_{i1} - h'_{i1}}{h_{i1} - h_1} = \frac{T_{i1} - T'_{i1}}{T_{i1} - T_1} \quad (3:39)$$

Where h'_{i1} and T'_{i1} are respectively the enthalpy and temperature of the air at the exit intercooler, h_1, T_1 and h_{i2}, T_{i2} being the corresponding properties of point 1, i_1 and i_2 respectively for a 3-stage compressor (**Figure 3.32**). The second part of Eq. (3:39) is obtained assuming constant specific heat of air.

3.7.3 Energy exchange in Multistage Compression

As mentioned previously, multistage compressor cylinder heads are usually cooled and further, the compressed air is cooled to reduce its temperature. Assuming perfect intercooling, an expression will now be derived to determine the energy abstracted as heat during compression and intercooling in every stage.

Let it be assumed that the compression curve is a polytropic with exponent n . during compression, the effect of cooling the cylinder is to abstract an amount of energy given by the first law equation

$$Q_c = W_c + \Delta U \quad (3:40)$$

As applied to a closed assembly. Here, W_c is the work of compression in a polytropic process $-mR(T_2 - T_1)/n - 1$ and ΔU is the change of internal energy $mc_v(T_2 - T_1)$. Thus, it is seen that:

$$\begin{aligned} Q_c &= \frac{mR(T_2 - T_1)}{n-1} + \frac{mR(T_2 - T_1)}{\gamma-1} \\ &= \frac{mR(n-\gamma)}{(n-1)(\gamma-1)}(T_2 - T_1) = \frac{mc_v(n-\gamma)}{(n-1)}(T_2 - T_1) \end{aligned} \quad (3:41)$$

After compression, the air enters the intercooler and is cooled at constant pressure to temperature T_1 . The energy transfer in intercooler is given by:

$$Q_i = mc_p (T_2 - T_1) \quad (3:42)$$

So the total energy exchange is:

$$\begin{aligned} Q = Q_i + Q_c &= m \left[c_p + c_v \frac{(n-\gamma)}{(n-1)} \right] (T_2 - T_1) \\ &= \frac{mn}{n-1} R (T_2 - T_1) \end{aligned} \quad (3:43)$$

It is thus seen that the total energy rejected is equal to the work of compression in each compressor stage.

3.8 Conclusion

In this chapter a model for a reciprocating linear piston air compressor was developed. This model contains different sub-models like cylinder head, driver, valves and heat transfer. This model is represented by two methods: EMR and bond graph. Each of these methods have their own strength but should be modified in order to be used in an open thermodynamic system. This was done using pseudo EMR and pseudo bond graph. Next, the results of the simulated model is represented. At the end since the final compression will be a multi-stage one, such aspects have been considered as well.

Chapter 4 Finned Piston Compressor

Analytical Model

4.1 Introduction

In this chapter, the goal is to develop a comprehensive model for the finned piston based on what was developed in Chapter 3 for a classic compressor. First the components of the finned piston and their functions are described together with the way the finned compressor works. Then a so-called Thermofluid-Electric analogy is introduced as the tool to model the finned piston. Then the principle of such analogy is described namely: Thermo-Electric and Pneumatic-Electric analogies. These analogies are first used to model a simple compressor and then extended to construct the finned piston model. At the end of this chapter some simulation results of finned compressor are presented and compared to the classic piston.

4.2 Finned Compressor Description

The principle of increasing the heat exchange surface through the use of differential pistons can be extended to the situation where the full volume occupied by a cylinder/piston unit is filled with imbricated fins as described in Chapter 1. In such a case, multiple layers of annular differential pistons are arranged within the same compression/expansion chamber, and correspond effectively to a concept of the integrated heat exchanger. Such geometry is represented in its principle in **Figure 4.1**. For simplicity only the upper half of the fins is represented. In such a case, one mobile assembly of differential layers is sliding inside of a fixed assembly of fins. In the center of the cylinder, there is a shaft for guiding the mobile equipment inside the fixed one, and that allows designing the system with a small distance between the fins. Considerations related to the inter-fin space will be done in relation with the calculation of the effect of a «dead» volume.

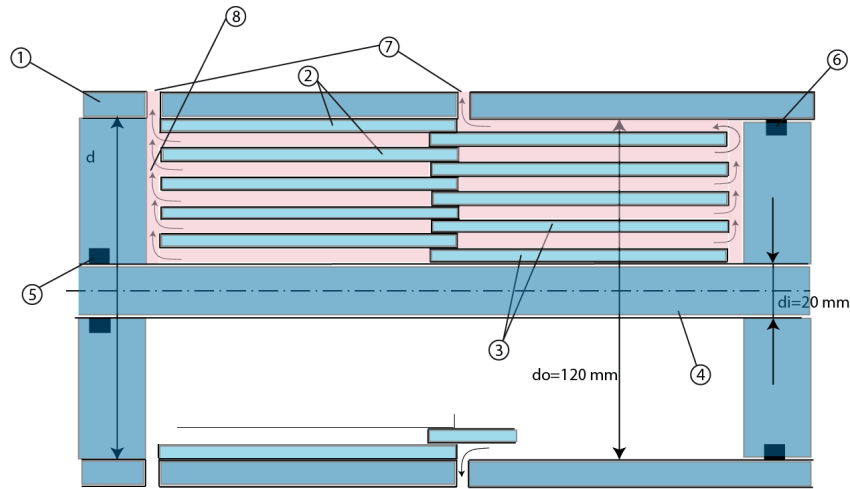


Figure 4.1 : Schematic representation of the Integrated Heat Exchanger Concept.

The parts numbered on the figure are:

- 1) External cylinder
- 2) Stator fins
- 3) Sliding fins
- 4) Guiding rod
- 5) Stator seal (rod-seal)
- 6) Piston-seal
- 7) Gas Inlet/outlet
- 8) Radial path

The inlet/outlet of the compressed/expanded gas in such a concept is realized through radial paths, allowing the access to the internal layers. The radial paths can be arranged on both sides of the cylinder, eventually at the whole periphery.

On the left side of **Figure 4.1**, the radial in/outlet is shown, and corresponds to the access to the annular compression/expansion annular chambers of the fixed (stator) part. In the middle of the figure, the radial in/outlet path is represented for the mobile (piston-side) annular chambers. It is evident that the two paths must be connected to the same in/outlet circuit or valve, using a manifold collector.

The force-active surface of such an Integrated Heat Exchanger Piston is equal to the full surface of a normal piston with identical external diameter, from which the occupied surface of the guiding shaft in the center must be subtracted.

It should again be noted that throughout this text, the metal parts are shown in blue, while the gas is shown in pink. In **Figure 4.2**, particularly the Main Compression Chambers (MCC) is shown in part a, with a sliding fin at the right side, pushing the air that is confined by two stator fins to the left. In part b) of the same figure, Inter Fin Space (IFS) is magnified which is surrounded by a sliding fin above and stator fin below it.

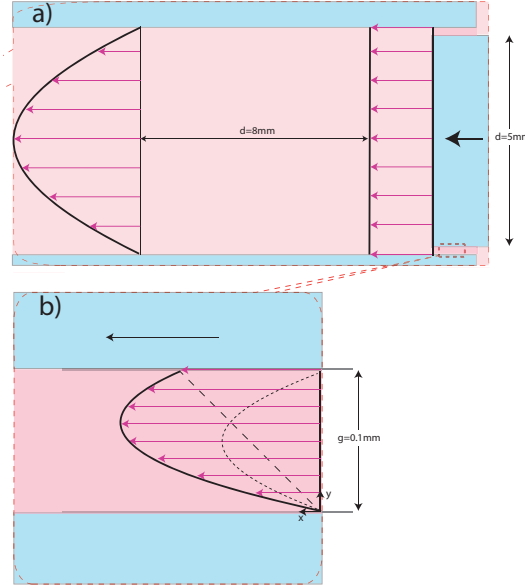


Figure 4.2 : Fluid flow in a) Main Compression Chamber (MCC) and b) Inter Fins Space (IFS).

4.3 Principle Of Thermoelectric Analogy

There is a great interest in using thermal resistance or thermoelectric analogy for modeling the system containing several layers. In this method, the heat flow is analogous to electrical current and temperature is analogous to electric voltage. One should note that thermal resistance of a medium depends on the geometry and thermal properties of the medium.

Heat flow through a layer can be written as:

$$\dot{Q} = \frac{T_1 - T_2}{R} \quad (4:1)$$

Where for conduction it can be written as

$$R_{Cond} = \frac{L}{kA} \quad (4:2)$$

Where R_{Cond} is the thermal resistance of the wall against heat conduction or simply the conduction resistance of the wall. And for convection can be written as

$$R_{Conv} = \frac{1}{hA} \quad (4:3)$$

Anyway the thermal resistance can also be expressed as

$$R_{wall} = \frac{\Delta T}{\dot{Q}} \quad (4:4)$$

Which is the ratio of the driving potential ΔT to the corresponding transfer rate \dot{Q} . This equation of heat transfer is analogous to the relation for electric current flow I , expressed as

$$I = \frac{Vo_a - Vo_b}{R_e} \quad (4:5)$$

Where R_e is the electric resistance and $V_a - V_b$ is the voltage difference across the resistance. Thus, the rate of heat transfer through a layer corresponds to electric current, the thermal resistance corresponds to electrical resistance, and the temperature difference corresponds to voltage difference across the layer. The same concept can be used to solve steady heat transfer problems that involve parallel or combined series-parallel arrangements. This concept can also be used for two- or even three-dimensional problems.

Consider a composite arrangement consisting of a layer of air (pink) and a layer of metal (blue) shown in **Figure 4.3**. It is assumed that the dominant heat transfer mode in the air is by convection, while in metal heat flows by conduction mechanism. In case (1) the layers are in series arrangement. It can be shown that total thermal resistance in this case is the addition of the resistances, while in case (2) where the layers of air and metal are in parallel, the total resistance is the multiplication of resistances over their sum. Thermal resistance network for combined series-parallel arrangement, can be described as the addition of the total of the parallel resistance and the resistance in series (case 3)[41].

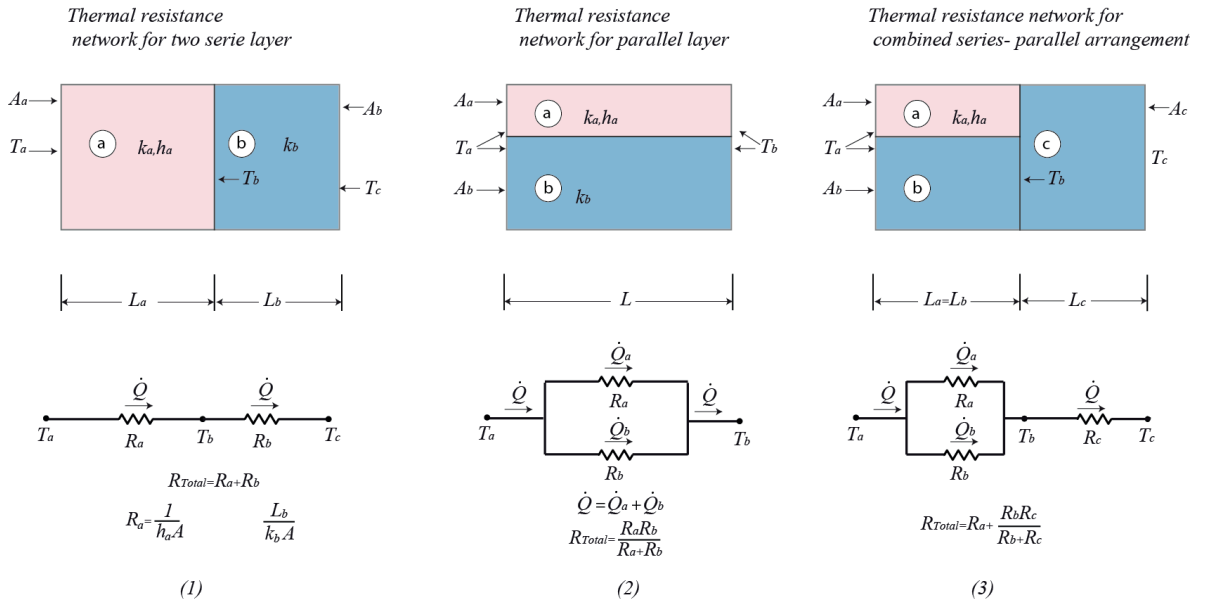


Figure 4.3 : Thermal resistance network for combined series-parallel arrangement.

4.4 Adaptation Of Thermo-Electric Analogy To Cylinder-Piston Assembly

In section 4.3 it is assumed that the heat flow is uniform along the system that means no heat is being stored in the body of layers. However in unsteady heat transfer analysis (which is the case for reciprocating compressors) this assumption is not always true, since a part of the heat can be stored in the metal. This will cause the introduction of a capacitor in the circuit. Consider a simple cylinder-piston assembly shown in **Figure 4.4**. While the piston compresses the gas, its temperature rises because the gas pressure increases. This acts as a heat generator, and since the temperature is being imposed by the cylinder head, it can be represented by a voltage source with a ground connection. The heat transfers to the first resistance R_1 , being the sum of convection resistance and half of conduction resistance in the metal.

$$R_1 = R_a + \frac{R_b}{2} \quad (4:6)$$

Where

$$R_a = R_{Conv} = \frac{1}{H_1 A} \quad (4:7)$$

In which convection coefficient H_1 can be defined for air with conductivity coefficient k_a and area A , as

$$H_1 = Nu \frac{k_a}{D_h} \quad (4:8)$$

Where Nusselt number for laminar flow in concentric annular passages are formulated by [39] by $\pm 20\%$ accuracy (it is described in more details in appendix I) for inner and outer annulus as

$$Nu_i = 7.54(r^*)^{-0.5} \quad (4:9)$$

$$Nu_o = 7.54(r^*)^{0.18}$$

Where r^* is the inner to outer annulus radius ratio:

$$r^* = \frac{r_i}{r_o} \quad (4:10)$$

And for a metallic cylinder in cylindrical coordinates with inner diameter of D_1 and outer diameter of D_2 and conductivity of k and thickness of l ,

$$R_b = R_{Cond,Metal} = \frac{\ln(D_2/D_1)}{2\pi l k} \quad (4:11)$$

So finally

$$\dot{Q} = \frac{T - T_w}{R_1} \quad (4:12)$$

One should note that as Kirchhoff current law indicates a part of the convected heat (\dot{Q}) will be stored in the wall (\dot{Q}_1) while a part will be released to ambient (\dot{Q}_2).

$$\dot{Q} = \dot{Q}_1 + \dot{Q}_2 \quad (4:13)$$

In the linear case a thermal capacitance can be defined such that

$$T_w = T_{w0} + \int_{t_0}^t \dot{Q}_1 dt \quad (4:14)$$

Where T_{w0} is the temperature $t = t_0$. The capacitance C can be found by assuming that the cylinder body does negligible work by expanding or contracting, so the changes in its internal energy are only the result of \dot{Q}_1 . Then if c is a *specific heat*,

$$c = \frac{\partial u}{\partial T} \quad (4:15)$$

Where u is the internal energy per unit mass

$$C = mc \quad (4:16)$$

And m is the mass of cylinder body.

From the other side \dot{Q}_2 that is the heat transfer between the metal and outside ambient air is

$$\dot{Q}_2 = \frac{T_w - T_{amb}}{R_2} \quad (4:17)$$

Where the second resistance R_2 , is the sum of half of the conduction resistance in the metal and convection resistance

$$R_2 = \frac{R_b}{2} + R_c \quad (4:18)$$

Where R_b was defined already in Eq. (4:11) and for the free convection from a cylinder, one can use the Rayleigh number computed approximately as

$$Ra = \frac{g c_p}{T v^2 \mu k} D^3 (T_w - T_{amb}) \quad (4:19)$$

Where g is the acceleration of gravity, T is the absolute temperature average of the surface of the cylinder and the environment (for an ideal gas only), v is the associated specific volume, k is the thermal conductivity, D is the diameter, and $T_w - T_{amb}$ is the temperature difference between the surface and the environment. For Ra in the usual wide range of 10^4 to 10^8 (for laminar flow), the Nusselt number is claimed by McAdams [83] to be well approximated by

$$Nu = 0.53 Ra^{0.25} \quad (4:20)$$

So the thermal resistance can be viewed as

$$R_c = R_{Conv,amb} = \frac{1}{\pi l k Nu} \quad (4:21)$$

Where L is the length of the cylinder. Finally, the heat flux that will be imposed to the cylinder head is

$$\dot{Q} = p\dot{V} + \dot{E}_e - \dot{E}_i + \dot{U} \quad (4:22)$$

The representation of such a model can be seen in **Figure 4.4**.

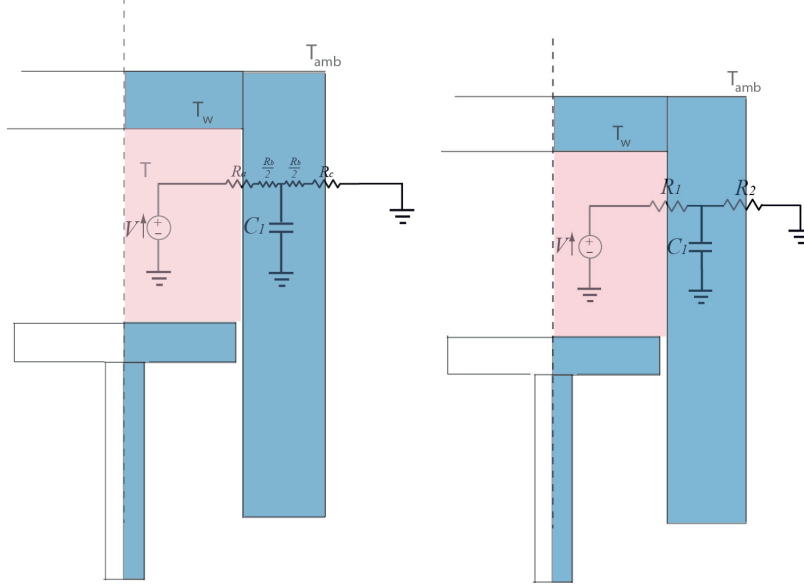


Figure 4.4 : Thermo-electric analogy for a cylinder-piston assembly.

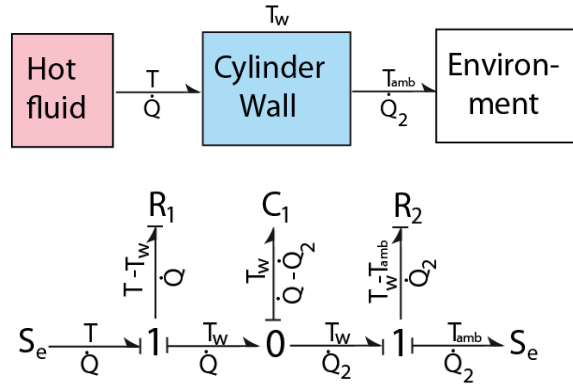


Figure 4.5 : Bond graph representation of the developed thermo-electric analogy.

The values of R_a , R_b and R_c are shown in **Figure 4.6** for three cycles. Because the values of air velocity and the inside area of cylinder surface changes alternatively over a cycle R_a is variable. It is observed that R_b value is very low compared to R_a and R_c . Also R_c can be decreased by applying a water jacket around the cylinder, so it seems the bottleneck in heat transfer enhancement is R_a .

This fact has been shown in **Figure 4.7**, similar to what is demonstrated by [41]. The passengers want to leave the island, and however there are enough ships ready in the harbor to take them to the mainland; the number of buses is not sufficient!

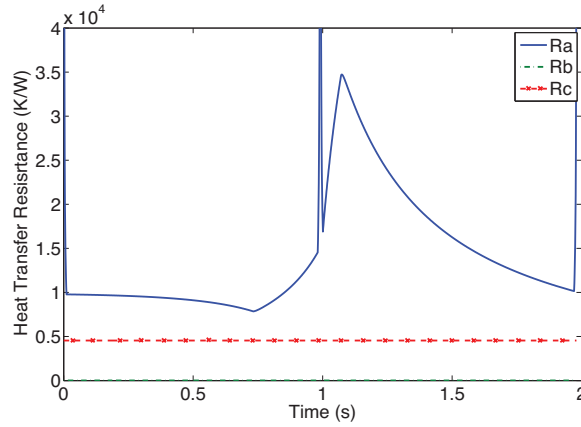


Figure 4.6 : Thermal resistance variation during one cycle.

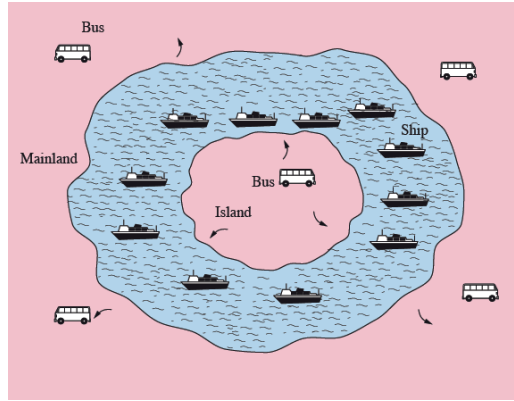


Figure 4.7 : Analogy between low convection heat transfer between compressed gas and cylinder body and shortage of bus in the island (concept taken from [41]).

4.5 Development of Thermo-Electric Analogy For The Finned Piston Model

The low rate of heat transfer in classic cylinders motivated to design a finned piston in order to increase the overall heat transfer coefficient. The advantages of such a piston is that it increases both heat transfer coefficient and heat transfer area. Consider again equation (4:8). By using a finned piston like the one in **Figure 4.8**, the hydraulic diameter will be 0.005 m instead of 0.125 m for a classic piston. Since, heat transfer coefficient is proportional to inverse of D_h . This means that heat transfer coefficient will be almost 25 times more than the classic piston. Apart from that it is interesting to evaluate the heat transfer area increment in finned piston compared to a classic piston.

Figure 4.8 shows a classic as well as a finned piston at Bottom Dead Center (BDC), where piston is at its full expansion and Top Dead Center (TDC) where it is at its full compression. **Figure 4.9** shows the heat transfer rate and temperature of a classic compressor over one cycle. It is instructive to notice that in reciprocating compressor the highest potential of heat transfer is at TDC (because of high temperature difference), but ironically the heat transfer area is very small since the piston is at its closest position to the cylinder head. The advantage of a finned piston is that the heat transfer area will remain constant and independent of the position of the piston, since there is a gap between fines and this allows the heat transfer to occur on the entire fines surface. **Figure 4.10** shows that the heat transfer

area is 52 times more at BDC and 1077 times more at TDC. As it will be seen later, this along with higher heat transfer coefficient leads to a dramatic increase in heat transfer amount.

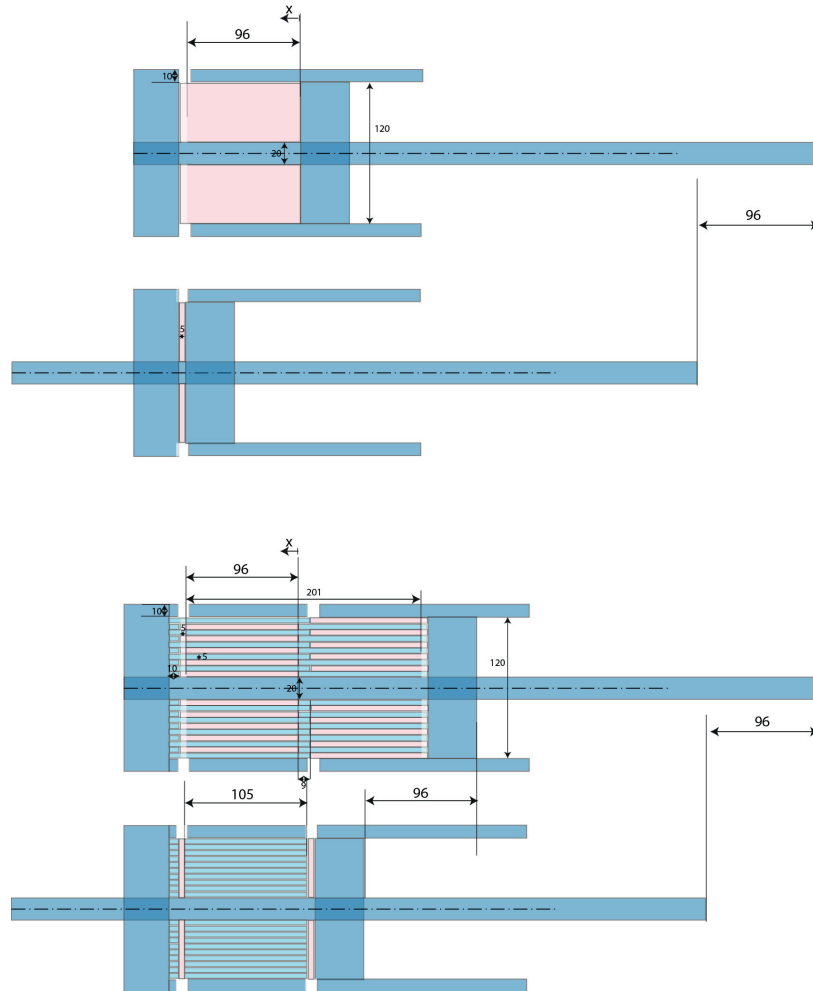


Figure 4.8 : Classic and finned piston positions at BDC and TDC

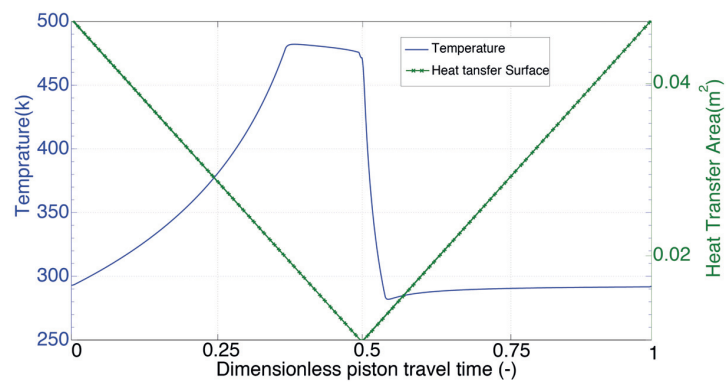


Figure 4.9 : Gas temperature and heat transfer area from gas to cylinder wall in classic compressor.

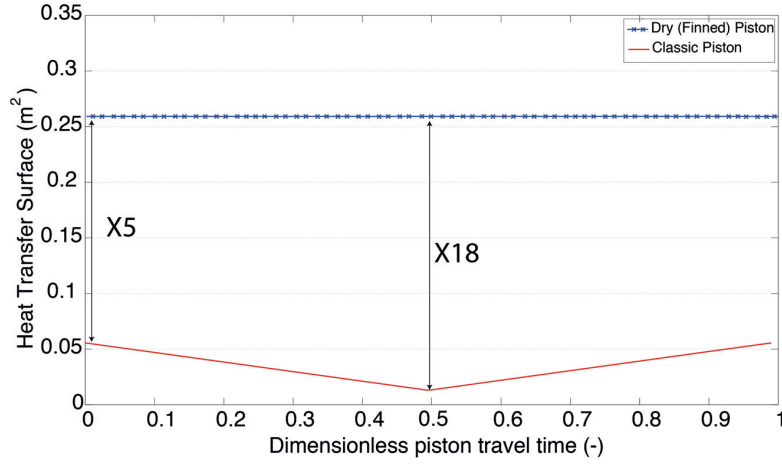


Figure 4.10 : Heat transfer area comparison during one cycle.

In **Figure 4.11** the equivalent circuit is constructed for a finned piston based on the same principles describe in section 3. In fact, air chambers (pink) can transfer the heat to their neighbor walls. As described in section 3, each resistant is the sum of the convection resistance and half of the conduction resistance of the neighbor wall. For example R_{11} is

$$R_1 = R_a + \frac{R_b}{2} \quad (4:23)$$

Generally an indexed resistance R_{ij} , where i is the number of chamber or its corresponding vertical fin, shows the heat transfer resistance between:

R_{i1} : air chamber and inner adjacent annulus in radial direction.

R_{i2} : air chamber and outer adjacent annulus in radial direction.

R_{i3} : air chamber and its corresponding vertical fin in axial direction.

R_{i4} : fin and upper cylinder wall in axial direction.

R_{i5} : air chamber and inner adjacent annulus (within inter fin space) in radial direction.

R_{i6} : air chamber and outer adjacent annulus (within inter fin space) in radial direction.

R_{i7} : fin and lower cylinder wall in axial direction.

One may notice that while the air chambers generate heat, a part of this heat will be stored in the fins and the rest will be released to the environment. Also to account for the heat transfer in axial direction a vertical network is implemented in the circuit. It is assumed that cylinder is axisymmetric around its axis. It should be reminded that most of the resistance and capacitors are nonlinear and variable with time (Like R_a in **Figure 4.6**). Vectorized code technique was used in programming to facilitate the computation of these values.

Another important consideration is the heat transfer within the inter fin space (There is a 0.1mm distance between the fins). Heat transfer in this area is called "Inter fins heat transfer" and contributes greatly to the total heat transfer, because the flow velocity is relatively high thanks to the very small area.

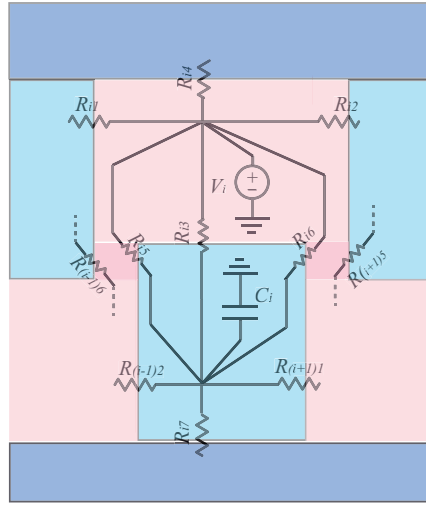


Figure 4.11 : Equivalent electrical circuit for thermo-electric analogy.

The Thermo-Electric network can be expanded to a finned piston with four chambers as shown in **Figure 4.12**. One should note that the model has been developed for 10 chamber (Complete piston), but for the sake of simplicity in demonstration only 4 chambers have been illustrated.

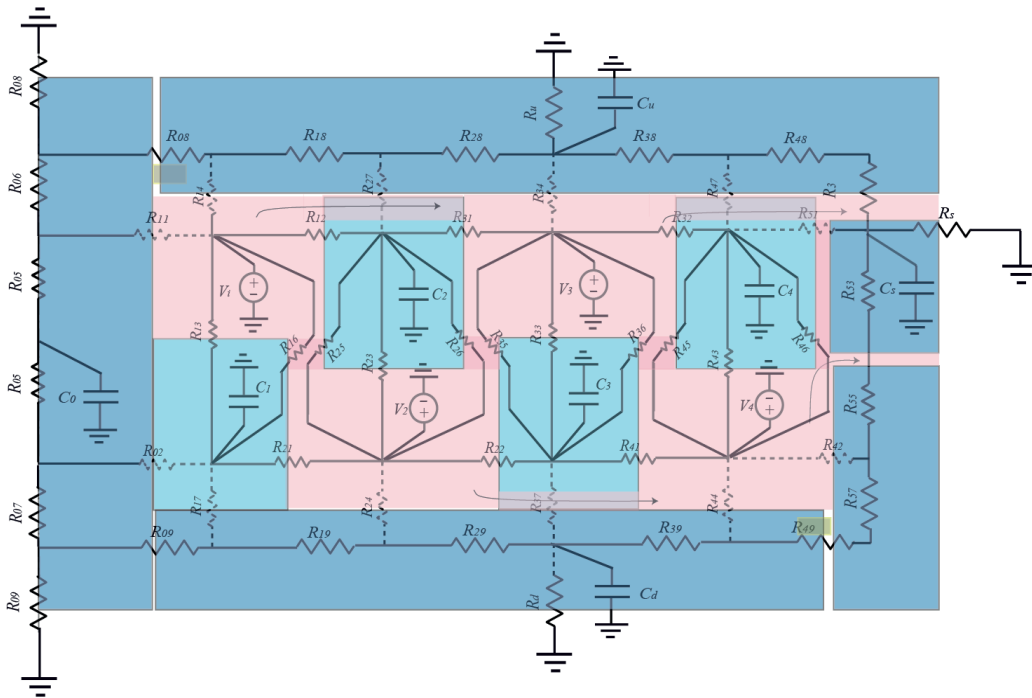


Figure 4.12 : Equivalent electrical circuit for thermoelectric analogy (entire piston).

Finally, the bond graph representation of the heat transfer part is shown in **Figure 4.13**.

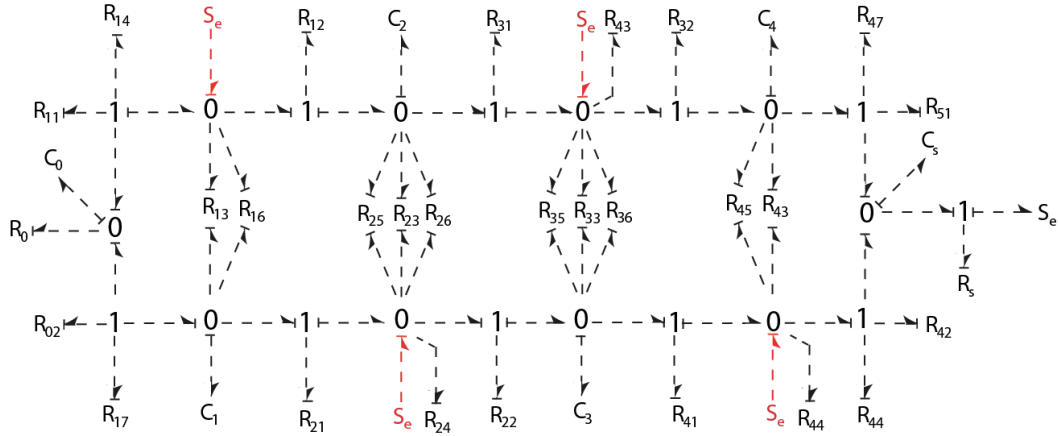


Figure 4.13 : Bond graph representation of the heat transfer in a finned compressor

4.5.1 State space equations

In studying complicated systems like the system described, there is an ideal opportunity to start the formulation in terms of significant physical variables and to generate simultaneous set of first-order equations. The state vector differential equations for the heat transfer part (neglecting dashed resistances in **Figure 4.12**) can be written as:

$$\dot{X} = AX + BU \quad (4:24)$$

$$Y = CX + DU \quad (4:25)$$

Considering wall temperatures as state variables, chamber temperatures as input and heat flow rate as the output:

$$X = \begin{bmatrix} T_{w1} \\ T_{w2} \\ T_{w3} \\ T_{w4} \end{bmatrix}; U = \begin{bmatrix} T_1 \\ T_2 \\ T_3 \\ T_4 \end{bmatrix}; Y = \begin{bmatrix} \dot{Q}_1 \\ \dot{Q}_2 \\ \dot{Q}_3 \\ \dot{Q}_4 \end{bmatrix} \quad (4:26)$$

Neglecting the dashed part of the circuit in **Figure 4.12**, the state matrixes A, B, C and D can be found as:

$$A = \begin{bmatrix} \frac{1}{m_{w1}c_{w1}} \left(\frac{1}{R_{21}} + \frac{1}{R_{13}} + \frac{1}{R_{16}} \right) & 0 & 0 & 0 \\ 0 & \frac{1}{m_{w2}c_{w2}} \left(\frac{1}{R_{12}} + \frac{1}{R_{31}} + \frac{1}{R_{23}} + \frac{1}{R_{25}} + \frac{1}{R_{26}} \right) & 0 & 0 \\ 0 & 0 & \frac{1}{m_{w3}c_{w3}} \left(\frac{1}{R_{22}} + \frac{1}{R_{41}} + \frac{1}{R_{33}} + \frac{1}{R_{35}} + \frac{1}{R_{36}} \right) & 0 \\ 0 & 0 & 0 & \frac{1}{m_{w4}c_{w4}} \left(\frac{1}{R_{32}} + \frac{1}{R_{43}} + \frac{1}{R_{45}} \right) \end{bmatrix} \quad (4:27)$$

$$B = \begin{bmatrix} \frac{1}{m_{w1}c_{w1}}\left(\frac{-1}{R_{13}} + \frac{-1}{R_{16}}\right) & \frac{1}{m_{w1}c_{w1}}\left(\frac{-1}{R_{21}}\right) & 0 & 0 \\ \frac{1}{m_{w2}c_{w2}}\left(\frac{-1}{R_{12}}\right) & \frac{1}{m_{w2}c_{w2}}\left(\frac{-1}{R_{23}} + \frac{-1}{R_{25}} + \frac{-1}{R_{26}}\right) & \frac{1}{m_{w2}c_{w2}}\left(\frac{-1}{R_{31}}\right) & 0 \\ 0 & \frac{1}{m_{w3}c_{w3}}\left(\frac{-1}{R_{22}}\right) & \frac{1}{m_{w3}c_{w3}}\left(\frac{-1}{R_{33}} + \frac{-1}{R_{35}} + \frac{-1}{R_{36}}\right) & \frac{1}{m_{w3}c_{w3}}\left(\frac{-1}{R_{32}}\right) \\ 0 & 0 & \frac{1}{m_{w4}c_{w4}}\left(\frac{-1}{R_{41}}\right) & \frac{1}{m_{w4}c_{w4}}\left(\frac{-1}{R_{43}} + \frac{-1}{R_{45}}\right) \end{bmatrix} \quad (4:28)$$

$$C = \begin{bmatrix} \frac{-1}{R_{11}} + \frac{-1}{R_{13}} + \frac{-1}{R_{16}} & \frac{-1}{R_{12}} & 0 & 0 \\ \frac{-1}{R_{21}} & \frac{-1}{R_{23}} + \frac{-1}{R_{25}} + \frac{-1}{R_{26}} & \frac{-1}{R_{22}} & 0 \\ 0 & \frac{-1}{R_{31}} & \frac{-1}{R_{33}} + \frac{-1}{R_{35}} + \frac{-1}{R_{36}} & \frac{-1}{R_{32}} \\ 0 & 0 & \frac{-1}{R_{41}} & \frac{-1}{R_{43}} + \frac{-1}{R_{45}} + \frac{-1}{R_{42}} \end{bmatrix} \quad (4:29)$$

$$D = \begin{bmatrix} \frac{1}{R_{11}} + \frac{1}{R_{12}} + \frac{1}{R_{13}} + \frac{1}{R_{14}} + \frac{1}{R_{15}} + \frac{1}{R_{16}} & 0 & 0 & 0 \\ 0 & \frac{1}{R_{12}} + \frac{1}{R_{22}} + \frac{1}{R_{23}} + \frac{1}{R_{24}} + \frac{1}{R_{25}} + \frac{1}{R_{26}} & 0 & 0 \\ 0 & 0 & \frac{1}{R_{31}} + \frac{1}{R_{32}} + \frac{1}{R_{33}} + \frac{1}{R_{34}} + \frac{1}{R_{35}} + \frac{1}{R_{36}} & 0 \\ 0 & 0 & 0 & \frac{1}{R_{41}} + \frac{1}{R_{42}} + \frac{1}{R_{43}} + \frac{1}{R_{44}} + \frac{1}{R_{45}} \end{bmatrix} \quad (4:30)$$

4.6 Pneumatic- Electric Analogy

It is common practice in hydraulics to choose pressure as effort (or potential) and volume flow as the flow variable.

In pneumatics or gases however, since the density is not constant and the flow can be regarded as compressible, mass flow is considered as the flow variable.

Hagen-Poiseuille law indicates that pressure drop and mass flow rate are related as [84]:

$$\Delta p = \frac{128\mu l}{\rho\pi d^4} \dot{m} \quad (4:31)$$

Comparing Eq. (4:31) to Ohm's law indicates that resistance in pneumatic systems is proportional to the length of the pipe and viscosity and is inversely proportional to the fourth power of diameter:

$$R = \frac{128\mu l}{\rho\pi d^4} \quad (4:32)$$

Ghafari et al. [85] have shown that the equivalent of capacitor in pneumatic systems is proportional to volume of the chamber containing the gas and is inversely proportional to polytropic index and temperature:

$$C = \frac{V}{nRT} \quad (4:33)$$

So, in case of isothermal compression, the capacitor will be linear.

It is possible to show that the equivalent of Inductor for a pipe with cross section of A and length of l , which contains a gas with density of ρ , is [85]:

$$L = \frac{\rho L}{A} l \quad (4:34)$$

But since the density in gases is very low, we can often neglect the effect of inertia in pneumatics. In This analogy pressure can be chosen as effort and mass flow will be the flow variable. By such an assignment the equivalent of resistance can be proved to be $128\mu l/\rho\pi d^4$ [84]. Where l and d are the length and diameter of the connecting channel, and μ is the viscosity. The equivalent of a capacitor in gas systems was found by [85] to be V/nRT .

The electrical circuit equivalent of the simple cylinder piston assembly is shown in **Figure 4.14**. One should note that the leak resistance in reservoir is practically infinity and is placed for the sake of correctness of the electrical circuit. The leak resistance in the cylinder is due to the fact that seals are not perfect and there is always an amount of air leaking to outside, decreasing the volumetric efficiency but the amount of the leak resistance is much higher than the valve resistance.

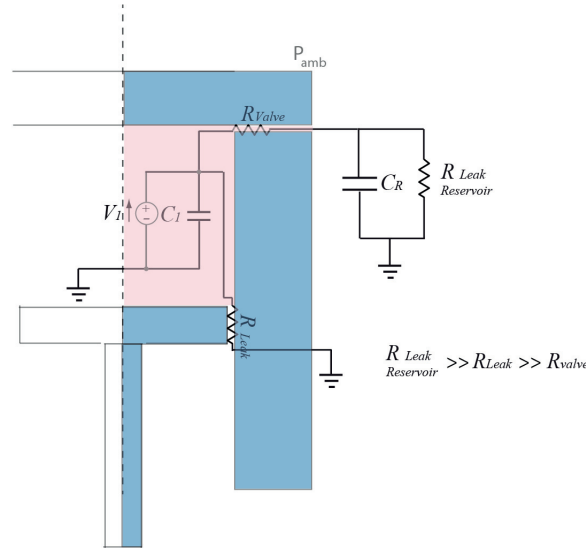


Figure 4.14 : Pneumatic-electric analogy for a cylinder-piston assembly.

The summary of the analogies used in this study is shown in **Table 4:1**.

Table 4:1 Table of equivalent variables for the different types of systems

Case	Bond graph	Flow variable	Effort variable	Compliance	Resistance
Electrical	Φ	I	ϕ	C	R
Thermal	T	\dot{Q}	T	mc	$\frac{x}{kA} \cdot \frac{1}{hA}$
Pneumatical	P	\dot{m}	p	$V/nR_g T$	$128\mu l/\rho\pi d^4$

4.7 Developement of Pneumatic- Electric Analogy for the Finned piston Model

Using the circuit developed in section 4.6 for a simple chamber, the equivalent circuit for pneumatic-electric analogy of the multiple chamber finned piston can be found in **Figure 4.15**. The upper chambers are connected by a small radial collecting channel that possesses resistance and capacitance effect at the same time (R_{13}, C_{13}, \dots). Also, the upper and lower chambers can exchange flow through the inner fin space (e.g. R_{12}, C_{23}, \dots). There are also two leakage resistances, since the finned piston has two seals.

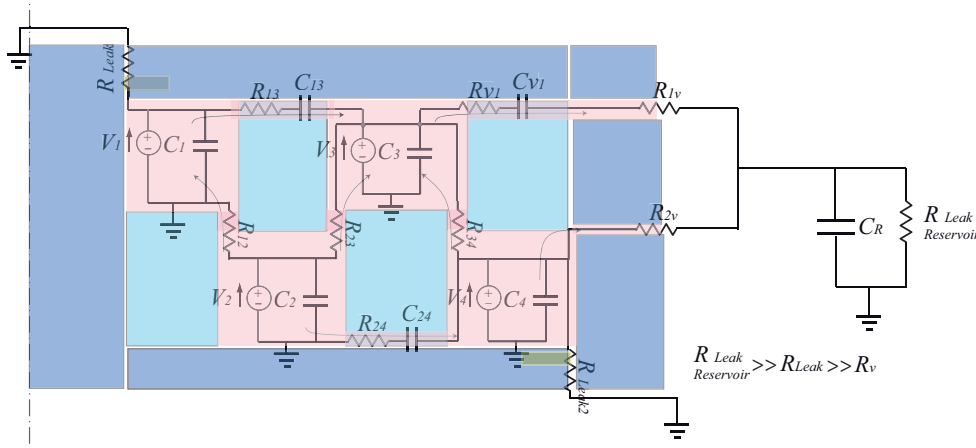


Figure 4.15 : Equivalent electrical circuit for pneumatic-electric analogy.

The bond graph representation of such a model can be seen in **Figure 4.16**.

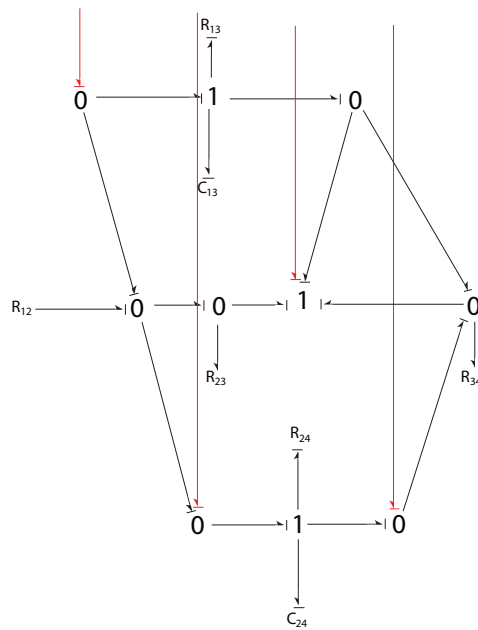


Figure 4.16 : Bond graph model of pneumatic part.

4.7.1 State space equations

Similarly for the pneumatic–electric analogy, considering chamber's pressure as state variables, reservoir and ambient pressure as input and outgoing mass flow as the output:

$$X = \begin{bmatrix} p_1 \\ p_2 \\ p_3 \\ p_4 \end{bmatrix}; U = \begin{bmatrix} p_{atm} \\ p_r \end{bmatrix}; Y = \begin{bmatrix} \dot{m}_{1v} \\ \dot{m}_{2v} \end{bmatrix} \quad (4:35)$$

The state matrixes A, B, C and D can be found as:

$$A = \begin{bmatrix} -\frac{1}{c_1}(\frac{1}{R_{12}} + \frac{1}{R_{13}} + \frac{1}{R_{11}}) & \frac{1}{c_1}(\frac{1}{R_{12}}) & \frac{1}{c_1}(\frac{1}{R_{13}}) & 0 \\ \frac{1}{c_2}(\frac{1}{R_{12}}) & -\frac{1}{c_2}(\frac{1}{R_{12}} + \frac{1}{R_{23}} + \frac{1}{R_{12}}) & \frac{1}{c_2}(\frac{1}{R_{23}}) & \frac{1}{c_2}(\frac{1}{R_{24}}) \\ \frac{1}{c_3}(\frac{1}{R_{13}}) & \frac{1}{c_3}(\frac{1}{R_{23}}) & -\frac{1}{c_3}(\frac{1}{R_{13}} + \frac{1}{R_{23}} + \frac{1}{R_{34}} + \frac{1}{R_{2v}}) & \frac{1}{c_3}(\frac{1}{R_{34}}) \\ 0 & \frac{1}{c_4}(\frac{1}{R_{24}}) & \frac{1}{c_4}(\frac{1}{R_{24}}) & -\frac{1}{c_4}(\frac{1}{R_{34}} + \frac{1}{R_{24}} + \frac{1}{R_{12}}) \end{bmatrix} \quad (4:36)$$

$$B = \begin{bmatrix} -\frac{1}{c_1}(\frac{1}{R_{11}}) & 0 \\ 0 & 0 \\ 0 & -\frac{1}{c_3}(\frac{1}{R_{1v}}) \\ -\frac{1}{c_4}(\frac{1}{R_{12}}) & -\frac{1}{c_4}(\frac{1}{R_{2v}}) \end{bmatrix} \quad (4:37)$$

$$C = \begin{bmatrix} 0 & 0 & -\frac{1}{c_3}(\frac{1}{R_{1v}}) & 0 \\ 0 & 0 & 0 & -\frac{1}{c_4}(\frac{1}{R_{2v}}) \end{bmatrix} \quad (4:38)$$

$$D = \begin{bmatrix} 0 & -\frac{1}{c_3}(\frac{1}{R_{1v}}) \\ 0 & -\frac{1}{c_4}(\frac{1}{R_{2v}}) \end{bmatrix} \quad (4:39)$$

4.8 Complete finned-piston model

The final application of such analogies is the developement of finned compressor model. This model will be based on the bond graph representation of the model of a classic piston seen in **Figure 4.13**.

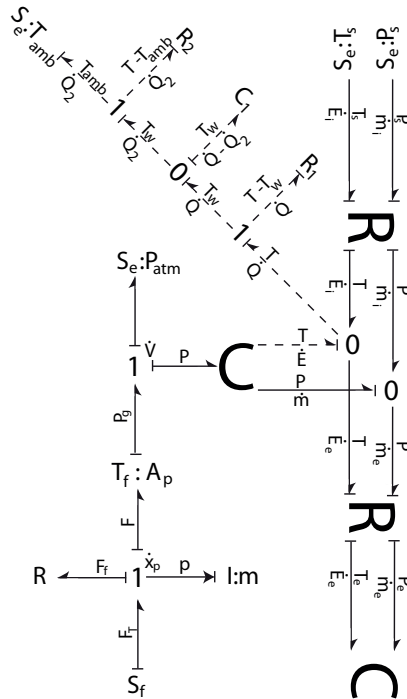


Figure 4.17 : Bond graph model of Classic piston.

Combining the two parts developed so far for four chambers, the complete bond graph model of a finned piston is represented in the **Figure 4.18**. As can be seen a part of the shaft power is converted to thermal energy in thermal bond. This energy will be transferred to ambient through the dotted bonds already shown in **Figure 4.13**. The rest of the shaft power is spent to increase the pressure of the gas through the hydraulic bond: the ambient air enters the compressor through the inlet valve (The upper capital R). Then it receives a part of the shaft power and its pressure rises. Finally it goes out through the outlet valve (The lower capital R) and is stored in a reservoir. One should note that during all this process the thermal and pneumatic bond are coupled to each other.

Each of the cylinder annulus are numerated and the aforementioned principles are applied to them while describing their connection to other chambers. One may not that such a bond graph representation can easily demonstrate the complicated interaction between the thermal and pneumatic elements of the system.

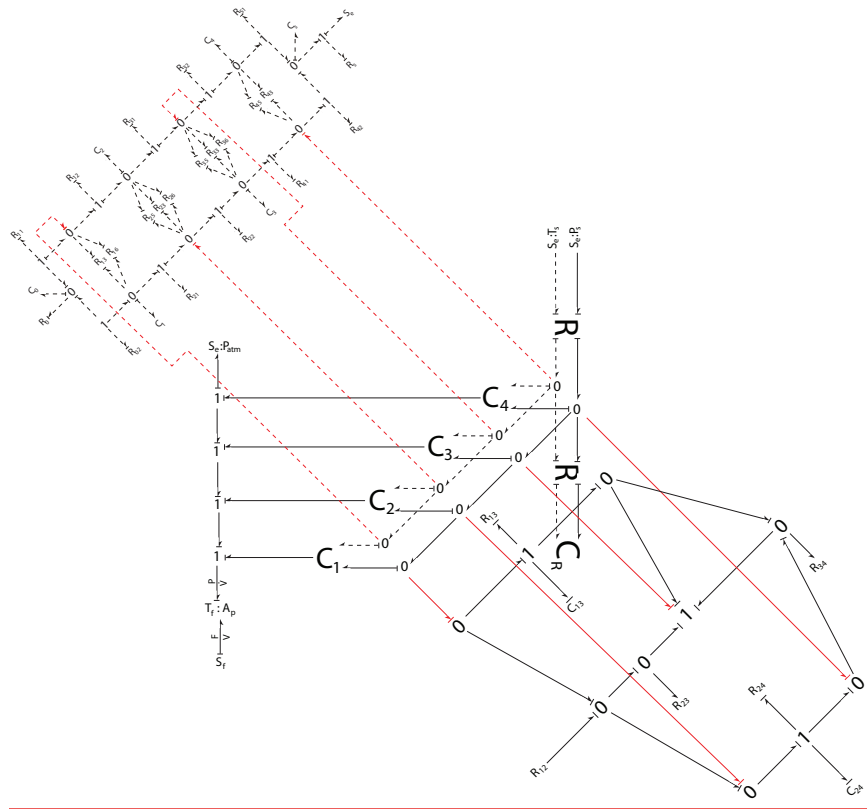


Figure 4.18 : Bond graph model of finned piston.

For more simplicity and compatibility with the finned piston geometry, it is possible to combine and couple thermal and pneumatic bonds, as shown in **Figure 4.19**. In this figure some of the resistances have been combined to give a simpler representation.

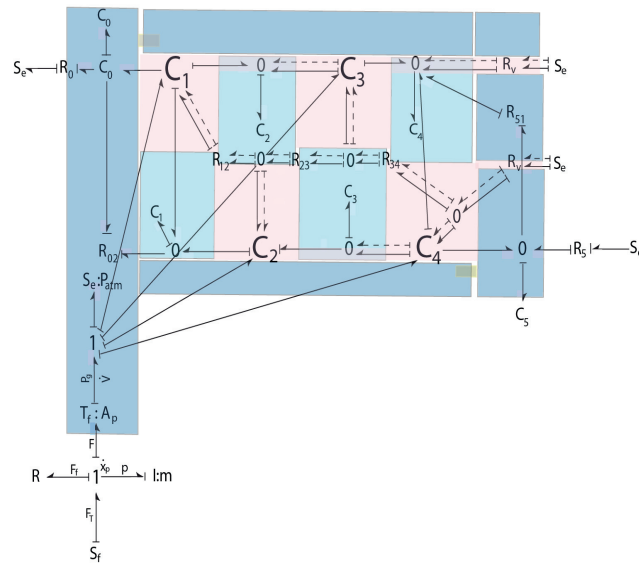


Figure 4.19 : Bond graph representation of finned piston model.

Also it is possible to show the finned compressor model a simplified EMR representation based on the model developed in chapter 3 as shown in **Figure 4.20**.

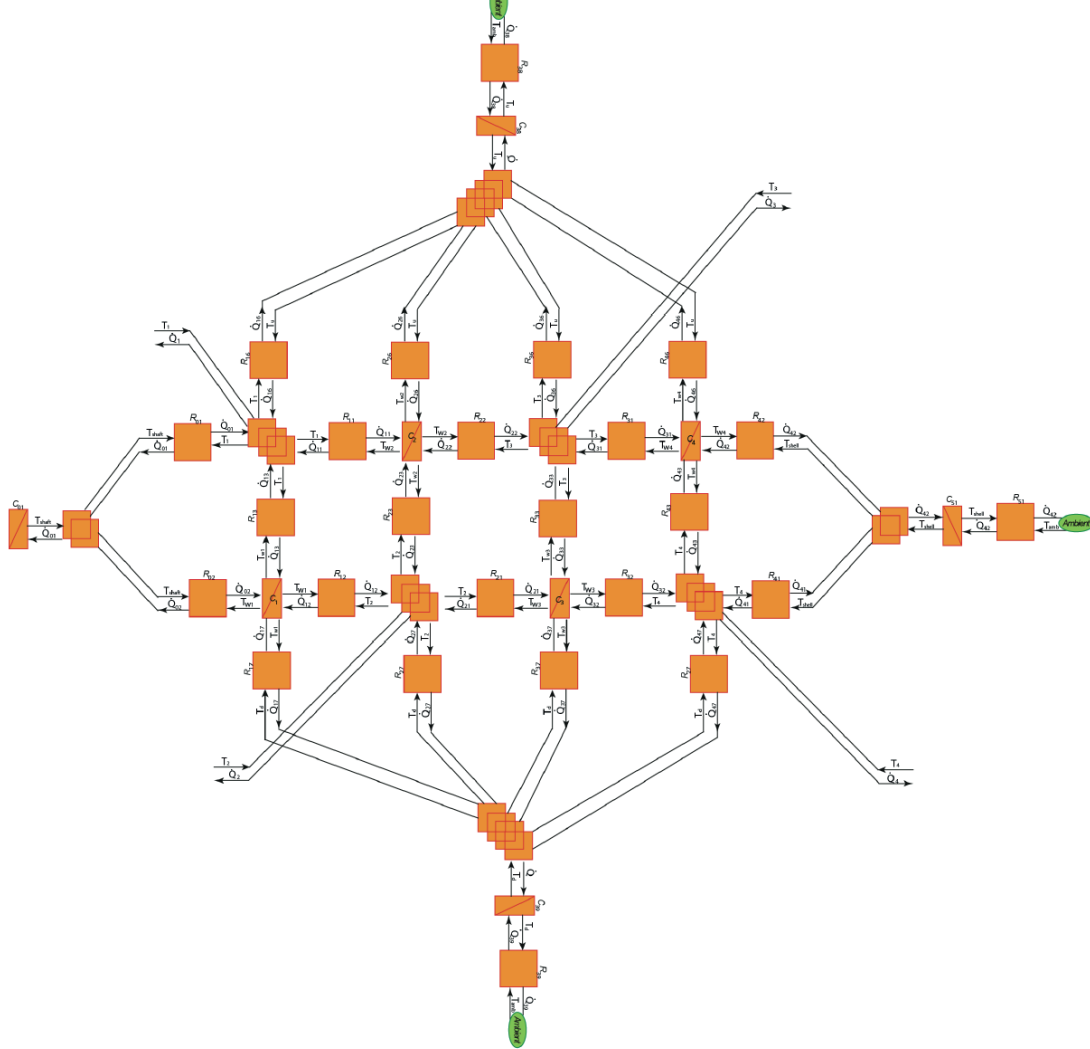


Figure 4.20 : EMR representation of finned piston model.

4.9 Simulation results

The complete model developed in Matlab Simulink is available in Appendix VI.

4.9.1 Model Inputs

The finned air compressor has a piston with outer diameter of 12 *cm* and inner diameter of 2 *cm* a stroke of 96 *cm*. The dead volume was supposed to be 5% of the displacement volume for each collecting channel. The period of a cycle is the same as before and equal to 1.98 seconds. The speed of the piston is constant during compression and expansion and is also equal to 100 (*mm s⁻¹*). The reservoir is the same as it was for classic compressor, and initially at ambient temperature and pressure and its volume is 25 *liters*, which is again 20 times more than cylinder volume. Other inputs

to the model required to estimate the gas compression efficiency for the finned piston compressors using the equations developed are available as input variables are presented in **Table 4:2**.

Table 4:2 Input variables to the numerical simulation of the classic piston model.

Constant	Symbol	Finned compressor	Units	Constant	Symbol	Finned compressor	Units
Maximum cylinder volume	V_{max}	0.0011	m^3	Reference dynamic viscosity	μ_0	$1.7 \cdot 10^{-5}$	$Pa \cdot s$
Dead Volume	V_0	0.000055	m^3	Initial temperature	T_0	293	KPa
Piston stroke	l	0.96	m	Initial pressure	p_0	100	KPa
Piston clearance	x_0	0.005	m	Maximum pressure	p_{max}	580	KPa
Piston Bore diameter	D_p	0.120	m	Inlet valve diameter	D_{vi}	0.006	m
Piston shaft diameter	D_0	0.02	m	Exit valve diameter	D_{ve}	0.006	m
Number of Chambers	N	10	—	Gap between fins	g	0.1	mm
Hydraulic diameter of main chambers	D_c	5	mm	Diameter of radial collecting channels	D_{rcc}	0.1	mm
Pressure compression ratio	p_r	5.8	—	Reservoir Volume	V_{res}	0.025	m^3
Cycle period	T_{period}	1.98	s	Cylinder thickness	t_{cyl}	0.02	m
Piston linear speed	\dot{x}_p	0.1	m/s	Cylinder mass	m_{cyl}	9.5	kg

The differential equations involved in heat transfer of such a transient multi-dimensional, multi layer system have time (t) as one independent variable in addition to cylindrical coordinates (r, x) and are very difficult (if not impossible) to solve analytically. The model for the entire finned piston was solved numerically using Matlab Simulink as an automated equation-solving program. A fixed-step size (0.00001 sample time) ode4 (Runge-kutta) solver is used, that can simulate the model in 3 minutes on a typical desktop computer. In comparison to other methods (Finite difference, time and frequency domain method...), this method simplifies (by lumping) the problem complexity at the model construction phase as opposed to computational phase. The resulting computations are simpler and therefore can be made with greater accuracy. Then results were compared to the equivalent classic piston for one complete cycle. **Figure 4.21 to Figure 4.24** show the main parameters during one cycle in a fixed pressure level (FLP) mode. Since one of the main concerns of this work is the average temperature of gas during compression, in **Figure 4.21** the temperature of each chamber was plotted along with the temperature of a classic piston. As it can be seen, due to the high convection in finned piston, the temperature of the gas decreases significantly during this discharge stage, while the gas temperature in the reciprocating piston remains nearly constant. Also, it is evident that the

temperature in finned chambers is much less than the classic piston. The reason why the temperature of chamber 1 and 4 are more is that they receive the inter heat transfer from one side while chambers 2 and 3 benefit from two sides. Likewise in **Figure 4.22** the pressure evolution is less steep in the chambers of finned piston that means being closer to isothermal line. **Figure 4.23** shows that the heat transfer rate is much higher in a finned piston compared to a classic one and finally **Figure 4.24** shows the effective work was decreased to a great extent for finned piston.

Figure 4.25 shows the mass contained in the compression chamber in the course of a cycle. This illustrates one drawback of finned piston compressor (or any other cooled compressor). Since the gas is cooler at the end of the discharge phase, its density is higher, which means more mass is trapped in the dead volume, so less mass is pumped. This decreases the volumetric efficiency or capacity of the finned compressor, however as it will be seen in chapter 6, eventually what is important is the «work consumed per unit of mass» which is less in case of a cooled or finned compressor. Similarly, the exergetic efficiency of a finned compressor is higher than a classic one. Finally, **Figure 4.26** shows the effective power evolution comparison between finned and classic compressor, which shows that the finned piston consumes less power during compression phase and recovers more work during expansion phase.

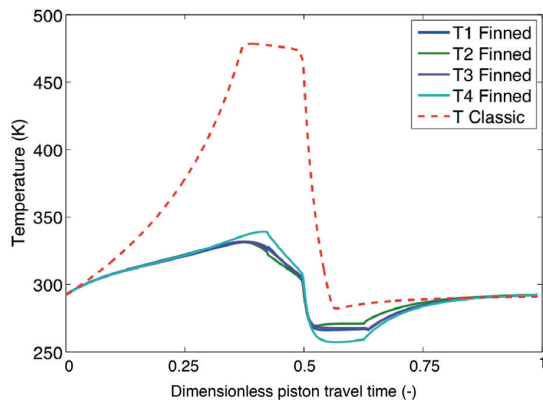


Figure 4.21 : Temperature evolution comparison.

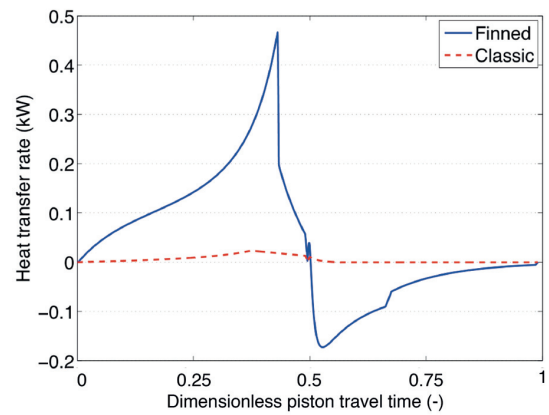


Figure 4.23 : Heat transfer rate comparison.

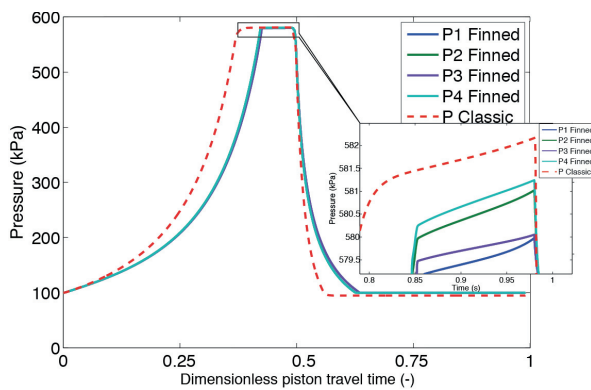


Figure 4.22 : Pressure evolution comparison.

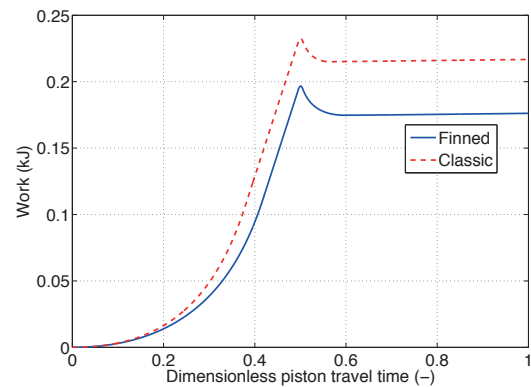


Figure 4.24 : Effective work comparison

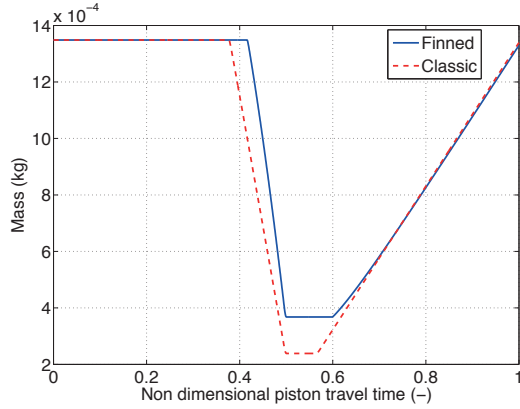


Figure 4.25 : Mass in the compression chamber.

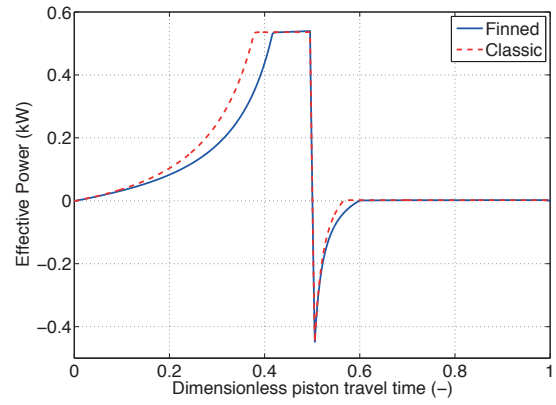


Figure 4.26 : Effective power comparison.

The results of the simulation for the finned compressor are summarized in **Table 4:3**.

Table 4:3 Summary of the results of the numerical simulation of the finned piston compressor model.

Constant	Symbol	Finned Compressor	Units
Effective Work	W_{eff}	0.176	kJ/cyc
Friction Work	W_{frc}	0.04	kJ
Total Work	W_{tot}	0.215	kJ
Discharged mass	m_{disch}	$0.98 \cdot 10^{-3}$	kg/cyc
Work per unit mass delivered	w_{eff}	179.6	kJ/kg
Volumetric efficiency	η_v	80.6	%
Exergy efficiency	$\eta_{x,cs}$	78.4	%
Isothermal efficiency	η_{iso}	87.4	%

4.10 Inter-Fin Heat Transfer

One aspect of the finned piston compressor that has a high potential for improving its performance is the heat transfer that happens in the small gap between fins ($g = 0.1 \text{ mm}$) and is referred to as Inter Fin Space (IFS) in this thesis.

Figure 4.27 shows the finned piston with only four chambers and symbolic dimensions (The space between the fins is represented larger than it is). The top and bottom sets of chambers are designed in a non-symmetric way, since the radial collecting channel is placed differently. This fact leads to a pressure difference between the top and bottom chambers. As described this causes a mass flow

between the two chambers, that can help in convection heat transfer in the very small gap between the fins (0.1 mm).

What makes the inter-fin heat transfer more advantageous is that hydraulic diameter will decrease to 0.0001 m (0.1 mm), which increases the heat transfer coefficient (according to Eq(4:40)) even more.

$$\dot{Q}(t) = \frac{Nu.k}{D_h} A_c (T - T_w) \quad (4:40)$$

This flow becomes more and more important as we reach the end of the compression stroke and becomes the dominant mode of heat transfer when the outlet valve is open (**Figure 4.32**).

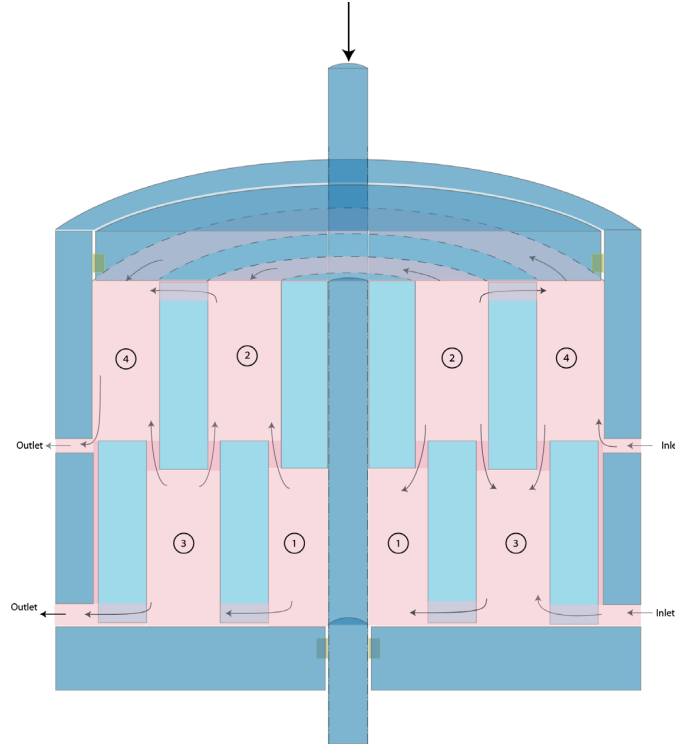


Figure 4.27 : Fluid flow direction in dry (finned) piston.

4.10.1 Pneumatic losses

Let us now focus on the losses associated with airflow between the inner-space fins. **Figure 4.28-a** shows such a typical gap of height about $g = 100$ micrometres, and width of πd where d is the diameter of corresponding annulus. Also, L is the length of fins, which varies along the cycle.

We suppose first that the thermal effects are negligible and the bond graph is shown by **Figure 4.28-b**. The mass flow is given in Eq. 1. And is related to volume flow as:

$$\dot{m} = \rho \dot{V} \quad (4:41)$$

Pressure drop and velocity of gas are related through friction factor as a general formulation [84]:

$$\Delta p = f \frac{L}{D} \frac{u^2}{2} \quad (4:42)$$

Hagen-Poiseuille law indicates that pressure drop and mass flow rate are related as [84]:

$$\Delta p = \frac{128\mu L}{\rho\pi d^4} \dot{m} \quad (4:43)$$

For a concentric annulus with gap of g and cross sectional area A_f of this relation can be written as:

$$\Delta p = \frac{12\mu L}{\rho A_f g^2} \dot{m} \quad (4:44)$$

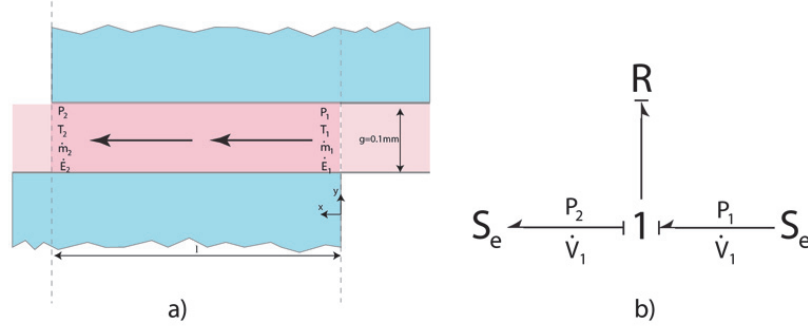


Figure 4.28 : Pneumatic resistance with the losses of a compressible fluid.

4.10.1 Conditions with thermal energy dissipation

Let us now examine the flow in the annular conduit through the same pneumatic resistance, which dissipates its energy by heating as shown in **Figure 4.29**.

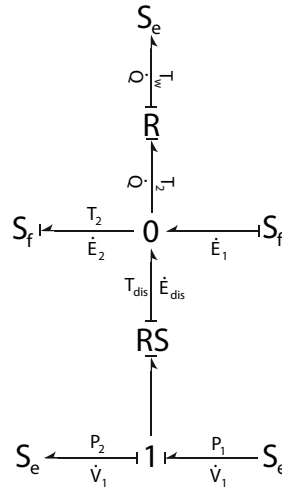


Figure 4.29 : Bond graph of energy dissipation in a resistance.

The dissipated power $P\dot{V}$ heats the air. On the bond graph the element R becomes multiport RS and dissipated energy \dot{E}_{dis} will be added to the internal energy of fluid \dot{E}_1 . The average temperature T_2 is calculated using the constitutive equations as follows:

$$\dot{E}_{dis} = (P_1 - P_2)\dot{V} \quad (4:45)$$

$$T_2 = \frac{1}{\dot{m}c}(\dot{E}_{dis} + \dot{E}_1 - \dot{Q}) \quad (4:46)$$

The total mass flow in IFS region, total dissipated power is shown in **Figure 4.30** and **Figure 4.31** respectively for two different gap distances and for a pressure gradient of $\Delta P = 1 \text{ kPa}$ between the upper and lower chambers. Also the heat flow in IFS region and total heat flow is shown in **Figure 4.32** for the same pressure gradient and gap.

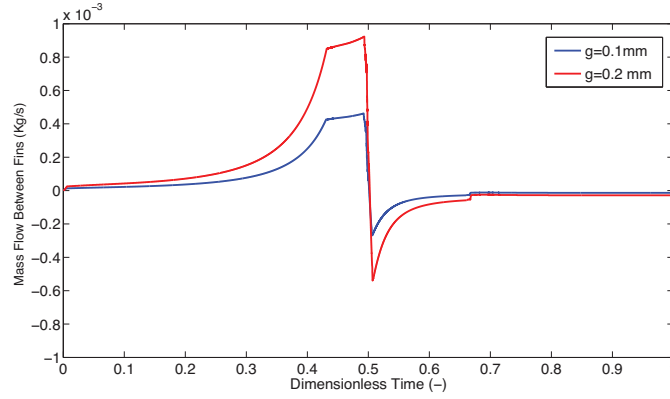


Figure 4.30 : Mass flow in the inter-fin space.

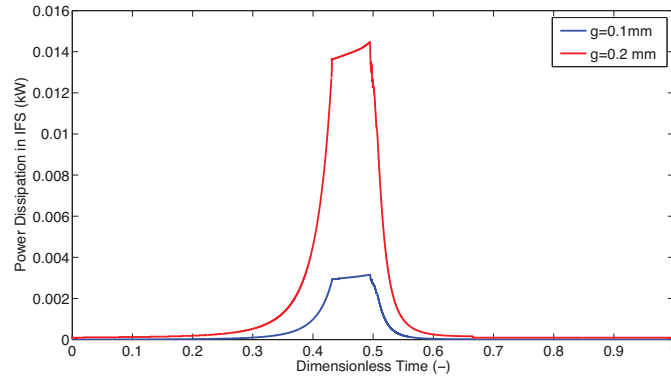


Figure 4.31 : Dissipated power in the inter-fin space.

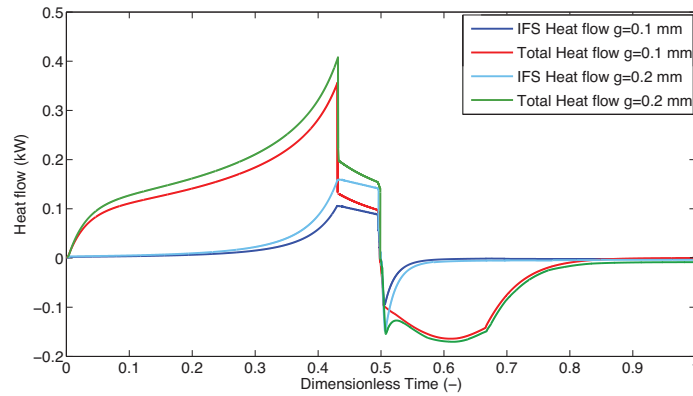


Figure 4.32 : Heat flow in the inter-fin space and total heat flow.

The effect of the gap between fins will be investigated as a parametric study in chapter 7.

4.11 Long term operation

Investigating the long-term performance of both compressors has arisen a major concern. The performance of both the classic and finned compressors change as the temperatures of its metal parts heat up. The finned compressor has an advantage when it has not been run for many cycles and is still relatively cool. But given enough run time it gets a lot hotter than the basic compressor, according to the simulations, and its performance suffers. The discharge air remains hotter in the basic compressor, but the temperature of the fins rise to about 409K (and the sleeve to 381K) whereas the sleeve in the basic compressor rises to a relatively cool 335K. It may take a few thousand cycles to reach equilibrium, which is not attempted experimentally, but with the simulations one can adjust initial temperatures until they do not change significantly over the course of one or just a few cycles.

Exergy efficiency of finned and classic compressor is plotted the in **Figure 4.33** over 200 cycles based on the definitions of equations (2:7)-(2:11). It can be seen from this figure, that the performance of the finned piston degrades with a sharper slope compared to classic piston compressor. Extrapolating the results, after about 10 minutes of operation, the performance of finned piston will be even poorer than the classic piston compressor. This necessitates the use of an external water jacket around the finned piston to keep its temperature almost at ambient and its performance as high as it is at the beginning of operation. However increasing the heat transfer on the external side is much easier than internal heat transfer between wall and gas, but is out of the scope of the current study.

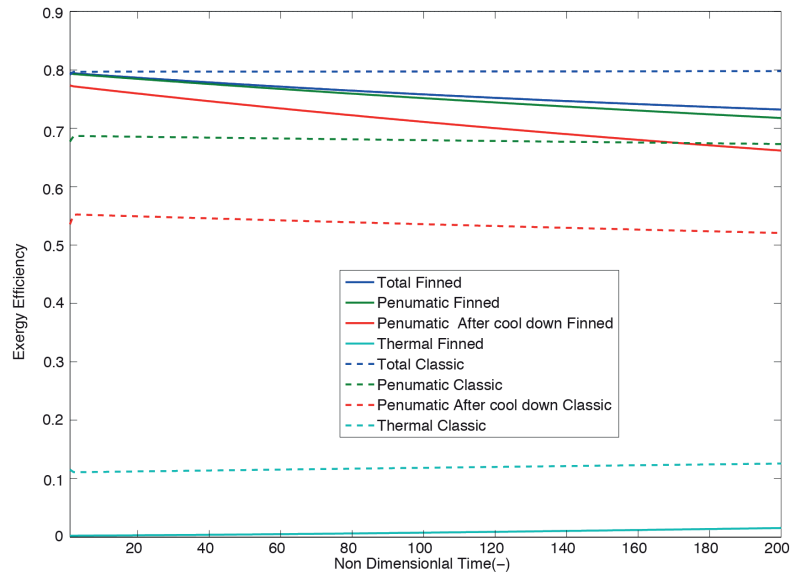


Figure 4.33 : Exergy efficiency degradation over time.

However we did not run the simulation for a very long time to reach thermal equilibrium, but for the first 100 cycles, It is shown in **Figure 4.34** that the temperature raise during filling process is higher in finned piston (and specially in fins) compared to classic piston. Please note that the total mass of finned piston is almost 3 times of its counterpart classic piston.

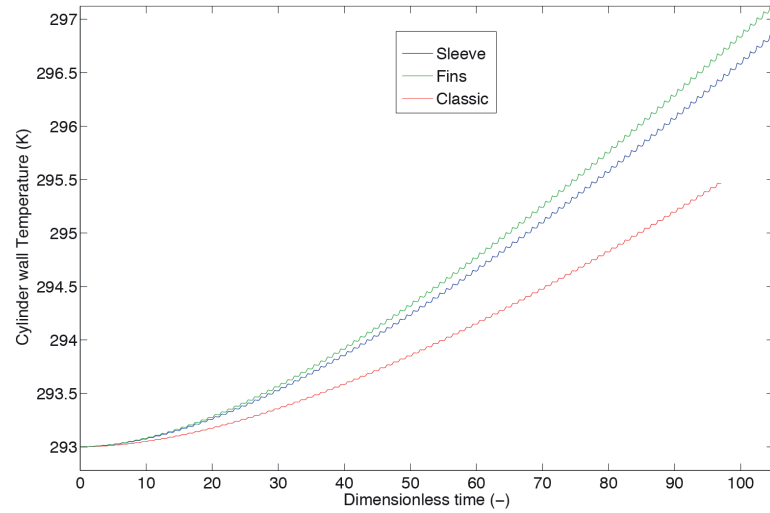


Figure 4.34 : fins and sleeve temperature of finned and wall temperature of classic piston compressors over filling period.

4.12 Conclusion

A complicated model for the finned piston was developed based on the model developed in Chapter 3 for a classic piston compressor. Thermo-Electric and Pnuematic-Electric Analgy is utilized to account for the sophisticated heat transfer and fluid flow that occurs in each layer and annular chambers. The model is simulated and compared to the results of the classic compressor already developed in chapter 3. Special attention is paid to inter-space heat transfer and fluid flow as well as long term operation and axial temperature distribution in fins.

Chapter 5 Finite Element Method

5.1 Introduction

Finite Element Method (FEM) has proved to be a very powerful tool in unsteady state thermo-fluid problems with complicated geometry. The moving mesh is the key to solve such problems. While analytic methods are mostly convenient to be used with a bulk method, FEM has the advantage of predicting the details of parameters distribution in the system over the whole process time. Moreover the graphical representation of the parameters evolution makes the FEM advantage double.

5.2 Generalities of Finite Element Model

Apart from the analytic studies done, it is of great interest to use a finite element model for having a visual demonstration of the parameters changes as the system evolves. Besides, the analytical model developed in previous chapters considers a uniform distribution of particles in cylinder, meaning one pressure one density and one temperature in the cylinder. In order to have a more detailed result on each area in the cylinder and study the flow and heat transfer, a FEM model is developed using COMSOL Multiphysics® and is compared to analytic model for both classic and finned piston compressors.

In order to allow some reasonable simulation times with a limited power for the computation, each of the compression stage has been modeled independently. The core of this chapter is to develop tools for the FEM modeling and the characterization of the three stages of a dry piston system. The geometries for all the stages are presented in this chapter, but only the modeling procedure for the first stage is described. The modeling approach for the next two stages is quiet similar, only pressure levels should be changed. The association of three pistons allows a compression process by stages: from 1 to 5.8 bars, from 5.8 to 34 bars, and from 34 bars up to 200 bars.

The main difficulty is there to study the heat transfer and fluid dynamics in a system where the topology is changing, as it is a piston regularly in movement. COMSOL as Finite Element Method software has been chosen, well dedicated for such a study.

As mentioned both classic and finned piston will be modeled. There are some common parts in modeling both compressors, which are related to definition of the driver motion and properties of material and initial and ambient conditions. These definitions will be covered in section 6.3. Then classic and finned piston will be described from the geometry and moving mesh and solver point of view.

5.3 Use of COMSOL Multiphysics®

There are some common parts in modeling both compressors, which are related to definition of the driver motion and properties of material and initial and ambient conditions. These definitions will be covered in section 6.3.1. Then classic and finned piston will be described from the geometry and moving mesh and solver point of view.

5.3.1 Global definitions

Independently from the structure, various parameters must be defined. The first set of parameters defines variables such as different pressure and temperature specifications:

- t_{per} defines the period of one cycle compression/expansion.

- T_{init} and P_{init} define the initial temperature and pressure.

- T_{amb} defines the ambient temperature around the piston.

- P_{ref} defines the reference pressure at which the air in the compression chamber will be expelled during compression. For the admission of air during expansion, the reference pressure we consider is the initial pressure P_{init} .

5.3.2 Definitions

What is notable in defining the global definitions, is to define the linear drive displacement as a piecewise linear function. The velocity of the piston can be derived by the derivative of the displacement, which is basically constant during compression and expansion, with the exception of start and stop transition periods. The function for defining the displacement is shown in **Table 5:1**. Velocity is defined in the variables as the derivative of displacement. The change of displacement and velocity is shown in **Figure 5.1**.

Table 5:1: Definition of a piecewise function for displacement.

Start	End	Function
0	0.99	$0.974*(0.1*t)$
0.99	1.98	0.99

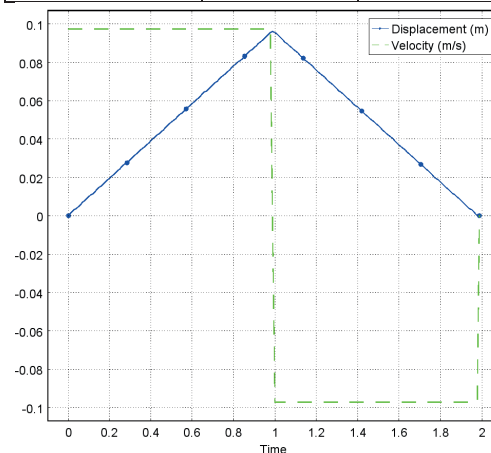


Figure 5.1 : Displacement and velocity of the piston in one cycle.

The last set of parameters is related to the main characteristics of the materials considered for modeling the stages.

- Solid part: Aluminum has been considered as the body of cylinder and the piston. The density, thermal conductivity and heat capacity is defined for these parts.
- The air: it is also defined with its density, its thermal conductivity, its heat capacity and its ratio of specific heats for the heat transfer study. It also defined with its dynamic viscosity for the fluid dynamics. It is obvious that these parameters are affected by temperature. This is taken into account in our model, at each simulation step of the calculation.

5.4 Classic piston

The general approach for modeling a cylinder-piston assembly with inlet and outlet will be described in this section.

5.4.1 Geometry

The geometry of the classic piston has been drawn in COMSOL environment. From the defined dimensions, we have directly drawn each stage directly with the CAD COMSOL interface. Such geometry with inlet/outlet valves is shown in **Figure 5.2** (right), where the blue part is air and grey part is the metallic cylinder piston assembly.

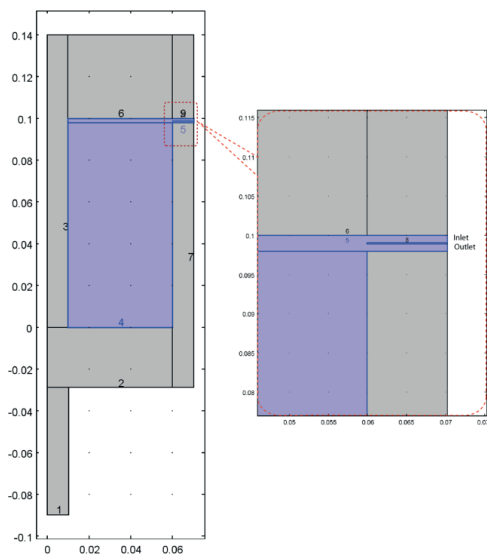


Figure 5.2 : Geometry of a classic cylinder-piston assembly with axial symmetry (left) and zoom on inlet/outlet area (right).

As each piston geometry has an evident symmetry along the vertical axe of the compression chamber, only half of the cylinder is drawn in a 2D plane. This allows reducing the simulation time and computational power. The geometry of the classic piston is proposed in **Figure 5.2** (left).

5.4.2 Moving mesh and meshes

The geometry of the classic piston can be divided into three parts to define the moving mesh:

- Cylinder, which is stationary: Fixed mesh.

- Piston, that moves without deformation: Prescribed deformation, which is equal to displacement defined already.
- Air, which both moves and deforms using a prescribed deformation defined as: $Displacement * (Y - A)/(-A)$, where A is the stroke of the piston.

Moving mesh specifies the way the mesh will be deformed as a function of the piston displacement. For each domain, the mesh displacement is defined. The definition of the mesh displacement must be strictly made, in order to give no degree of liberty for the solver to choose by itself the way the meshes could move. This is required to avoid any mesh inversion, which could lead to a decrease of the simulation accuracy. The moving mesh during compression of the classic piston is illustrated in **Figure 5.3**.

Once the classic piston model is implemented, calculations must be operated for 38'000 elements of meshes. The average element quality is 0.99, for a mesh area close to 0.014.

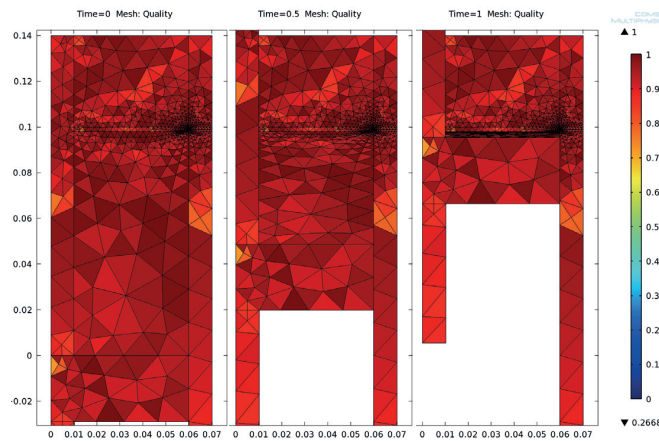


Figure 5.3 : Mesh of the classic piston for full expansion mid-travel and full compression respectively.

5.4.3 Heat Transfer

Heat transfer inside the cylinder occurs through both convection and conduction in gas, convection from gas to solid and conduction inside solid. Besides, a part of the heat will be stored in the body of the metal. For this reason we have considered conjugate heat transfer to consider all this effects.

The main parameters needed for this solver are the density, the thermal conductivity, and the heat capacity of the air and the aluminium. The ratio of specific heats for the air only is also needed. We remind that the air parameters are function of the pressure and the temperature. It is taken into account at each simulation step.

Moreover, the parts of the geometry that will move should be specified to the solver. This is the reason why in **Figure 5.4** some domains (part of the geometry which are the mobile part of the piston) must be specified by translational motion rules.

For the air, pressure work should be also specified.

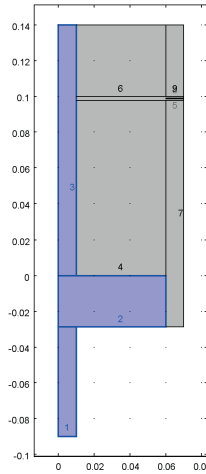


Figure 5.4 : Translational motion for the piston.

The boundary conditions must be defined for heat transfer solver. Considering again the geometry defined in **Figure 5.4**.

- The left side of the geometry is defined to have symmetry conditions.
- The outer sides of the geometry is set to have convection cooling.
- Inlet: the boundary is defined by Laminar inflow with an entrance pressure of $\max(P_{in}, P_{init})$ and entrance length of 0.1.
- Outlet: the boundary is defined by laminar outflow with an exit pressure of $\min(P_{out}, P_{ref})$ and exit length of 0.1.
- For all the boundaries except the inlet and the outlet, the condition is a wall with no slip condition.
- As seen in **Figure 5.5**, two kind of wall are defined. A fixed wall for the fixed part of the piston, and a moving wall for the moving part of the piston. The speed of the moving wall is defined by the speed of the piston

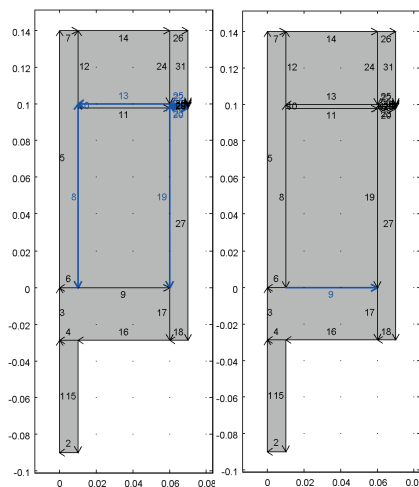


Figure 5.5 : Boundary conditions with no slip condition (left) for fixed wall and moving wall (right) respectively.

5.4.4 Study

The solver uses a time-dependent compiler, and dependent are T, u (velocity) and p. The range of the study is equal to one complete cycle of compressor (0,1.98) with time step of 0.01 seconds.

5.5 Finned piston

The general approach is the same as described for a classic piston, so only the additional items or differences will be described in this section. But here all the three stages are defined.

5.5.1 Geometry

Each geometry of the stage of the dry piston system has been predefined. From the defined dimensions, we have directly drawn each stage directly with the COMSOL CAD interface. Each stage has been considered separately from the two others. Moreover, the direct structural environment of each stage has not been considered. This last simplification is justified by the assumption that the temperature of the solid part of each stage does not vary significantly for few cycles compression/expansion, with no heat transfer between the solid part of the piston and their environment.

As each piston geometry has an evident symmetry along the vertical axe of the compression chamber, we have only drawn the half of each stage, in a 2D plane. This allows reducing the simulation constraints in time and in needed computational power. The geometry of each stage is proposed in **Figure 5.6**.

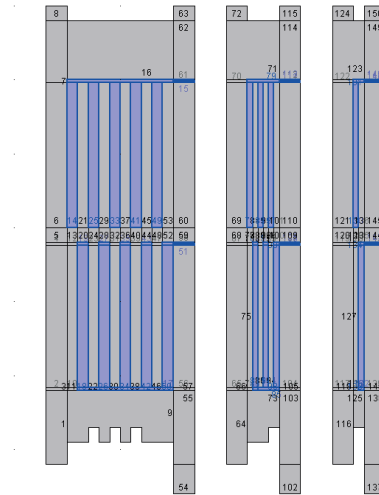


Figure 5.6 : The three stages of the compressor.

The geometry of the finned piston with two inlets and outlets is sketched showing air and metallic areas respectively with blue and grey colours as shown in **Figure 5.7**. On the other hand, **Figure 5.8** shows that the fins are not in contact with each other but a layer of air flow between them. This as will be seen later will enhance the heat transfer.

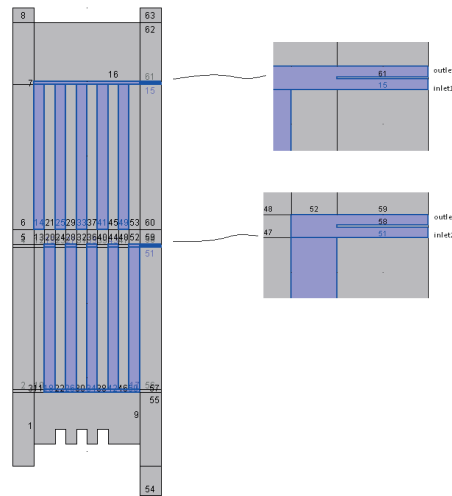


Figure 5.7 : Geometry of finned piston with outlets and inlets.

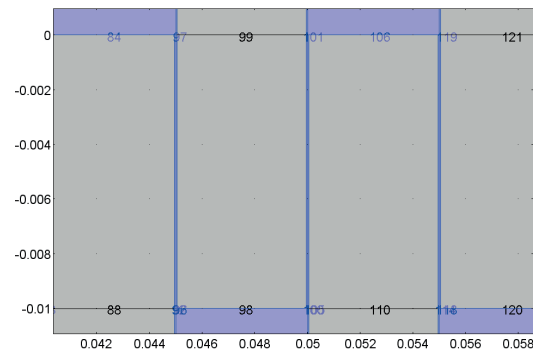


Figure 5.8 : The air can flow Inter fin space.

The principal of applying moving mesh is the same as described for classic piston. One can see the mesh distribution during compression and expansion in **Figure 5.9**.



5.5.2 Heat Transfer

114

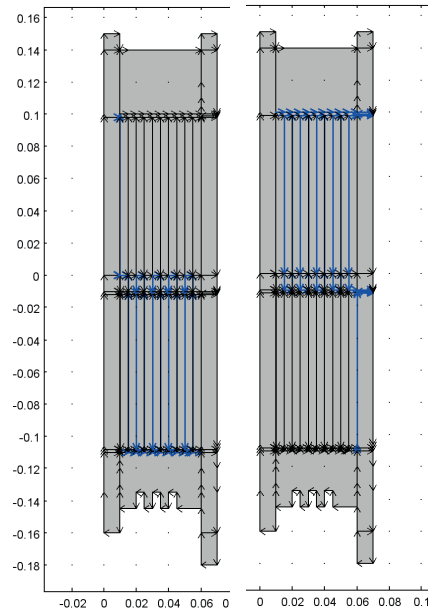


Figure 5.11 : Boundary conditions with no slip condition for fixed wall and moving wall respectively.

5.6 Results

Thanks to the analytic simulation it is possible to verify the finite element results. The results are shown for one complete cycle of compressor operation.

Figure 5.12 shows the volume change from full expansion (TDC) to full compression (BDC). The comparison is based on the fact that both compressors should have the same dead volume and displacement volume. Pressure evolution is shown in **Figure 5.13**. As it can be seen, the pressure raise is less steep for finned piston since the process is closer to isothermal conditions. The analytic and COMSOL results match very well during compression but the deviation of results is a bit more during expansion.

Figure 5.14 shows the temperature change for both pistons. As expected temperature raise is much less for finned piston thanks to increased heat transfer area. The COMSOL model predicts less steep increase at the beginning, but steeper increase at the end of compression compared to the analytical model. **Figure 5.15** and **Figure 5.16** are related to the power and work comparison respectively. As it is obvious the work is the area under power curve. The difference of the power (or work) between analytic and FEM result is 4.2% for classic and 1.7% for finned piston.

Figure 5.17 shows the mass change in one cycle. One can see that the mass remaining in the cylinder is more for the finned piston. This is no surprise because since the temperature increase is less, the density will be higher at the end of compression, and with the same volume the mass of air remaining in the finned compressor will be higher as a result. This fact results in lower volumetric efficiency in a more isothermal compression, which is a draw back of the finned piston.

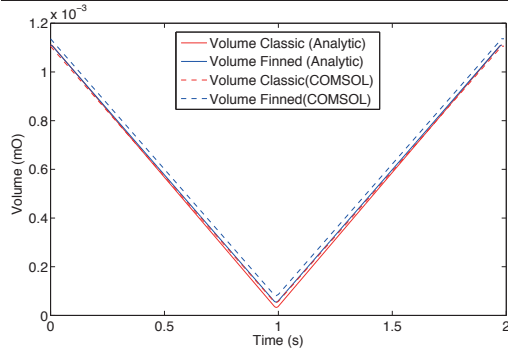


Figure 5.12 : Volume change during in one cycle.

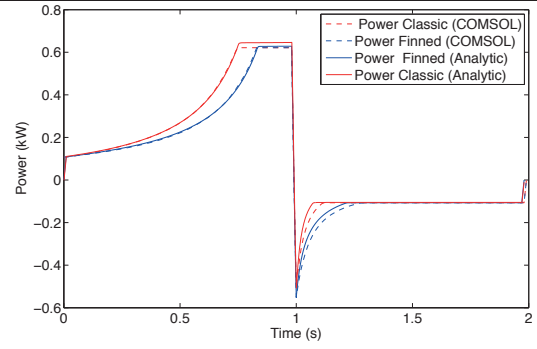


Figure 5.15 : Power evolution in one cycle.

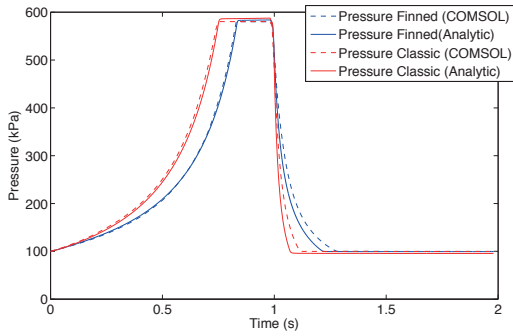


Figure 5.13 : Pressure evolution in one cycle.

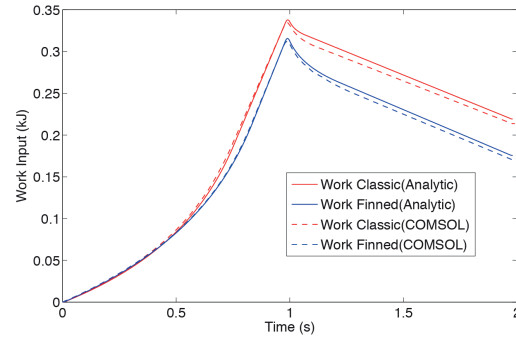


Figure 5.16 : Work during in one cycle.

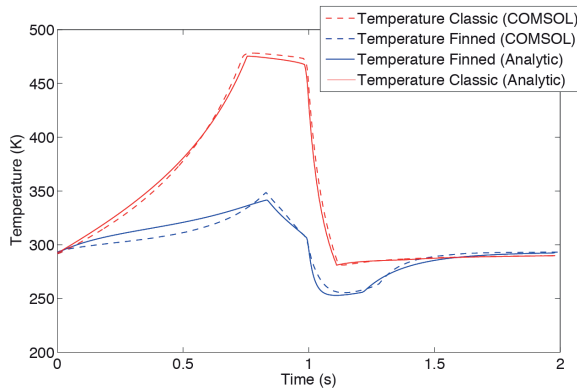


Figure 5.14 : Temperature evolution in one cycle.

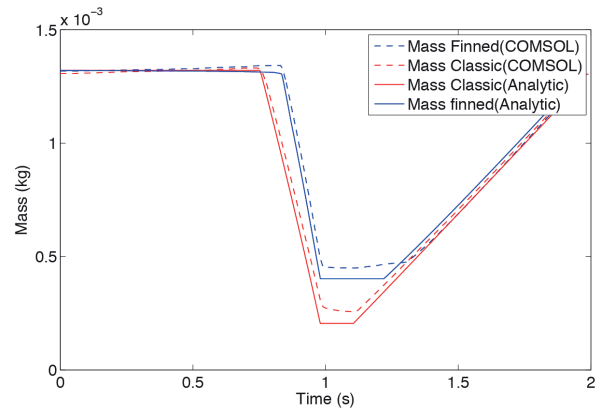


Figure 5.17 : Mass change in the cylinder head in one cycle

5.6.1 2D plots

First two-dimensional result is observed for the temperature gradient. This temperature gradient is plotted in **Figure 5.18** for the middle of the compression process. One may notice that the maximum temperature at the same time is much less for the finned piston.

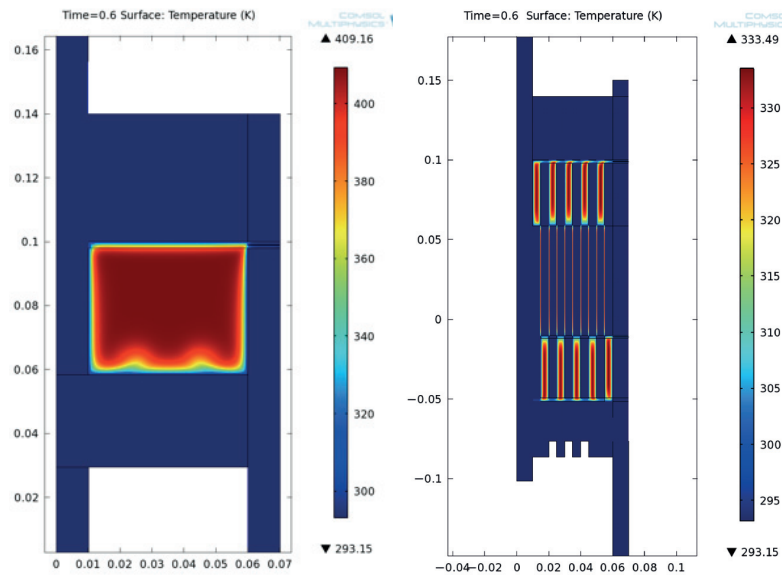


Figure 5.18 : Temperature gradient – mid of last expansion travel.

Figure 5.19 illustrates the velocity magnitude in colour and velocity field in arrows. One can notice the flow in the very small Inter-Fins Space (IFS). This air circulation will enhance the heat transfer the more the compressor approaches the end of the compression.

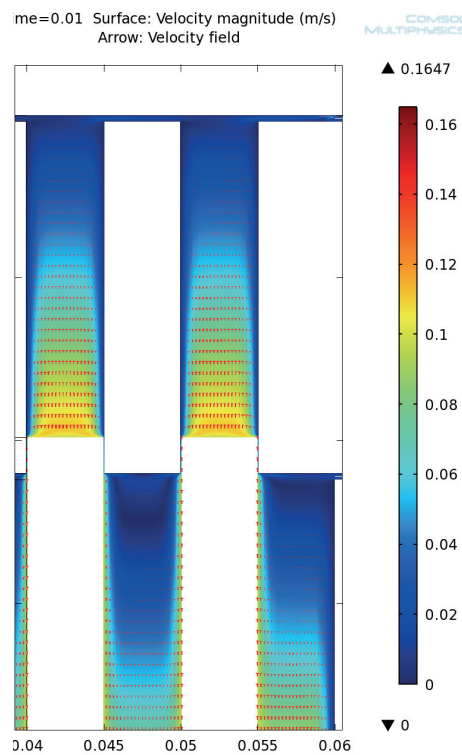


Figure 5.19 : Velocity of air movement in the chambers and inter fin space.

5.7 Temperature distribution along the fins

Heat transfer in the fins is unsteady with changing boundary conditions, and an analytical solution requires constructing an electrical circuit inside the fins instead of just two conduction resistance (as shown in **Figure 4.12**) which is cumbersome. However, one may obtain a better approximation of axial temperature distribution in the fins at any given time using FEM method. The results are given in **Figure 5.20** after 20, 40, 60, 80 and 100 cycles of operation in Filling Mode(FM). While the cylinder head is always at ambient temperature, the maximum temperature along the fins occurs very close to the fin base where the gas is compressed the most at the end of the compression cycle and convects its heat to the fins. The effect of the convection from the hot gas is also apparent at the tip of the fins.

The results confirm that the temperature variation along the fins is less than 1% after $N \times 100$ cycles. Hence, the assumption of mean bulk temperature in fins has only 1% error which is valid accurately.

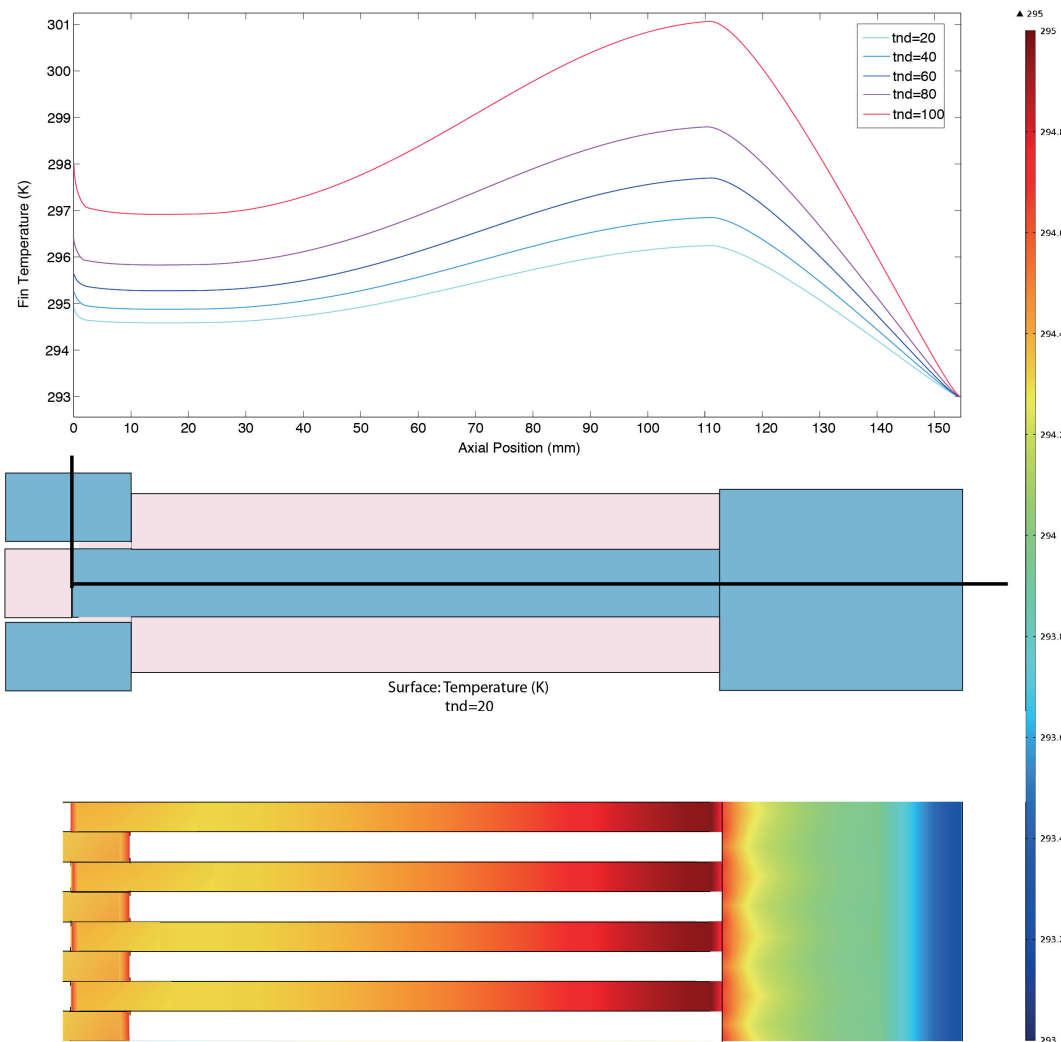


Figure 5.20 : fins and sleeve temperature of finned piston compressor over filling period.

5.8 Conclusions

Finite Element Method (FEM) which can be fitted in multidimensional models category has proved to be a very powerful tool in unsteady state thermofluid problems with complicated geometry. The moving mesh is the key to solve such problems.

While analytic methods are mostly convenient to be used with a bulk method, FEM has the advantage of predicting details of parameters distribution in the system over the whole process time. Moreover the graphical representation of the parameters evolution makes the FEM advantage double.

However one should not forget that without the insight that the analytical methods provide, FEM softwares could be a blackbox for the users and the user first should have necessary knowledge about the physics of the problem.

The results of achieved using FEM method shows very good compatibility with analytic ones. The best approach is to use both analytic and FEM methods to have insight to the physics as well as accuracy and results for parameters distribution.

Chapter 6 Experimental Method

6.1 Introduction

Experimental verification is an essential step in validating the theoretical results. Two different piston compressors (classic and finned) were tested on the same setup with identical driver, sensors and reservoir. In this chapter, first the prototype development will be described. Then, for each compressor, the same procedure of testing is followed:

1. Running the compressor, without connecting it to the reservoir (which will be called No Load Mode).
2. Running the compressor, connecting it to the reservoir (which will be called Load Mode or Filling Mode). In this case the reservoir pressure rises from atmospheric pressure to a given pressure.

One may note that the effective work to compress the gas will be taken into account only in the load mode. The theoretical results will be verified by experiment in each step.

The classic method for experimental verification in compressor technology is implementing a pressure transducer, calculating volume of the gas chamber based on the piston displacement and finally to provide the p-V curve [58]. However in the case of finned piston compressor, considering the limited space between cylinder and fins, it is not practical to insert a pressure or temperature sensor in the compression chamber. Also since this compressor is compact and delicate, instead we opted to measure the power indirectly by installing a force sensor on the driver shaft and multiply it by velocity to secure the instantaneous power. Integrating power curve can produce the work consumed.

The drawback of this method is that friction and other losses should be taken into account in the simulation. However, these losses will be seen to be very small compared to the compression work.

6.2 Loss characterization

6.2.1 Sliding force

One of the major sources of friction in a kinematic reciprocating piston is the sliding friction of the piston seals. As mentioned previously in Chapter 3, The sliding friction is a function of the inside diameter of the piston ring, the vertical height of the piston ring, sliding friction coefficient and pressure of the gas in the chamber. The complete manufacturer data of the seals and friction associated with them is available in Appendix III.

6.2.2 Valve losses analysis

Check valves allow the fluid to flow in one direction like a diode. Flow through valves (specially spring backed check valves) is very complex, and in industrial applications a theoretical analysis is generally not plausible. Therefore, minor losses are determined experimentally, usually by the manufacturers of the valves. However analytical model introduced in Appendix III can be used, the manufacturer data is applied in this section to verify the experimental results.

The losses of two seemingly identical valves by two different manufacturers, for example, can differ by a factor of 2 or more. Therefore the particular manufacturer data should be consulted in the calculation of pressure drop and losses associated with it. The valves used for the finned piston are a set of (1/8) inch Swagelok check-valves (4C series). These valves have been replaced later by SMC Japan valves. The complete data sheet of all the valves can be found in appendix IV.

Figure 6.1 shows the components of the check valve and **Figure 6.2** shows the manufacturer data to determine the flow rate as a function of pressure drop and inlet pressure. These data has been integrated in the model in the form of a look up table.

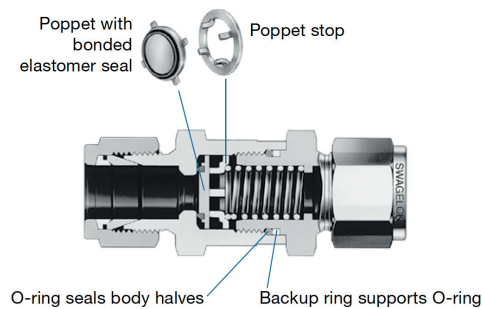


Figure 6.1 : Check valve components

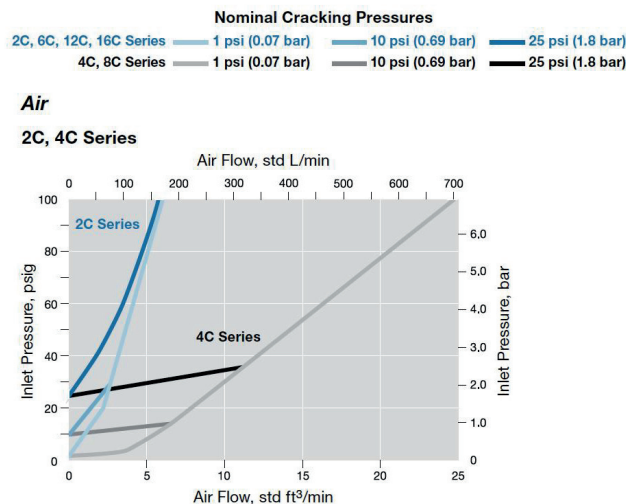


Figure 6.2 : Manufacturer data for determining mass flow from inlet pressure and pressure drop.

6.3 Driver setup description

The velocity has been set to be linear and constant during compression and expansion mode except at the very beginning and end of each movement. Velocity and piston position is shown in **Figure 6.3**. The force was recorded using Kistler sensor, and the velocity was measured using a built-in so-called oscilloscope in the Indra-work program designed to command the compressor. Then the two measurements were synchronized using programming techniques. Instantaneous power consumption was derived using the multiplication of force and velocity in LabView. It should be mentioned that here, velocity is cause and force exerted by the gas is the effect, from the causality point of view.

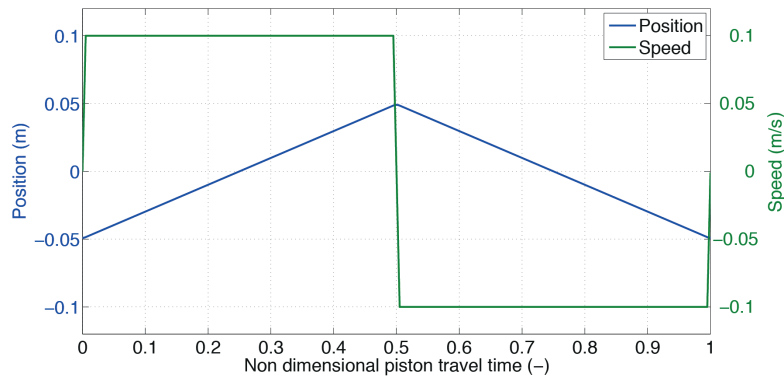


Figure 6.3 : Position and speed of piston during one cycle.

The test-bench includes an electrical motor to provide needed work, a ball-screw driver for transforming rotational to linear movement, a place for the piston compressor to be connected through transmission linear shaft and apparatus needed for controlling speed and measuring force, temperature and pressure (**Figure 6.4**).

6.4 Experimentation for a classic piston

First the classic compressor is installed on the test setup using dedicated flange connection.

6.4.1 Setup Description

The CP96 SB125-100W SMC cylinder used in this experiment is basically a linear actuators, with 125mm Bore size and 100mm stroke (Details and technical drawings of the piston are available in appendix V). These Non-Lubricated actuators are used for straight-line movement in a single or double acting manner, and are available with reed or solid-state switches for position detection.

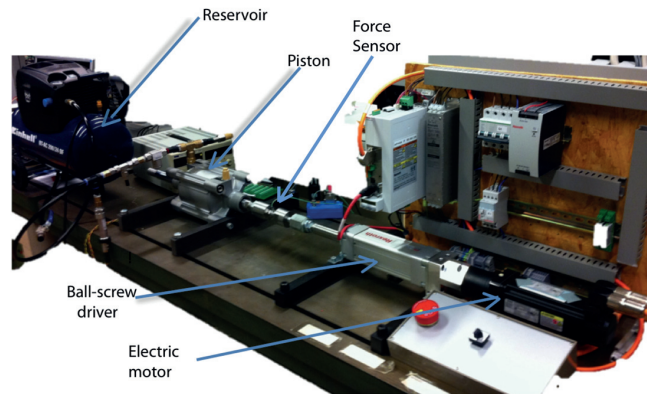


Figure 6.4 : Experimental setup.

The schematic configuration of the setup is shown in **Figure 6.5**. There are two anti-return valves one at the inlet just after the air filter, and one after the compressor outlet. The temperature sensors are placed after the anti return valve. The compressor is connected to the reservoir using a flexible tube in load mode.

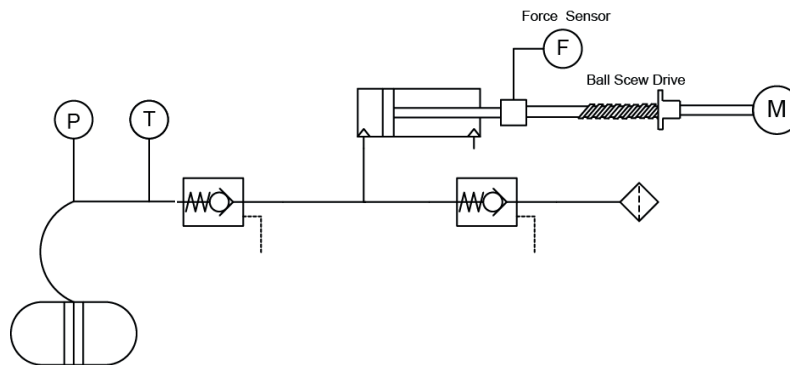


Figure 6.5 : Setup circuit schematic in filling mode.

The experimentations on the compressor setup were done under two conditions: No-load and Filling mode.

Figure 6.6 shows the experimental and calculated force and velocity In No-load mode. Since friction force always resists against any movement, friction force and velocity always have opposite signs causing a negative power. However since the work input to compressor is considered positive by convention, friction power (in **Figure 6.7**) sign is reversed.

Experimental friction force in **Figure 6.6** indicates a stick-slip friction behavior. The spikes and counter-spikes at the beginning and end of the compression and expansion is due to the inertia effect of piston mass, that is already discusses in section 3.5.5.

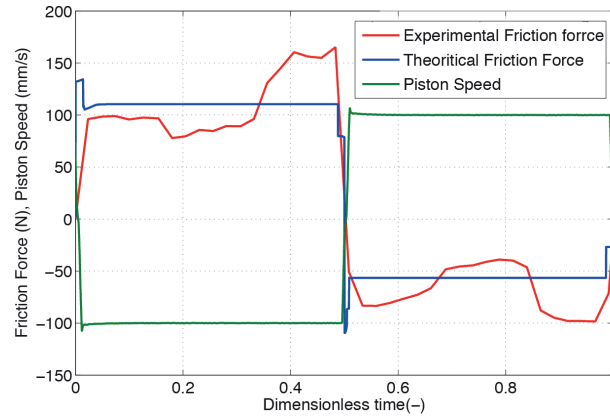


Figure 6.6 : Friction force and speed in classic compressor (No Load mode).

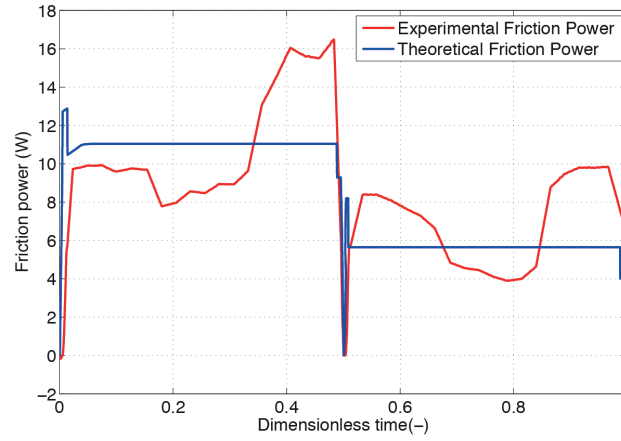


Figure 6.7 : Friction power in classic compressor (No Load mode).

In the next step the compressor will be connected to the reservoir, which is called “Load Mode”.

The pressure and power raise evolution for classic compressor in load mode is shown in **Figure 6.8** and **Figure 6.9** respectively.

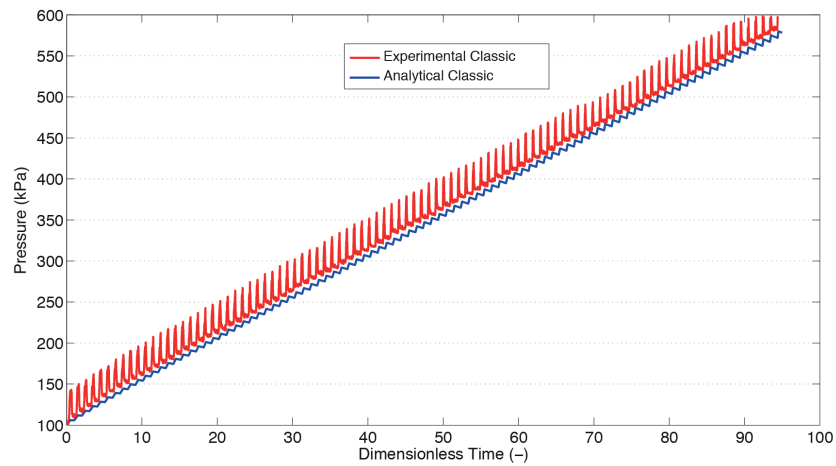


Figure 6.8 : Pressure evolution in reservoir for filling load mode in classic compressor.

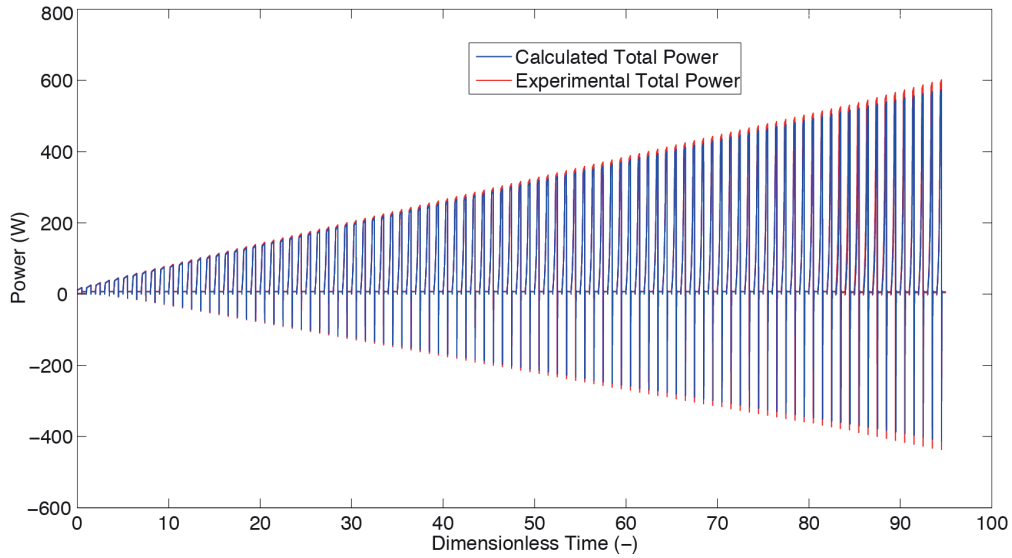


Figure 6.9 : Experimental and analytical power in load mode for classic compressor.

The force and velocity is shown in **Figure 6.10** and corresponding power in **Figure 6.11** for zoomed areas on a selected cycle (50th for example). The generality of the model shows good agreement with experimental results, both in they way pressure and power raise as well as the shape of the power curve in any individual cycle. The only visible difference is in the expansion part which can be correlated to friction due to special shape of the seals in expansion mode, which may need a very deep study on the dry friction between seals and piston in reverse direction and is out of the scope of the current research. The difference between the calculated and experimental power is 4.8 % Mean Absolute Error (MAE) for the whole range and 5% error in the input work over the filling time (Integral of the power curve).

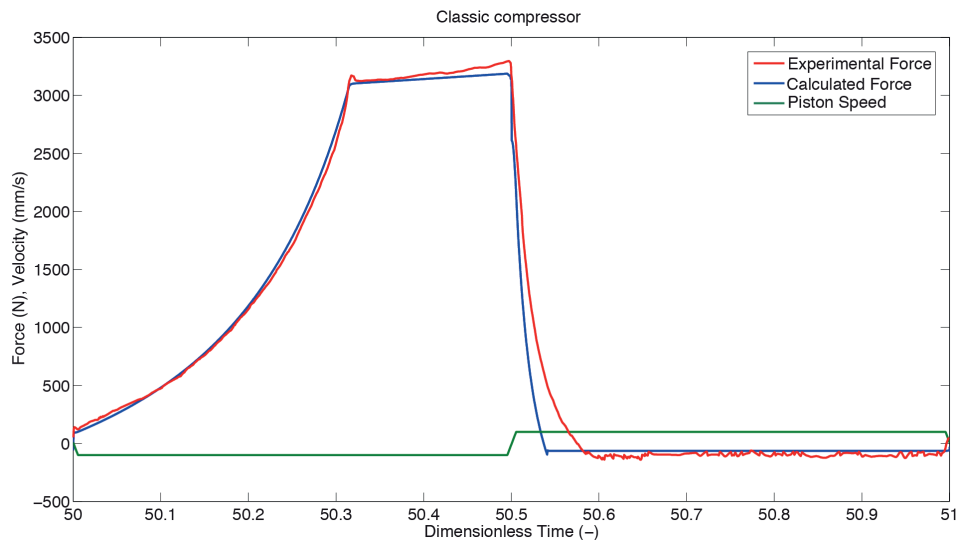


Figure 6.10 : Experimental and analytical Force and velocity in load mode (50st cycle) in classic compressor.

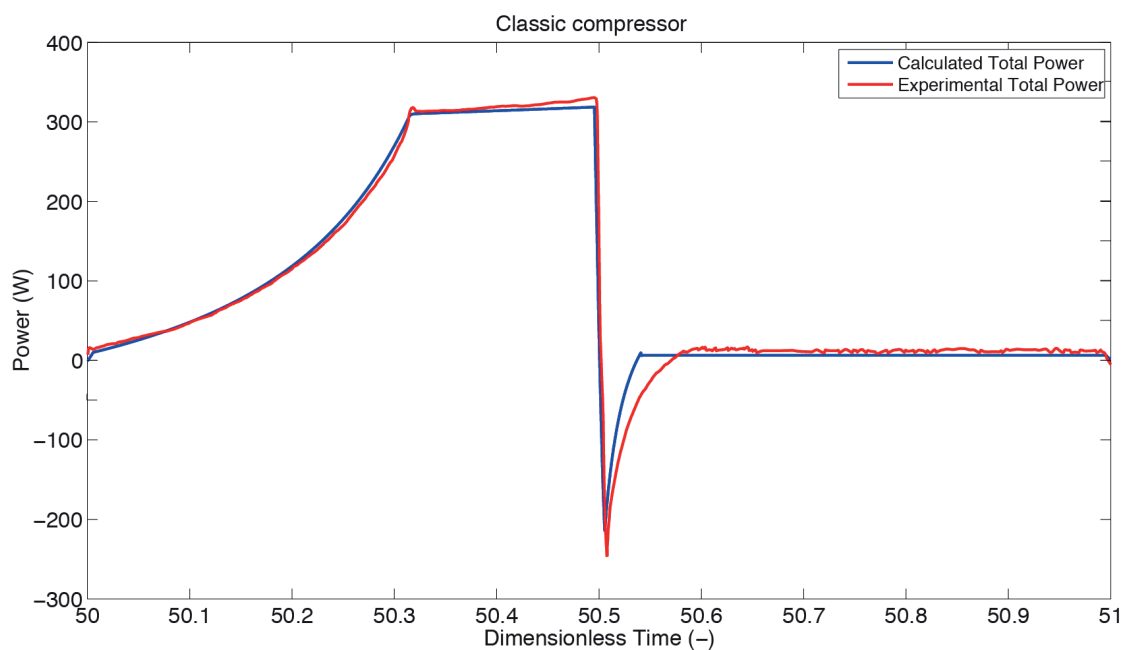


Figure 6.11 Experimental and analytical power in load mode (50st cycle) in classic compressor.

Figure 6.12 shows the amount of effective, friction and their sum which is total work, as well as final exergy content of reservoir during the charging process of the reservoir with the classic compressor. One may note that valve losses is already included as a part of the effective work. The final values are reported in **Table 6:2** and used for calculation of efficiency.

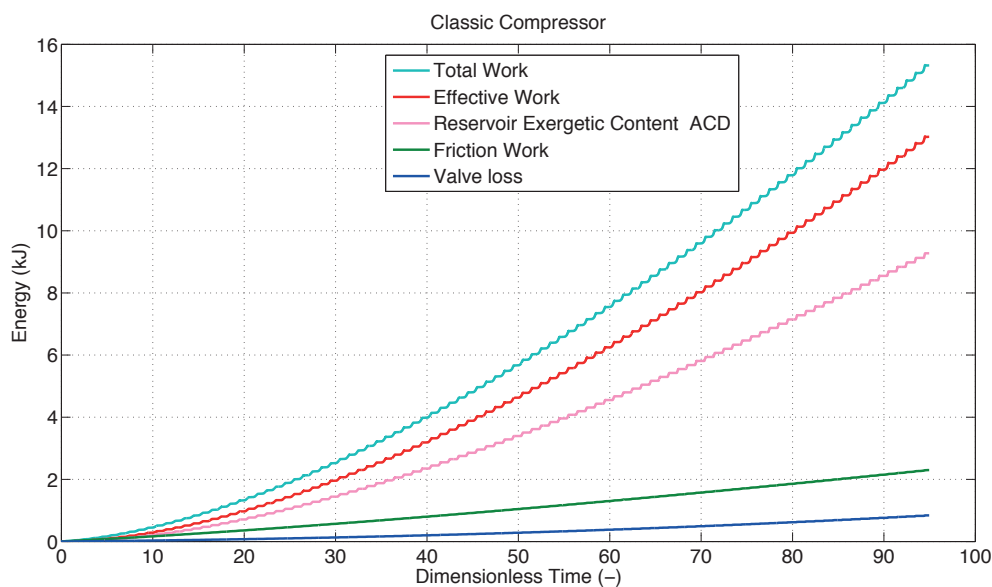


Figure 6.12 : Effective, friction and total work and reservoir exergy content after cool down for classic compressor.

6.5 Experimentation for Finned compressor

The finned piston uses the same setup, driver mechanism and velocity profile described earlier, but due to its special design has two inlets and outlets, instead of one. The two outlets will be joined together using a tee and connected to reservoir in filling mode. (**Figure 6.13**).

6.5.1 Setup Description

To evaluate and characterize the performance of developed finned piston, it is implemented in the test bench that has been already realized. First the finned piston was fabricated from aluminum with a high tolerance to avoid friction and leaks (**Figure 6.14**). The test bench like before includes an electrical motor to provide needed work, a ball-screw driver for transforming rotational to linear movement, as before, The finned cylinder and apparatus needed for controlling speed and measuring force, temperature and pressure. (**Figure 6.15**)

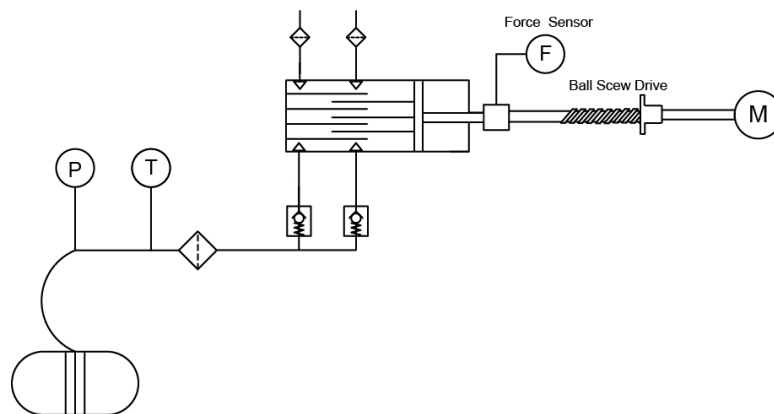


Figure 6.13 : Setup schematic circuit in filling mode.

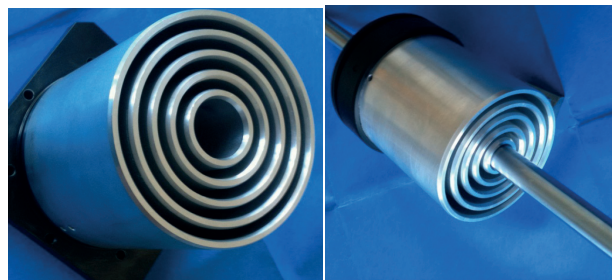


Figure 6.14 : Fix and mobile part of the finned piston cylinder.

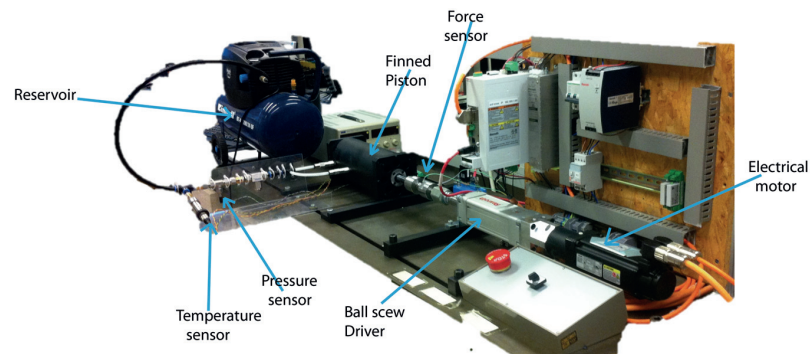


Figure 6.15 : Finned piston experimental setup

In order to characterize the losses in the finned piston system, first the compressor itself is tested without being connected to check valves and sensors. The data for force and velocity are recorded by corresponding sensors. Figure 6.16 shows the experimental force and velocity in no load mode and corresponding power.

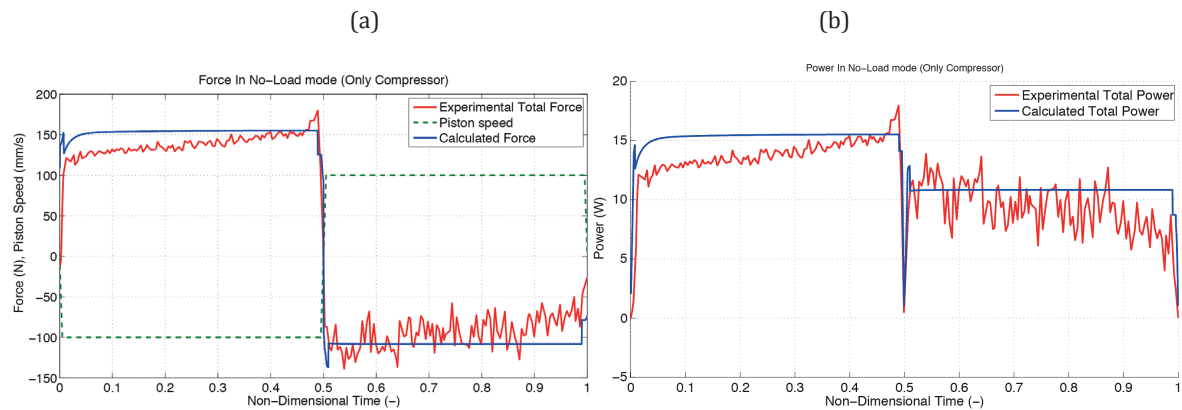


Figure 6.16 : Experimental and analytical (a) Force and velocity (b) power in no-load mode in finned piston compressor.

This is used to characterize the seal friction parameters. These parameters and also other geometrical parameters of the seals are shown in Table 6:1.

Table 6:1 input variable to the numerical simulation of the frictional forces in classical compressor.

Constant	Symbol	Value	Units
Piston ring sliding friction coefficient in compression	ϕ_1	0.2	-
Piston ring sliding friction coefficient in expansion	ϕ_2	0.15	-
Piston ring vertical height	σ	0.005	m

Piston ring preload fraction	$\alpha_{preload}$	0.2	-
Maximum gas pressure	$P_{gas,max}$	580	kPa

In the next step the compressor will be connected to the reservoir, which is called “load mode”.

The pressure and power raise evolution is shown in **Figure 6.17** and **Figure 6.18**. For finned piston compressor, since the heat transfer coefficient relation (4:9) has an uncertainty of $\pm 20\%$, the curves of pressure raise has been plotted for these values as well. As expected, the model prediction of the pressure curves matches very well the experimental pressure, with the experimental pressure falling within the $\pm 20\%$ uncertainty error of heat transfer coefficient.

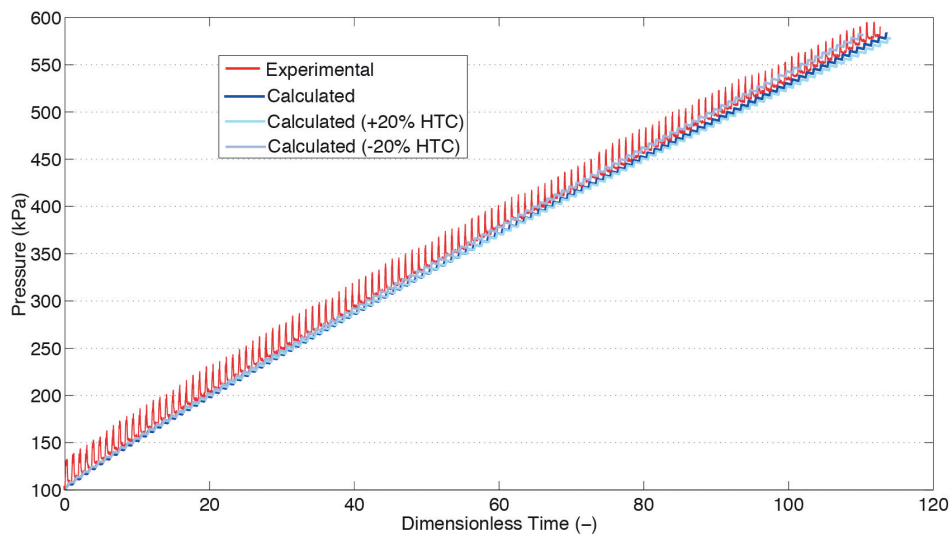


Figure 6.17 : Experimental and analytical pressure increase in finned piston compressor.

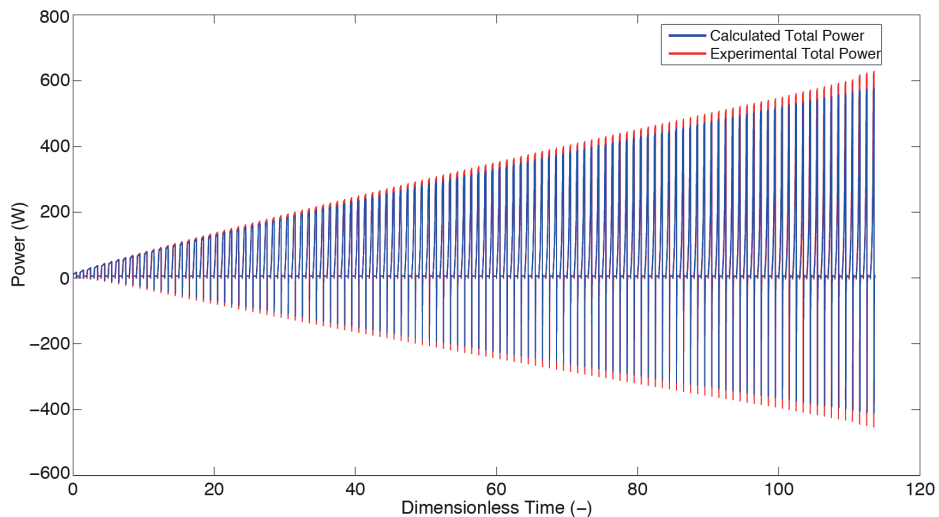


Figure 6.18 : Experimental and analytical power raise in finned piston compressor.

For the finned piston as well, the prediction of the model shows a reasonable match with experimental results, both in the way pressure and power raise as well as the shape of the power curve in any

individual cycle. The force and velocity is shown in **Figure 6.19** and corresponding power in **Figure 6.20** for zoomed areas on a selected cycle (50th). The prediction of the model shows good agreement with experimental results, both in they way pressure and power raise as well as the shape of the power curve in any individual cycle. The only visible difference is in the expansion part as was seen for classic compressor. The difference between the calculated and experimental power 3.1 % MAE for the whole range and 4% for the work input over the filling time (Integral of the power curve).

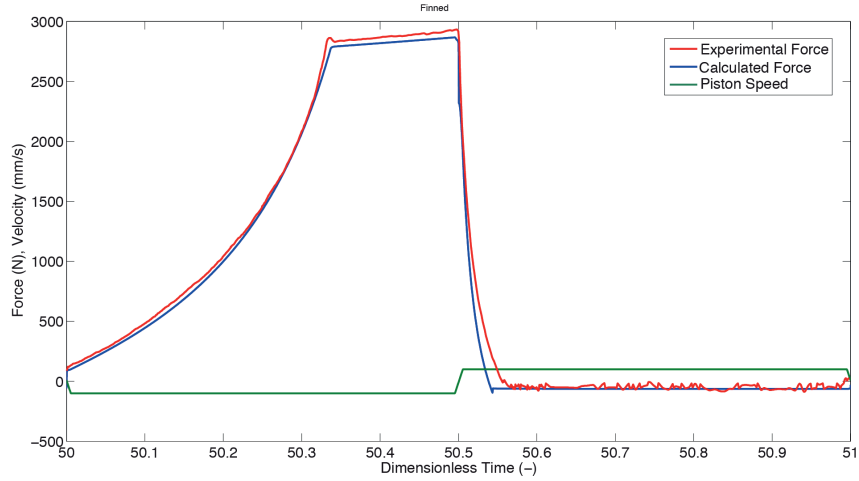


Figure 6.19 : Experimental and analytical force and velocity in load mode (50th cycle).

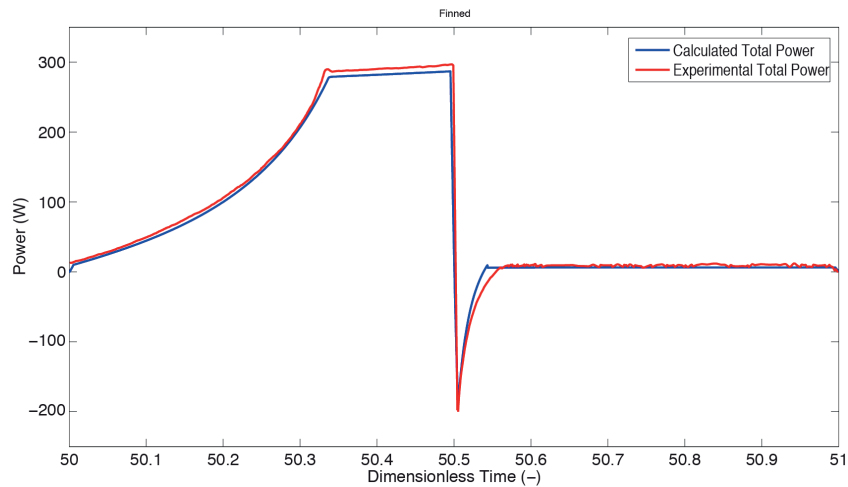


Figure 6.20 : Experimental and analytical power in load mode (50th cycle).

The experimental force is compared to model prediction in **Figure 6.21** for 100th cycle. But in **Figure 6.22**, the effect of uncertainty in heat transfer coefficient shown as it is seen for pressure rise. Experimental power falling within model prediction with $\pm 20\%$ heat transfer coefficient accuracy.

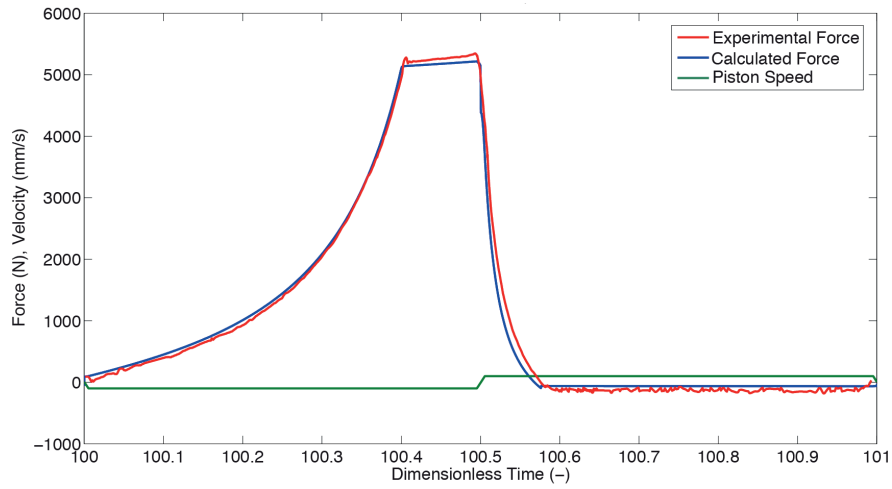


Figure 6.21 : Experimental and analytical Force and velocity in load mode (100th cycle).

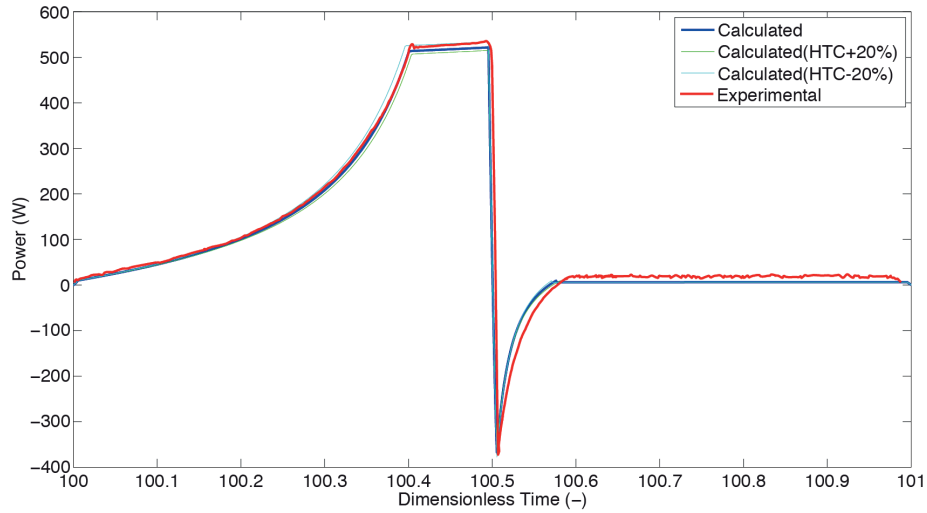


Figure 6.22 : Experimental and analytical power in load mode (100th cycle).

Figure 6.23 shows the amount of effective, friction and their sum which is total work, as well as final exergy content of reservoir during the charging process of the reservoir. If one compares **Figure 6.23** and **Figure 6.12**, it can be observed that the ratio of final reservoir exergetic content to effective (or total) work is more in the case of finned compressor as compared to the classic compressor. This fact will be seen also **Table 6:2**.

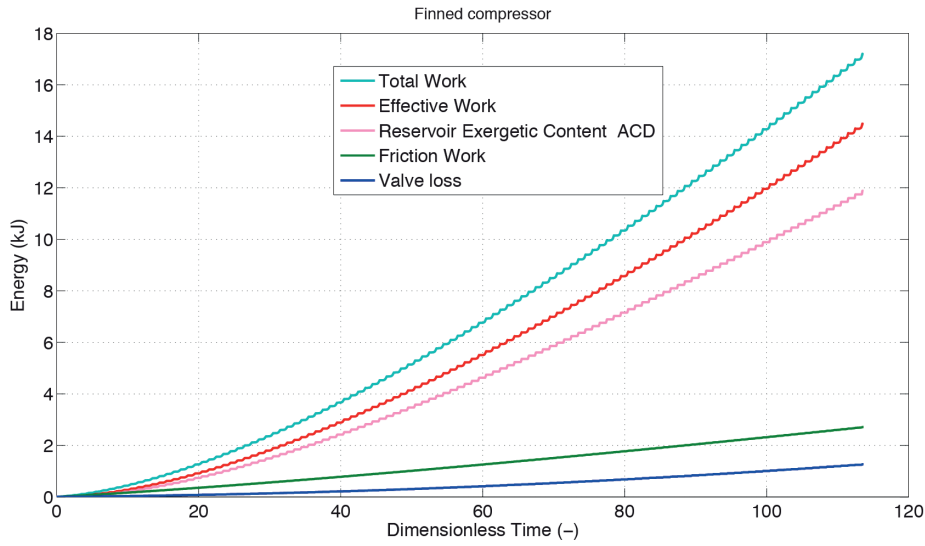


Figure 6.23 : Effective, friction and total work and reservoir exergy content after cool down for finned compressor.

The outer sleeve of finned compressor surface is measured with an infrared thermometer and compared to simulation (**Figure 6.24**) and it agreed relatively well.

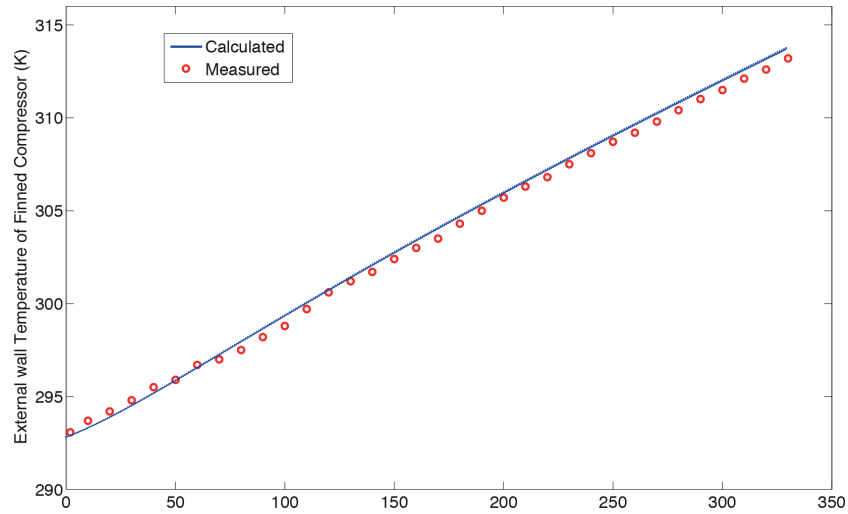


Figure 6.24 : Measured and calculated temperature for finned compressor sleeve.

6.6 Comparision

In this section, the performances of both the classic and finned piston are compared. Both pistons have the same surface area and the same stroke, so the dead and displacement volume is the same.

Figure 6.25 shows the evolution in compressors discharge pressure during the filling of the reservoir and also after stopping charging and cool down of the reservoir. It is evident that the finned piston fills the reservoir in longer time (114 cycles instead of 93 cycles). Because the finned piston should have a longer filling time, since it is more isothermal.

One of the other results recorded from the test bench is related to the discharge temperature at the output of both the classical and the finned compressors. The temperature profile of the output of the classic and finned compressor is represented in **Figure 6.26** and **Figure 6.27** respectively. The temperature raise is much less in finned piston, which shows a higher isothermal efficiency.

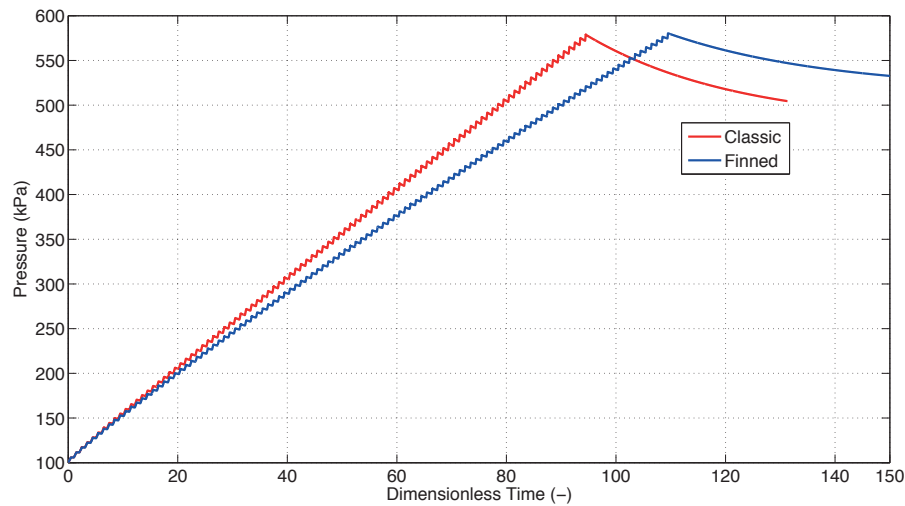


Figure 6.25 : Pressure evolution during filling the reservoir up to 5.8 Bar and after cool-down.

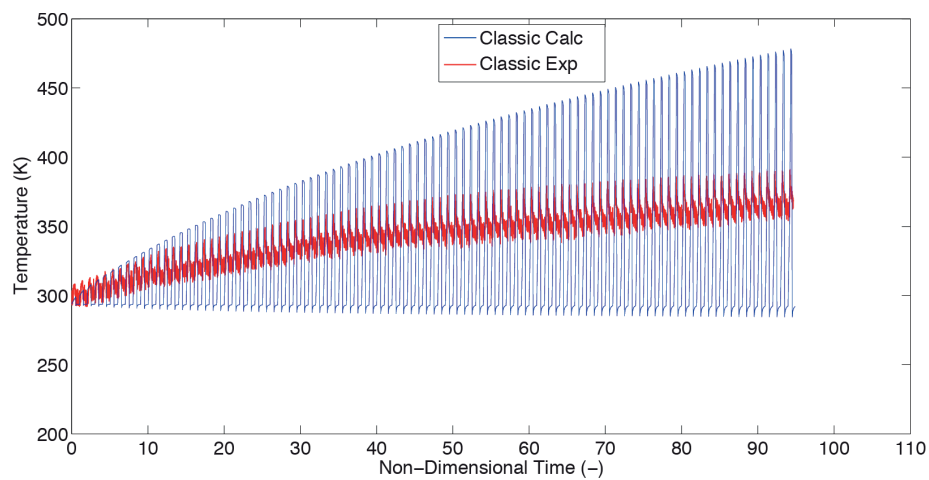


Figure 6.26 Temperature evolution for classic piston compressor during filling the reservoir.

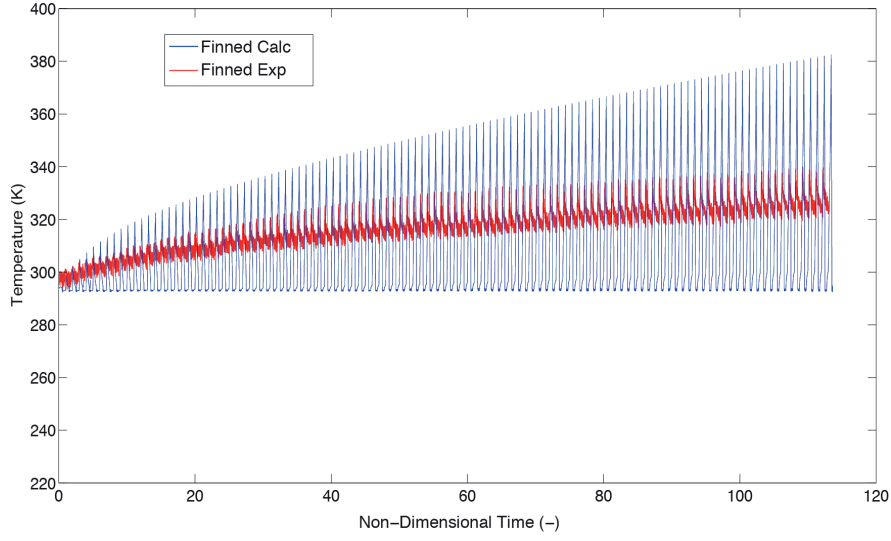


Figure 6.27 Temperature evolution for finned piston compressor during filling the reservoir.

As discussed in chapter 2, in CAES the goal is to store energy in a reservoir in the form of compressed air, and then recover it later.

In order to find the efficiency of the compression and storage process, one can divide the reservoir exergetic content after cool down to effective or total work delivered to compressor in **Figure 6.12** or **Figure 6.23**.

Another similar approach is to divide the work done by the compressor to the maximum extractable energy content of the reservoir. As mentioned in chapter 2, the work potential (exergy) of the compressed air in vessel with volume of V and pressure p_2 can be found based on Eq.(2:26) from the Eq. (6:1)

$$X_2 = p_2 V \left(\frac{1}{p_2} + \ln(p_2) - 1 \right) \quad (6:1)$$

For a reservoir with a volume of $V = 25 \text{ Lit}$, the final exergy content of the reservoir can be calculated for each compressor.

For the case of the classic compressor, the initial pressure of the reservoir is $p_{2i} = 5.8 \text{ Bar}$, but after a sufficient time and letting the reservoir to cool down, the pressure will reduce to $p_{2f} = 4.9 \text{ Bar}$. Hence, the energy content of the reservoir is equal to 8.86 kJ.

For the case of the finned piston compressor, however the initial pressure of the reservoir reaches to the same $p_{2i} = 5.8 \text{ Bar}$, but after the cool down it, the pressure reduces only to $p_{2f} = 5.25 \text{ Bar}$. This is due to the fact that the inlet temperature is lower and the pressure drop is less compared to the classic piston. Hence, the energy content of the reservoir is equal to 11.93 kJ.

The work in both cases can be calculated from the integral of the effective power curve (load mode and no load mode difference) during filling process.

$$W = \int [F_{LM}(t) - F_{NLM}(t)]v(t)dt \quad \text{From } t = 0 \text{ to } t = t@p = 5.8 \text{ Bar} \quad (6:2)$$

The efficiency can be defined based on Eq. (2:31) as:

$$\eta_{x,cs} = \eta_{x,comp} \cdot \eta_{x,stor} = \frac{X_1}{W_c^+} \frac{X_2}{X_1} = \frac{X_2}{W_c^+} \quad (6:3)$$

Or considering also the friction losses as:

$$\eta_{x,cs}^f = \frac{X_2}{W_c^+ + W_f} = \frac{X_2}{W_t^+} \quad (6:4)$$

The energy consumptions and exergetic efficiency is summarized in **Table 6:2**.

Table 6:2 Compression and storage exergetic efficiency in filling mode comparison between the pistons.

	Friction Work (kJ)	Compression Work (kJ)	Total Work (kJ)	Final Exergy content (kJ)	$\eta_{x,cs}^f$ (%)	$\eta_{x,cs}$ (%)
Classic piston compressor	2.12	13.14	14.82	8.86	59.7	67.4
Finned piston compressor	2.6	14.3	16.9	11.93	70.6	84

The results show that however the finned piston has a slightly higher friction loss, it consumes less effective energy for compressing the gas, showing higher exergetic efficiency since the compression process is closer to isothermal conditions.

Chapter 7 Sensitivity Analysis

7.1 Introduction

In the finned compressor under the study, the effect of various parameters, such as clearance volume, stroke length to bore diameter, operating speed, etc. must be well understood. In this chapter a parametric study was conducted to study the effect of these parameters. Compressor parameters: clearance volume, stroke length, stroke length to bore diameter ratio, cylinder wall temperature, velocity, number of fins and gap between fins--were varied systematically. Performance parameters: volumetric efficiency, consumed energy, total heat transfer, discharged mass and consumed energy per unit of mass discharged (per cycle) and exergy efficiency—were studied as the compressor parameters were varied. All simulated results are based on the prediction of the model developed for the finned piston in Chapter 4 and for FLP between 1 to 5.8 Bar. The results reveal interesting potential of improving performance by using optimized design variables.

7.2 Performance Parametres

It is important to define appropriate parameters to evaluate the compressor performance. The performance indicators in compressors can be divided into three categories

7.2.1 Mass Flow of Compressed Gas Delivered

It is important to measure the mass flow delivered by the compressor. The higher the amount of mass delivered the higher the capacity of compressor is. Another indicator in this domain that has a close correlation with discharged mass is volumetric efficiency η_v , which is defined as:

$$\eta_v = \frac{\text{Volume of the gas intake per cycle}}{\text{stroke or swept volume}} \quad (7:1)$$

7.2.2 Work Consumed by the Compressor

Another important parameter of the compressor is the consumed work. This parameter can be defined as the work consumed per cycle or work consumed per unit of time which is corresponding to power. Since the isothermal compression is the ideal process for compression, in the context of finned compressor, the efficiency parameter for evaluating work can be compared to this work. So, the isothermal efficiency (ratio), which is defined as:

$$\eta_{iso} = \frac{\text{Ideal work of isothermal compression}}{\text{Actual work of compression}} \quad (7:2)$$

7.2.3 Exergetic Efficiency

Assuming an steady state operation with a fixed exhaust pressure level, the exergetic efficiency can be defined as shown in Chapter 2 the exergy content of the gas stream after cool down divided by the total work delivered to the compressor:

$$\eta_{ex} = \frac{\dot{E}_{ex,c}}{\dot{W}_c} \quad (7:3)$$

Exergy efficiency may also be defined including losses (friction and vicious dissipation)

$$\eta_{ex} = \frac{\dot{E}_{ex,c}}{\dot{W}_c + \dot{W}_f} \quad (7:4)$$

Where the stream exergy of the outlet gas from the compressor after cool-down is:

$$\dot{E}_{ex,c} = \dot{m}_e R T_e \ln \left(\frac{p_e}{p_{amb}} \frac{T_{amb}}{T_e} \right) \quad (7:5)$$

For more detailed calculation of efficiency terms please see Appendix II.

Figure 7.1 shows the relation between inlet and outlet state variables, simulation equations, constitutive relations and performance parameters in a compressor.

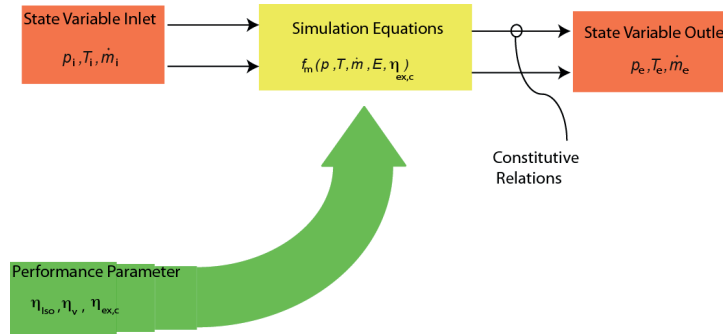


Figure 7.1 : Input and output variables and performance parameters of the system.

7.3 Finned compressor parametric study

In this section we have simulated the aforementioned model for a finned compressor and will investigate the effect of changing design variables including clearance volume, stroke length, stroke length to bore diameter ratio, cylinder wall temperature and velocity on performance parameters.

7.3.1 Effect of clearance volume

Clearance volume, which significantly affects the performance of the compressor, is an important factor in compressor design. The sensitivity of compressor performance to change in clearance volume is shown in **Table 7:1** and **Figure 7.2** and **Figure 7.3**.

Table 7:1 Effect of clearance volume on performance parameters of the finned compressor.

Clearance volume	3.5%	5.5%*	7.5%
	(-36%)		(+36%)
$\eta_v(\%)$	88.5	80.6	72.5
	(+10%)		(-10%)
Consumed energy (kJ/cycle)	0.193	0.176	0.157
	(+10%)		(-10%)
Discharged Mass (kg/cycle)	$1.24 * 10^{-3}$	$0.98 * 10^{-3}$	$0.842 * 10^{-3}$
	(+26%)		(-14%)
Consumed energy per mass unit (kJ/kg)	174	179.6	186.3
	(-3.2%)		(+3.7%)
$\eta_{iso}(\%)$	87.6	87	85.5
	(+0.8%)		(-1.7%)
$\eta_{ex}(\%)$	80.68	78.4	74.3
	(+3%)		(-5%)

* Base-line condition

The value in () is the percentage change from the base line.

One may observe that with increasing the clearance volume, the volumetric efficiency decreases dramatically. This is logical since the gas at the discharge pressure is trapped in the clearance volume at the end of compression. This trapped gas is expanded until its pressure is lower than the intake pressure (atmospheric pressure here). The increase of clearance volume, therefore, increases the amount of trapped gas, causes the inlet valve to open later, and decrease the volumetric efficiency as shown in **Figure 7.2**.

Also, decreasing the clearance volume, isothermal and exergetic efficiency also increases due to the fact that the compression effective work per unit mass decreases.

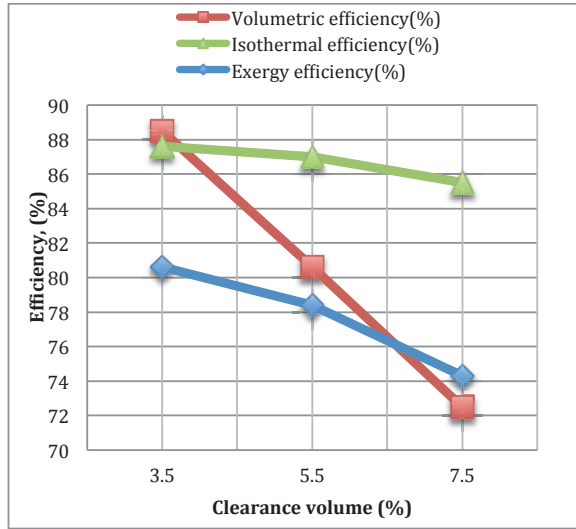


Figure 7.2 : Variation in volumetric, isothermal and exergetic efficiency.

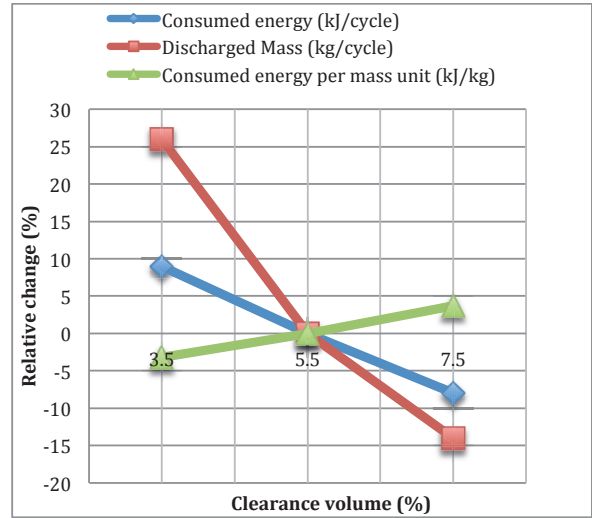


Figure 7.3 : Variation in consumed energy, discharged mass and consumed energy per mass unit.

One may also observe that an increase in volumetric efficiency enhances the actual delivered capacity, the discharged mass, and consumed energy. **Figure 7.3**, shows that the slope of the discharged mass is higher than the consumed energy as the clearance volume decreases. Therefore, reducing clearance volume can efficiently enhance the work per unit mass.

7.3.2 Effect of velocity

One of the most interesting parameters to investigate is velocity. One may observe that as shown in **Figure 7.4** the linear speed is changed from 25 to 200 mm/s versus the dimensionless time. **Figure 7.6**, which shows the time in horizontal axis, however shows that for a lower linear velocity it takes longer time to complete the cycle, which means longer period time. Since the velocity is lower, the mean gas velocity is lower and so as shown in **Figure 7.5**, the Reynolds number is lower. This leads to lower convection heat transfer rate (**Figure 7.6**). However, since the total heat transfer (**Figure 7.7**) is the integral of heat transfer rate over the period time, the total heat transfer is higher in a cycle with longer period. This leads to lower exhaust temperature (**Figure 7.8**) and lower total work required (**Figure 7.9**). Here it should be noted that friction was shown to be constant since friction losses are independent of speed (please see Eq.3:24).

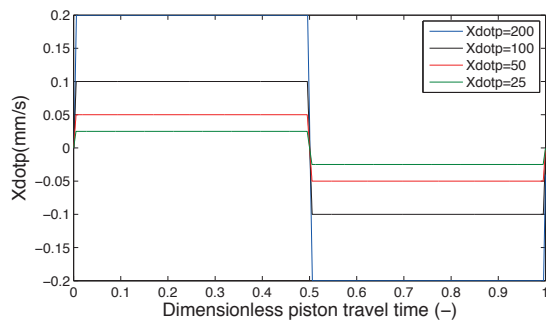


Figure 7.4 : Linear velocity.

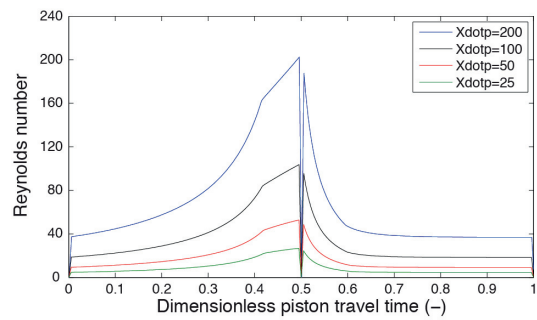


Figure 7.5 : Reynolds number.

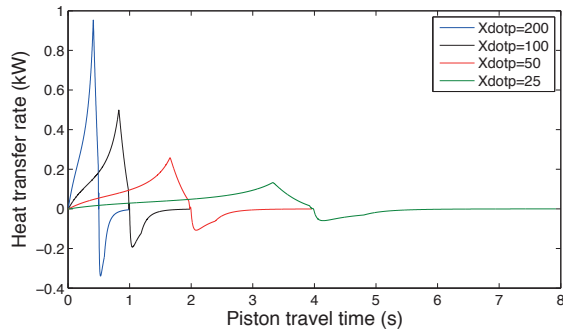


Figure 7.6 : Heat transfer rate.

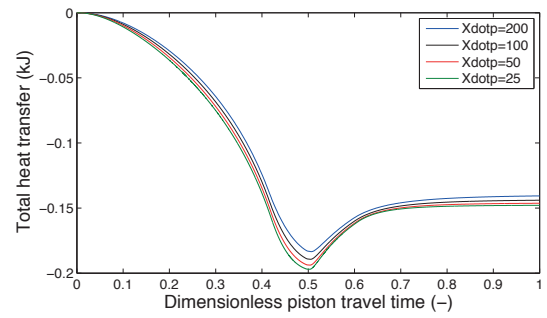


Figure 7.7 : Total heat transfer.

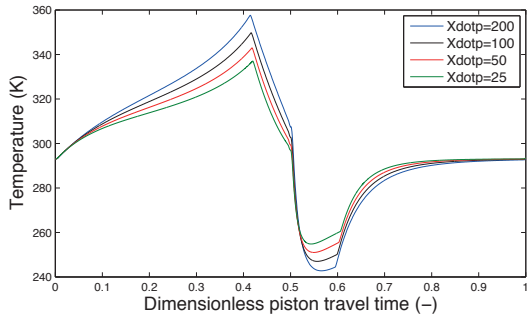


Figure 7.8 : Gas temperature.

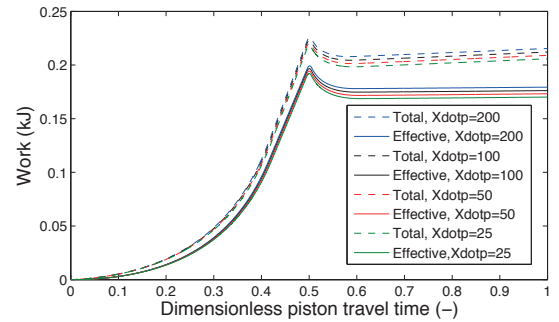


Figure 7.9 : Total work.

This fact is shown in **Table 7:2** as well. It is apparent from this table and **Figure 7.10**, which however by reducing velocity, the consumed energy and mass discharged per cycle decrease, but the consumed energy per unit mass also decreases. This means lower operating speed is beneficial in compressors, since it lets the gas to exchange more heat and get closer to isothermal operation (**Figure 7.11**), however decreases the capacity of the compressor. The interesting observation in this section is that the amount of friction work is independent of the velocity (by keeping the geometry unchanged). Because since the friction force is almost constant and independent of velocity (please see Eq.3:24), the friction work is proportional to the area under velocity curve, which is practically equal for all the cases, since higher velocity is compensated by lower operation time.

Table 7:2 Effect of Velocity on performance parameters.

Linear velocity (mm/s)	200	100*	50	25
Consumed energy (kJ/cycle)	0.1794 (+1.8%)	0.1762	0.1732 (-1.7%)	0.1701 (-3.6%)
Discharged Mass (kg/cycle)	0.9854×10^{-3} (+0.55)	0.98×10^{-3}	0.9768×10^{-3} (-0.4%)	0.9734 (-0.6%)
Consumed energy per mass unit (kJ/kg)	182.04 (+1.5)	179.6	177.32 (-1.2%)	174.66 (-2.7%)
Heat transfer (kJ/cycle)	0.1407 (-2.2%)	0.144	0.1463 (+1.6%)	0.1479 (+2.7%)

Discharged gas temperature (k)	357.6 (+2.2 %)	349.8	342.8 (-2%)	336.9 (-3.7%)
Friction Losses (kJ/cycle)	0.036 (0%)	0.036	0.036 (0%)	0.036 (0%)
$\eta_{ex}(\%)$	75.6 (-2.3 %)	77.8	79.49 (+2.1%)	81.4 (+4.4%)

* Base-line condition

The value in () is the percentage change from the base line

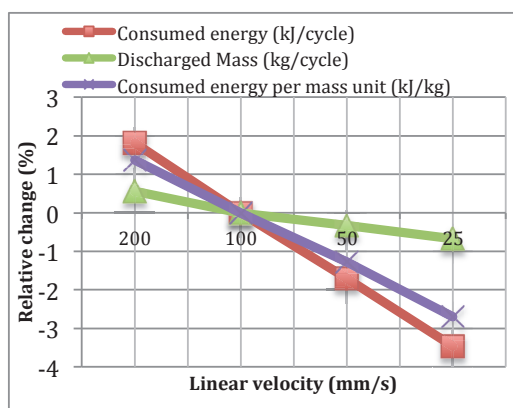


Figure 7.10 : Variation in consumed energy, discharged mass and consumed energy per mass unit.

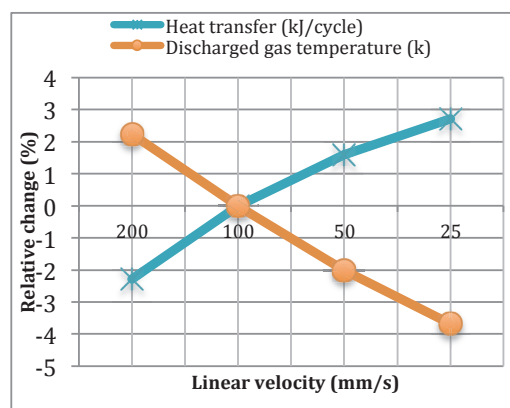


Figure 7.11 : Variation in Heat transfer and discharged gas temperature.

Since the operating speed is the only parameter that can be varied experimentally a sensitivity analysis is conducted on it. This is accomplished by examining the sensitivity of the input work to change in compressor linear speed in filling mode. The test results were compared with model prediction on a Parody diagram and it was found that the work input to fill the reservoir up to 5.8 Bar matched the experimental results within 1% MAE with all points falling within $\pm 2\%$ of experimental results. The input work has a trend, which tended to under predict the work at low speed and over predict it in medium speed and again under predict it in higher speed (**Figure 7.12**).

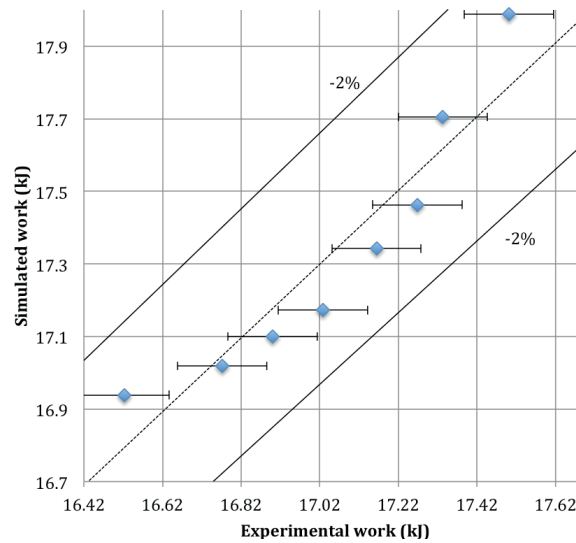


Figure 7.12 : Simulated compared against experimental input work for finned piston compressor for filling mode up to 5.8 Bars.

7.3.3 Effect of Cylinder Wall(Fins) Temperature

In reality the wall (fins) temperature is not constant and not a design parameter, but a variable parameter affected by heat transfer. In this section however, wall temperature is assumed constant in the model, so changing it from a sub-ambient temperature to a higher amount can reflect the effect of lower to higher heat transfer. In this study the wall temperature is changed from 250 K to 450 K. **Figure 7.13** shows the change of work while **Figure 7.14** shows the change of different efficiencies. Evidently the lower wall temperature corresponds to lower work and higher isothermal and exergetic efficiencies, however the delivered mass (**Figure 7.15**) and volumetric efficiency decrease.

In other words, whenever the fins and walls are cooled, the value of polytropic factor during compression will be lower than k , since cooling tends to make the process nearly isothermal. Again during expansion of the air in the dead volume, an effectively cooled cylinder head tends to make the process isothermal. As a result the volume of the air trapped in the dead volume (at the end of compression stroke) will be greater than what it would be if it was isentropic.

Hence the volumetric efficiency of the finned compressor is adversely affected by effective cooling of fins cylinder head and walls, though the work input for compressing unit of mass is reduced (**Figure 7.16**).

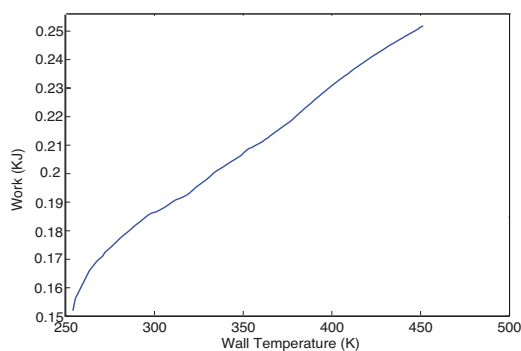


Figure 7.13 : Effective Work change with wall(fins) Temperature.

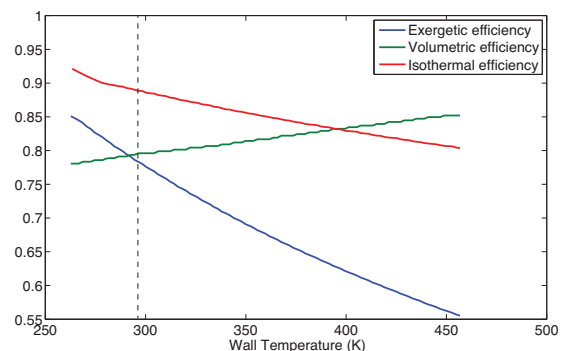


Figure 7.14 : Efficiency change with wall(fins) Temperature.

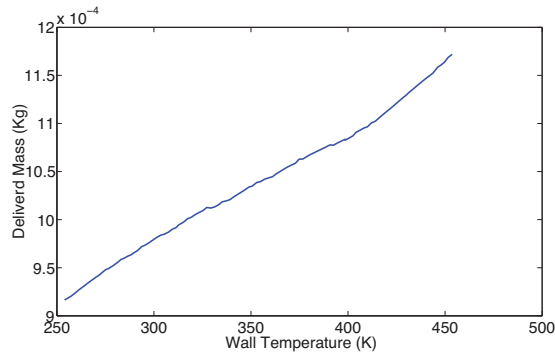


Figure 7.15 : Discharged mass change with wall(fins) Temperature.

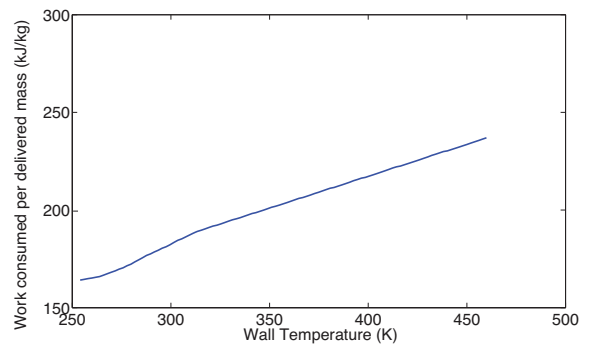


Figure 7.16 : Work Consumed per delivered mass change with wall(fins) Temperature.

7.3.4 Effect of Stroke Length to Bore Diameter (L/D)

Different stroke length means different cylinder length. A cylinder becomes shorter when the stroke length is decreased. A compressor with a shorter cylinder is more compact and economical. Hence, the stroke length to diameter is an important factor in determining the manufacturing cost of compressor.

Volumetric efficiency changes slightly with different stroke lengths because the percentage of clearance volume is fixed. So this performance parameter was not included in the results. Keeping the volume (dead and displacement) fixed, the ratio of L/D is changed from 0.1 to 2.34 (**Figure 7.17**). It should be reminded that in a cylinder the minimum surface area for a fixed volume would occur when the length is equal to diameter.

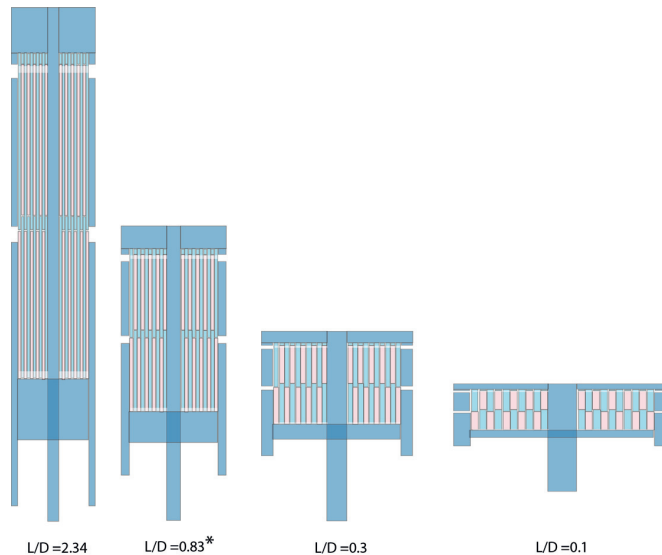


Figure 7.17 : Finned piston geometry for different length to diameter ratio(*=Base case).

In this part the length of compressor (and stroke as a result) will increase but the piston period remains the same. So a piston with longer stroke (**Figure 7.19**) will have a higher velocity (**Figure 7.18**).

It is apparent that longer stroke means higher speed, which leads to higher Reynolds number and higher convection heat transfer coefficient (**Figure 7.20**). This together with increased heat transfer area and also

reduced hydraulic diameter (see Eq.(4:40)). As a result, the total heat removed from the gas will increase (with the period being the same) (**Figure 7.21**), leading to lower temperature of the exhaust gas (**Figure 7.22**). Also the discharged mass decreases slightly as seen in section 7.3.3(**Figure 7.23**).

This in turn will lead to lower work requirement. However in this section (by changing the geometry) one may note that the friction work will increase as a result of increased speed.

Figure 7.24 shows that compression work decreases with increased piston length, but friction increases with piston length. What is interesting is that overall; the total consumed energy per mass has a minimum when L/D ratio is equal to 1.43. This leads to a maximum in exergetic efficiency (**Figure 7.25**)

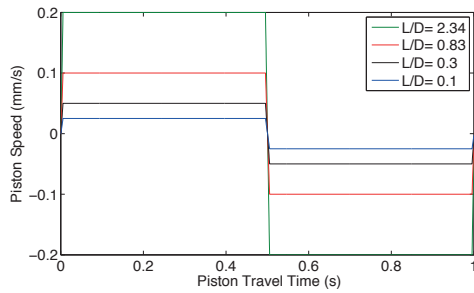


Figure 7.18 : Linear velocity.

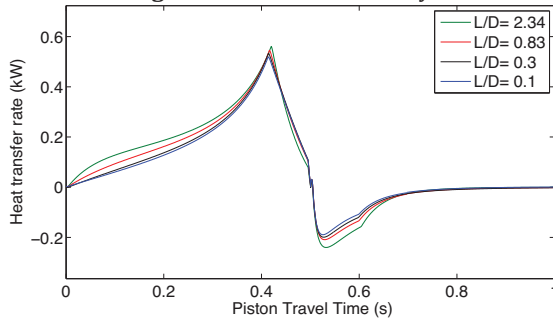


Figure 7.20 : Heat transfer rate.

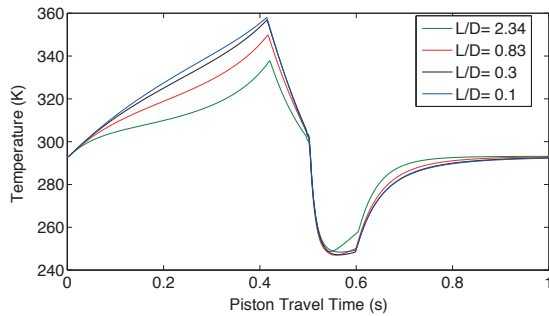


Figure 7.22 : Gas temperature.

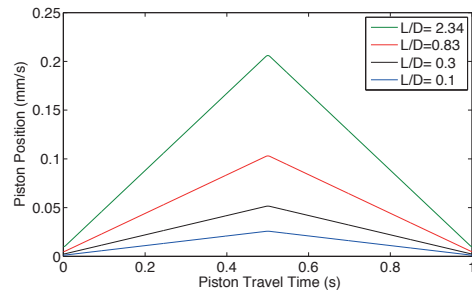


Figure 7.19 : Piston position.

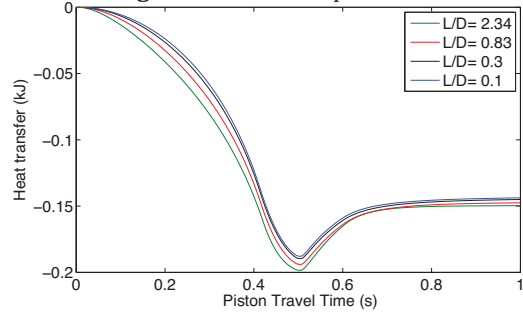


Figure 7.21 : Total heat transfer.

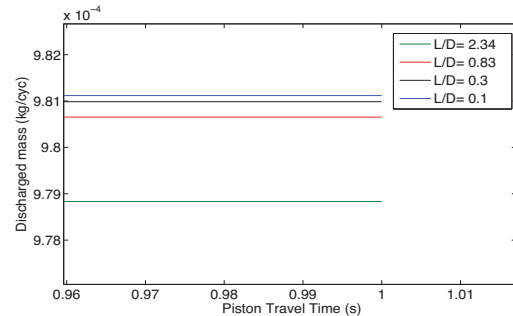


Figure 7.23 : Discharged mass.

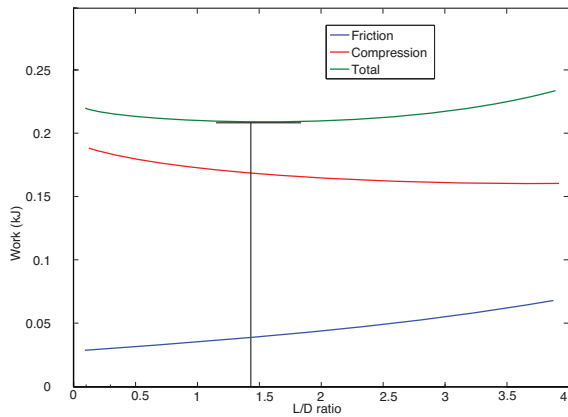


Figure 7.24 : Work change with L/D ratio.

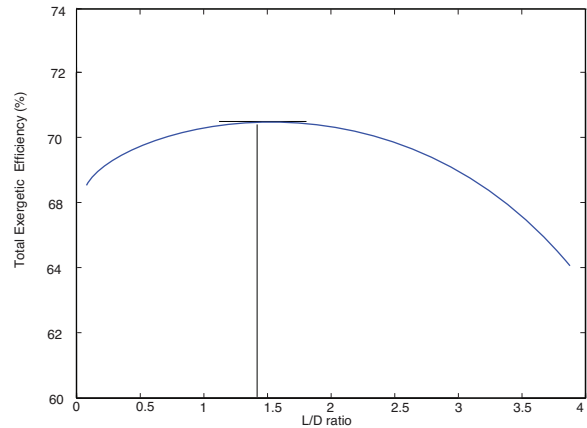


Figure 7.25 : Total exergetic efficiency (including friction) change with L/D ratio.

7.3.5 Effect of Number of Fins

The number of fins is proportional to heat transfer surface and also increased number of fins in a given space means lower hydraulic diameter, which in turn according to Eq.(4:40), (4:9) and (4:10) means higher Nusselt number and convective heat transfer coefficient. Hence increasing the number of fins in a given volume improves the performance theoretically. However, the drawback is that the energy lost as viscous dissipation (Eq. (4:44)) in IFS will increase dramatically. In **Figure 7.26** the exergetic efficiency is shown as a function of number of fins. The green curve represents the efficiency neglecting the friction and viscous dissipation (Eq.(7:3)), while the blue curve shows exergetic efficiency taking into account such losses (Eq.(7:4)). Nevertheless, manufacturing a finned piston with such a thin width and narrow gap is not practical.

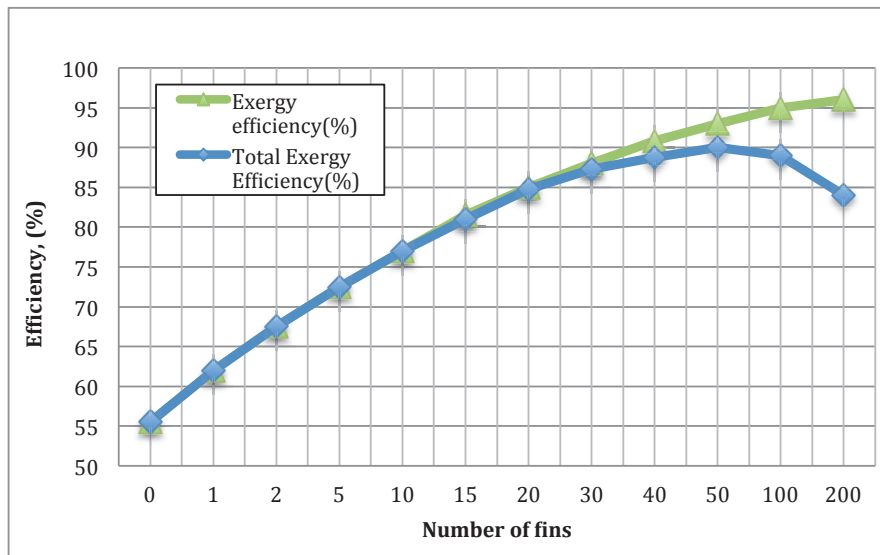


Figure 7.26 : Efficiency change with number of fins.

7.3.6 Effect of gap between fins

It is interesting also to study the effect of the gap between fins on performance parameters in the compressor in FLP mode with $PR = 5.8$. Evidently increasing the gap increases the dead volume of the

compressor (Figure 7.27). This in turn will decrease the discharged mass and volumetric efficiency (Figure 7.28).

On the other hand, the heat transfer and consequently compression work and also dissipated pneumatic energy depends on the pressure gradient between fins. Figure 7.29 shows that for a given pressure gradient increasing the gap decreases the compression work and increases the pneumatic dissipation. However, finally all the aforementioned parameters should be considered into η_{ex} . According to Figure 7.30 for a given pressure gradient, exergetic efficiency reaches a maximum for a specific gap between fins. This value of gap between fins increases with increment of Δp .

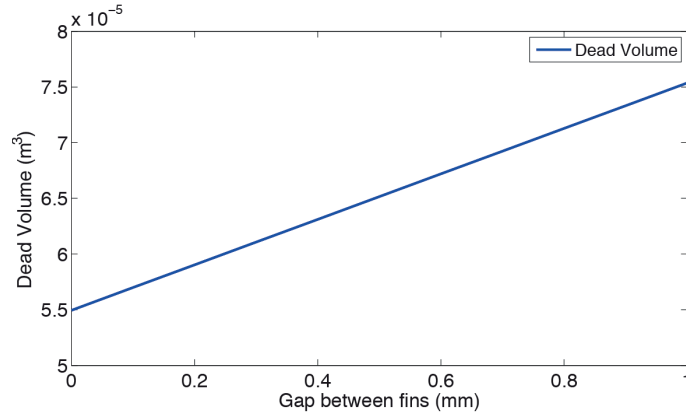


Figure 7.27 : Influence of g_{IFS} on dead volume

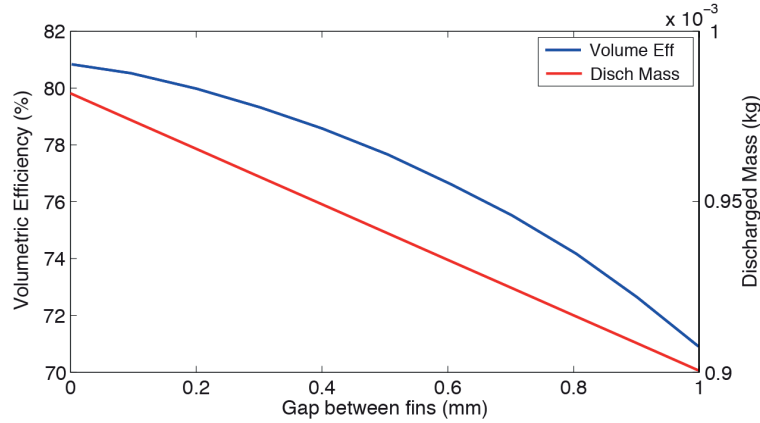


Figure 7.28 : Influence of g_{IFS} on discharged mass and η_{vol}

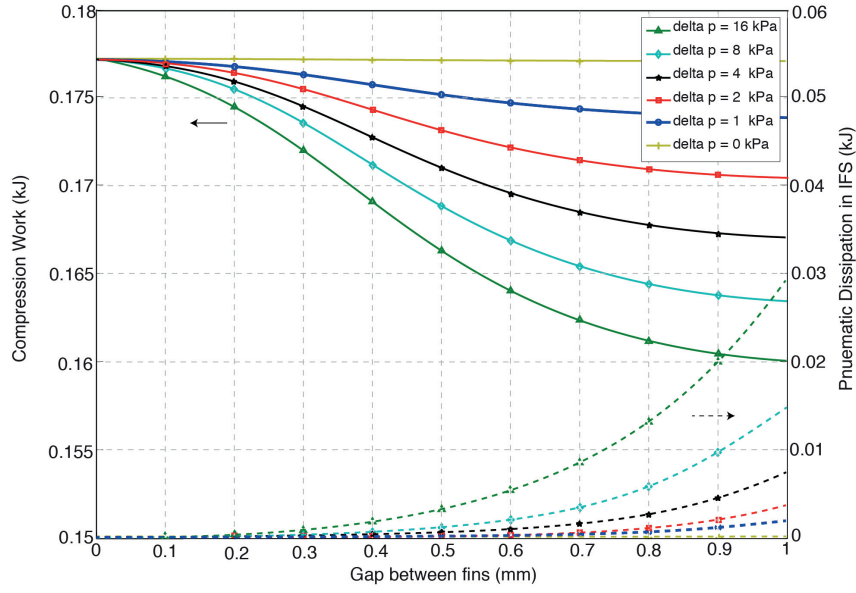


Figure 7.29 : Influence of g_{IFS} and Δp on compression work and pneumatic dissipation in IFS. (Initial $\Delta p=1$ kPa for current design).

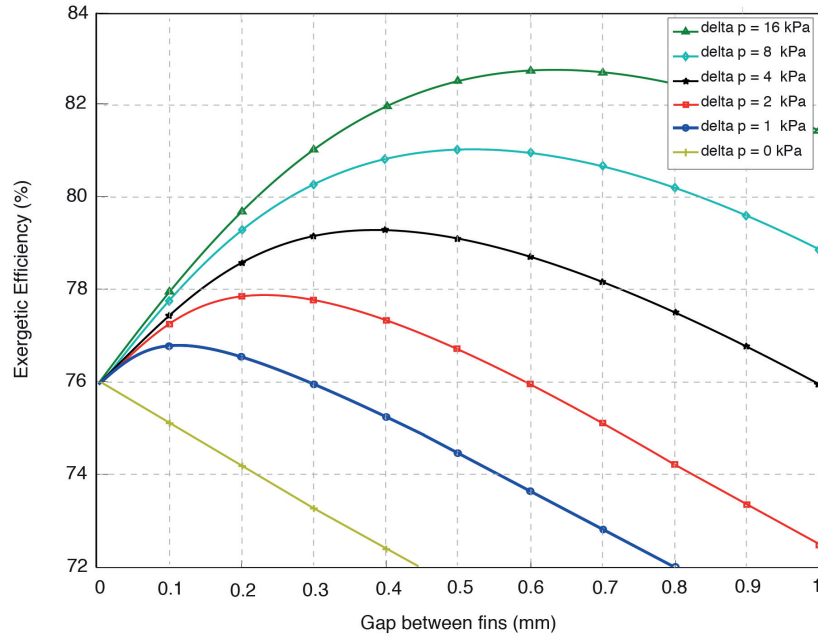


Figure 7.30 : Influence of g_{IFS} and Δp on η_{ex} (Initial $\Delta p=1$ kPa for current design).

7.4 Conclusion

In this chapter, the effect of different parameters on performance of the finned piston compressor is investigated. It was found that exergetic efficiency is the most comprehensive parameter for evaluating the compressor performance for CAES applications and contains the effect of delivered mass as well as consumed work, so only this performance parameter was selected in the last sections. Among these parameters, some like clearance volume are better to be as small as possible however

their minimum is restricted by design limitations. Others like operating speed also need to be at their minimum for the compressor to be efficient, however this decrease the capacity of the delivered air, so other parameters should be considered in their selection. Among these parameters L/D ratio and gap between fins are very interesting since there is an optimum value for them regarding efficiency. The maximum exergetic efficiency is obtained when length is almost equal to 1.4 times of diameter, but the gap between fins is a function of pressure gradient as well. For the current pressure gradient the current gap is optimum. Finally wall temperature (that is shown that should be minimum for better efficiency) for example, is not a design parameter, but a consequence of enhanced heat transfer.

Chapter 8 Conclusion and Future Research

8.1 Achieved results

Applying the existing compressor/expanders for isothermal CAES systems have a few drawbacks, but these can be addressed by employing some innovative concepts like Directly Integrated Exchangers (DIE). Since the same design will be used in expansion mode, the interest in approaching isothermal condition is double. The same concept can be applied to multistage compression/expansion for reaching high compression ratios. By doing so, inter-heaters and intercoolers may be avoided, resulting in pressure drop and equipment cost.

A comprehensive thermodynamic study has been done on CAES regarding the level of isothermy. It was shown that only an analysis based on 1st law of thermodynamics is not sufficient to evaluate the performance of an isothermal CAES system. The 2nd law of thermodynamics has to be taken into account and combining these two, the exergetic efficiency was defined and used as the effective performance evaluation term in this study.

A step by step and modular approach is employed in modelling the finned piston compressor and the graphical representation was used to demonstrate such a model. First the model is developed for a basic compressor by attaching all the subsystems of a compressor. This model is used as a basis for the finned piston compressor model: several compression chambers are connected to represent the annular compression chambers and their heat and mass transfer interaction were taken into account using thermo and pneumatic-electric analogies.

The models were verified using dedicated test benches. The results reveal an increase of 16% in exergetic efficiency by using finned compressor.

This study has shown that a comprehensive modelling approach can indeed be used for predicting the performance of both classic and finned linear reciprocating compressors. The sensitivity analysis in combination with experimental validation of the prototype compressors shows the general approach for modelling finned compressor is relatively strong, as relatively few modifications to the model were needed to present the finned piston compressor.

This model was exercised to determine the important parameters when designing a finned compressor. It was discovered that the finned compressor is highly sensitive to dead volume and moderately sensitive to change in operational speed and stroke to diameter ratio. Changes to the finned piston geometry shows that there is an optimum value for length to bore diameter ratio and gap between fins, however the general sensitivity of the model to these parameters is relatively small.

In **Figure 8.1** one can see the situation of CAES technology regarding thermal characteristics from isothermal to adiabatic compression. Performance indicators are plotted as a function of polytropic factor for FLP mode with PR=5.8. The polytropic factor was changed from 1.4 to 1 (Adiabatic to Isothermal) the arrow shows the direction of progress towards isothermal behaviour. The red line is the position of classic piston ($n=1.35$), while the blue one is the finned piston ($n=1.12$). One can see that the isothermal efficiency has increased from 76 % to 87% as a result of increase in overall heat transfer coefficient from 1.42 to 25.1(W/K). Also, average outlet temperature has decreased from 446 K to 325 K and the work done per cycle decreased from 0.21 kJ to 0.17 kJ. However, There is still a huge potential for improvement.

Noticing the second plot in **Figure 8.1** shows that approaching toward higher isothermal efficiencies is very difficult, because the overall heat transfer coefficient increases logarithmically toward isothermal, and an ideal piston needs almost 100 times more overall heat transfer coefficient. This means almost 100 more time fins in the same volume, which is practically impossible. On the other hand the viscous dissipation in such a configuration will also increase dramatically. This balance of heat transfer to viscous forces and also construction costs requires a design optimization, which is beyond the scope of this work. The objective function can be compression-storage efficiency and the decision variables are geometrical dimension (e.g. fin width or stroke to diameter ratio) as well as operational conditions (e.g. speed...). A study is done on the effect of each individual parameter on performance, but a comprehensive optimization can also be done to improve the design taking into account the effect of each parameter on the others.

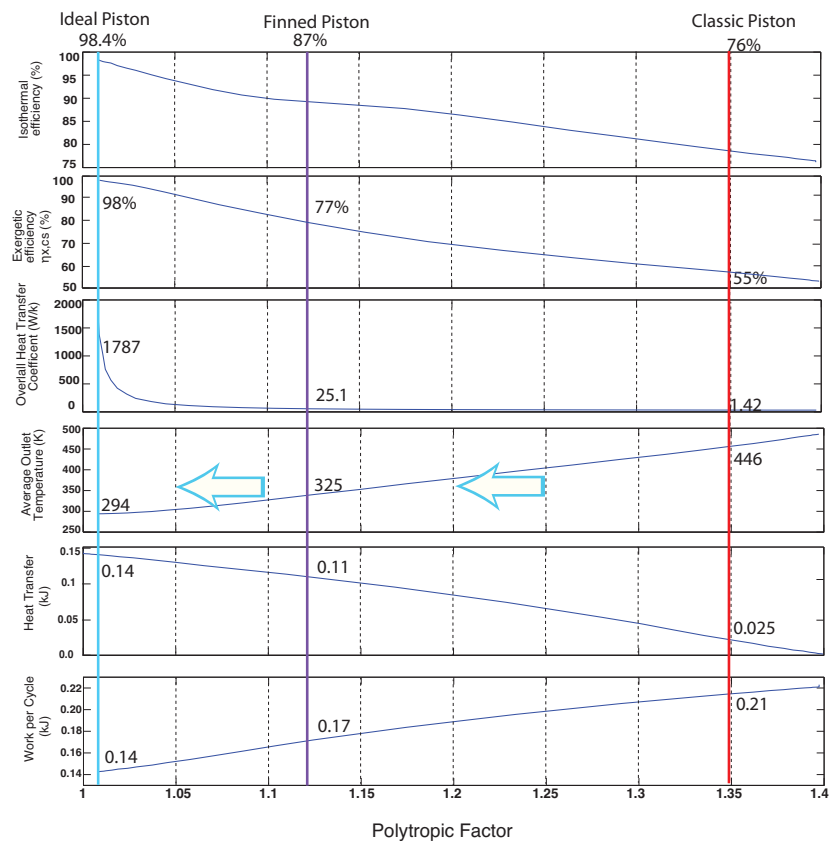


Figure 8.1 : Placement of Finned piston in the roadmap (Results for FLP mode with PR=5.8).

8.2 Future Research

It was concluded from the previous section that to reach the isothermal compression, the overall heat transfer coefficient (heat transfer coefficient multiplied by the heat exchange area) should be increased by orders of magnitude, and even some changes in the design by performing an optimization can only increase the efficiency by few percents. Hence, the level of isothermal or exergetic efficiency reached by a metallic finned piston is limited.

This is mainly due to poor convection heat transfer coefficient between air and metal, which is a property of the material. An alternative solution can be using another medium with higher heat convection coefficient such as water. It is natural, has a high heat capacity and density and thermal convection when it moisturizes the walls forming a liquid film. Moreover, the liquid can also be used as a medium to carry heat into and out of the compression chamber.

8.2.1 Liquid piston

One of the most promising solutions in this regard can be utilizing columns of water to compress the air. In fact it has been one of the first solutions to reach isothermal condition realized by LEI at EPFL. This has been carried out by introducing a new concept of water-hydraulic gas compression/expansion called “liquid piston”.

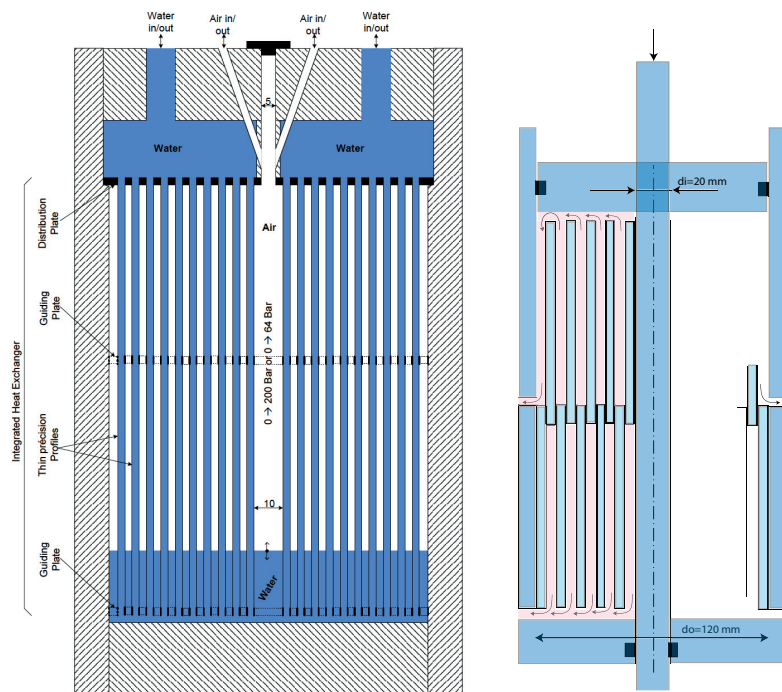


Figure 8.2 : Liquid piston geometry (Left) and Dry (Finned) piston geometry (Right).

Liquid piston has shown promising future for isothermal CAES in recent years, but still the thermo fluid analysis of the hydraulic-pneumatic aspects (which revealed to be the bottleneck of the system) was not studied in detail. This technology lacks a model that can describe and predict the thermal behavior of the integrated heat exchanger. This can provide an insight to the physics in the system and provide a tool to optimize the design. However complexity of the geometry and dynamic behavior of

the system with different and changing flow regimes and thermal properties poses a challenge. In section 3 an approach will be described to face the mentioned difficulties.

Modeling a reciprocating compressor deals with a series of complicated thermo-fluid phenomena's occurring simultaneously in a relative short period of time. This will be more complex in the case of a liquid piston, since the geometry is more complex and compression involves water circulation.

A precise dynamic (unsteady state) model should be obtained to predict the behavior and characterize the performance of the system.

However, these complexities can be addressed using similar techniques developed already in this thesis and will be described in more details in the next section.

Once such a model is developed a parameter study or an optimization can be done on the liquid piston to optimize its performance.

Liquid piston (**Figure 8.2** left) benefits from the same concept of heat transfer surface increase in a finned piston(**Figure 8.2** right), but on the other hand, uses columns of water instead of metal to compress the air.

Liquid piston has its own strength:

- Because a liquid can conform to an irregular chamber volume, the surface area to volume ratio in the gas chamber can be increased using a liquid piston. This creates near-isothermal operation, which decreases energy lost to heat generation.
- A liquid piston eliminates gas leakage and replaces sliding seal friction with viscous friction.
- The liquid can also be used as a medium to carry heat into and out of the compression chamber.
- Besides introducing directly integrated heat exchangers eliminates the cost and size problems of external heat exchangers and the pressure drop and temperature difference associated with them.
- Water has a high heat capacity and density and thermal convection when it moisturizes the walls.

However, water air interface introduces two new challenges that should be addressed:

- Two phase flow due to partial evaporation of water in air,
- Entrainment (diffusion) of a portion of the gas in the liquid at high pressures.

8.2.2 Methodology

The effective work will be to analyze the liquid piston from the thermodynamics, heat transfer and fluid mechanics point of view. This project comprises an analytic study, a CFD study and verification of the results using an experimental test bench.

8.2.3 Analytic model

The most important part in every research is to provide an insight into the physics of the problem by understanding the mechanisms involved. In the case of the liquid piston an analytic mode should be

developed based on the principles of mass and energy conservation as well as constitutive laws of thermodynamics. First a single bore will be studied from the heat transfer and fluid flow mechanism. As carried out for the case of dry piston a similar analogy between heat transfer and electric circuits can be proposed in **Figure 8.3**. For example, the heat generated as the result of air compression will be transferred radially out to the walls by convection. At the end this basic models can be put together to form the final model for the entire system.

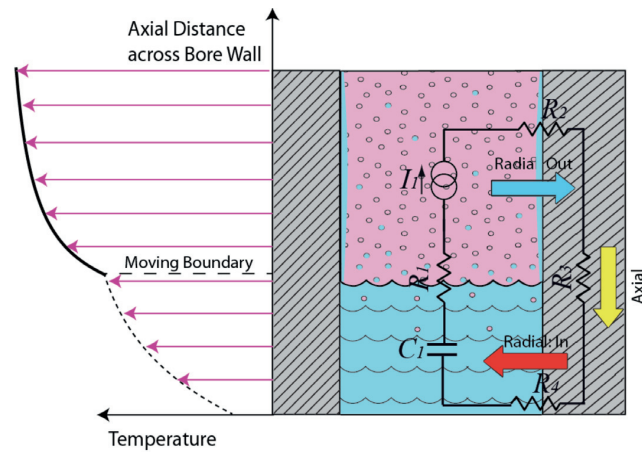


Figure 8.3 : Heat transfer mechanisms and assumed temperature profile across the bore wall.

8.2.4 FEM model

For the sake of simplicity, the analytical modeling is based on the assumption that parameters has a uniform distribution in each chamber, assuming one temperature, pressure, etc. in each chamber. However, it is of great interest to develop a finite element model that can predict the distribution of the parameters throughout the system over time. This provides a graphical representation of the heat and mass transfer process. A sample of such a model for one bore can be seen in Figure 3.

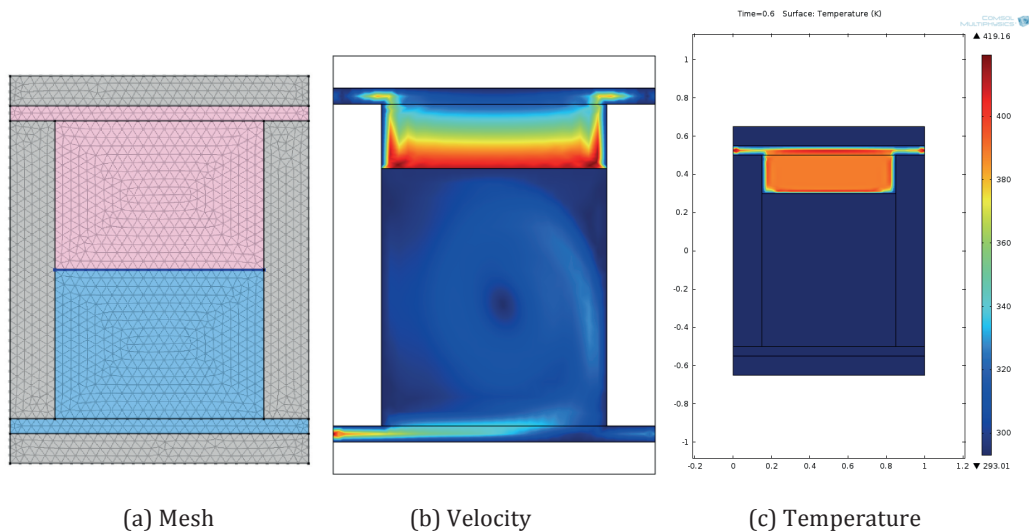


Figure 8.4 : Heat transfer mechanisms and assumed temperature profile across the bore wall.

Bibliography

- [1] Yang, Z., J. Zhang, M. Kintner, Meyer, X. Lu, et al. "Electrochemical Energy Storage for Green Grid." 2010.
- [2] *Energy Storage Association*. <http://energystorage.org> (accessed July 2012).
- [3] Cavallo, A. "Controllable and affordable utility-scale electricity from intermittent wind resources and compressed air energy storage (CAES)." *Energy* 32 (2009): 120–127.
- [4] Lund, H., and G. Salgi. "The role of compressed air energy storage (CAES) in future sustainable energy systems." *Energ. Convers. Manage* 50 (2009): 1172–1179.
- [5] Williams, S. Succar and R. H. *Compressed air energy storage: Theory, resources, and applications for wind power*. Technical report, Princeton, New Jersey: Princeton Environmental Institute, 2008.
- [6] Jakiel, C, S Zunft, and A Nowi. "Adiabatic compressed air energy storage plants for efficient peak load power supply from wind energy: the European project AA-CAES." *International Journal of Energy Technology and Policy* 5 (2007): 296-306.
- [7] Eckard, R. "CAES Compressed Air Energy Storage Worldwide." Rockville, MD, USA,: SBI Energy, 2010.
- [8] Lemofouet, S., and A. Rufer. "A hybrid energy storage system based on compressed air and supercapacitors with Maximum Efficiency Point Tracking." *IEEE Transaction on Industrial Electronics, Vol.53, No 4,08.2006*. 53, no. 4 (08 2006).
- [9] Reller, A., Rufer, A., & Cyphelly, I. "Usage of compressed air Storage System." Swiss Federal Office of Energy Report., 2004.
- [10] Kenschke, T. "Dispered energy storage - raising the productivity of renewable energy sources with cutting-edge energy storage solutions." *Proceedings. Eurosolar/Energieagentur NRW meeting*. Germany, 2003.
- [11] Kepshire, D. D. "Demonstration of Isothermal Compressed Air Energy Storage to Support Renewable Energy Production." Washington D.C. : Update conference US DOE ESS, 2010.
- [12] Lehman, J. "Air storage gas turbine power plants: a major distribution for energy storage." *Proc. Int. Conf. Energy Storage*. Brighton UK., 1981. 327 – 336.
- [13] Hoffeins H., H. "Air storage gas turbine power plant." *Energy Supply*. , 1994.
- [14] McBride , T, and D Kepshire. *ICAES innovation: foam-based heat exchange*. Seabrook, NH, USA : SustainX, Inc., 2014.
- [15] Coney, M.W., Stephenson, P.L., Malmgren, A., Linnemann, C., Morgan, R.E., Richards, R.A., Huxley, R. and Abdallah, H. "Development Of A Reciprocating Compressor Using Water Injection To Achieve Quasi Isothermal Compression." *International Compressor Engineering Conference*. Purdue University, 2002.
- [16] *Isothermal Compressed Air Energy Storage - SustainX*. 1 July 2012. <http://www.sustainx.com/technology-isothermal-caes.htm>.
- [17] Lemofouet, S, and A Rufer (Dir). *Investigation and optimisation of hybrid electricity storage systems based on compressed air and supercapacitors*. Thèse EPFL, n° 3628, 2006.
- [18] *Publications - Herrick lab*. <https://engineering.purdue.edu/Herrick/Publications/compressor14.pdf> (accessed December 10, 2014).

References

- [19] Favrat, D. "Thermodynamics and energy systems analysis, from energy to exergy." Lausanne: EPFL Press, 2010.
- [20] Soedel, W. *Design and Mechanics of Compressor Valves*. West Lafayette, IN: Purdue University Press, 1984.
- [21] Kdambi, V, and M Prasad. *An Introduction to Energy Conversion*. Vol. II. Wiley Eastern Private, 1974.
- [22] Wu, Ta-The. *High-pressure heat transfer in reciprocating gas compressors*. Ph.D Thesis, The Pennsylvania state university, 1994.
- [23] Chen, K, and G, A Karim. "Evaluation of the Instantaneous unsteady heat transfer in rapid compression-expansion machines,," (proc Instn Mech Engrs) 212, no. Part A (1998).
- [24] Bollinger. System and method for rapid isothermal gas expansion and compression for energy storage. US Patent US 8240146 B1. 14 Aug 2012.
- [25] Cavallini A, Doretto L, Longo G.A., Rossetto L, Bella B., Zannerio A., "Thermal analysis of a hermetic reciprocating compressor." *International Compressor Engineering Conference*. West Lafayette, IN, USA., 1996. 535-540.
- [26] Stouffs, P., M. Tazerout, and P. Wauters. "Thermodynamic analysis of reciprocating compressors." *International Journal of Thermal Science*, 2001: 52-66.
- [27] Sun., Si-Ying, and Ting-Rong Ren. "New method of thermodynamic computation for a reciprocating compressor: Computer simulation of working processes." *International Journal of Mechanical Science* 37 (1995): 343 -353.
- [28] Adair, R.P., et al. "Instantaneous heat Transfer to the Cylinder Wall in Reciprocating Compressors." *Proc. of the Purdue Compressor Technology Conf*. West Lafayette, IN, USA., 1972. 521-526.
- [29] Annand, W. D. "Heat transfer in the cylinders of reciprocating internal combustion engines." *Proc. Instn Mech. Engrs* 177(36) (1963): 973-996.
- [30] Kornhauser, A. *Gas-wall heat transfer during compression and expansion*. PhD thesis, Massachusetts Institute of Technology, Cambridge, MA., 1989.
- [31] Nusselt, W. "Der Waermeuebergang in der Verbrennungskraftmaschine." *Z. Ver. Dt. Ing.*, no. 67 (1923): 692.
- [32] Eichelberg, G. "Some new investigations on old combustion engine problems." *Engineering* 148, no. 547 (1939).
- [33] Woschni, G. "A universally applicable equation for the instantaneous heat transfer coefficient in the internal combustion engine." *SAE paper 670931*, 1967.
- [34] Lekic, U, and J.B.W Kok. "Heat Fows in Piston Compressors." *5th european Thermal-Sciences Conference*. The Netherlands, 2008.
- [35] Kim, J, and E Groll. "Feasibility study of a bowtie compressor with novel capacity modulation." *International Journal of Refrigeration* 30 (8) (2007): 1427-1438.
- [36] Todescat, M. L., Fagotti, F., Prata, A. T., Ferreira, R. T. S. "Thermal energy analysis in reciprocating hermetic compressors." *Proceedings of International Compressor Engineering Conference at Purdue*, 1992. 1419-1428.
- [37] Chung, Seo Yoon, Gwang Hoon Rhee, and Hyung Jin Sung. "Direct numerical simulation of turbulent concentric annular pipe flow: Part 1: Flow field." *International Journal of Heat and Fluid Flow* 23, no. 4 (August 2002).
- [38] Chung, Seo Yoon , and Hyung Jin Sung. "Direct numerical simulation of turbulent concentric annular pipe flow: Part 2: Heat transfer." *International Journal of Heat and Fluid Flow* 24, no. 3 (June 2003).
- [39] Shah, R. K., and A. L. London. "Laminar flow forced convection in ducts: a source book for compact heat exchanger analytical data / Publisher: New York: Academic Press, (1978)." (Academic Press) 1978.
- [40] Incropera, F., Dewitt, D.,. *Fundamentals on heat and mass transfer*. New york: John Wiley and sons, 1996.
- [41] Cengel, Y., and A. Ghajar. *Heat & Mass Transfer*. McGraw-Hill, 2010.

References

- [42] Paschkis, V. "Electrical analogy method for the investigation of transient heat flow problems." *Industrial heating* 9 (1942): 1162-1170.
- [43] Paschkis, V., Heisler, M.P., "The accuracy of lumping in an electric circuit, representing heat flow in cylindrical and spherical bodies." *J. appl. Phys.* 17 (1946): 246-254.
- [44] Del Cerro, F. e. "The Teaching of Unsteady Heat Conduction Using the Thermo-electric Analogy and the Code pspice. Nonlinear Models. ." *International Conference on Engineering Education and Research "Progress Through Partnership". VSB-TUO, Ostrava* . 2004.
- [45] Jena, C, N Sarbhai , and R Mulaveesala. "Pulsed Thermography Simulation: 1D, 2D and 3D Electro-Thermal Model Based Evaluation." *Proc. National Seminar on Non-Destructive Evaluation*. 2006.
- [46] Chen, Y, N Halm, EA Groll, and JE Braun. "A comprehensive model of scroll compressors, part II: overall scroll compressor modeling." *Proceedings of the 2000 International Compressor Engineering Conference at Purdue*. West Lafayette, IN: Purdue University, 2000. 725-734.
- [47] Faulkner, H. *An investigation of instantaneous heat transfer during compression and expansion in reciprocating gas handling equipment*. Massachusetts Institute of Technology., 1983.
- [48] Chiu, C. P., and T.S Wua. "Study of Air Motion in Reciprocating Engine Using AN Algebraic Grid Generation Technique." *Numerical Heat Transfer, Part A: Applications* 17, no. 3 (1990): 309-327 .
- [49] Katopodes, F.V, A.M.J Davis, and H.A. Stone. "Piston flow in a two-dimensional channel. *Physics of Fluids* 12(5), 1240." *Physics of Fluids* 5, no. 5 (2000): 1240.
- [50] Meleshko, V.V. , and T.S. Krasnopolskaya. "Piston Stokes flow in a semi-infinite channel." *C. R. Acad. Sci. Paris, Série Iib*, 329, 2001: 1-6.
- [51] Pollak, E., W. Soedel, R. Cohen, and F. J. Friedlaender. "On the resonance and operational behavior of an oscillating electrodynamic compressor." *Journal of Sound and Vibration* 67, no. 1: 121-133.
- [52] Song, XG, L Wang, SH Baek, and YC Park. "Transient Analysis of a Spring-Loaded Pressure Safety Valve Using Computational Fluid Dynamics (CFD)." *ASME Pressure Vessels and Piping Conference*. 2009. , 253-258.
- [53] Chabane, S, S Plumejault, D Pierrat, and M Bayart. "Vibration and chattering of conventional safety relief valve under built up back pressure." *3rd IAHR International Meeting of the Workgroup on Cavitation and Dynamic Problems in Hydraulic Machinery and Systems*. Brno, Czech Republic, 2009.
- [54] Habing, R. *Flow and Plate Motion in Compressor Valves*. Universiteit Twente, 2005.
- [55] Aigner, R, G Meyer, and H Steinrück. "Valve Dynamics and Internal Waves in a Reciprocating Compressor." *5th Conference of the EFRC*. Prague, 2007.
- [56] Heywood , J.B. "Internal combustion engine fundamentals." New York: McGraw-Hill, Inc, 1988.
- [57] Bell, I, E Groll, J Braun, and T Horton. "A computationally efficient hybrid leakage model for positive displacement compressors and expanders." *International Journal of Refrigeration* 36, no. 7 (November 2013): 1965-1973.
- [58] Fan, Z, and Z Chen. "A Calculating Method for Gas Leakage in Compressor." *International Compressor Engineering Conference*. West Lafayette: Purdue University, 1994.
- [59] Dennis F. Li, Steve M. Rohde & Hazem A. Ezzat. "An Automotive Piston Lubrication Model." *A S L E Transactions* 26, no. 2 (1983).
- [60] Ren, T, and J Neels. "Advantages of Non-lubricated CNG Compressors." *IMW Industries*. <http://www.imw.ca/documents/The%20Benefits%20of%20Non-Lubricated%20Compressors.pdf> (accessed 2014).
- [61] Lewis, M.W.J. " Wear and friction of PTFE seals ." *Lubr. Eng* 42 (1986): 152-158.
- [62] Bradshaw, C. *A Miniature-Scale Linear Compressor for Electronics Cooling*. Vol. Dissertation. West Lafayette, Indiana: Purdue University, Dissertation, 2012.

References

- [63] Mathison, M. *Modeling and evaluation of advanced compression techniques for vapor compression equipment*. Purdue University, Dissertation, 2011.
- [64] Chen, Y, N.P Halm, E.A Groll, and J.E Braun. "A Comprehensive Model of Scroll Compressors Part I: Compression Process Modeling." *International Compressor Engineering Conference*. West Lafayette: Purdue University, 2000.
- [65] Kim, J, and E.A Groll. "Bowtie Compressor With Novel Capacity Modulation Part 2: Model Validation and Parametric Studies." *International Compressor Engineering Conference*. West Lafayette: Purdue University, 2006.
- [66] Coney, M.W., Stephenson, P.L., Malmgren, A., Linnemann, C., Morgan, R.E., Richards, R.A., Huxley, R. and Abdallah, H., "Development Of A Reciprocating Compressor Using Water Injection To Achieve Quasi Isothermal Compression ." *International Compressor Engineering Conference*. West Lafayette: Purdue University, 2002.
- [67] Van de Ven, J.D., Li, P.Y. "Liquid piston gas compression." *Appl Energy*, doi:10.1016/j.apenergy.2008.12.001, 2009.
- [68] Kim, Y.M., J.H. Lee, and D. Favrat. "Potential and evolution of compressed air energy storage: energy and exergy analyses." *Entropy* 14 (2012): 1501–1521.
- [69] Elmegaard, B., and W. Brix. "Efficiency of Compressed Air Energy Storage." *The 24th International Conference on Efficiency, Cost, Optimization, Simulation and Environmental Impact of Energy Systems*. 2011.
- [70] Bejan, A., and M.J. Moran. "Thermal design and optimization." John Wiley & Sons,, 1996.
- [71] Karnopp, D.C. "State variables and pseudo bond graphs for compressible thermofluid systems." *J. Dynamic Syst., Measure. Control, Trans. ASME* 101, Serie G., No.3 (1979).
- [72] Engja, H. "Bond graph model of a reciprocating compressor ." *Journal of the Franklin Institute* 319, no. 1-2 (January–February 1985).
- [73] Karnopp, D.C., Rosenberg R.C. "System dynamics: Modeling and Simulation of Mechatronic systems." (Wiley) 2000.
- [74] Thoma, J., Ould Bouamama, B.,. *Modeling and Simulation in Thermal and Chemical Engineering*. Springer, 2000.
- [75] Hissel, D., Péra, M.C., Bouscayrol, A., Chrenko, D.,. "Energetic Macroscopic representation of a fuel cell." (Revue Int de Génie Électrique) 1295-490X, 11 (4–5). (2008): 603–623.
- [76] Borutzky, W.,. *Bond graph methodology; development and analysis of multidisciplinary dynamic system models*. Springer: London, 2009.
- [77] Chrenko, D. *Energetic macroscopic representation modeling and control of a low temperature fuel cell system fed by hydrocarbons*. Ph.D Thesis, the University of Franche-Comte. , 2008.
- [78] Bouscayrol, A., Davat ,B., De Fornel, B. et al. "Multi- converter multi-machine systems: application for electromechanical drives." (Eur Phys J Appl Phys.) , 10 (2), 131–147. (2000).
- [79] Bouscayrol, A., Schoenfeld, R., et al. "Different energetic descriptions for electromechanical systems." , *Eur Conf Power Electron Appl*, p. 10. 2005.
- [80] Chrenko, D., Coulié, J., Lecoq S., Péra, M.C., Hissel, D. "Static and dynamic modeling of a diesel fuel processing unit for polymer electrolyte fuel cell supply." *Int J Hydrogen Energy*, 34, 1324–1335. , 2009.
- [81] Charles, Passut A, and Ronald P Danner. "Correlation of idealgas enthalpy,Heat capacity and Enthalpy." *Ind. Eng. Chem. Process Des. Develop.* 11, no. 4 (1972).
- [82] Tastavi, A. *Compresseurs volumétriques*. Lausanne, Switzerland: EPFL Press., 1983.
- [83] Holman, J.P. *Heat Transfer*,. Edited by 7th Ed. McGraw-Hill , 1990.
- [84] Çengel, Y. A., and J. Cimbala. *Essentials of Fluid Mechanics: Fundamentals and Applications*. McGraw-Hill, fifth ed. , 2008.
- [85] Ghafari A., Maghsoudpour A. and Pourmomtaz A., *Control and dynamic systems, Second ed*. Tehran: K.N.Toosi University Publications (In Persian), 2006.

References

- [86] Wien, W. "Lehrbuch der Hydrodynamik." Leipzig: Hirzel, 1900. 247.
- [87] Lamb, H. "Hydrodynamics." New York: Dover, 1932.
- [88] Lakshmanan, N. M. Natarajan and S. M. "Analytical method for the determination of the pressure drop in rectangular ducts." *Indian Chem. Eng.* 12 (2) (1970): 68-69.
- [89] Lundberg R.E., McCuen P.A. and Reynolds, W.C. "Heat transfer in annular passages. Hydrodynamically developed laminar flow with arbitrarily prescribed wall temperatures or heat fluxes." *Int. J. Heat Mass Transfer* 6 (1963): 495-529.

Appendix

I. Flow Characteristics in Concentric Annulus

Regarding the special geometry in a finned piston, the classic formulation of Nusselt number in the piston compressor is not applicable anymore. Since the piston speed is low, the flow stays laminar. Both thermal and hydrodynamic entry lengths are quite short compared to the length of the fins (**Figure AI.1**), so the flow can be considered fully developed in the annular space.

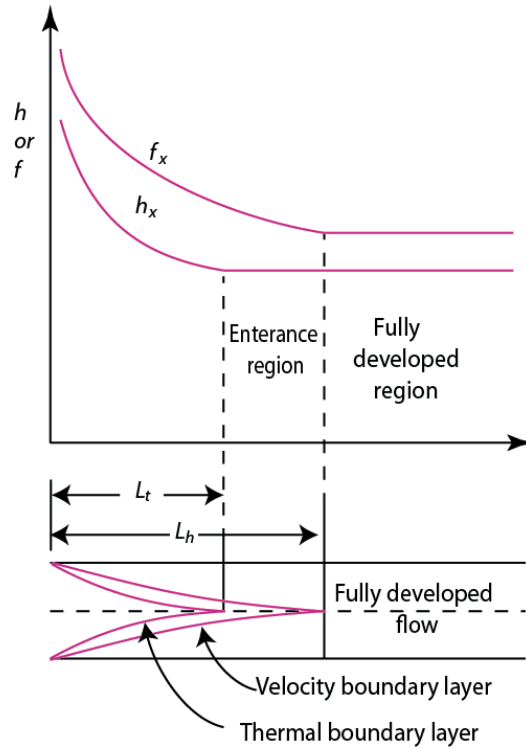


Figure AI.1: Thermal and hydrodynamic entry length.

I.1 Fluid Flow

It is also interesting to study the flow profile in the finned piston. In the space between two stationary fins (**Figure AI.2-b**) the flow is induced by moving piston. This kind of flow has been studied in many works [49]-[50]. In summary the flow is uniform near the piston and parabolic and fully developed at a distance of:

$$L_{t,lam} \approx 0.05ReD$$

$$L_{h,lam} \approx 0.05RePrD$$

Reynolds number is variable during a cycle (since the temperature and hence the density varies), however its average value can be calculated by:

$$Re = \frac{\rho VD}{\mu} = \frac{VD}{\nu} = \frac{0.1(m/s) * 5 * 10^{-3}(m)}{1.6 * 10^{-5}(m^2/s)} = 32$$

For such low Reynolds number the flow regime is absolutely laminar. For $Re = 32$ and $Pr = 0.67$, the hydrodynamic and thermal entry lengths are:

$$L_{h,lam} \approx 8 \text{ mm}$$

$$L_{t,lam} \approx 5.36 \text{ mm}$$

In this distance the flow is in transition mode.

But in the gap between the fins (**Figure AI.2-b**) the flow is a combination of a Couette flow and Poiseuille flow. The resulting pressure and velocity field can be found by superposition method respectively as [84]:

$$P = P_0 + \frac{\partial P}{\partial x} x - \rho g z$$

$$u = \frac{Vy}{h} x - \frac{1}{2\mu} \frac{\partial P}{\partial x} (y^2 - hy)$$

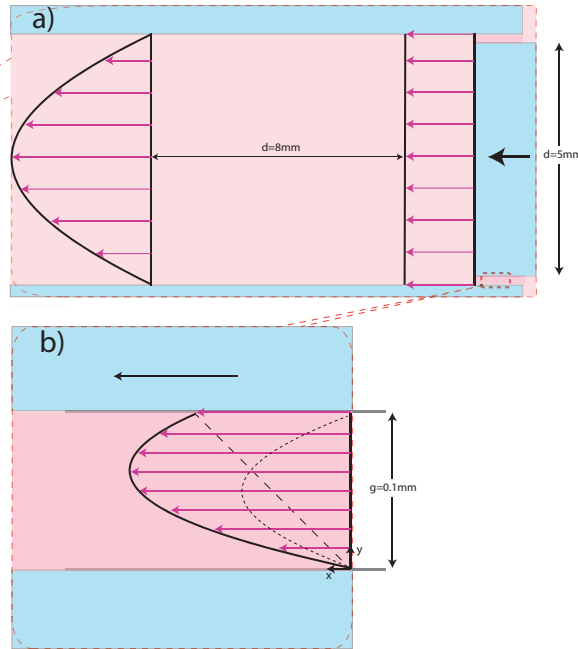


Figure AI.2 Velocity profile in inter fins space.

The solution to hydrodynamic problem for fully developed flow through an annular duct (**Figure AI.3**) has long been known.

An important parameter in this geometry is inner to outer annulus radius:

$$r^* = \frac{r_i}{r_o}$$

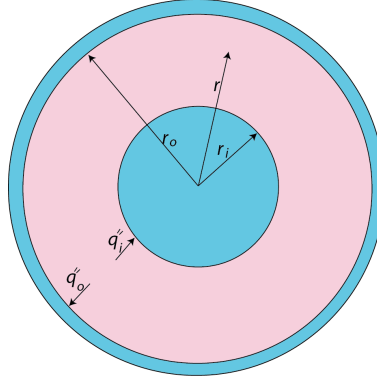


Figure AI.3 : A concentric circular annular duct

It is found in the early textbooks such as those by Wien [86] and Lamb [87]. The velocity profile and corresponding friction factor are given by Lundberg et al. [89] as

$$u = -\frac{c_1 r_o^2}{4} \left[1 - \left(\frac{r}{r_o} \right)^2 + 2r_m^{*2} \ln \left(\frac{r}{r_o} \right) \right]$$

$$u_m = -\frac{c_1 r_o^2}{8} [1 - r^{*2} - 2r_m^{*2}]$$

$$\frac{u_{max}}{u_m} = \frac{2(1 - r_m^{*2} + 2r_m^{*2} \ln r_m^*)}{1 + r^{*2} - 2r_m^{*2}}$$

$$f_i Re = -\frac{c_1 D_h}{u_m} \left(\frac{r_m^2 - r_i^2}{r_i} \right)$$

$$f_o Re = -\frac{c_1 D_h}{u_m} \left(\frac{r_o^2 - r_m^2}{r_o} \right)$$

$$f Re = \frac{16(1 - r^{*2})^2}{1 + r^{*2} - 2r_m^{*2}}$$

where

$$r_m^* = \frac{r_m}{r_o} = \left[\frac{1 - r^{*2}}{2 \ln \left(\frac{1}{r^{*2}} \right)} \right]$$

Where c_1 represents the pressure gradient parameter and can be shown as:

$$c_1 = \frac{dP}{dx} \frac{\mu}{g_c}$$

and r_m designates the radius where the maximum velocity occurs ($\partial u / \partial r = 0$); f_i and f_o designates the Fanning friction factor at the inner and outer walls, respectively; f stands for the perimeter average Fanning friction factor, which is related to f_i and f_o as

$$f = \frac{f_i r_i + f_o r_o}{r_i + r_o}$$

All of the foregoing results were recalculated by Shah and London [39]. The fRe factors are also presented in **Figure AI.4**.

Natarajan and Lakshmanan[88] presented the following simple formula for fRe.

$$fRe = 24(r^*)^{0.035}$$

also hydrodynamic entry length can be presented as:

$$L_{hy}^+ = 0.6(r^*)^{-0.8}$$

And finally incremental pressure drop as:

$$K(\infty) = 0.6(r^*)^{-0.7}$$

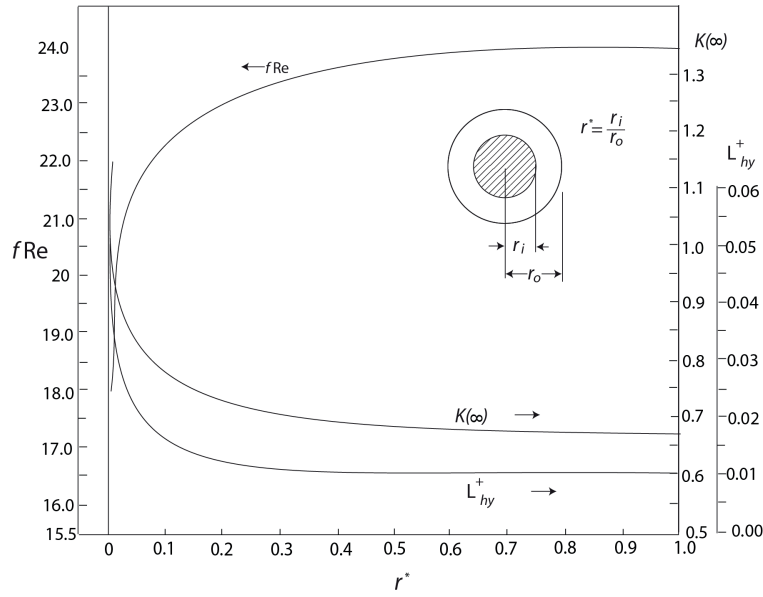


Figure AI.4 : Concentric annular ducts: fRe, $K(\infty)$ and L_{hy}^+ for fully developed laminar flow.

I.2 Heat transfer

Lundberg et al.[89] systematically approached the fundamental solution for heat transfer problems. They presented extensive results for the dimensionless temperatures, heat fluxes, and Nusselt numbers as a function of r^* . Based on their equations, the detailed results were computed by Shah and London [39]. The Nusselt number for the case where the constant specified temperature of both walls are equal, can be obtained from **Figure AI.5**.

One may not that when the dimensionless ratio approaches unity; the Nusselt number will approach the case of two parallel plates, which is reported by Shah and London [39] to be 7.54.

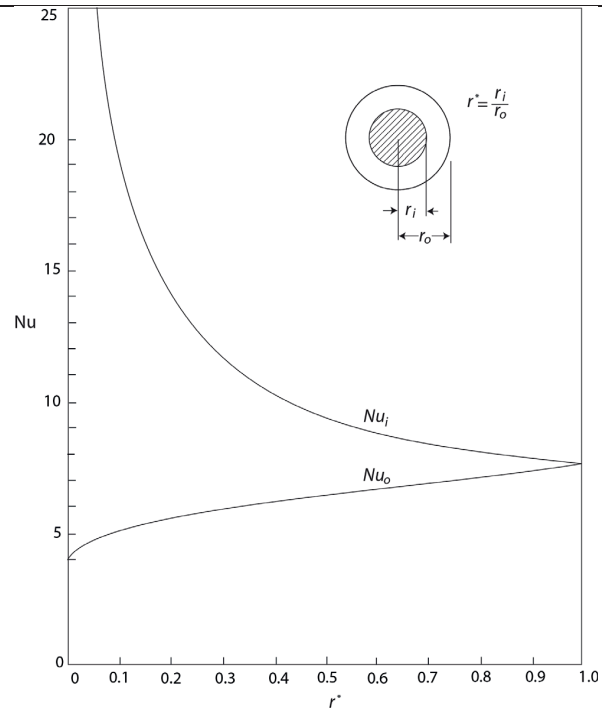


Figure AI.5 : concentric annular ducts: Nusselt number for constant temperatures on both walls for fully developed laminar flow

The values of convective heat transfer equations has been calculated in the finned piston model, based on the tabulated data from the aforementioned sources.

Similar to correlation for fRe a similar correlation can be defined for Nu_i and Nu_o as:

$$Nu_i = 7.54(r^*)^{-0.5}$$

$$Nu_o = 7.54(r^*)^{0.18}$$

A II. Other Efficiency Definitions

II.1 Introduction

Apart from exergetic efficiency that was defined in chapter 2, there are other efficiencies that are used widely in compressor technology literature, and were reference in the text. In this appendix the most important ones will be described together with analysis of their change with some important compressor parameters like pressure ratio and polytropic factor.

II.2 Isothermal Efficiency

The isothermal efficiency (ratio) can be defined as the isothermal work divided by the actual work of compression:

$$\eta_{iso} = \frac{w_{isothermal}}{w_{actual}} = \frac{n-1}{n} \ln\left(\frac{p_2}{p_1}\right) / \left[1 - \left(\frac{p_2}{p_1}\right)^{n-1/n}\right] \quad (\text{AII:1})$$

The variation of isothermal efficiency with polytropic factor for different pressure ratios is shown in **Figure AII.1**, which shows that the isothermal efficiency decreases with both pressure ratio and polytropic factor.

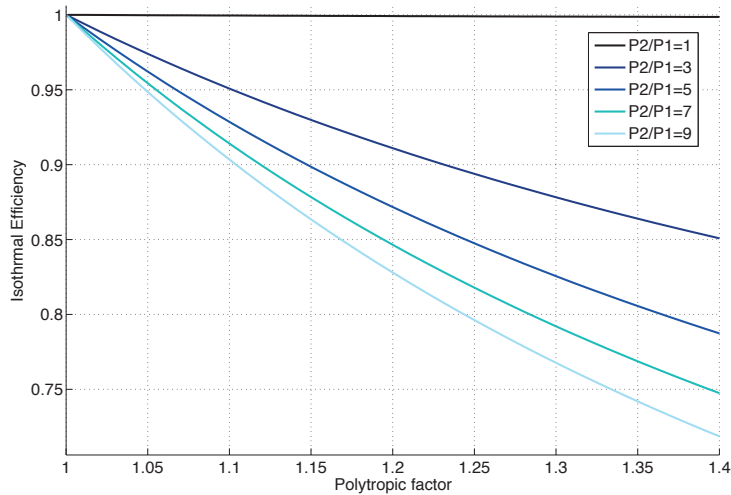


Figure AII.1: Isothermal efficiency vs. polytropic factor.

II.3 Volumetric Efficiency

With the ideal gas equation of state, the theoretical mass contained within a single cylinder compressor can be formulated in terms of suction volume, $V_1 - V_4$, or discharge volume, $V_2 - V_3$, assuming no leakage during a cycle. This mass is

$$m = \frac{p_1(V_1 - V_4)}{RT_1} = \frac{p_2(V_2 - V_3)}{RT_2} \quad (\text{AII:2})$$

And is process-dependent, because the values of V_2 and V_4 are functions of n . The mass-flow rate, \dot{m} , is simply

$$\dot{m} = f_c \frac{p_1(V_1 - V_4)}{RT_1} = f_c \frac{p_2(V_2 - V_3)}{RT_2} \quad (\text{AII:3})$$

Where f_c is the number of intake strokes per unit time (or the compressor rotational frequency in (RPM/60)). The terms $P1/RT1$ and $P2/RT2$ in Eq. (AII:3) can be viewed as a density at a specific suction state or a specific discharge state; the product of this density with the volume yields the mass flow per cycle.

We can simplify Eq. (AII:3) by introducing the volumetric efficiency, η_v that is defined by [21]

$$\eta_v = \frac{\text{Volume of the gas intake per cycle}}{\text{Stroke or swept volume}} = \frac{V_1 - V_4}{V_1 - V_3} \quad (\text{AII:4})$$

Where in **Figure AII.2** points 1-4 are the start of the compression, discharge, expansion and intake processes respectively.

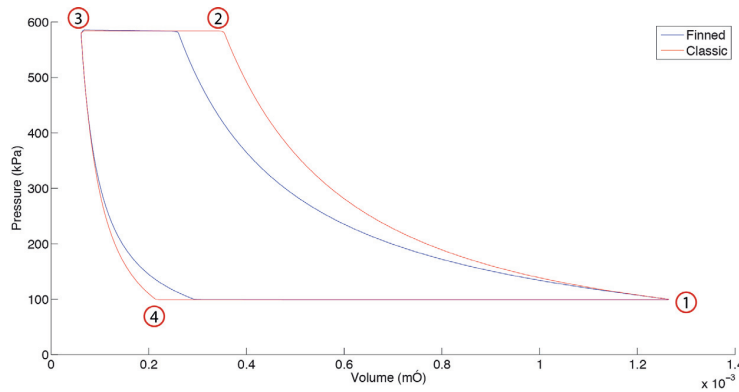


Figure AII.2: Starting point of four different processes on a p-V diagram.

Volumetric efficiency can be defined also in terms of flow rate as the ratio between the actual volume flow rate in the compressor inlet and the displacement rate of the compressor (maximum theoretical flow rate):

$$\eta_v = \frac{\dot{V}_i}{\dot{V}_D} = \frac{\dot{m}v_i}{f_c V_D} \quad (\text{AII:5})$$

Where v_i is the specific volume of inlet gas and V_D is the maximum volume of suction process.

Rearranging Eq. (AII:3) and introducing Eq. (AII:4) into the resulting equation yields

$$\dot{m} = f_c \frac{(V_1 - V_4)p_1(V_1 - V_3)}{(V_1 - V_3)RT_1} = f_c \eta_v \frac{p_1 V_s}{RT_1} = \eta_v \dot{m}_s \quad (\text{AII:6})$$

Where V_s is the swept volume of inlet gas and \dot{m}_s is the swept mass flow rate. To determine how the theoretical mass flow rate, \dot{m} , depends on compressor geometry and process, we manipulate Eq. (AII:6) such that it is a function of only the clearance, CL , the pressure ratio, p_2/p_1 , and the polytropic exponent, n . The result is [21]:

$$\eta_v = 1 + CL \left[\left(\frac{p_2}{p_1} \right)^{1/n} - 1 \right] \quad (\text{AII:7})$$

Eq. (AII:7) is plotted as a function of n for different $CL = V_c/V_s = V_3/(V_1 - V_3)$ and Pr in **Figure AII.3**.

Clearly, the value of volumetric efficiency, and thus, the mass-flow rate, decreases with increasing clearance and pressure ratio. Besides, increasing n increases volumetric efficiency.

In other words, whenever the cylinder is cooled, the value of n during compression will be lower than k (where $k=c_p/c_v$, since cooling tends to make the process nearly isothermal. Again during expansion of the air in the dead volume, an effectively cooled cylinder head tends to make the process isothermal. As a result the volume of the air at the end will be greater than what it would be if it was isentropic. Hence the volumetric efficiency of the compressor is adversely affected by effective cooling of cylinder head, though the work input for compression is reduced. The effect of friction and other conditions during the expansion and compression tend to make the n_e the expansion index slightly greater than n , though it is the practice to assume $n_e = n$ for most calculations.

Also, **Figure AII.2** confirms the results from **Figure AII.3**. We can see that in **Figure AII.2** while $V_1 - V_3$ (the denominator of Eq. (AII:4)) is constant for all cases, $V_2 - V_3$ (the numerator of Eq. (AII:4)) decreases while we go closer to isothermal conditions, hence with the definition offered, there is a trade-off between isothermal efficiency and volumetric efficiency.

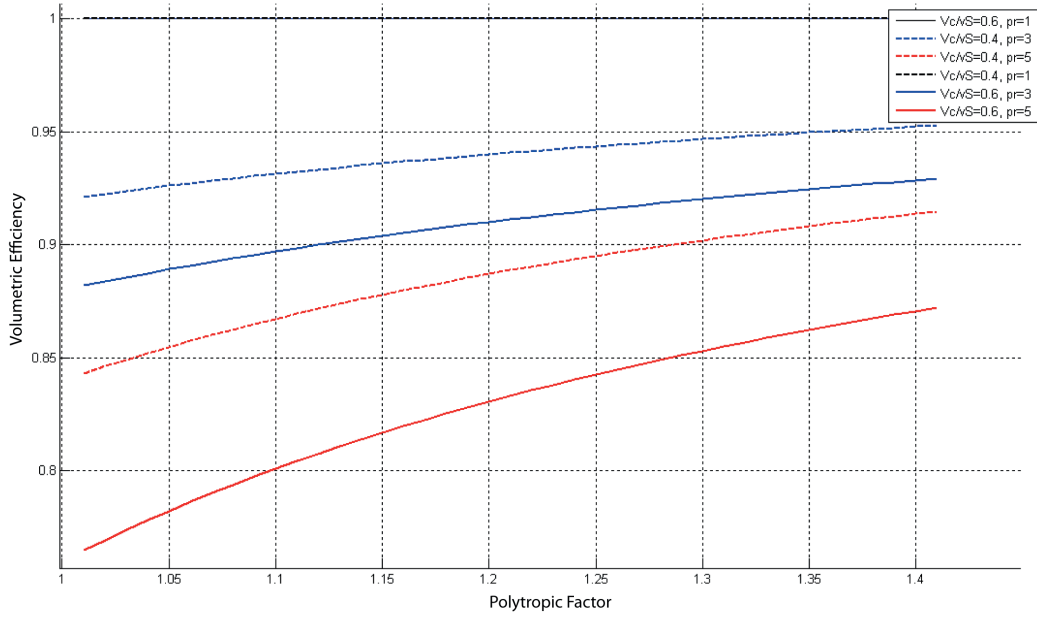


Figure AII.3: Volumetric Efficiency vs Polytropic coefficient

II.3 Efficiency of delivery

One of the other efficiencies that have a close relation to volumetric efficiency is the efficiency of delivery. This term can be defined as the “ratio of the mass of gas delivered per cycle compared to the mass of gas contained in the swept stroke volume at nominal suction conditions”,

$$\lambda = \frac{\text{Mass of the gas delivered per cycle}}{\text{mass of gas contained in the swept stroke}} = \frac{m_1 - m_3}{m_1} \quad (\text{AII:8})$$

This ratio is illustrated for classic and finned compressor in **Figure AII.4**. It is evident that the efficiency of delivery is lower for a finned piston. As described in Chapter 7, this is because the gas density is higher at the end of compression (point 3) and with the same dead volume, the trapped mass higher for finned piston.

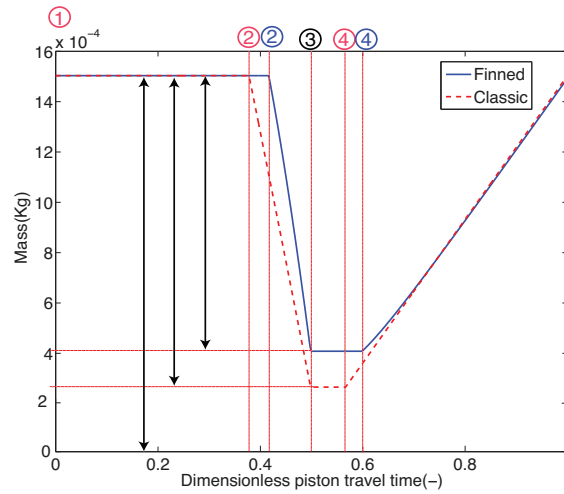


Figure AII.4: Efficiency of delivery for classic and finned piston.

A III. Dynamic Valve Model

As mentioned in the literature review, Kim and Groll [35], have developed a reliable model for predicting dynamic behavior in spring backed valves. This model is adapted to the check valves in this study. However since the operation speed is low, as it will be seen later, the effect of valve vibration is not much in this case. Besides including the valve dynamic model in the comprehensive model makes the simulation very slow (Considering the number of cycles required to fill the reservoir). Anyway this study is presented in this part of appendix for further information. **Figure AIII.1:** and **Figure AIII.2:** show respectively the components and schematic of a preloaded spring-backed check valve.

The dynamic valve model is based on the same principles already described in chapter 3 for a static valve model, but here the valve opening area is not constant, but a function of valve lift shown by Eq. (AII:1)

$$\dot{m} = f(P_{high}, P_{low}, A(x_{valve})) \quad (AII:1)$$

Valves are modeled as single degree of freedom lumped element in vibration system. The valve lift is obtained by solving a second order differential equation provided by force balances of valve poppet plate.

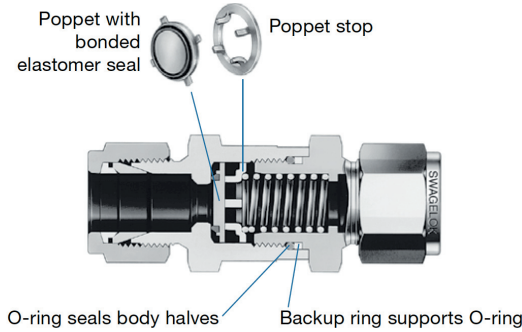


Figure AIII.1: Preloaded spring-backed check valve components.

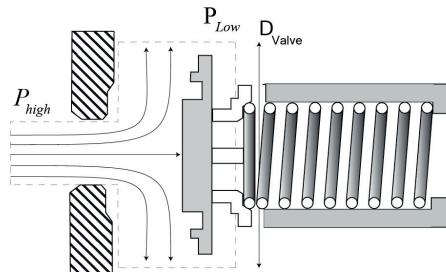


Figure AIII.2: schematic of the preloaded spring-backed check valve components.

Valves are modelled as Single degree of freedom lumped element, vibration system. And model is discretized into two modes:

- Pressure-dominant operation
- Mass-Flux-dominant operation

III.1 Pressure Dominant Mode

The main acting forces on the valve plate are a pressure force, a spring force and drag force. Where C_D is a drag coefficient for a round plate, which is 1.17.

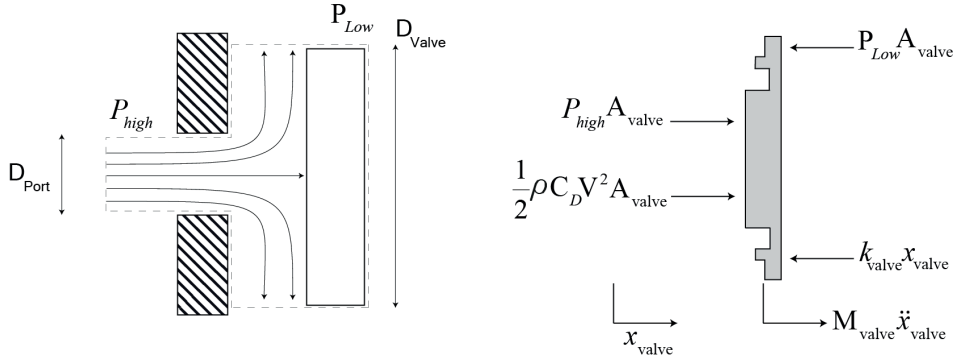


Figure AIII.3 : Free body diagram of valve plate in pressure dominant mode.

Based on the free body diagram of **Figure AIII.3**, the equation of motion can be written as Eq. (AII:2)

$$M_{valve} \ddot{x}_{valve} + k_{valve} x_{valve} = \frac{1}{2} \rho C_D V^2 A_{valve} + (P_{high} - P_{low}) A_{valve} \quad (\text{AII:2})$$

III.2 Mass-flux Dominant Mode

After a given distance from seat, the pressure difference diminishes and the mass-flux effect dominates the motion. **Figure AIII.4** shows the free body diagram of the valve plate in this mode.

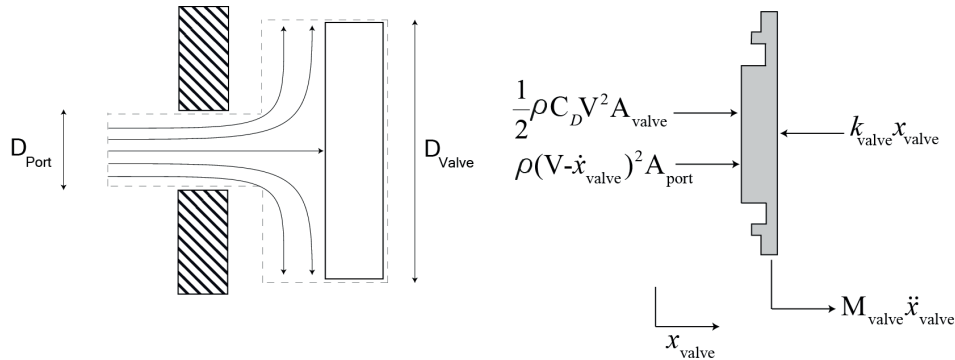


Figure AIII.4 : Free body diagram of valve plate in mass-flux dominant mode.

Equation of motionin of this mode can be described as Eq. (AII:3)

$$M_{valve}\ddot{x}_{valve} + kx_{valve} = \frac{1}{2}\rho C_D V^2 A_{valve} + \rho(V - \dot{x}_v)^2 A_{port} \quad (AII:3)$$

Switch between modes of operation happens when flow rates of each mode are equal:

$$\rho V(\pi D_{valve} x_{valve}) = \rho V \frac{\pi}{4} (D_{port})^2 \quad (AII:4)$$

Solving for transitional lift yields:

$$x_{tr} = \frac{(D_{port})^2}{4D_{valve}} \quad (AII:5)$$

Two second-order, non-linear, ordinary differential equations must be solved numerically. For the parametes described in **Table A III.1**.

Table A III.1: Valve parameters.

Mass	Spring Constant	Damping Coefficient	Port Diamete	Valve Diameter
$M(kg)$	$k(N/m)$	CD	$D_{valve}(mm)$	$D_{port}(mm)$
0.01	300	1.2	4.5	5

Valve responds like a second order system as can be seen from **Figure AIII.5**.

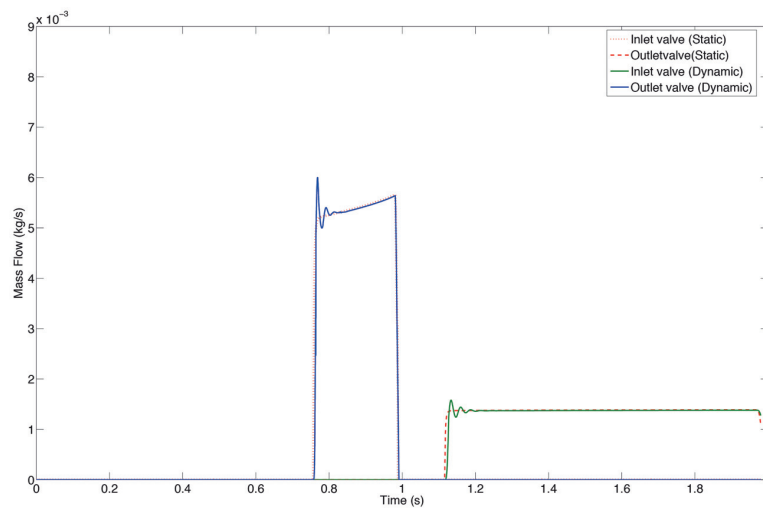


Figure AIII.5 : Mass flow of dynamic and static valve model.

Also the p-V diagram of the compressor with dynamic valve model is shown in **Figure AIII.6**.

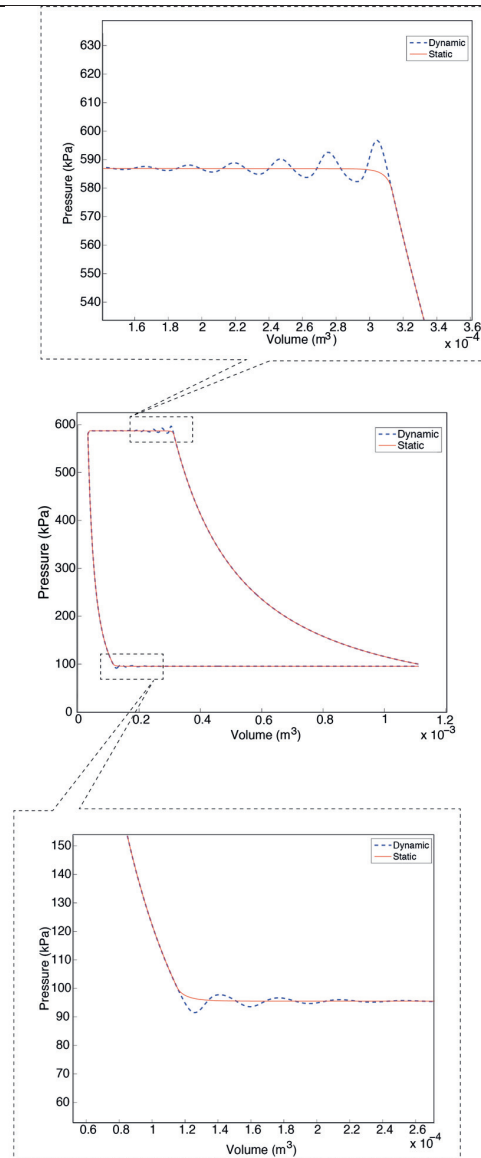


Figure AIII.6 : p-V diagram of valve dynamics.

The bond graph of the preloaded check valves are shown in **Figure AIII.7**. Suction and discharge from compressor is through preloaded valves. Lifts of these valves are limited by stoppers. Bond graph of such a valve is modeled considering all these constraints. The force due to gas pressure is created on the lower vertical bond.

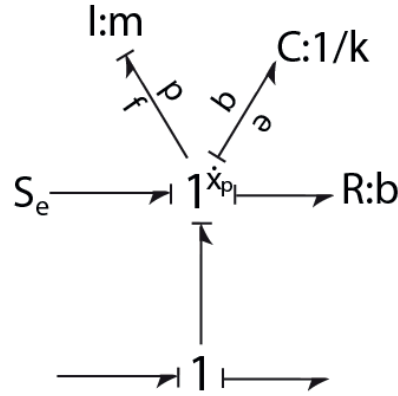


Figure AIII.7 : Bond graph of the dynamic preloaded valve model.

I is the inertia of the valve . Element C together with modulated source S_e models the valve spring force due to pre-compression and when restrained by the stopper. When the valve is in contact with either the seat or the stopper, the value of R is switched to high value for structural damping; else a nominal air damping is considered. If one concentrates closely on the energy in the system, associating a momentum p or displacement q variable with each distinct energy element:

$$f = p/m \quad (\text{AII:6})$$

$$e = k * q \quad (\text{AII:7})$$

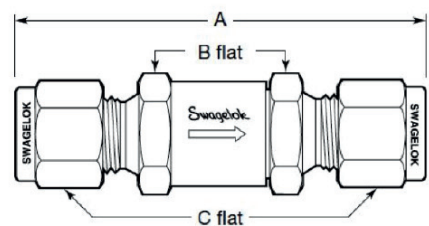
As it is seen from **Figure AIII.6**, the dynamic valve behaviour fluctuates around the static valve behaviour and the upper and lower parts almost cancel each other out. So, in long term, the oscillatory effect can be neglected with regards to power consumption aspect of the compressor.

A IV. Data sheets

IV.1 Swagelok Valve Data sheet

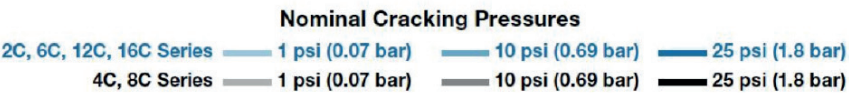
SS-4C4-1/3

C Series



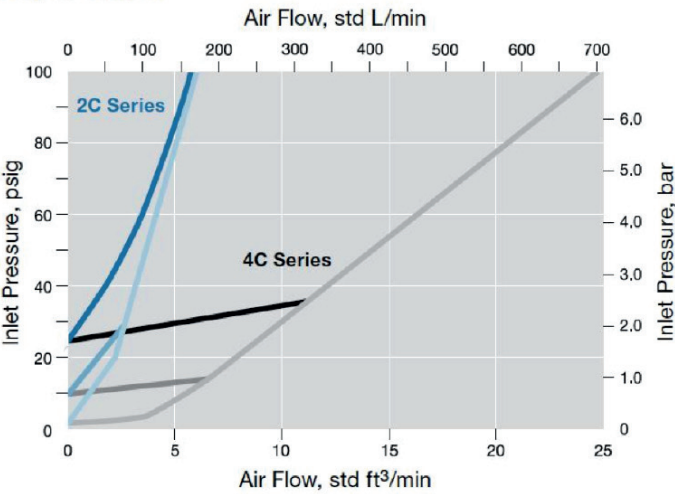
End Connections		Basic Ordering Number	Series	Dimensions, in. (mm)		
Inlet/Outlet	Size			A	B	C
Fixed Cracking Pressure, C Series						
Female NPT	1/8 in.	SS-4C4-	4C	1.89 (48.0)	5/8	

C Series



Air

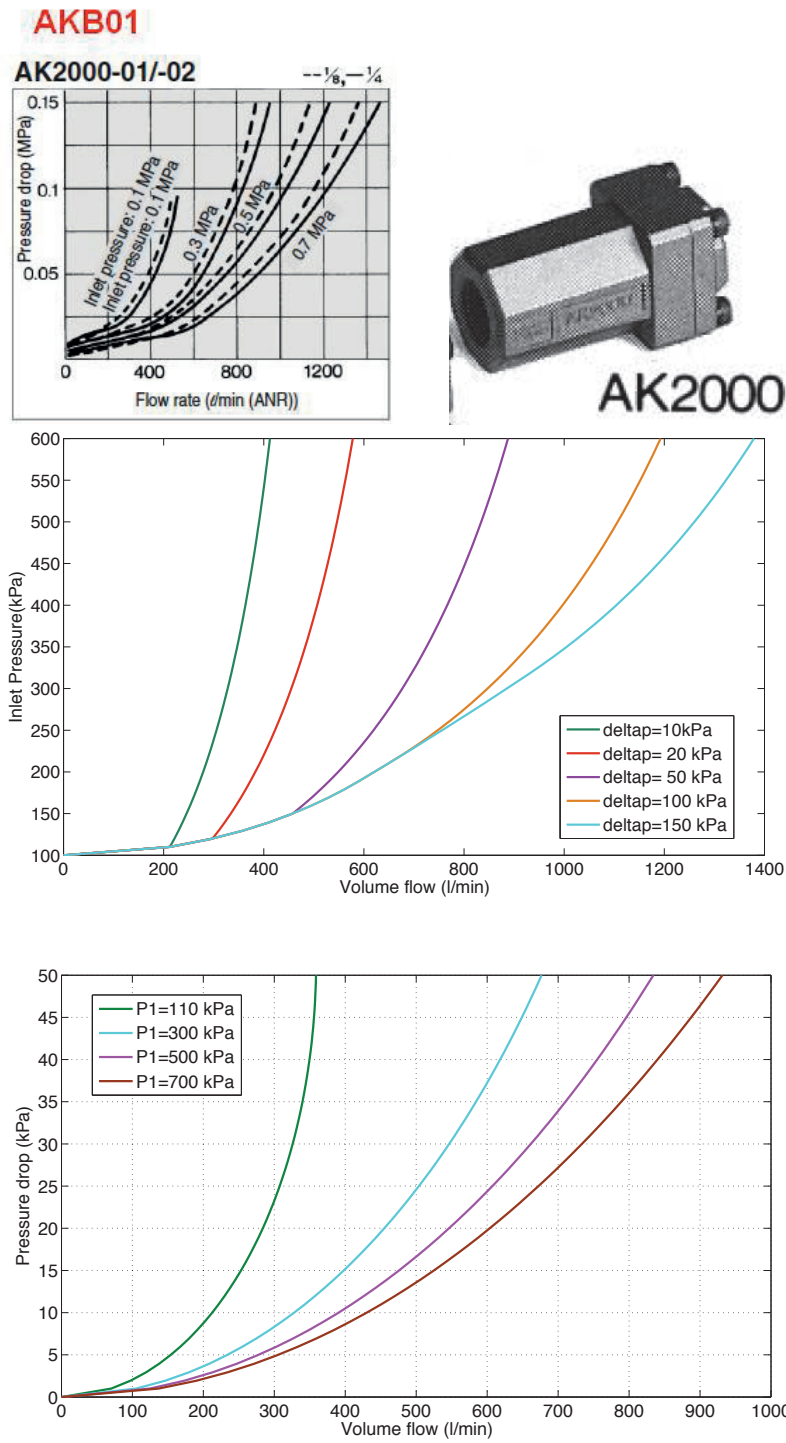
2C, 4C Series



IV.2 SMC Valve Data sheet

Model

Model	Port size	Effective area (mm ²)	Weight (g)
AK2000-01	1/8	25	105



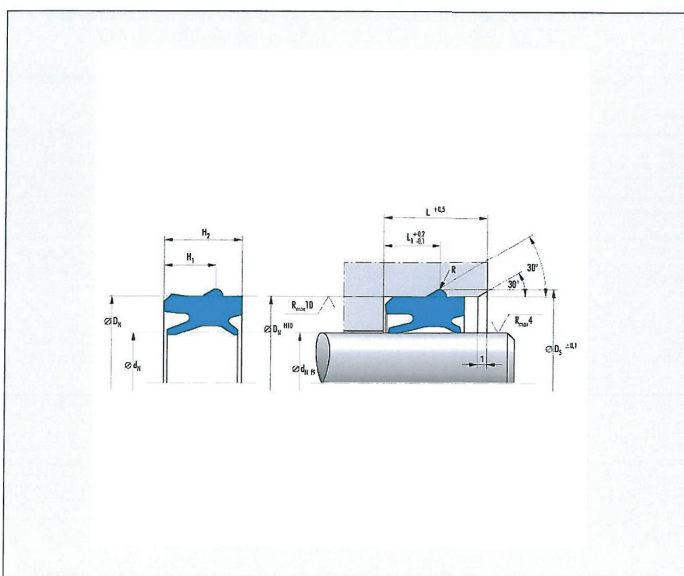
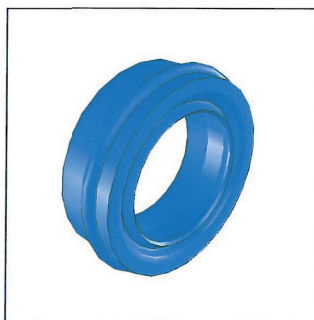
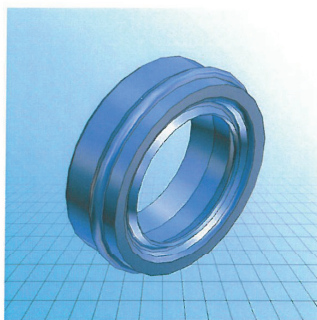
IV.3 Seals datasheet



Combi seal
AUNIPSL

PDF DATASHEET

© 1992 - 2010 CADENAS GmbH

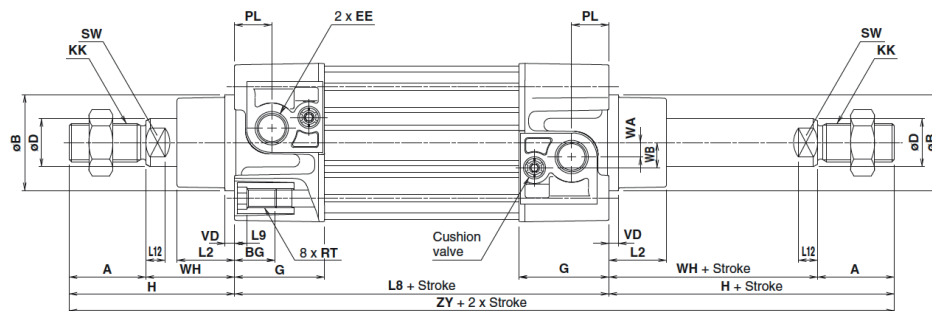


IDNR (Numéro de référence)	
ARTIKELNR (Order number)	407287
DN1 (mm)	20
DN (mm)	30
NUT (Groove)	without Groove
H1 (mm)	7
H2 (mm)	10.4
DS (mm)	32.2
L (mm)	13
L1 (mm)	7.7
R (mm)	1.1
Ring pre-pressure (kPa)	120

A V. Technical drawings

V.1 Classic Piston

CP96S(D)B



Bore size (mm)	A	øB d11	øD	EE	PL	RT	L12	KK	SW	G	BG	L8	VD	VA	WA	WB	WH	ZZ	ZY	E	R	L2	L9	H
125	54	60	32	G 1/2	19	M12 x 1.75	13	M27 x 2	27	58	20	160	6	6	17	15	65	285	398	144	110	40	—	119

Figure AV.1: Schematic and dimension of classic SMC piston.

V.1.1 Calculating the effective surface

Bore and shaft diameters are:

$$\phi B = 0.125 \text{ m}$$

$$\phi D = 0.032 \text{ m}$$

The effective surface is calculated as:

$$A = \pi(\phi B^2 - \phi D^2)/4 = 0.0114 \text{ m}^2$$

$$V = A * \text{Stroke} = 0.0114 * 0.1 = 0.00114 \text{ m}^3 = 1.14 \text{ Lit}$$

V.2 Finned Piston

The geometry of finned piston is shown in **Figure AV.2** and **Figure AV.3**.

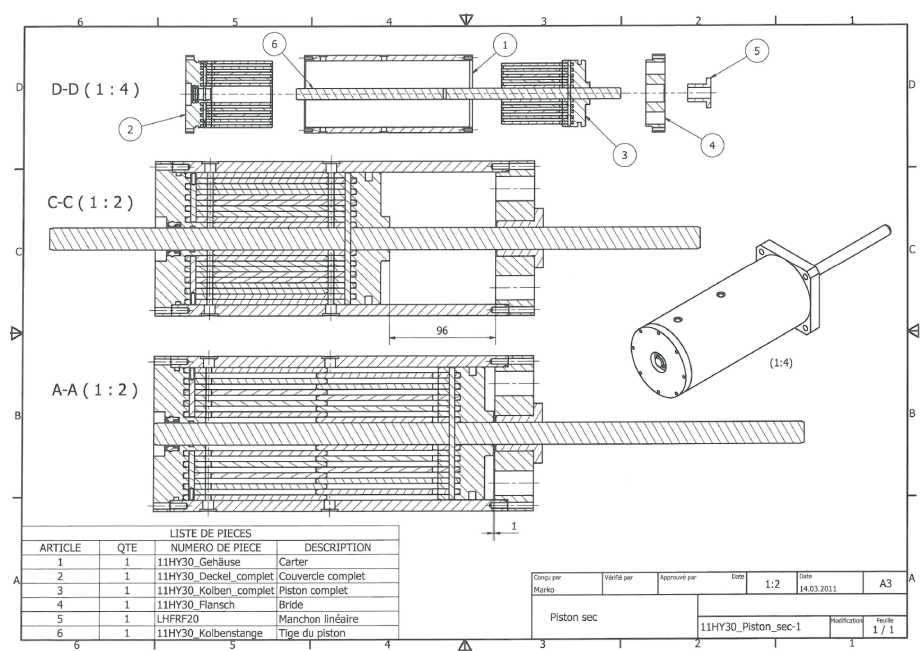


Figure AV.2: Technical drawing of the finned piston(Axial section view).

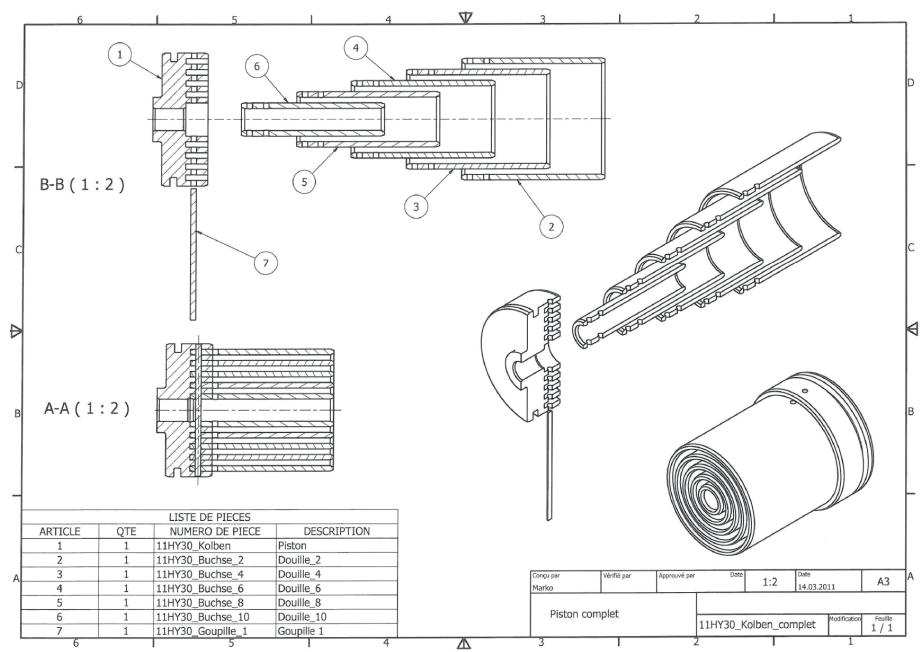


Figure A V.3: Technical drawing of the finned piston (Exploded view).

Outside and inside diameters are:

$$\phi do = 0.12 \text{ m}$$

$$\phi di = 0.02 \text{ m}$$

The effective area of finned piston can be calculated as:

$$A = \pi(\phi do^2 - \phi di^2)/4 = 0.011 \text{ m}^2$$

$$V = A * \text{Stroke} = 0.011 * 0.1 = 0.00114 \text{ m}^3 = 1.10 \text{ Lit}$$

A VI. Simulink Model Representation

The model was simulated in Matlab Simulink®. **Figure A VI 1** shows the overall model blocks, including chambers, the walls between them, inter fin spaces, collecting channels and valves. **Figure A VI 2** shows the details of the model for a typical chamber. One may note that to avoid complexities all the causality relations are integral causality (pay attention on the integration on mass and energy equations). The values are used to calculate temperature and pressure through constitutive relations. A fixed-step size (0.00001 sample time) ode4 (Runge-kutta) solver is used, that can simulate the model in 3 minutes on a typical desktop computer.

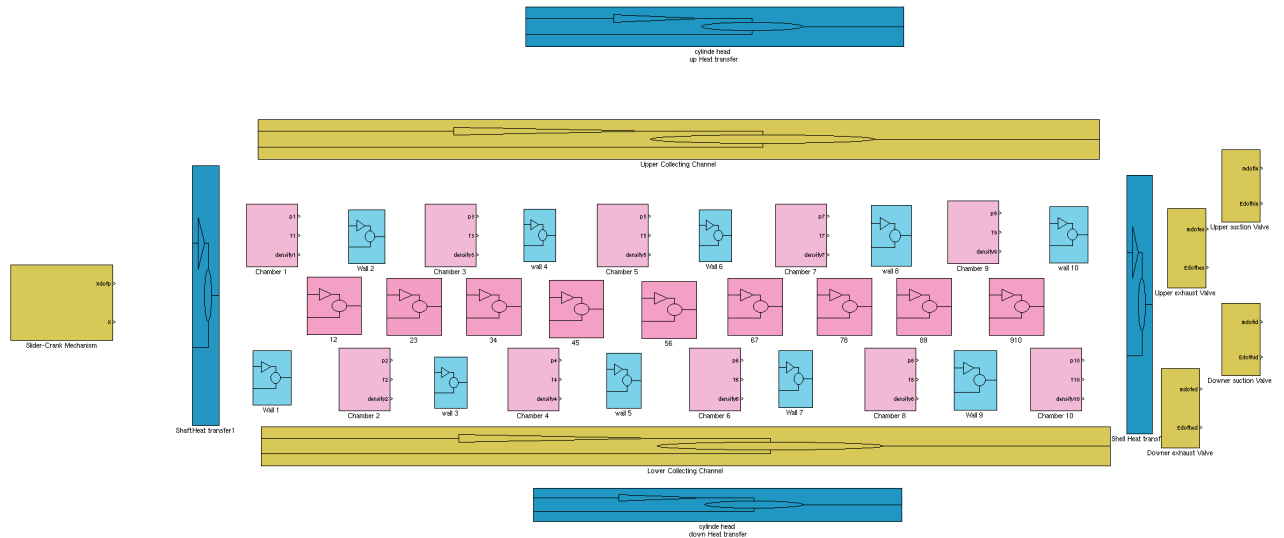


Figure A VI.1: Implementation of the finned model compressor in Simulink.

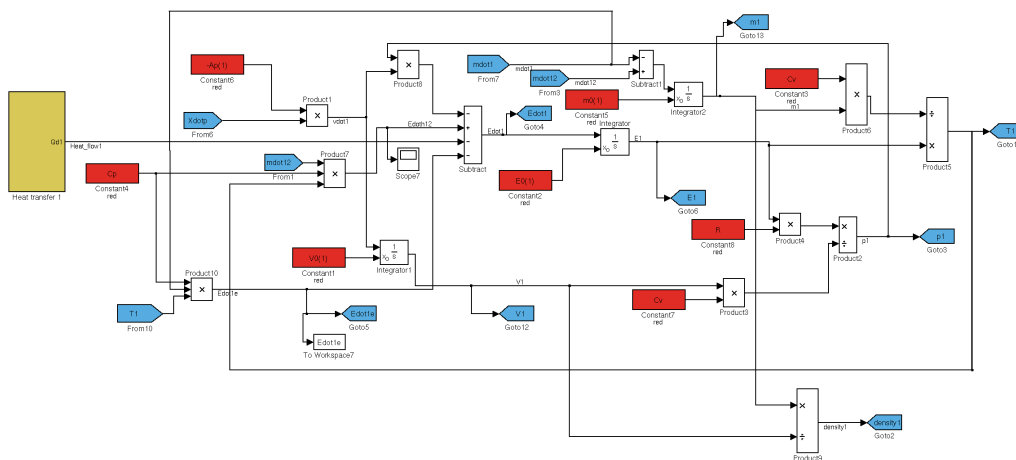


Figure A VI. 2: First chamber model in Simulink.

Figure A VI. 3 shows the IFS model in Simulink between 1st and 2nd chamber. Mass flow is calculated by multiplying pressure difference of the chambers and reverse of resistance of IFS. **Figure A VI. 4** shows the details of the upper valve.

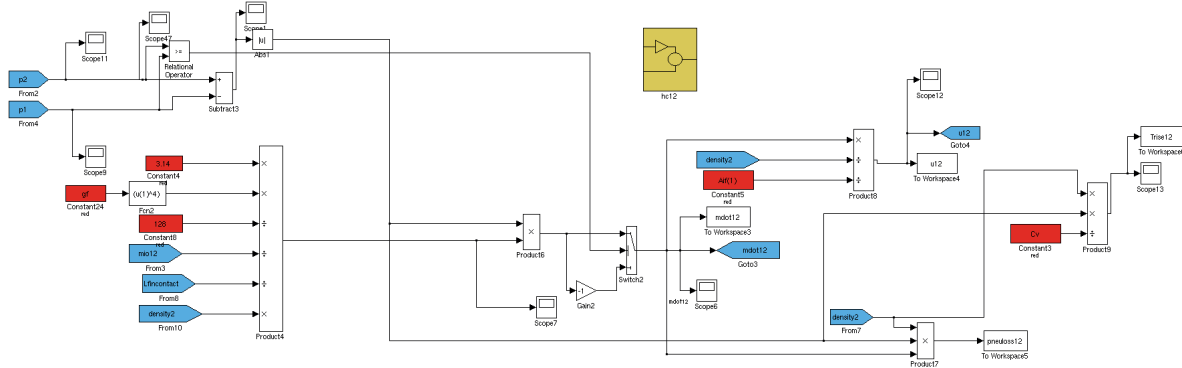


Figure A VI. 3: IFS model in Simulink between 1st and 2nd chamber.

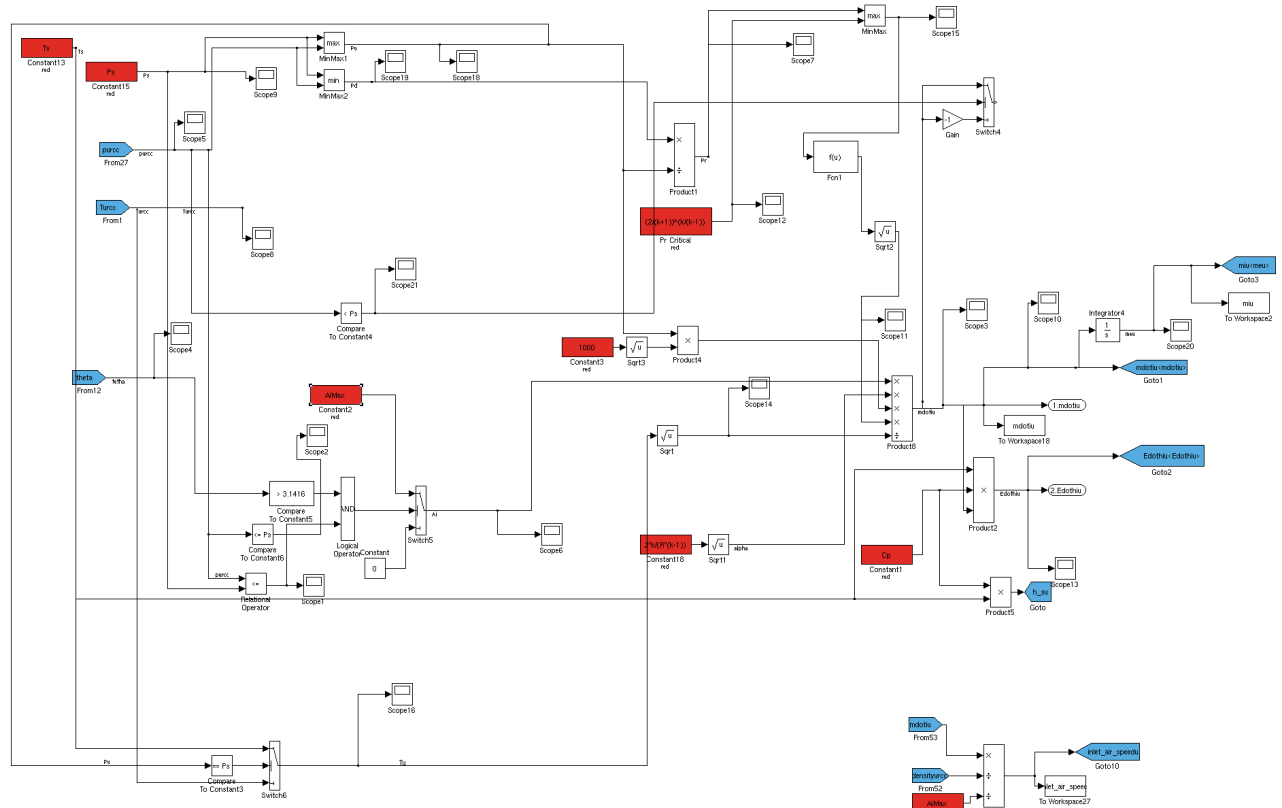


Figure A VI. 4: Upper suction valve model in Simulink between.

Curriculum Vitae

Mahbod Heidari
EPFL
STI-IEL-LEI
Station 11
1015 Lausanne

Born in Jul. 12, 1984
Nationality :Iranian
Permit B
+41 78 7706773
mahbod.heidari@epfl.ch

Education

2015 (exp.) PhD in Energy engineering at EPFL
2010-2014 Energy engineering studies at EPFL
2007-2010 Master in Energy systems at Manchester University/KNTU
2002-2007 Bachelor in Mechanical Engineering studies at K.N.Toosi University of Technology

Professional Membership

2002-present American Society of Mechanical Engineers (ASME)
2007-2010 Association of Energy Engineers (AEE)

Professional Experience

2010-2014 Research Assistant at Industrial Electronics Laboratory, EPFL.
2007-2010 Plant Piping engineer at IRITEC

Technical Skills

Modelling, Simulation and analysis of thermo fluidal systems unsteady state analysis of open thermodynamic systems
Energy Integration Application of Pinch and cogeneration technics to energy systems
Energy Conversion, Storage and Management With focus on renewable energies
Optimization Linear and non-linear multi-objective programming
Finite Element Analysis Fluid flow and Heat Transfer analysis with COMSOL

Projects

PhD Thesis

I am working on a finned piston compressor, a new and promising machine, which can be used in isothermal Compressed Air Energy Storage (CAES). My main goal was to improve the energetic performance of current reciprocating compressors. By this technique the excess electrical energy during off-peak time can be stored and used later on during the peak-time electricity demand. The list of my publications is available at: <http://people.epfl.ch/cgibin/people?id=201109&op=publications&lang=en&cvlang=en>

2010-2011 Modelling and optimization of the fast recharge of the compressed air car in the area of energetic efficiency.
2009-2010 Investigation of mixed refrigeration cycle efficiency in NGL plants.
2008-2009 Exergy analysis for low temperature refrigeration systems used in Natural Gas Liquid Recovery plants.

Languages

English Fluent (iBT TOEFL Score=90; GRE General Score=1200)
French Proficient
Persian Native Language

Personal Information

30 years old, Single, Iranian Citizenship, Permit B

Journal Articles

M. Heidari, S. Wasterlain, P. Barrade, F. Gallaire and A. Rufer, Energetic Macroscopic Representation of A Linear Reciprocating Compressor Model, International Journal of Refrigeration (2015), 10.1016/j.ijrefrig.2014.12.019.

M. Heidari, A. Rufer and J. R. Thome, Heat And Mass Transfer Modelling In A Finned Reciprocating Compressor, Part I: Heat Transfer Using Thermo-Electric Analogy, Applied Thermal Engineering (2014), In Review.

M. Heidari, A. Rufer and J. R. Thome, Heat And Mass Transfer Modelling In A Finned Reciprocating Compressor, Part II: Mass Transfer Using Pneumatic-Electric Analogy, Applied Thermal Engineering (2014), In Review.

M. Heidari, A. Rufer and D. Favrat, Energy And Exergy Analysis Of Isothermal Compressed Air Energy Storage Systems, Journal of Applied Energy (2015), In Review.

Conference Proceedings

Increasing Exergetic Efficiency Through Convective Heat Transfer Enhancement in a Finned Reciprocating Compressor

Heidari, M. and Rufer, A.

First Thermal Fluids Engineering Summer Conference, New york, USA, 2015.

Thermo-Electric Analogy Method For Computing Transient Heat Transfer In A New Reciprocating Finned Piston Compressor

Heidari, M., Rufer, A., Thome J. R.

15th International Heat Transfer Conference (IHTC15), Kyoto, Japan, 2014.

On The Strategies Towards Isothermal Gas Compression And Expansion

M. Heidari, S. Lemofouet and A. Rufer,

22nd International Compressor Engineering Conference at Purdue, West Lafayette, Indiana, 14-17 July 2014.

Bond Graph Model Representation of a New Reciprocating Finned Air Compressor

M. Heidari and A. Rufer.

11th International Conference on Bond Graph Modelling and Simulation. Monterey, CA, USA. July 6-10, 2014.

Fluid Flow Analysis of a New Finned Piston Reciprocating Compressor Using Pneumatic Analogy

M. Heidari and A. Rufer.

3rd International Conference on Fluid Dynamics and Thermodynamics Technologies (FDTT2014), Antalya, Turkey, 21-23 April 2014.

Computational Fluid Dynamics Comparison of Classic and Finned Piston Reciprocating Linear Air Compressor Using COMSOL

M. Heidari, P. Barrade and A. Rufer

COMSOL European Conference, Cambridge, United Kingdom, September 16-17, 2014.

Analysis and Development of a New Compressor Device Based on The New Finned Piston

Mahbod Heidari, Alfred Rufer

International Conference on Compressors and their Systems, London, UK.

9 - 10 September 2013

Finite Element Modelling and simulation of a Three-Stage Air Compressor Based on Dry Piston Technology.

M. Heidari, P. Barrade and A. Rufer.

COMSOL European Conference, Stuttgart, Germany, October 26-28, 2011.